# Ligand-specific regulation and signalling by the neuromedin U 2 receptor

Thesis submitted for the degree of Doctor of Philosophy

at the University of Leicester

by

Heider Shaheed Jawad Qassam BSc, MSc

Department of Cell Physiology and Pharmacology

University of Leicester

May 2019

# ABSTRACT Heider Qassam


## Ligand-specific regulation and signalling by the neuromedin U 2 receptor

Neuromedin U receptor 2 (NMU2) is a Family A, G protein-coupled receptor (GPCR) for both neuromedin U (NmU) and neuromedin S (NmS), particularly within the CNS where effects include the suppression of feeding behaviour and increased energy expenditure suggesting an anti-obesity target. Although NMU2 preferentially activates $G\alpha_{q/11}$, it is unclear which signalling underlies physiological outcomes or if the ligands generate different responses. Here, NMU2 signalling and regulation have been explored, including using a protocol of brief ligand exposure to match exposure patterns of peptidergic receptors *in vivo*.

In HEK293 cells stably expressing human (h) NMU2, hNmU-25 and hNmS-33 evoked similar $Ca^{2+}$ signalling, although resensitisation required only 6 h following brief (5 min) exposure to hNmU-25 but more than 6 h following hNmS-33. Activation of the mitogen-activated protein kinases (MAPKs) ERK, P38 and JNK, was more sustained following brief exposure to hNmS-33 compared to hNmU-25. NMU2 phosphorylation was increased by both ligands and inhibition of protein kinase C (PKC) reduced this by ~50%. Phosphorylation was more sustained following brief exposure to hNmS-33 than hNmU-25. Sustained challenge with either ligand sustained the recruitment of arrestin 2 and 3 to NMU2. Ligand removal resulted in loss of arrestin interaction that was slower for arrestin 2 but similar for the two ligands. This suggests that following brief exposure to hNmS-33, sustained NMU2 phosphorylation does not sustain arrestin recruitment and arrestin recruitment is not responsible for sustained MAPK activation. Five phosphorylated serine or threonine residues were identified in the *C*-terminus of NMU2 by mass spectrometry. Mutation of these reduced phosphorylation by both ligands and phosphorylation was abolished by PKC inhibition. Mutation of seven other serine/threonine residues reduced phosphorylation by hNmU-25 more than hNmS-33, suggesting different phosphorylation patterns. Mutation of all fourteen *C*-terminal serine/threonine residues abolished agonist-dependent phosphorylation. These data highlight ligand-dependent NMU2 signalling and regulation, particularly following brief ligand exposure. Such ligand dependence may be relevant to other GPCRs but their consequence to physiology and implications for drug discovery require further study.

# ACKNOWLEDGEMENTS

First, I would like to acknowledge my sponsor, The Higher Committee for Education in Iraq (HCED) for letting me grab this PhD opportunity. I would like to express my special appreciation and thanks to my supervisor, **Associate Professor Gary B. Willars**. I would like to thank you for all the encouragement, support, guidance and supervision throughout my PhD study. Thank you very much for your time you have spent on preparation and correction of my talks, posters and thesis. Thank you very much for giving me an opportunity to be a co-author of scientific papers. I would like to thank you for giving me great trust and for allowing me progress as a research scientist in molecular pharmacology. I would like to thank my second supervisor **Associate Professor Nina Storey** for your encouragement, support and guidance. Special thanks go to **Dr. Adrian J. Butcher** (UK Dementia Research Institute at the University of Cambridge, UK) for training in the techniques of receptor phosphorylation and BRET assays in addition to your invaluable advice.

Next, I would like to thank my PhD committee members: **Professor John Challiss** and **Professor Christine E. Pullar** for their contribution towards the project and my progress.

Many thanks to all members in Department of Molecular and Cell Biology at the University of Leicester who have supported me during may PhD study, particularly **Dr Lorenza Francescut** and **Mr. Raj Mistry**.

Many thanks go to the Protein and Nucleic Acid Chemistry laboratory (PNACL) and Protein Expression laboratory (PROTEX) for their services, in particular mass spectrometric analysis and DNA sequencing. Thank you to all of my lab mates and friends I have met in the department during my PhD study, both past and present: **Dr.Niachang Li**, **Dr**. **Omar Bahattab**, **Dr. Ali Janabi**, **Shou Wang** and **Dr. Karrar Kamoona**.

Special thanks go to my father and mother for their support and patience. Your prayers have allowed me to progress so far. Finally, thank you to my wife, **Aula**. You have always believed in me and I would not be here without you. We have been together all the way through the PhD journey with hope for a successful future. I would like to express my thanks to my children, **Fatima**, **Mustafa** and my little boy **Hassan** who was born in the third year of my PhD study. You are the best gift from God.

*This thesis is dedicated to my father, my mother, my wife and my children*

***Heider***

# PUBLICATIONS

## Peer-reviewed publications:

Alhosaini K, Bahattab O, **Qassam H**, Challiss J, Willars GB (2018). Ligand-specific signaling profiles and resensitization mechanisms of the neuromedin U2 receptor. *Mol Pharmacol.* 94:674–688.

Brimson JM, Safrany ST, **Qassam H**, Tencomnao T (2018). Dipentylammonium binds to the sigma-1 receptor and protects against glutamate toxicity, attenuates dopamine toxicity and potentiates neurite outgrowth in various cultured cell lines. *Neurotox Res.* 34:263-272.

## Abstracts:

**Qassam HS**, Butcher AJ, Tobin AB, Willars GB. (2016) Ligand-dependent temporal patterns of signalling and receptor phosphorylation at NMU2. British Pharmacology Society (2016), London, UK.
http://www.pa2online.org/abstract/abstract.jsp?abid=33149&period=64

**Qassam HS**, Butcher AB & Willars GB (2018). Ligand-dependent profiles of NMU2 signalling: relationships to receptor phosphorylation and arrestin recruitment. 7th RSC /SCI symposium on GPCR in Medical Chemistry, Verona, Italy.

# Contents

# List of figures

# List of tables

# ABBREVIATIONS

| | |
|---|---|
| **$[Ca^{2+}]i$** | Intracellular calcium concentration |
| **AC** | Adenylyl cyclase |
| **ACTH** | Adrenocorticotropic hormone |
| **AGRP** | Agouti-related peptide |
| **AP2** | Adaptor protein-2 |
| **ARC** | Arcuate nucleus |
| **ATP** | Adenosine triphosphate |
| **BMI** | Body mass index |
| **bp** | Base pair |
| **BRET** | Bioluminescence resonance energy transfer |
| **BSA** | Bovine serum albumin |
| **cAMP** | Adenosine cyclic-3,5-monophosphate |
| **CCR7** | Chemokine receptor |
| **CD44** | Cluster of differentiation |
| **cDNA** | Complementary DNA |
| **CHO** | Chinese hamster ovary |
| **CKK** | Cholecystokinin |
| **CNS** | Central nervous system |
| **CREB** | cAMP response element binding protein |
| **CRH** | Corticotrophin-releasing hormone |
| ***C*-terminal** | Carboxy-terminal |
| **Cy3B-pNmU-8** | pNmU-8 fluorescently tagged at *N*-terminal with Cy3B |
| **DAG** | Diacylglycerol |
| **DDT** | Dithiothreitol |
| **DMEM** | Dulbecco's modified Eagle‟s medium |
| **DMN** | Dorsomedial nucleus |
| **DMSO** | Dimethyl sulphoxide |
| **DNA** | Deoxyribonucleic acid |
| **dNTPs** | Deoxyribonucleotide triphosphate |
| **DPBS** | Dulbecco's phosphate-buffered saline |
| **$EC_{50}$** | Concentration given 50 % of the maximal response |
| **ECE-1** | Endothelin-converting enzyme 1 |
| **ECL** | Extracellular loop |
| **EDTA** | Ethylenediaminetetraacetic acid |
| **EGF** | Epidermal growth factor receptor |
| **eGFP** | Enhanced green fluorescent protein |
| **ELISA** | Enzyme-linked immunosorbent assay |
| **Endo H** | Endoglycosidase H |

| | |
|---|---|
| **Epac** | Exchange protein activated by cAMP |
| **ER** | Endoplasmic reticulum |
| **ERK** | Extracellular signal-regulated kinase |
| **FBS** | Fetal bovine serum |
| **FBS** | Fetal bovine serum |
| **Fluo-4-AM** | Fluo-4-acetoxymethylester |
| **FM3** | Previous name of neuromedin U type 1 receptor |
| **FM4** | Previous name of neuromedin U type 4 receptor |
| **FSH** | Follicle-stimulating hormone |
| **FSK** | Forskolin |
| **G418** | Geneticin |
| **$GABA_B$** | Gamma-aminobutyric acid receptor type B |
| **GDP** | Guanosine diphosphate |
| **GEF** | Guanine nucleotide exchange factor |
| **GLP-1** | Glucagon-like peptide |
| **GPCR** | G protein-coupled receptor |
| **G-protein** | Heterotrimeric guanine nucleotide-binding protein |
| **GRK** | G protein-coupled receptor kinase |
| **GTP** | Guanosine triphosphate |
| **HA** | Hemagglutinin |
| **HBSS** | Hanks' balanced salt solution |
| **HEK** | Human embryonic kidney |
| **HEK-NMU1** | HEK 293 cells stably expressing NMU1 |
| **HEK-NMU2** | HEK 293 cells stably expressing NMU2 |
| **hNmS-33** | Human NmS-33 |
| **hNmU-25** | Human NmU-25 |
| **HRP** | Horseradish peroxidase |
| **IBMX** | Isobutylmethylxanthine |
| **ICL** | Intracellular loop |
| **ICV** | Intracerebroventricular |
| **$IP_3$** | Inositol 1,4,5-trisphoshate |
| **IV** | Intravenous |
| **JNK** | c-JUN *N*-terminal kinase |
| **KHB** | Krebs-HEPES buffer |
| **LB** | Luria broth |
| **LH** | Luteinising hormone |
| **LHA** | Lateral hypothalamic area |
| **MAPK** | Mitogen-activated protein kinase |
| **MC4R** | Melanocortin-4 receptor |

| | |
|---|---|
| **MEM** | Minimum essential medium |
| **MOP** | mu opioid receptor |
| **mRNA** | Messenger RNA |
| **nLUC** | Nanoluciferase |
| **NmS** | Neuromedin S |
| **NmU** | Neuromedin U |
| **NMU1** | Neuromedin U receptor subtype-1 |
| **NMU2** | Neuromedin U receptor subtype-2 |
| **NMU2-HA** | Neuromedin U receptor subtype-2 tagged with HA at *C*-terminal |
| **NmU-IL** | NmU-like immunoreactivity |
| **NPY** | Neuropeptide Y |
| ***N*-terminal** | Amino-terminal |
| **PAR2** | Protease-activated receptor 2 |
| **PCR** | Polymerase chain reaction |
| **PDBu** | Phorbol 12,13-dibutryate |
| **$pEC_{50}$** | Negative logarithm of the concentration given 50 % of the maximal response |
| **$PIP_2$** | Phosphatidylinositol 4,5-bisphosphate |
| **PKA** | Protein kinase A |
| **PKC** | Protein kinase C |
| **PNGase F** | Peptide N-glycosidase F |
| **pNmU-25** | Porcine NmU-25 |
| **POMC** | Pro-opiomelanocortin |
| **PP2A** | Protein phosphate type 2 A |
| **PTH1R** | Parathyroid hormone type 1 receptor |
| **PTX** | Pertussis toxin |
| **PVDF** | Polyvinylidene difluoride |
| **PVN** | Paraventricular nucleus |
| **PYY** | Peptide YY |
| **RGS** | Regulator of G protein signalling |
| **RLuc** | Renilla luciferase |
| **RNA** | Ribonucleic acid |
| **RT** | Room temperature |
| **S1P1** | Sphingosine-1-phosphate receptor 1 |
| **SAPKs** | Stress-activated protein kinases |
| **SCN** | Suprachiasmatic nucleus |
| **SDS** | Sodium dodecyl sulfate |
| **SERCA** | Sarcoplasmic/endoplasmic reticulum $Ca^{2+}$ATPase |
| **siRNA** | Small/short interfering RNA |
| **SNX27** | Sorting nexin 27 |

| | |
|---|---|
| **SON** | Supra optic nucleus |
| **SST2** | Somatostatin type 2 receptor |
| **TBST** | Tris buffered saline with tween |
| **TEMED** | N, N, N‟, N‟-tetramethylethylenediamine |
| **UII** | Urotensin II |
| **VMN** | Ventromedial nucleus |
| **WHO** | World health organisation |
| **YFP** | Yellow fluorescent protein |
| **α MSH** | α melanocyte-stimulating hormone |

# 1 Chapter one: General introduction

## 1.1 Obesity

Obesity remains a growing public health concern facing populations around the world. It is a risk factor for other diseases that play crucial roles in increasing of the rate of morbidity and mortality (Behary *et al.*, 2015). Although several medications have been approved for treatment of obesity, others have been excluded for their side effects. The neurmedin system might be potential therapeutic target for treatment of obesity.

Obesity is defined simply as an increase in the deposition of fat as a result of a disruption of the balance between food consumption and energy expenditure (Behary *et al.*, 2015; Valsamakis *et al.*, 2017). The most common measurement or indicator used to determine if individuals are overweight is called the body mass index (BMI). This is derived by dividing the total body weight (measured in kg) over the square of the individual height (measured meteres) (Sweeting, 2007). The BMI is used to categorise individuals as overweight and obesity according to criteria defined by the World health organisation (WHO). For example, people who have a BMI between 25 - 29.9 kg / $m^2$ are considered as overweight while individuals with a BMI over 30 kg / $m^2$ are considered obese (WHO Obesity and Overweight, 2016). Concerns have been raised as the prevalence of obesity have increased over recent years and are still increasing. For example, globally 1.9 billion adults and 41 million children (under five-age group) are overweight (WHO Obesity and overweight, 2016). In the UK, estimates indicate that about one third of adults are obese, with a BMI over 30 kg / $m^2$.

### 1.1.1 Obesity associated diseases

Obesity is not only a disease state by itself but also a risk factor for more than 20 other critical conditions that increase morbidity and mortality. This includes Type II diabetes mellitus in which the vast majority of patients are overweight and obesity is biggest risk factor for this condition, hypertension, stroke, cardiovascular disease, dyslipidaemia, cancers, and genitourinary system problems. Hence, there is an urgent need to provide therapeutic options to treat and/or prevent obesity, particularly with the presence of limited options to date (Upadhyay *et al.*, 2018).

### 1.1.2 Food consumption and energy expenditure: central and peripheral regulation of eating behaviours

Like other physiological processes, body fat composition is highly regulated. Changes in this parameter is a result of the imbalance between the energy input and energy output (Kim *et al.*, 2018). Different mechanisms contribute to the regulation of feeding behaviour. Peripheral regulation of feeding occurs through a variety of gut peptides **(Figure 1.1)**. For example, at the start of food ingestion, levels of these peptides increase thereby influencing both the amount of food intake and the frequency (Kim *et al.*, 2018). Glucagon-like peptide (GLP-1), cholecystokinin (CKK), and peptide YY (PYY) are examples of satiety peptides, which are secreted upon food ingestion from enteroendocrine cells of gastrointestinal tract (Cummings *et al.*, 2007). Both GLP-1 and PYY play important roles in regulation of feeding. Intravenous (IV) treatment with GLP-1 decreases body weight in individuals of normal weight and in individuals that are either overweight or have Type II diabetes mellitus (Holst, 2007; Sandoval *et al.*, 2015). Likewise, in mouse of obesity produced by PYY knockout, the administration of PYY reduced weight (Batterham *et al.*, 2006). CCK is also a satiety-regulating molecule that is released from the duodenum. It is an anorexic peptide that mediates its effects via two receptors, CCK type A and type B (Steinert *et al.*, 2017). The satiety produced by CCK is thought to be via CCK type A receptor rather than the CCK type B receptor as antagonising the CCK type A receptor increases food intake (Steinert *et al.*, 2017). Leptin, a hormone related to satiety, is a circulating protein synthesised in adipose tissue. It mediates its action in the CNS by cognate receptor (Bjorbaek, 2009). In the hypothalamic regions and ARC, the leptin receptor (ObRb) is expressed playing a crucial role in regulating biological action of leptin, particularly energy intake, energy expenditure and body fat regulation (Sainz *et al.*, 2015). Leptin is key in the regulation of body fat content. For example, decreased food consumption was associated with peripheral or central administration of leptin while increased food consumption was occurs in states of leptin deficiency (Halaas *et al.*, 1997). Mice-deficient either leptin or its cognate receptors ($lep^{ob/ob}$, $lep^{db/db}$ respectively) are obese, hyperphagic and resistant to insulin and hyperglycaemic (Bjorbaek, 2009). In contrast to the effects of leptin, ghrelin, a gut hormone secreted from stomach, is an orexigenic protein with high circulating levels during fasting and low levels during fed states (Kim *et al.*, 2018). Indeed, the ICV administration of ghrelin to the rats resulted in a rapid onset of food

eating that was brief despite the fact that ghrelin also had plays a role in the long-term regulation of body mass (Tschop *et al.*, 2000).

The central regulation of feeding behaviour is also a critical factor influencing on the balance between feeding and energy expenditure. Understanding the molecular bases of this regulation is therefore of particular interest, particularly in terms of the potential treatment of obesity. Feeding and energy regulate complex processes that depend on the integration of many signals. This includes information on nutritional status and energy levels gathered by the brain, which is responsible for processing these signals and responding appropriately to regulate feeding (Williams *et al.*, 2001). The hypothalamus is considered a key regulator of feeding and energy expenditure by acting on signals arising from both peripheral and central regions (Magni *et al.*, 2009). This central regulation is further complicated by different regions within the hypothalamus interacting through a variety of neuropeptides, which provide attractive anti-obesity targets (Boughton *et al.*, 2013). These interacting regions include arcuate nucleus (ARC), paraventricular nucleus (PVN), dorsomedial nucleus (DMN), ventromedial nucleus (VMN) and lateral hypothalamic area (LHA). In the ARC, which is a one of the most extensively studied areas, two populations of hypothalamic neurons are involved; one functions to stimulate feeding behaviour and includes neuropeptide Y (NPY) and agouti-related peptide (AGRP) and other is pro-opiomelanocortin neuron (POMC) which has suppressant effects on feeding **(Figure 1.1)** (Kim *et al.*, 2018). The receptors for leptin and insulin are also expressed on these neurons and have a role in the regulation of POMC and NPY/AGRP pathways. It has been reported that POMC and NPY/AGRP pathways are modulated by leptin and insulin through activating the anorexigenic and orexigenic effects of the POMC and NPY/AGRP pathways respectively (Schwartz *et al.*, 2000). In the POMC producing neurons within the ARC, the binding of leptin to its receptor mediates the transcription of POMC peptide precursor. This, in turn, is cleaved and increases the production of α melanocyte-stimulating hormone (α MSH) which is an anorexic peptide that mediates its effects via melanocortin -4 receptor (MC4R) (van der Klaauw, 2018). It has been demonstrated that administration of α MSH to rodents reduces eating and increases consumption of energy, which can be blocked by inhibition of MC4R (Adage *et al.*, 2001). In contrast, NPY/AGRP producing neurones which communicate through the PVN-ARC axis are responsible for orexigenic effects by secreting a variety of neuropeptides such as NPY and AGRP that result in increased food

intake (Sternson *et al.*, 2014). NPY is an orexigenic neuropeptide that is abundantly expressed in the brain (Abdalla, 2017). It has been shown that NPY levels increase in the fasting state but decrease after eating, highlighting its role in regulating feeding (Wynne *et al.*, 2005). In mice, the direct and continuous administration of NPY resulted in rapid increase in food intake and the development of obesity (Raposinho *et al.*, 2001). Leptin also regulates NPY by attenuating its synthesis (Erickson *et al.*, 1996). Within the NPY/AGRP neurons, the orexigenic AGRP is synthesised and mediates its effects by binding to the MC4R. This results in the inhibition of the constitutive activity of MC4R and induces receptor endocytosis by acting as an inverse agonist (Nijenhuis *et al.*, 2001). In the cases where energy supply restricted, the NPY/AGRP producing neurones suppress the POMC pathway (Sato *et al.*, 1988). Overall, the central and peripheral regulatory mechanisms described are well-established aspects of satiety, hunger and energy expenditure. However, the complexity of these mechanisms draws attention to the possibility of new strategies for the generation of novel therapeutic agents. Some previously marketed anti-obesity drugs have been withdrawn due to the development of a variety of unwanted effects, adding further impetus to the generation of more selective molecules (Boughton *et al.*, 2013). Indeed, neuropeptides and their receptors can be future therapeutic targets controlling the central and peripheral regulation of eating and energy expenditure (van der Klaauw, 2018). For example, neuromodulators like lorcaserin or molecules mediating similar actions of the endogenous neuropeptides (MC4R agonists) caused a reduction in human body mass (Burke *et al.*, 2014).

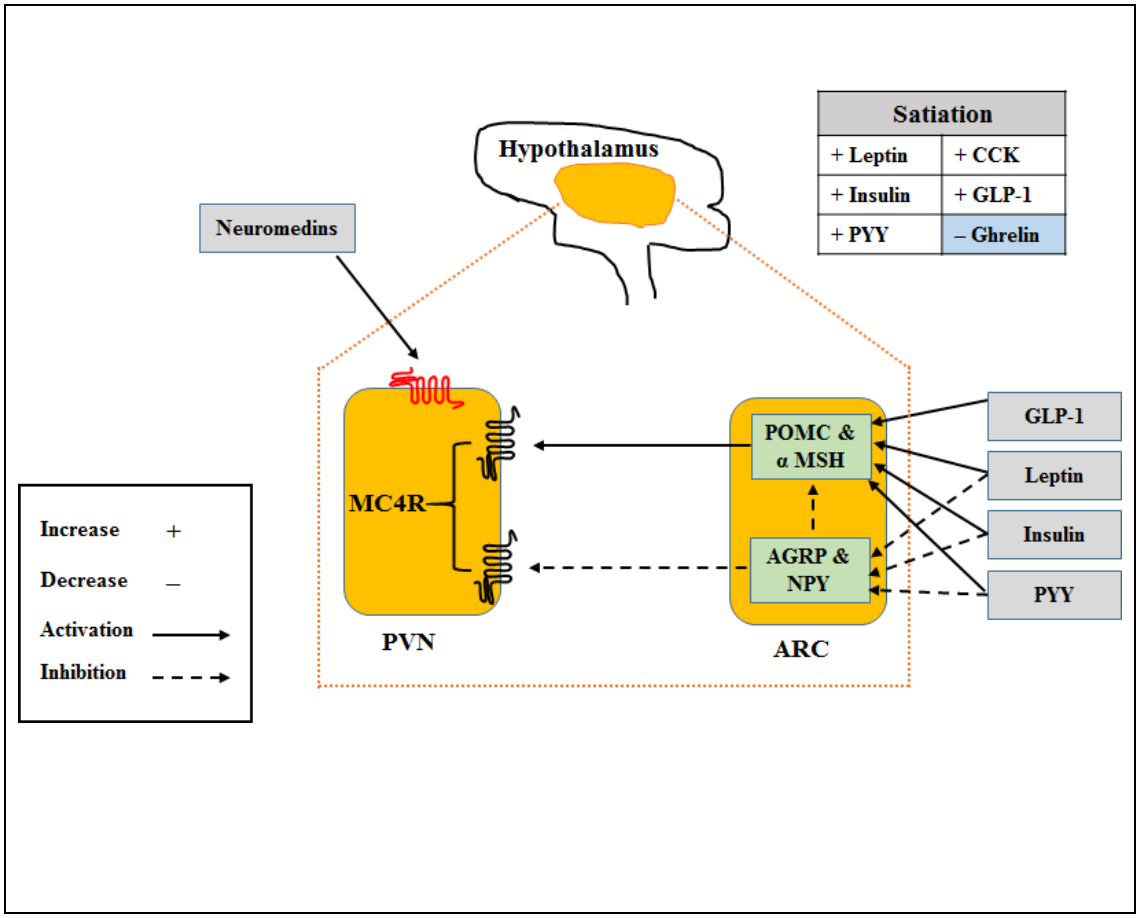


**Figure 1.1 Central and peripheral signals involved in the regulation of feeding and energy homeostasis**

CCK, PYY and GLP-1 are released from the gastrointestinal tract following food intake. Both leptin and insulin are delivered into the circulation from adipocytes and cells of pancreas respectively to regulate the long-term energy storage. Ghrelin is a peptide hormone in which it is found with high and low concentrations in the fasting state and after eating respectively. Two populations of the neurons are controlled by a variety of peptide molecules including POMC, NPY and AGRP. Abbreviations in the text.

### 1.1.3 Current options and future pharmacotherapy for the treatment of obesity

Obesity is a one of the leading causes of public health issues based on its pathophysiological and economic implications worldwide (Zhang *et al.*, 2012). It is associated with a list of chronic diseases **(Section 1.1.1)** and is well-established that there is a link between the increasing prevalence of obesity and the increased number of deaths from cardiovascular diseases and cancers, particularly liver cancers (Calle *et al.*, 2003; Shrager *et al.*, 2012; Jensen *et al.*, 2014). Furthermore, a considerable amount of evidence indicates the positive effects of weight loss on such obesity-associated diseases. Reductions in body weight have ameliorative influences on obesity-related risk factors (Fujioka, 2010; Henry *et al.*, 2013; Jensen *et al.*, 2014; Kushner *et al.*, 2014). Hence, with the increasing prevalence of obesity globally, options for the management of obesity is required. Different approaches are currently used to treat obesity including lifestyle modification (diet restriction and physical exercise), pharmacotherapy and bariatric surgery (Patel, 2015). Lifestyle changes are the first-line treatment for obesity (Jensen *et al.*, 2014) and both low-calorie food intake and physical exercises are essential in reducing body weight (Wing *et al.*, 2006; Rock *et al.*, 2010). However, limitations associated with compensatory biological changes generally lead to a regain of weight by increasing food seeking and decreasing satiation (Makaronidis *et al.*, 2018). Pharmacological approaches can be used as adjuvant therapy to overcome these compensatory mechanisms and promote continued lifestyle modification (Greenway, 2015). Bariatric surgery is a powerful surgical procedure with estimates of around 500,000 surgical operations performed globally each year (Angrisani *et al.*, 2015). Such intervention is generally considered for individuals with a BMI $\geq$ 40 or those with obesity-related diseases that have a BMI $\geq$ 35 and who are unable to manage life-style modifications (Jensen *et al.*, 2014; Khorgami *et al.*, 2017). However there are several drawbacks that associated with such surgery with a possibility of bleeding, suture failure or infections (Benaiges *et al.*, 2017).

In view of the difficulties associated with life-style modifications and surgery to treat obesity, pharmacotherapy remains a crucial option for management although options are limited because of lacking of consistent efficacy or adverse effects. Individuals with a BMI ($\geq$ 30) or BMI ($\geq$ 27) with obesity-associated diseases are eligible for pharmacotherapy (Jensen *et al.*, 2014). Furthermore, a pharmacotherapeutic approach is considered the next option if life-style modification fails (Gadde *et al.*, 2018). Although

a variety of medications for the management of obesity have been introduced over the last two decades, many of them have been withdrawn due to unacceptable side effects (Narayanaswami *et al.*, 2017). Medications are classified into three categories: drugs that interfere with lipid absorption; drugs that reduce eating and; those that increase energy expenditure **(Table 1.1)** (Narayanaswami *et al.*, 2017; Gadde *et al.*, 2018).

**Table 1.1 Drugs approved for the management of obesity**

| **Medication** | **Mode of action** | **Side effects** |
|---|---|---|
| Orlistat | Lipase inhibitor, restricts the absorption of fat from the gastrointestinal tract | Oily stool, anal oil leak from anus and fecal incontinence |
| Combination of phentermine and topiramate<br><br>Phentermine<br><br>Topiramate | Noradrenaline transporter inhibitor, acts by activation of POMC-producing neurones<br>GABA agonist, reduces appetite | Constipation, dry mouth, dizziness paresthesia and insomnia |
| Lorcaserin | Selective $5HT_{2c}$ agonist, induces feeling of fullness | Nausea, dry mouth, constipation, fatigue, dizziness, headache cough and hypoglycaemia |
| Liraglutide | GLP-1 agonist, reduce appetite | Hypoglycemia, nausea, vomiting diarrhea, abdominal pain, constipation, fatigue, dyspepsia and headache |
| Combination of naltrexone and bupropion<br>Naltrexone<br><br>Bupropion | Non-selective opioid receptor blocker.<br>Noradrenaline and dopamine transporter inhibitor activates POMC producing neurones to deliver α MSH leading to increase in the energy expenditure and decrease eating | Dry mouth nausea, vomiting, diarrhea, dizziness, insomnia and headache |

Limited options do not work for all because of side effects and compliance issues highlight the need for the development of novel therapeutic targets with safe, better efficacy and lower adverse effects, particularly with explosive figures of both obesity and related conditions. There is a strong possibility that the brain-gut peptides; neuromedin

system might be future targets, attracting attentions of the researchers for their potential as anti-obesity targets.

## 1.2 Neuromedin U and structurally-related neuromedin S: discovery and difference between species

Neuromedin U (NmU) is a brain-gut peptide belonging to the neuromedin family. Originally, this peptide was separated in the 1980s from porcine spinal cord based on its ability to contract uterine smooth muscle (Kangawa *et al.*, 1983; Minamino *et al.*, 1985). The structurally-related but distinct peptide neuromedin S (NmS) was discovered later and found to be particularly abundant in the suprachiasmatic region of the brain, hence the suffix S (Mori *et al.*, 2005). Other members of the neuromedin family also exist and distribute in a variety of tissues with a myriad of biological activities in many systems, including neuromedins type B and C, neurokinin B and A, substance K and neurotensin like peptide (Brighton *et al.*, 2004a). Two versions of porcine NmU were originally purified, a twenty-five amino acid version, porcine neuromedin U-25 (pNmU-25) and a shorter eight amino acids version with similar bioactivity, porcine neuromedin U-8 (pNmU-8) (Minamino *et al.*, 1985). The shorter form is likely to be a result of cleavage of the longer version at a dibasic cleavage site including two arginines $R^{16}$ and $R^{17}$ prior to the last eight amino acids **(Figure 1.2)** (Fisher *et al.*, 1988). Isolation and purification of NmU from different species such as human (Austin *et al.*, 1995), rabbit (Kage *et al.*, 1991), frog (Domin *et al.*, 1989), dog (O'Harte *et al.*, 1991a) and chicken (O'Harte *et al.*, 1991b; Domin *et al.*, 1992), mainly resulted in NmU-25 analogues with the exception of rat that had twenty-three amino acids while chicken and guinea pig had nine amino acids (Minamino *et al.*, 1988; Murphy *et al.*, 1990; O'Harte *et al.*, 1991b). Recently, a variety of versions of NmU have been isolated from several species including, NmU-17 from the skin of the Asian red toad (Lee *et al.*, 2005) and NmU-21, -25 and -38 from the brain of goldfish **(Figure 1.2; A)** (Maruyama *et al.*, 2008). Several forms of NmS have been isolated from different species such as human (hNmS-33) mouse (mNmS-36), rat (rNmS-36) and both fNmS-17 and fNmS33 from bombina frogs (Mori *et al.*, 2005; Chen *et al.*, 2006) **(Figure 1.2; B)**.

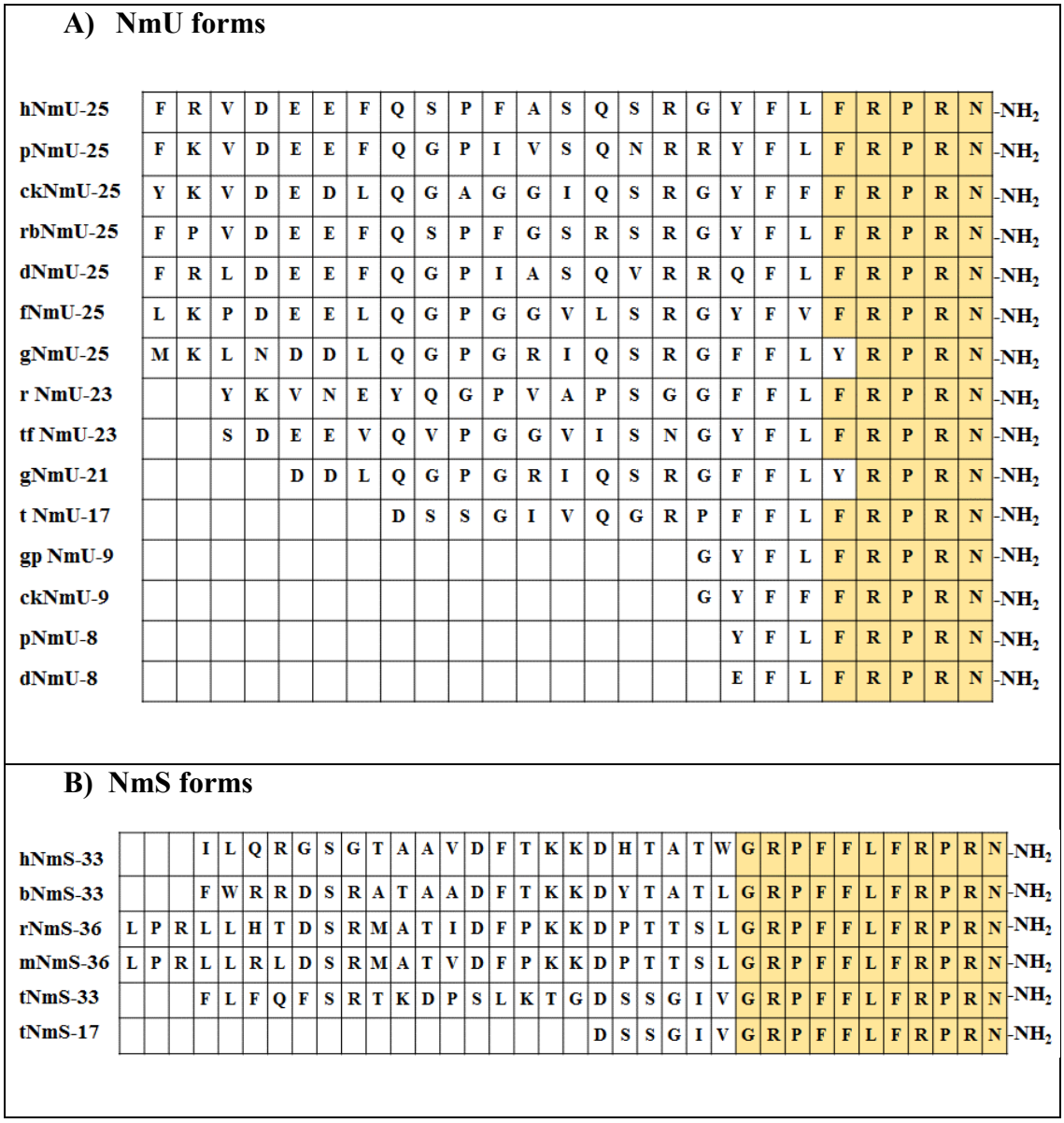


**Figure 1.2 Amino acid sequences of different forms of NmU and NmS from several species**

Amino acid residues of the different versions of NmU and NmS. A) NmU forms isolated from mammals, birds, amphibia and fish. B) NmS forms from mammals and amphibia. All NmU and NmS versions among species share the *C*-terminal amidation of asparagine (-$COONH_2$). The last five amino acid residues (F-R-P-R-N) are conserved between all NmU and NmS versions (highlighted in yellow) except for the goldfish. NmS from all species isolated to date share eleven amino acid residues at the *C*-terminus. Abbreviations: human (h), porcine (p), chicken (ck), rabbit (rb), dog (d), frog (f), tree frog (tf), goldfish (g), toad (t), guinea pig (gp), rat (r), mouse (m), bovine (b).

### 1.2.1 Structure-activity relationships of NmU and NmS

The structural constancy of NmU isoforms, at least within the *C*-terminal region among species suggests its importance for function (Brighton *et al.*, 2004a). Two key aspects within the NmU structure are highly conserved among species, including the *C*-terminal amidation of asparagine (N) and the last five amino acids at the *C*-terminus of the NmU peptides (F-R-P-R-N-$NH_2$) (Mitchell *et al.*, 2009). In the canine NmU-8 (sequence of $pE^1$ $F^2$ $L^3$ $F^4$ $R^5$ $P^6$ $R^7$ $N^8$ -$NH_2$ where pE is pyroglutamic acid), substitution of phenylalanine $F^2$ or $F^4$ with amino acids such as A, Y, W, T, E, H or cyclohexylalanine caused a reduction in smooth muscle contractility of chicken crop preparation, highlighting the importance of these residues for biological activity (Kurosawa *et al.*, 1996). Furthermore, substitution at positions 2, 4, 5, 6, 7 and 8 with either glycine or the corresponding D-form amino acids in pNmU-8 (H-$Y^1$ $F^2$ $L^3$ $F^4$ $R^5$ $P^6$ $R^7$ $N^8$-$NH_2$) reduced its ability to contract chicken crop smooth muscle (Hashimoto *et al.*, 1991). In rat NmU-23 ($Y^1$ $K^2$ $V^3$ $N^4$ $E^5$ $Y^6$ $Q^7$ $G^8$ $P^9$ $V^{10}$ $A^{11}$ $P^{12}$ $S^{13}$ $G^{14}$ $G^{15}$ $F^{16}$ $F^{17}$ $L^{18}$ $F^{19}$ $R^{20}$ $P^{21}$ $R^{22}$ $N^{23}$-$NH_2$) and structurally related analogues, the $F^{16}$ - $N^{23}$ fragment plays a major role in muscle contraction while segments from position 6 to 9 and 13 to 15 seem to be critical for the peptide potency in both, chicken crop smooth muscle and rat uterus contraction assays (Sakura *et al.*, 1991). The amide moiety bound to the carboxylic acid side chain of all NmU isoforms also plays a role in receptor activity. For instance, deletion of the amide group from pNmU-8 abolished activation of human and mouse receptors in recombinant systems and contraction of uterine smooth muscle (Minamino *et al.*, 1985; Sakura *et al.*, 1991; Funes *et al.*, 2002). In contrast to the highly conserved *C*-terminal region of NmU isoforms, the *N*-terminal region has a low level of homology. Evidence suggests that this region is crucial for potency and stability (Mitchell *et al.*, 2009). Using an isolated uterus contractility approach, previous research has established that rNmU-25 is three fold more potent than tNmU-17 which had a similar last eight amino acids to rNmU-25 but had a great variation in the *N*-terminus compared to other NmU peptides ($EC_{50}$: 0.5 nM and 1.6 nM for rNmU-25 and tNmU-17 respectively) (Lee *et al.*, 2005). Furthermore, in terms of the stability of peptide, *N*-terminal amino acids substitution is found to have a critical role in increasing the resistance of the peptide to the enzymatic degradation. For example, NmU with an *N*-terminal- modified side chain showed greater proteolytic resistance and longer half-life (Hashimoto *et al.*, 1995; Sakura *et al.*, 1995). Collectively, these studies outline a critical role for the *N*-terminus of NmU peptides in the determination of binding strength of NmU with its cognate receptors, and stability of the peptide.

Although coded by a separate gene, NmS shows strong similarity to NmU, having the same seven amino acid residues and an amidated asparagine at the *C*-terminus **(Figure 1.2)**. However, there are variations within the *N*-terminal region (Mori *et al.*, 2008) **(Figure 1.2)**. Furthermore, NmS is not a splice variant of the NmU and the genes for the two prepropeptides containing NmU or NmS localise to different chromosomes, namely 4q12 and 2q11.2 respectively (Mori *et al.*, 2005). Given the importance of both *C*- and *N*-terminal regions in the biological activity and peptide-receptor interaction, characterisation of NmU and the structurally-related NmS, particularly at the level of receptor signalling is of interest, in respect of possible pathophysiological and functional differences. Unfortunately, no information is available regarding interactions of either hNmU-25 or hNmS-33 with either receptor subtype.

### 1.2.2 Peripheral and central localisation of NmU and NmS

Several lines of evidence, particularly in human and rat, have shown that NmU is ubiquitously distributed through the body. In the rat, NmU-like immunoreactivity (NmU-LI) is found in considerable levels in the small intestinal tract, mainly in the duodenum and jejunum (Domin *et al.*, 1987; Augood *et al.*, 1988; Honzawa *et al.*, 1990; Austin *et al.*, 1994). It is also detected in the nerve cell bodies within the enteric nervous system (Ballesta *et al.*, 1988). Furthermore, levels of NmU-LI are detected within the genitourinary system such as ovaries, fallopian tubes, urethra, ureter, prostate and testis (Augood *et al.*, 1988; Ballesta *et al.*, 1988; Honzawa *et al.*, 1990). In human, northern blotting demonstrated significant levels of NmU mRNA expression in the gastric system which were much higher in the jejunum (Austin *et al.*, 1995). In the rat brain, high concentrations have been found in different regions, including the hypothalamus, striatum, medulla oblongata, anterior pituitary and cingulate gyrus (Domin *et al.*, 1987; Fujii *et al.*, 2000; Szekeres *et al.*, 2000). In Man, moderate concentrations have been detected in the medial frontal gyrus and cingulate gyrus as well as relatively low to moderate levels in the substantia nigra, medulla oblongata, thalamus, hypothalamus and locus coleus (Brighton *et al.*, 2004a; Mitchell *et al.*, 2009; Mori *et al.*, 2016). NmS may display more restricted localisation, particularly in the central nervous system. In the hypothalamus mRNA levels of NmS are detected. More specifically, high mRNA levels have been found in the suprachiasmatic nucleus (SCN) along with same expression within the hypothalamus, including the PVN, ARC and supraoptic nucleus (SON) (Mori

*et al.*, 2005). Peripherally, NmS expression is restricted to a small number of tissues such as testis and spleen (Gajjar *et al.*, 2017).

### 1.2.3 Physiology and pathology of the NmU and NmS

Since NmU and NmS were reported, they have attracted considerable interest given their association with a range of pathophysiological effects.

#### 1.2.3.1 NmU functions

##### 1.2.3.1.1 Smooth muscle contractility

The contraction of rat uterus smooth muscle led to initial identification of pNmU-25 and pNmU-8 (Minamino *et al.*, 1985). NmU has the ability to provoke the smooth muscle contraction in several tissues, particularly in the gastric and genitourinary systems. However, there are some differences among species in the ability to activate the smooth muscle contractility. For example, urinary bladder in rat, mouse, rabbit and guinea pig does not respond to NmU although it causes contraction of man and dog urinary bladder (Westfall *et al.*, 2002). NmU also contracts the human ascending colon (Jones *et al.*, 2006). Furthermore, knockout of NMU1 in mice inhibits smooth muscle contraction although knockout of NMU2 has not effect (Prendergast *et al.*, 2006; Dass *et al.*, 2007). However, in other systems such as genitourinary tract, smooth muscle contraction appears to be mediated by both receptors (Martinez *et al.*, 2015). Moreover, it has also been shown that NmU has a prokinetic effect in mouse colon and that is mediated by NMU1, thereby attracting attention as a useful pharmacological candidate for gastric motility disorders (Dass *et al.*, 2007).

##### 1.2.3.1.2 Eating and energy regulation

There is a growing body of literature highlighting that NmU is a crucial player in regulating aspects of feeding behaviour. The expression of the peptide with its receptors along the brain-gut axis, which is important in controlling feeding and energy expenditure, support this. Indeed, the direct intracerebroventricular (ICV) administration of NmU or its analogues cause anorexigenic effects through reducing eating and its related behaviours in various species (Howard *et al.*, 2000; Kojima *et al.*, 2000; Nakazato *et al.*, 2000; Niimi *et al.*, 2001; Ivanov *et al.*, 2002; Hanada *et al.*, 2003; Bechtold *et al.*, 2009; Egecioglu *et al.*, 2009; Peier *et al.*, 2009). In addition, the transgenic overexpression of NmU in mice results in a reduction in weight gain (Kowalski *et al.*, 2005). Conversely, it has been demonstrated that the central administration of NmU

antisera increased eating (Kojima *et al.*, 2000; Jethwa *et al.*, 2005). Furthermore, NmU levels are decreased in the ventromedial hypothalamus under fasting conditions (Howard *et al.*, 2000). Collectively, these studies outline a critical role for NmU in the central regulation of feeding that is consistent with its hypothalamic expression. The effects of NmU appear to not only influence feeding but also energy homeostasis. Indeed, ICV administration of NmU increases body temperature, heat production, oxygen consumption and locomotor activity highlighting its role in regulation of energy expenditure (Howard *et al.*, 2000; Nakazato *et al.*, 2000; Hanada *et al.*, 2001; Ivanov *et al.*, 2002; Wren *et al.*, 2002; Hanada *et al.*, 2003; Novak *et al.*, 2006). Much uncertainty still exists about the mechanisms that underpin the regulation of eating behaviour and energy expenditure by NmU although there are some suggestions. First, c-Fos, an indicator of neuronal activity, was found in an abundant levels in oxytocin-producing neurones of both the PVN and SON regions following stimulation with NmU (Niimi *et al.*, 2001). Additionally, administration of oxytocin suppressed eating, suggesting that the activation of these neurons mediate the suppressive effect of NmU on eating (Brighton *et al.*, 2004a; Martinez *et al.*, 2015). Second, there is an evidence that NmU might mediate its effects on feeding and energy homeostasis, at least partly via the corticotrophin-releasing hormone (CRH) axis. Indeed, the effects of administered NmU on eating end energy expenditure are lost in mice lacking CRH (Hanada *et al.*, 2003). Furthermore, the suppression of feeding and the mRNA levels of CRH induced by central administration of CRH were suppressed in NmU knockout mice (Morley *et al.*, 1982; Hanada *et al.*, 2004). Taken together, these studies support the notion that CRH might be a regulator of the NmU effects on feeding and energy homeostasis. Third, leptin, a hormone released from adipocytes and a crucial regulator of feeding, is also correlated with NmU. Indeed, leptin causes NmU release from hypothalamic explants (Wren *et al.*, 2002). It has also been demonstrated that the satiation-associated effects of leptin following intraperitoneal administration were suppressed following injection of anti-NmU antisera into satiated rat (Jethwa *et al.*, 2005). A likely explanation is that leptin might act as an upstream regulator of NmU. Conversely, administration of leptin reduced body mass, although knockout of NmU reduced this, suggesting that leptin might partially influence NmU functions (Hanada *et al.*, 2004; Jethwa *et al.*, 2005). Lastly, in addition to the direct effects of NmU on eating and energy expenditure when injected into the PVN and ARC of the hypothalamus, it also has a delaying action when administered to the medial preoptic (MPO) area of the hypothalamus which is involved in reproductive functions and

increases in NPY after eating (Wren *et al.*, 2002). Furthermore, some neuropeptides involved in the regulation of feeding are also affected after transgenic modification of NmU expression (knockout and overexpression). It has been reported that NmU-overexpression in mice increases both NPY and POMC mRNA expression although AGRP mRNA remained unchanged (Kowalski *et al.*, 2005). In contrast, mice lacking NmU showed a reduction in POMC mRNA levels despite no changes in that of NPY and AGRO (Hanada *et al.*, 2004). These studies clearly indicate that there is a relationship between NmU and feeding-regulated neuropeptides in regulating food intake and energy balance.

Several lines of evidence highlight an involvement of NmU receptors in mediating the effects of NmU on eating behaviour, particularly NMU2 which is now well known as a key player in controlling eating and body weight (Hosoya *et al.*, 2000; Howard *et al.*, 2000; Raddatz *et al.*, 2000; Shan *et al.*, 2000). For example, knockout of NMU2 in mice inhibits the effects of NmU on eating-associated aspects (Bechtold *et al.*, 2009; Peier *et al.*, 2009). Furthermore, knockout of NMU2 in the hypothalamic region increases seeking towards fat-enriched food and binge-related eating (Benzon *et al.*, 2014; McCue *et al.*, 2017).

As NmU plays a critical role in eating behaviour and energy expenditure this system might provide therapeutic opportunities for the treatment of obesity. Different molecules derived from NmU structure have been successfully developed, generally with higher potency and stability than NmU *in vivo* (Ingallinella *et al.*, 2012; Neuner *et al.*, 2014; Micewicz *et al.*, 2015; Kaisho *et al.*, 2017; Kanematsu-Yamaki *et al.*, 2017; Nagai *et al.*, 2018). However, it is unclear whether NmU is a suitable therapy in obese individuals as it has been reported that the chronic administration of NmU in rodents does not influence eating behaviour (Thompson *et al.*, 2004). Little is currently known about the regulation of signalling, particularly at the level of receptors, including desensitisation, resensitisation, and post-translation modifications that might need further characterisations to answer some questions that have been raised in this context.

#### 1.2.3.1.3 Influence on stress

NmU receptors are abundantly expressed in the PVN and have a critical role in the stress response through releasing CRH. CRH, in turn, induces release of adrenocorticotrophic hormone (ACTH) from anterior pituitary gland. Finally ACTH mediates the production

and secretion of cortisol from adrenal glands. Hence, the PVN is an essential regulator of the hypothalamus, pituitary and adrenal glands (Brighton *et al.*, 2004a; Gajjar *et al.*, 2017). It is now well established from a variety of studies performed in rats that ICV injection of NmU provokes a stress response (Kojima *et al.*, 2000; Hanada *et al.*, 2001; Wren *et al.*, 2002; Gartlon *et al.*, 2004; Zeng *et al.*, 2006). The increased plasma levels of ACTH, adrenaline and corticosterone hormones that are known to be induced by the stress response are also reported following either ICV or subcutaneous administration of NmU (Malendowicz *et al.*, 1993; Ozaki *et al.*, 2002; Sasaki *et al.*, 2008). Furthermore, it has been demonstrated that stress-associated behaviours mediated by NmU are blocked by pre-treatment with anti-CRH antibodies or CRH antagonists (Hanada *et al.*, 2001). Moreover, mice lacking CRH showed no locomotor activity following NmU administration (Hanada *et al.*, 2001). Apart from action in the hypothalamus, it has been found that NmU may have peripheral effects on the stress response. Thus, NmU caused the release of steroids from the adrenal cortex, which decreased following pre-incubation with CRH inhibitors (Malendowicz *et al.*, 1994b; Malendowicz *et al.*, 1994a). Collectively, these studies outline a critical role for NmU in the hypothalamo-pituitary adrenal axis.

#### 1.2.3.1.4 Influence on reproductive hormones

Several lines of evidence demonstrate the effects of NmU on female reproductive hormones. Indeed, ICV injection of rats with NmU increases plasma levels of oxytocin and vasopressin (Ozaki *et al.*, 2002; Quan *et al.*, 2003). In the interstitial cells of the ovary, challenge with NmU caused the activation of the extracellular signal-regulated kinase (ERK) pathway and progesterone release via the NMU2 receptor (Lin *et al.*, 2013). In contrast, treatment of rats with NmU inhibited both luteinising hormone (LH) and follicle-stimulating hormone (FSH) release from the pituitary gland (Fukue *et al.*, 2006). Furthermore, young mice lacking NmU showed both a high puberty index, which is determined by the LH : FSH ratio, and increased vaginal opening (Fukue *et al.*, 2006). Thus, NmU may play a role in delaying aspects of puberty by inhibition of the gonadotrophin hormones.

#### 1.2.3.1.5 Influence on insulin release

NmU mRNA is expressed in the pancreas (Fujii *et al.*, 2000; Hedrick *et al.*, 2000; Szekeres *et al.*, 2000). In addition, NmU receptors, particularly NMU1, has been demonstrated in pancreatic rat islets at both mRNA and protein levels, suggesting a

potential role of NmU in the regulation of insulin synthesis and/or release (Kaczmarek *et al.*, 2006). Indeed, a recent study showed NMU1 expression in isolated human pancreatic cells and that treatment with NmU inhibits insulin secretion from these cells (Alfa *et al.*, 2015). Furthermore, both NmU and NMU1 are expressed in mice pancreatic cells and NmU treatment inhibits insulin release *in vivo* and *in vitro*, thereby, providing further evidence for a role of NmU in glucose homeostasis (Zhang *et al.*, 2017).

#### 1.2.3.1.6 Cardiovascular effects

The circulatory system is also affected by NmU, which appears to have a pressor effect. Data from several sources have identified increased blood pressure following IV injection of NmU. These increases were not associated with changes in heart rate, implying local vasoconstriction (Minamino *et al.*, 1985; Sumi *et al.*, 1987; Gardiner *et al.*, 1990; Chu *et al.*, 2002; Westfall *et al.*, 2002). The elevation of blood pressure following the central administration of NmU is mediated by enhanced sympathetic activity (Tanida *et al.*, 2009; Rahman *et al.*, 2011; Rahman *et al.*, 2012; Rahman *et al.*, 2013). In individuals suffering from heart failure as result of cardiovascular complications such as ischemic heart diseases or dilated cardiomyopathy, high levels of NmU mRNA have been detected in the left ventricle, highlighting its role in cardiac hemodynamic regulation (Gajjar *et al.*, 2017). There has also been suggestion that the release of NmU from adipose tissues might lead to elevated blood pressure in obese patients but this needs to be confirmed (Martinez *et al.*, 2015).

#### 1.2.3.1.7 Bone mass formation

NmU appears to play a vital role in the regulation of bone formation. Apart from its contribution with NmU in regulation of feeding behaviour **(Section 1.2.3.1.2)**, Leptin, is considered a crucial regulator for bone mass remodelling by decreasing the bone formation, and this effect might correlate with the NmU effects. (Saper *et al.*, 2002; Hamrick *et al.*, 2004; Hamrick *et al.*, 2005; Cirmanova *et al.*, 2008). Indeed, mice lacking NmU have increased bone mass as a result of increased bone formation (Sato *et al.*, 2007). In addition, decreased bone mass was observed following treatment of wild-type mice with an NMU2 receptor agonist (Sato *et al.*, 2007). Furthermore, in NmU-deficient mice the inhibition of bone formation by leptin was reduced, suggesting that NmU might act as a downstream mediator of leptin and this effect of NmU appears to be mediated by CNS as revealed by cell-based assays (Sato *et al.*, 2007). Application of NmU to rat osteoblast-like cells induces proliferation through NMU2, highlighting a direct effect of

NmU on bone (Rucinski *et al.*, 2008). Recently, a study in European children identified an association between NmU gene polymorphisms and bone density, suggesting that the NmU system might also be a useful therapeutic target for the treatment of bone diseases (Gianfagna *et al.*, 2013).

#### 1.2.3.1.8 Pain

NmU is found within the spinal cord **(Section; 1.2.2)**, particularly in sensation-related sites, which suggests a role in pain-related behaviours. Indeed, the central administration of NmU increases nociception in both rat and mouse (Cao *et al.*, 2003; Yu *et al.*, 2003; Moriyama *et al.*, 2004). In NmU-knockout mice, a lowered pain is observed in heat plate and formalin tests compared to wild-type mice (Nakahara *et al.*, 2004a). NMU2 may play a particularly important role in such effects. Thus, mice lacking NMU2 showed a reduction in pain in response to painful stimuli or NmU treatment. In contrast, NMU1-dificient mice did not show any differences compared to wild-type mice in response to the painful stimuli (Zeng *et al.*, 2006; Torres *et al.*, 2007).

#### 1.2.3.1.9 Cancer

NmU expression levels tend to alter in different types of cancers. Studies have demonstrated that a lower NmU gene expression is seen in isolated cells of oesophageal squamous carcinoma; in agreement with reduced cell proliferation in this form of cancer after NmU administration (Alevizos *et al.*, 2001; Yamashita *et al.*, 2002). Such data suggest that NmU can act as a tumour suppressor. In other forms of cancers such as ovarian cancer (Euer *et al.*, 2005), acute myeloid leukaemia (Shetzline *et al.*, 2004) and urinary bladder cell carcinoma (Wu *et al.*, 2007), NmU mRNA is overexpressed. It has been reported in both human pancreatic cancer and canine cancers of peripheral nervous sheaths, NMU2 expression is increased, highlighting a potential role of NmU and NMU2 in the deterioration of these cancers (Ketterer *et al.*, 2009; Klopfleisch *et al.*, 2013). Furthermore, both NmU and NMU2 are co-localised in endometrial cancer cells and are associated with increasing the migration and proliferation of these cells by influencing the expression levels of adhesion molecules such as CD44 and integrin α 1, which are involved in the progression of endometrial tumours (Lin *et al.*, 2016). Compared to the healthy breast cells, breast carcinomas show an increase in the levels of NmU mRNA; this increase is an indicator for poor prognosis, particularly with breast cancer cells expressing high levels of NMU2, suggesting its role in the progression of certain tumours by NMU2-related effects (Garczyk *et al.*, 2017). These finding suggest that NmU has

paradoxical effects (tumour suppressor versus tumour inducer) and this system might be a future pharmacological target for these types of cancers.

#### 1.2.3.2 NmS functions

##### 1.2.3.2.1 Circadian clock

Restriction of NmS to SCN, a centre for biological clock regulation, suggests a vital role in circadian rhythm control (Mori *et al.*, 2008). It has been reported that ICV injection of NmS to rats induces phase shift in circadian control of locomotion which was stronger than that induced by NmU (Mori *et al.*, 2005). NmS mRNA is expressed at high levels within the SCN during daylight whilst these levels decreased during the night (Mori *et al.*, 2005). NmS expression was unchanged when rats were exposed to a long-term period of darkness, implying its importance in circadian regulation (Mori *et al.*, 2005). Moreover, it has been demonstrated the NmS-producing neurones in the SCN play a crucial role in the regulation of circadian rhythm behaviour by acting as pacemakers and influencing molecular clock neurones (Lee *et al.*, 2015). NMU2 is expressed in the SCN and thought to be responsible for the effects of NmS on circadian rhythm (Nakahara *et al.*, 2004b). Together, these studies provide important insights into the role of NmS and NmU and NMU2 in regulating the circadian clock, which is consistent with their influences on eating behaviour and energy homeostasis as it is a one of the potential aspects that links to the obesity through its controlling a network of transcription mechanisms that regulates a variety of vital processes ranging from glucose transport to gluconeogenesis, adipogenesis and lipolysis (Bray *et al.*, 2007; Kalsbeek *et al.*, 2007; Kohsaka *et al.*, 2007).

##### 1.2.3.2.2 Feeding

Food seeking was reduced in a concentration-dependent fashion following ICV administration of NmS in rats; this influence was greater with NmS than NmU (Ida *et al.*, 2005). Furthermore, central injection of NmS in mice supressed body weight and increased body temperature and locomotor activity (Peier *et al.*, 2009). Orexigenic effects of ghrelin, NPY and AGRP neuropeptides were also attenuated after administration of NmS (Mori *et al.*, 2008). The mRNA levels of anorexic peptides such as CRH and POMC and secretion of the α-MSH increased following ICV injection of either NmS or NmU, although NmS was more potent than NmU (Nakahara *et al.*, 2010). Data from several studies suggest that the central actions of NmS on food intake and energy expenditure are mediated particularly by NMU2 which is known to be predominant in the central nervous

system **(Section 1.3.2.2)**. Indeed, acute ICV injection of NmS in NMU2-deficient mice did not reduce food intake or produce an increase in temperature and locomotor activity that were seen in the wild-type mice (Nakahara *et al.*, 2010). Another study also showed that the effects of NmS on feeding and metabolic regulation were absent in mice lacking NMU2 (Bechtold *et al.*, 2009). On the other hand, knocking NMU2 out specifically in the PVN using viral-mediated RNAi caused an increase in eating and body weight in mice fed with a high-fat diet, whilst mice maintained under normal food remained unchanged (Benzon *et al.*, 2014). Furthermore, in female but not male, mice lacking NMU2 showed an increase in body weight, particularly when fed a fat-dense diet, providing a suggestion that sex might be critical in determining the role of NMU2 in regulating eating and energy homeostasis. (Egecioglu *et al.*, 2009). Together these studies indicate a role of NMU2 in mediating the effects of NmS on feeding and energy expenditure, with evidence linking NMU2 regulation to some critical factors such as diet preference and sex difference.

#### 1.2.3.2.3 Urinary output

Plasma levels of the anti-diuretic hormone, vasopressin increased in response to ICV injection of NmS and this was associated with a lower production of urine (Sakamoto *et al.*, 2007). Vasopressin is produced and released in the SON and PVN where NMU2 is expressed. Indeed, ICV administration of NmS resulted in an increase in the level of c-Fos expression in these regions, suggesting its anti-diuretic effect might be through the modulation of release of vasopressin from the PVN and SON (Sakamoto *et al.*, 2007).

#### 1.2.3.2.4 NmS and reproductive hormones

It is now well established that ICV injection of NmS increases c-Fos expression in both the PVN and SON (Ida *et al.*, 2005; Mori *et al.*, 2005). Furthermore, immunostaining showed increased levels of c-Fos in oxytocin-producing neurones following NmS administration (Sakamoto *et al.*, 2008). Moreover, NMU2 is expressed in oxytocin-producing neurones, providing a suggestion that NmS might have a role in oxytocin release (Qiu *et al.*, 2005). Indeed, central administration of NmS in rats mediated oxytocin release from these regions and elevated milk secretion (Sakamoto *et al.*, 2008). NmS expression levels in female adult also change during the oestrus cycle, for example, increasing in the proestrus phase (Gajjar *et al.*, 2017). ICV injection of NmS induced the release of the LH in the oestrus phase with evidence of moderate increases in the

metestrus phase (Mori *et al.*, 2008). Collectively, these studies outline a critical role for NmS in female gonadotrophic axis.

## 1.3 Receptors for NmU and NmS

Two receptors termed NMU1 and NMU2 are originally identified as receptors for NmU and NmS. These receptors were named FM3 (known as NMU1) and FM4 (known as NMU2) before discovery and deorphanisation. NMU1 is localised within human chromosome 2q37.1 whilst NMU2 is at 5q33.1 (Fujii *et al.*, 2000; Hedrick *et al.*, 2000; Hosoya *et al.*, 2000; Howard *et al.*, 2000; Raddatz *et al.*, 2000; Shan *et al.*, 2000; Szekeres *et al.*, 2000). NMU1 was cloned from a murine T-lymphocyte complementary DNA (cDNA) and human cDNA libraries as a result of some similarity to the ghrelin receptor and neurotensin receptor which are respectively 33 % and 29 % of homologous (Tan *et al.*, 1998). Based on the NMU1 sequence, NMU2 was subsequently identified and purified from a variety of species including human, mouse and rat (Tan *et al.*, 1998; Hosoya *et al.*, 2000; Howard *et al.*, 2000; Raddatz *et al.*, 2000; Shan *et al.*, 2000; Funes *et al.*, 2002). NMU1 and NMU2 have some sequence homology (45 - 50 %) with some homology to other receptors such as the growth hormone receptor and motilin receptor (~ 30 % homology) in addition to the ghrelin and neurotensin receptors highlighted above (Brighton *et al.*, 2004a). With respect to the potential initiation codon of translation of both receptors, two potential methionines are found at the beginning of *N*-terminus generating putative short or long versions of the receptors with evidence suggests that the shorter one might be more recognisable by Kozak sequence which is a sequence promoting translation process (Brighton *et al.*, 2004a). Recombinant expression of NMU1 or NMU2 was used to screen different putative ligands using multiple functional assays. This led to identification of NmU as a natural ligand for both receptors (Mitchell *et al.*, 2009).

### 1.3.1 Main structural features of NMU1 and NMU2

Both receptors have characteristic features of Family A GPCRs **(Figure 1.3)**. For example, NMUs have a well-conserved ERY pattern in their sequence which is a conserved E/DRY motif among the members of Family A (Audet *et al.*, 2012). Specifically this motif is located between the third transmembrane domain and beginning of the second intracellular loop and plays critical role in maintaining the inactive state of the receptor, ligand binding and G-protein activation (Rasmussen *et al.*, 2011; Audet *et al.*, 2012; Gyombolai *et al.*, 2015; Di Pizio *et al.*, 2016). Another structural element

similar to other members of Family A is found in the 6$^{th}$ transmembrane domain of both NMUs; this motif is a WCxP pattern (where x is any amino acid) and seems to be an essential component for GPCR activation (Trzaskowski *et al.*, 2012; Topiol *et al.*, 2015). Two cysteine amino acids forming a disulphide bridge in the majority of Family A receptors are located in the second extracellular loop and above the third transmembrane domain of both receptors **(Figure 1.3)**. This disulphide bridge is thought to have a role in maintaining a stable conformation in response to ligand binding (Zhou *et al.*, 2000; Wheatley *et al.*, 2012). In the *N*-terminal region of NMUs, there are two potential *N*-linked asparagine glycosylation sites. NMU2 also has a potential glycosylation site in the second extracellular loop. These glycosylation sites are likely to be critical in stabilising the second extracellular loop or providing a space for ligand binding by shifting away of the direction of the loop (Wheatley *et al.*, 2012). Serine, threonine and tyrosine sites in the intracellular domains and *C*-terminal of both receptors provide potential sites for receptor phosphorylation by kinases, including the second messenger kinases (protein kinase A (PKA) or protein kinase C (PKC); and G-protein receptors kinases (GRKs) (Brighton *et al.*, 2004a). Although there are consensus sites on NMUs for second messenger kinases within the *C*-terminal and intracellular loops, GRKs consensus sites are lacked (Brighton *et al.*, 2004a). To date, it is unknown if NMU1 and NMU2 are phosphorylated in response to agonist occupation which is relevant to the regulation of cell signalling by these receptors (Tobin, 2008).

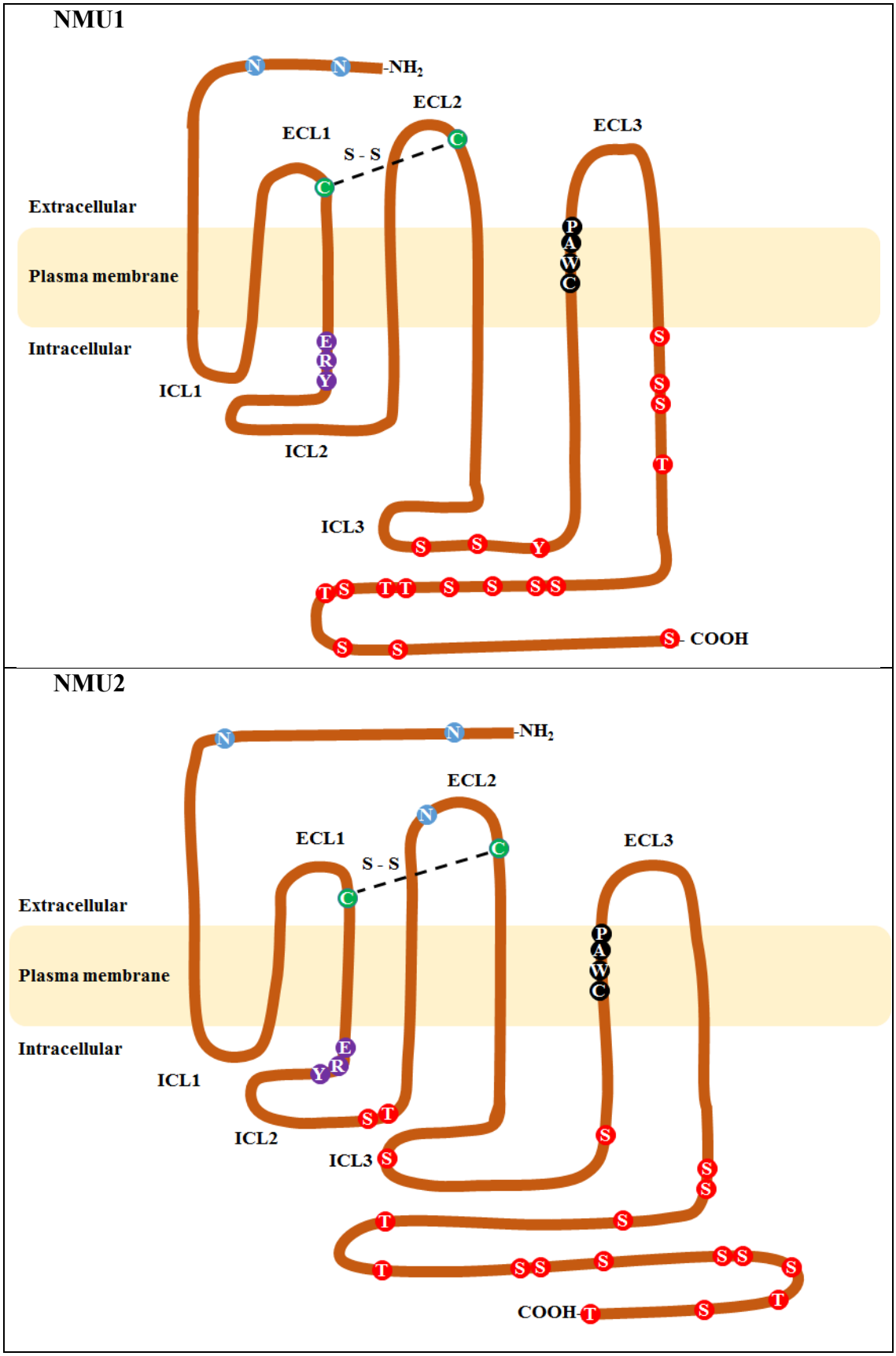


**Figure 1.3 Schematic diagram showing the main structural charactersitics of NMU1 and NMU2 sequences**

The putative seven transmembrane helices of NMU1 and NMU2 are generated by HMMTOP software (Tusnady *et al.*, 2001). The main motifs similar to Family A GPCRs are highlighted, namely the E/DRY (indicated in purple) and CWxP (indicated in black) motifs. Two potential *N*-linked asparagine glycosylation for NMU1 and three for NMU2 are highlighted in blue (N). Two cysteine residues forming a disulphide bridge (s-s) are indicated in green (c). Potential serine (S), threonine (T) and tyrosine (Y) sites of both receptors highlighted in red are located in the *C*-terminal and ICL3 of both NMU1 and NMU2 in addition to ICL2 of NMU2. Abbreviations: ECL (extracellular loop), ICL (intracellular loop).

### 1.3.2 NMU1 and NMU2 distribution

The issue of NMU1 and NMU2 tissue localisation has been controversial. Divergent methods, including dot blotting, Northern blotting, PCR and *in-situ* hybridisation have demonstrated different findings in a range of species. To date there has been general agreement that NMU1 is peripherally located, whereas NMU2 is restricted to the central nervous system (Brighton *et al.*, 2004a; Mitchell *et al.*, 2009; Martinez *et al.*, 2015; Smith *et al.*, 2019). Although distribution has been examined across a range of mammalian and non-mammalian species that this will focus on example of mammalian species.

#### 1.3.2.1 Peripheral and central localisation of NMU1

In man, NMU1 expression is detected in high levels in the periphery, mainly in the small intestine and stomach but it has also been found in other tissues including adrenal cortex, bone marrow, trachea, lung, pancreas, mammary gland, heart and blood cells, particularly T-lymphocyte and natural killer cells (Hedrick *et al.*, 2000; Howard *et al.*, 2000; Raddatz *et al.*, 2000; Szekeres *et al.*, 2000; Westfall *et al.*, 2002). In rat, moderate to high concentrations have been found in jejunum, ileum, duodenum, spleen, lung, caecum, colon and rectum (Gartlon *et al.*, 2004; Hsu *et al.*, 2007). NMU1 mRNA levels are found at high levels in the gastrointestinal tract, heart, skin, lung and testes of chicken (Wan *et al.*, 2018).

Centrally, undetectable copies of NMU1 mRNA have been found in the central nervous system in both human and rat although low mRNA levels were detected in amygdala (Gartlon *et al.*, 2004). In chicken, although the levels of NMU1 mRNA were weak in cerebellum, midbrain, and hindbrain, moderate levels have been detected in the hypothalamus (Wan *et al.*, 2018). Furthermore, low levels of NMU1 expression have also been found in the tissues of pig including cerebral cortex cerebellum and spinal cord (Li *et al.*, 2017b). All of the studies reviewed here support the view that NMU1 is predominantly distributed in the periphery.

#### 1.3.2.2 Peripheral and central localisation of NMU2

In human, NMU2 has been reported in the periphery with high mRNA levels detected in the testis whilst low to moderate levels have also been found in thymus, spleen, trachea, lung, thyroid gland, pancreas, adrenal gland, liver and gastrointestinal tract (Hosoya *et al.*, 2000; Raddatz *et al.*, 2000; Shan *et al.*, 2000; Westfall *et al.*, 2002). In the rat, different peripheral regions have been screened with moderate to high NMU2 levels

detected in uterus and ovaries (Fujii *et al.*, 2000; Hosoya *et al.*, 2000; Gartlon *et al.*, 2004). Furthermore, low NMU2 mRNA levels were seen in small intestine, large intestine, stomach, lung, thymus, salivary gland, bladder and testis (Fujii *et al.*, 2000; Hosoya *et al.*, 2000; Mitchell *et al.*, 2009). In the chicken, a range of peripheral regions has been tested for NMU2 existence. However, NMU2 mRNA levels were appeared in limited regions in the periphery such as muscle, skin and subcutaneous fat (Wan *et al.*, 2018). In pig, high NMU2 mRNA levels were found in the testis and pancreas with moderate levels detected in the lungs, heart, adrenal gland, ovaries, stomach, kidney and spleen although low levels were also seen in the colon and thyroid gland (Yang *et al.*, 2012; Li *et al.*, 2017b).

Several lines of evidence however suggest that NMU2 is predominantly localised in the central nervous system. In human NMU2 expression is restricted in regions of the brain and spinal cord such as, cerebral cortex, hippocampus, hypothalamus and medulla oblongata, with low levels detected in amygdala, cerebellum and dorsal root ganglia (Howard *et al.*, 2000; Raddatz *et al.*, 2000; Shan *et al.*, 2000). In rat, high levels of NMU2 expression were found in the hypothalamus, particularly in the PVN, ependymal layer of the third ventricle, ARC, SCN and hippocampus (Howard *et al.*, 2000; Guan *et al.*, 2001; Graham *et al.*, 2003; Nakahara *et al.*, 2004b). It has also been reported that NMU2 is expressed in the nucleus accumbens and ventral tegmental area in the rat brain (Kasper *et al.*, 2018; Smith *et al.*, 2019). The spinal cord, hypothalamus, cerebral cortex, midbrain and medulla oblongata demonstrated considerable mRNA levels of NMU2 in the pig (Yang *et al.*, 2012; Li *et al.*, 2017b). In chicken, high levels of NMU2 mRNA were observed in hypothalamus with evidence showing low levels in cerebellum, midbrain, hindbrain (Wan *et al.*, 2018). Collectively, these studies highlight the central distribution of receptors which was coincided with the distribution of cognate ligands (NmU and NmS) and the reported key role in CNS functions such as feeding behaviour and energy expenditure.

## 1.4 Cell signalling through GPCRs

### 1.4.1 Introduction to GPCR structure and families

NmU and structurally-related NmS are endogenous ligands that mediate their actions via two receptors, NMU1 and NMU2. These receptors are classified within the members of Family A belonging to GPCRs superfamily and play important roles in range of pathophysiological events **(Section 1.2.3)**. In particular, these receptors and potentially particularly NMU2 present possible targets for the treatment of obesity **(Section 1.1.2)**. Therefore, an understanding of the activation, signalling and regulation of these receptors is of particular interest.

GPCRs are membrane-associated proteins that comprise a huge superfamily of receptors in mammalian cells and account for approximately 800 genes within the human genome (Lander *et al.*, 2001; Venter *et al.*, 2001; Gurevich *et al.*, 2018a). In addition to regulating many physiological processes, they are important pharmacological targets as they represent targets of a large proportion of approved medications (Santos *et al.*, 2017; Sriram *et al.*, 2018). Currently, about 35 % of therapeutically-used drugs interact with these receptors. (Diaz *et al.*, 2018; Sriram *et al.*, 2018; Islam *et al.*, 2019). Despite more than 800 GPCRs, only a relatively small proportion are targeted; this leaves many potential targets including ~ 100 orphan GPCRs for which the endogenous ligands have yet to be identified (Islam *et al.*, 2019).

Within the mammalian GPCRs superfamily there are three main families, having seven helical domains with variations in length and function, particularly the *N*-terminus, extracellular loops, intracellular loops and *C*-terminal side chain (Gurevich *et al.*, 2018a). These families are designated as A, B, and C **(Figure 1.4)** (Pierce *et al.*, 2002). Family A represents the largest with 672 members including adrenergic receptors, angiotensin receptors, histamine receptors opioid receptors, opsin receptors and olfactory receptors (Millar *et al.*, 2010; Erlandson *et al.*, 2018). The first receptor was crystallised allowing its structure to be determined by X-ray crystallography was rhodopsin (Palczewski *et al.*, 2000), followed more recently by others including beta 1, beta 2 adrenergic receptors, histamine receptor (H1) and muscarinic receptors (M2 and M3subtype) (Rasmussen *et al.*, 2011; Shimamura *et al.*, 2011; Kruse *et al.*, 2012; Miller-Gallacher *et al.*, 2014; Weichert *et al.*, 2014). The main structural features of this family were explained in **Section 1.3.1**. Family B comprises ~ 25 receptors that are targets for hormones, including growth hormone releasing hormone, glucagon, secretin, vasoactive intestinal peptide

parathyroid hormone and calcitonin and characterises by intermediate *N*-terminal domain length which is a binding site for ligand (Pierce *et al.*, 2002). The smallest number of GPCRs is classified within the Family C, including gamma aminobutyric acid receptors, calcium-sensitive receptors and metabotropic glutamate receptors (Pierce *et al.*, 2002). These members are characterised by having a large *N*-terminal side chain with Venus fly trap like structure (Muto *et al.*, 2007).

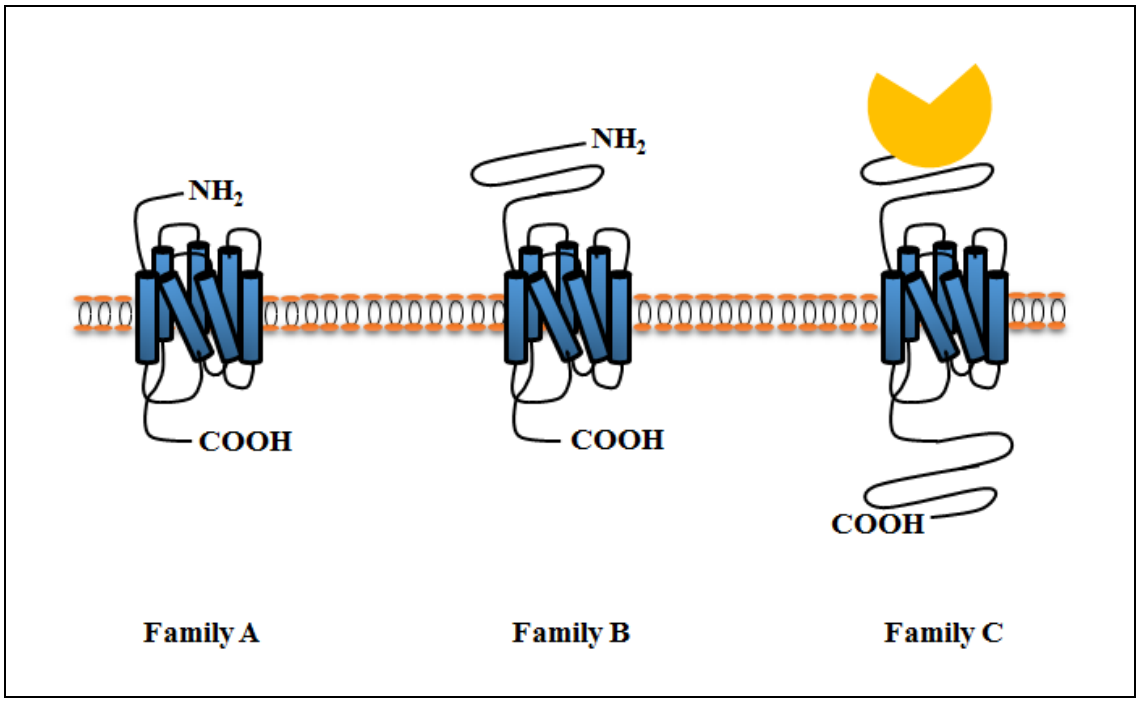


**Figure 1.4 Three major families of GPCRs**

Three GPCRs families grouped based on sequence similarity and extracellular *N*-terminal domain length. Family A GPCRs represent the largest with a relatively short *N*-terminal domain. Family B GPCRs are smaller in number than Family A GPCRs but have *N*-terminal domain longer than Family A GPCRs. Family C GPCRs have a unique *N*-terminal domain like Venus fly trap.

### 1.4.2 GPCR activation and intracellular signalling

#### 1.4.2.1 GPCR signalling via heterotrimeric G-proteins

Classically, GPCRs mediate their actions by activation of heterotrimeric G-proteins, although other mechanism including intracellular signalling mediated by arrestins has also been established **(Section 1.4.2.4.1)** (New *et al.*, 2007; Wang *et al.*, 2018). These heterotrimeric G-proteins comprise three subunits, α, β and γ in which the α subunit is responsible for the binding of guanosine diphosphate (GDP) and guanosine triphosphate (GTP) and the β and γ subunits act as a one unit (βγ dimer) (Hamm, 1998; Pierce *et al.*, 2002). Extracellular ligands such as neuropeptides, neurotransmitters and hormones exert their influence via binding to seven transmembrane receptors on the cell surface. Ligand binding, in turn, causes conformational changes in the receptor culminating in the coupling and activation of G-proteins. More specifically, under resting condition (basal state), GDP is associated with the G-protein α subunit (Gα) which together with β and γ subunits form an inactive complex at the plasma membrane (Wong, 2003). Ligand binding causes conformational change in receptor and this facilitates G-protein binding that then drives GDP dissociation. GDP is then replaced by cellular GTP on the Gα subunit followed by the release of GTP-bound Gα subunit from the βγ dimer. Both the GTP-bound Gα subunit and released βγ dimer are then free to activate various effectors (Cabrera-Vera *et al.*, 2003; Syrovatkina *et al.*, 2016). The GTP is subsequently hydrolysed to GDP via the intrinsic activity GTPase of the Gα subunit. This leads to reassembly of the heterotrimeric G-proteins and termination of G-protein signalling (De Vries *et al.*, 2000; Ross *et al.*, 2000). The intrinsic GTPase activity is enhanced by a family of proteins named regulators of G-protein signalling (RGS) **(Figure 1.5)**.

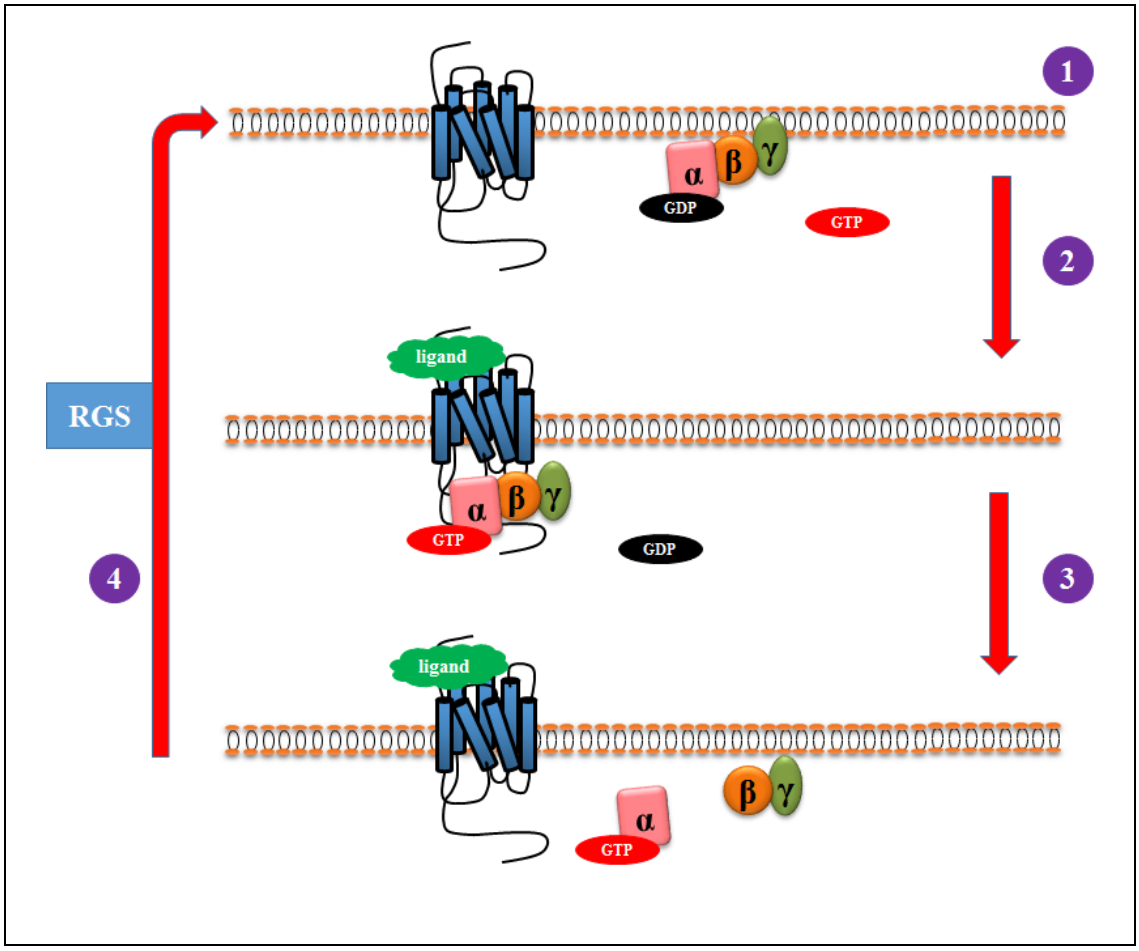


**Figure 1.5 Ligand-induced G-protein activation**

The scheme shows the activation and termination of G-protein signalling. 1) Under the basal state, heterotrimeric G-proteins (α, β and γ subunits) are attached at the cell surface membrane by lipid anchor. 2) Ligand binding causes association of the receptor and G-protein and exchange of GDP for GTP on the Gα subunit. 3) The GTP-linked Gα subunit and βγ dimer are released to interact with various downstream signalling pathways. 4) Signal termination occurs through GTP hydrolysis to GDP by the intrinsic GTPase activity of the Gα subunit, which leads to re-association of the heterotrimeric G-protein in preparation for another round of signalling.

GPCRs can couple to G-proteins belonging to four families of Gα subunits. These include $G\alpha_q$ which comprises five members ($G\alpha_q$, $G\alpha_{11}$, $G\alpha_{14}$, $G\alpha_{15}$ and $G\alpha_{16}$), $G\alpha_s$ has two members ($G\alpha_s$ and $G\alpha_{olf}$), $G\alpha_i$ includes nine members ($G\alpha_{i1}$, $G\alpha_{i2}$, $G\alpha_{i3}$, $G\alpha_{oA}$, $G\alpha_{oB}$, $G\alpha_{t1}$, $G\alpha_{t2}$, $G\alpha_g$ and $G\alpha_z$) and $G\alpha_{12}$ consists of two members ($G\alpha_{12}$ and $G\alpha_{13}$) (Syrovatkina *et al.*, 2016). β and γ subunits are encoded by five and twelve genes respectively. The various forms are differently distributed in the body and share the same general biochemical activities (Syrovatkina *et al.*, 2016). The Gα subunit has two main domains which are GTPase and α-helical domains (Sprang *et al.*, 2007). In the core of Gα subunit, between the GTPase and α-helical domains, there is a deep pocket that is responsible for GDP or GTP binding (Syrovatkina *et al.*, 2016).

The activation of $G\alpha_q$ members leads to activation of phospholipase C (PLC) which hydrolyses phosphatidylinositol 4,5-bisphosphate ($PIP_2$) to 1,4,5-inositol triphosphate ($IP_3$) and diacylglycerol (DAG). $IP_3$, in turn, binds to $IP_3$ receptors, thereby releasing $Ca^{2+}$ from the endoplasmic reticulum (ER) and activating protein kinase C (PKC) via DAG (Werry *et al.*, 2003). $G\alpha_s$ stimulation causes adenylyl cyclase (AC) activation, resulting in cyclic adenosine 3,5-monophosphate (cAMP) synthesis from adenosine triphosphate (ATP). Increased intracellular cAMP concentration activates protein kinase A (PKA), exchange protein activated by cAMP (Epac) and regulates cyclic nucleotide-gated ion channels (Wettschureck *et al.*, 2005). Binding to $G\alpha_i$ subtypes, inhibits AC leading to lower cAMP levels (Milligan *et al.*, 2006). $G\alpha_{12/13}$ activated by GPCRs causes redistribution of GTPases such as p115RhoGEF from cytosol to the membrane resulting in activation of guanine nucleotide exchange factor (GEF). This is in turn, mediating GDP/GTP replacement (Fukuhara *et al.*, 2001; Dutt *et al.*, 2004). GTPases such as Rho that are regulated by $G\alpha_{12/13}$-binding GPCRs play important physiological roles in, for example, angiogenesis, proliferation and cell migration (Heasman *et al.*, 2008) **(Figure 1.6)**.

Apart from the Gα subunits, Gβγ dimer plays critical roles in mediating the activation of a variety of downstream proteins such as PLC, AC, voltage-gated $Ca^{2+}$ channel and inwardly rectifying $K^+$ channel. This βγ-mediated signalling is primarily initiated by the largest and ubiquitously distributed $G\alpha_i$ family (Khan *et al.*, 2013; Syrovatkina *et al.*, 2016).

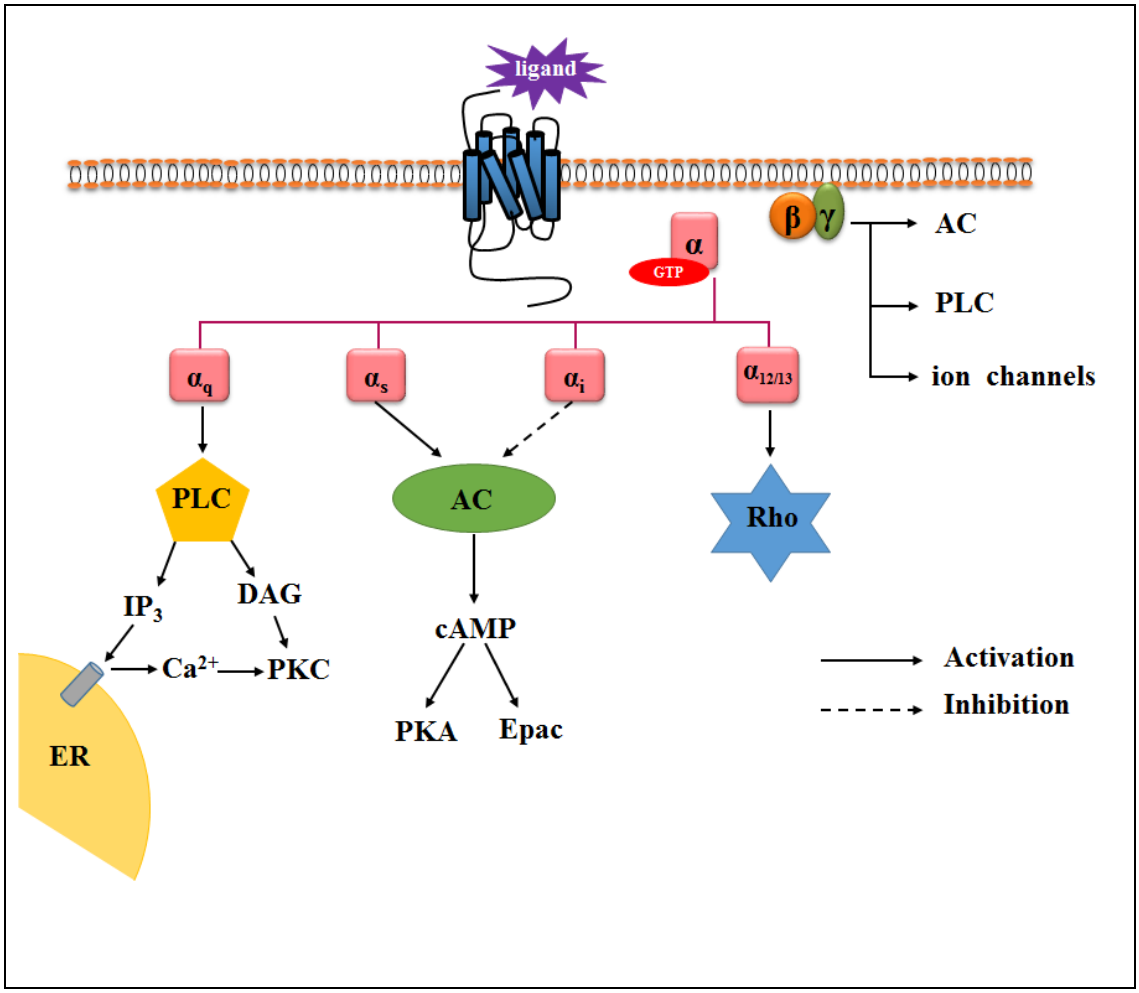


**Figure 1.6 GPCR signalling through Gα and Gβγ subunits**

The scheme shows that ligand binding to the receptor leads to association of G-proteins with the receptor and subsequent G-protein activation. Following activation, the GTP-bound Gα subunit and the βγ dimer dissociates and signal to a variety of effectors. $G\alpha_q$ subtypes stimulate PLC and generate the $IP_3$ and DAG. $G\alpha_s$ activation stimulates AC mediating conversion of ATP to cAMP which then activates PKA and Epac and regulates a variety of ion channels. In contrast, $G\alpha_i$ subunit inhibits AC, thereby inhibiting cAMP production. $G\alpha_{12/13}$ mediates Rho activation. Gβγ dimer (primarily from $G\alpha_i$ subunit) mediates activation of a variety of downstream effectors. Abbreviations are within the text.

#### 1.4.2.2 GPCRs induce the signalling pathways of the mitogen-activated protein kinases (MAPKs)

GPCR activation is also often associated with activation of MAPK cascades (Goldsmith *et al.*, 2007). In mammals, there are four cascades including extracellular signal-regulated kinases 1 and 2 (ERK1 and ERK2), c-JUN *N*-terminal kinase (JNKs) or stress-activated protein kinases (SAPKs), P38 kinases and ERK5 (Plotnikov *et al.*, 2011). Each cascade contains three different kinases starting from upstream to downstream that are responsible for a signalling cascade **(Figure 1.7)**. These include MAPKKK, MAPKK and MAPK. The signal, which is mediated by a receptor induces phosphorylation of upstream MAPKKK. The phosphorylated MAPKKK triggers phosphorylation of MAPKK and this kinase phosphorylates the downstream MAPK which translocate to nucleus resulting in activation of several transcription molecules (Sarma *et al.*, 2012). When signals are initiated, they are amplified by sequential phosphorylation and activation of these kinases that ultimately lead to phosphorylation of a variety of regulatory target proteins by the downstream kinases (ie. The MAPKs) (Goldsmith *et al.*, 2007). A variety of GPCRs activate MAPK signalling cascades via G-proteins and play critical roles in modulating a myriad range of regulatory gene responses, thereby control many cellular activities such as proliferation, differentiation, migration, growth, stress responses and apoptosis (Gutkind, 2000; Kranenburg *et al.*, 2001; Werry *et al.*, 2005). The first cascade is the ERK1 and ERK2 family, representing the prototype of the MAPKs, which play critical roles in a variety of signalling mediated by many GPCRs (Seger *et al.*, 1995a). In their simplest form, the signals mediated by such receptors transduce to the GTPase, termed Ras which is, in turn, activated at the cell surface by guanine nucleotide exchange factor and adaptor protein GRB2 (growth factor receptor bound protein 2) resulting in attraction of components of upstream MAPKKK, particularly Raf-1 and B-Raf thereby leading to recruitment and activation of these kinases (Plotnikov *et al.*, 2011). The signals are then transmitted to the second components of the cascade which is a MAPKK in the form of MEK1 or MEK2 (MEK1/2) by serine phosphorylation followed by activation of ERK1 and ERK2 (Seger *et al.*, 1995b; Shaul *et al.*, 2009). Thereafter, ERK1/2 phosphorylates and activates a variety of intracellular substrates, thereby promoting ERK1/2-dependent cellular responses such as proliferation, differentiation, survival and apoptosis (Yoon *et al.*, 2006) **(Figure 1.7)**.

Different stimuli including stress and many GPCRs are also able to activate P38 (Goldsmith *et al.*, 2007; Coulthard *et al.*, 2009). Stimulation of the P38 cascade by either GPCRs or stress mediates signal transduction to the small adaptor proteins GTPases (the MAPKKK component) which then phosphorylate and activate the second level of the cascade including MKK3 and MKK6. These MAPKKs activate and phosphorylate different forms of P38 (α, β, γ, and δ) (Plotnikov *et al.*, 2011) **(Figure 1.7)**. Ultimately, P38 targets and regulates a variety of cellular responses relating to this signalling cascade.

JNK, is a recognised regulator of a variety of intracellular and extracellular stress responses (hence named the SAPKs) (Davis, 1994). The activation of JNK pathway can be also mediated by GPCR signalling (Gutkind, 2000; Goldsmith *et al.*, 2007). Following GPCR activation, the signal is transmitted to the first level of the cascade (MAPKKK) by GTPases of the Rho family such as Rac1 and CDC42. This results in phosphorylation and activation of the kinases. The activated kinases at the MAPKKK level also activate the MAPKKs such as MKK4 and MKK7 by phosphorylation of their serine and threonine residues (Wang *et al.*, 2007). Activation of JNK by MAPKK phosphorylation plays a critical role in phosphorylating and activating a variety of subcellular molecules that target the transcription of various genes that regulate a variety of cellular processes including inflammation, apoptosis, cytokine production and metabolism (Dhanasekaran *et al.*, 2008; Huang *et al.*, 2009; Rincon *et al.*, 2009; Plotnikov *et al.*, 2011) **(Figure 1.7)**.

ERK5 is activated by a variety of stimuli in addition to GPCRs (Nishimoto *et al.*, 2006; Wang *et al.*, 2006; Goldsmith *et al.*, 2007). Stimulation of this cascade mediates phosphorylation and activation of MAPKKKs including MEKK2 and MEKK3, which leads to activation of MEK5 by phosphorylation of serine and threonine residues (Chao *et al.*, 1999; Plotnikov *et al.*, 2011). Thereafter, ERK5 phosphorylates and activates a variety of cytoplasmic and nuclear signalling proteins thereby playing important roles in regulating many pathophysiological process. However, much less is known about its functions compared to other MAPKs and might involve arrange of diseases (Plotnikov *et al.*, 2011).

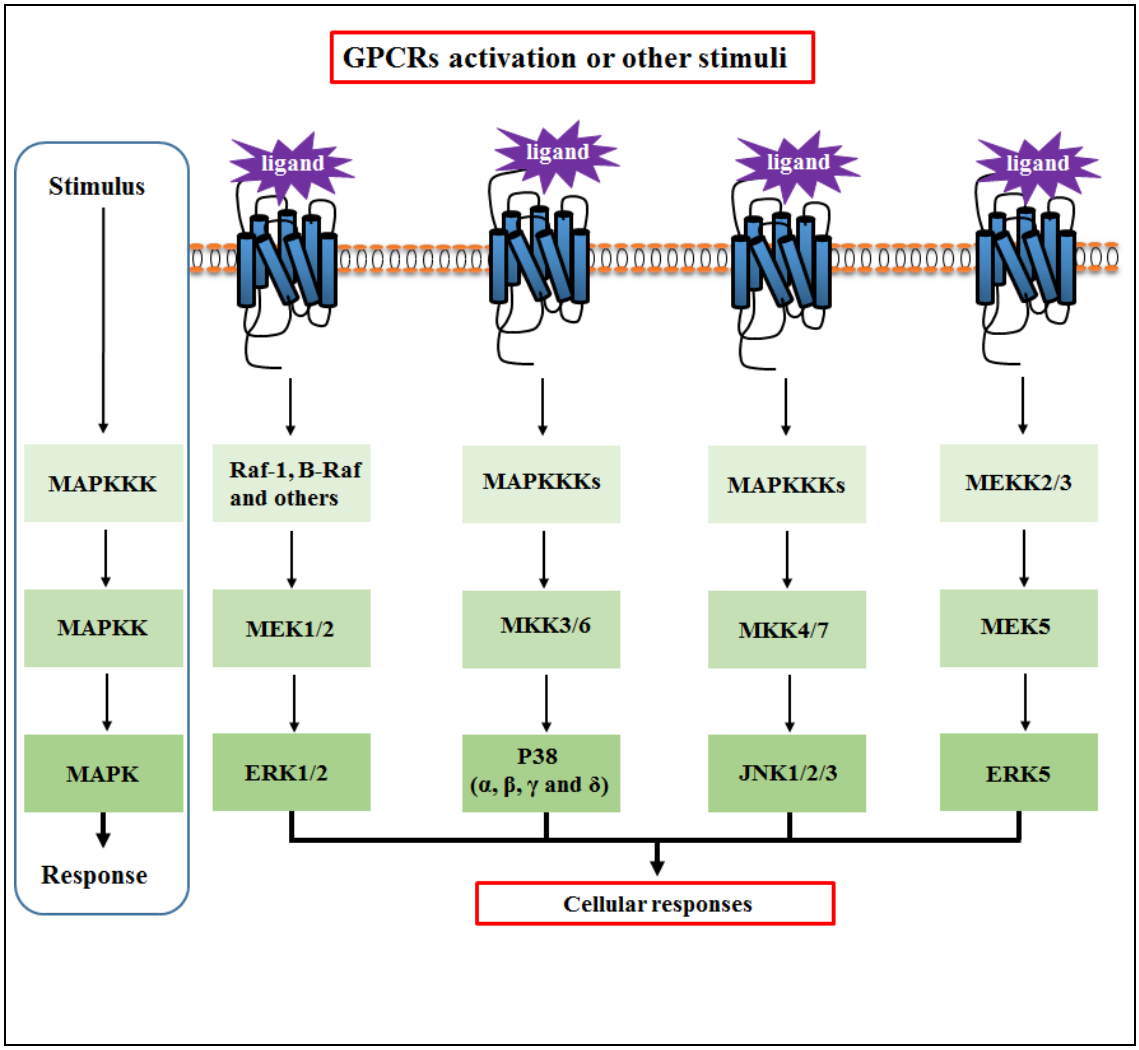


**Figure 1.7 MAPK signalling cascades**

The scheme shows the sequential activation of each MAPK cascade. The kinases of each component in the cascade can phosphorylate and activate other kinases in the next level of the cascade resulting in a variety of pathophysiological responses.

### 1.4.2.3 NMU1 and NMU2 signalling pathways

Intracellular signalling pathways in response to NMU1 and NMU2 activation have been studied predominantly in recombinant systems. Upon agonist activation, NMU1 and NMU2 increase phospholipase activity and increase intracellular $Ca^{2+}$ concentrations (Fujii *et al.*, 2000; Hedrick *et al.*, 2000; Hosoya *et al.*, 2000; Howard *et al.*, 2000; Kojima *et al.*, 2000; Raddatz *et al.*, 2000; Szekeres *et al.*, 2000; Funes *et al.*, 2002; Micewicz *et al.*, 2015; Alhosaini *et al.*, 2018). $Ca^{2+}$ responses are insensitive to pertussis toxin (PTX), which inhibits activation of $G\alpha_i$, highlighting coupling to $G\alpha_q$ (Brighton *et al.*, 2004b).

Activation of either NMU1 or NMU2 with NmU also results in ERK1/2 activation which was unchanged by PTX, again highlighting a likely contribution of $G\alpha_q$ (Brighton *et al.*, 2004b). Furthermore, hNmU-25 and hNmS-33 are able to activate both ERK1/2 and P38 in HEK-293 cells expressing NMU2 (Alhosaini *et al.*, 2018). Whether such signalling G-protein-dependent signalling or G-protein-independent requires further study.

Activation of both NMU1 and NMU2 have been shown to attenuate forskolin-induced cAMP accumulation (Aiyar *et al.*, 2004; Brighton *et al.*, 2004b). Furthermore, pre-treatment with PTX reduced the inhibitory effect of NmU on the forskolin-mediated cAMP increase (Brighton *et al.*, 2004b). Moreover, activation of recombinant human NMU2 inhibited isoproterenol-mediated increases in cAMP in HEK-293 with stable expression of NMU2 in PTX-sensitive manner (Sampson *et al.*, 2018). Considering all of these studies, it seems that both receptors are at least in recombinant systems, able to couple to $G\alpha_i$.

### 1.4.2.4 Regulation of GPCR signalling

#### 1.4.2.4.1 Receptor phosphorylation and desensitisation

GPCRs play critical roles in controlling a variety of cellular functions by transducing and regulating the signalling arising from a myriad of extracellular stimuli (Rajagopal *et al.*, 2018). However, when such signalling remains active (overstimulation), it has the potential to be harmful and can result in, for example, abnormal cell function and growth. Therefore, in a healthy cell, signalling by agonist binding to the receptor is generally controlled by a variety of pathways to reduce excessive signalling in a process termed desensitisation (Pierce *et al.*, 2002). Upon agonist activation, the receptor undergoes conformational changes leading to receptor phosphorylation by serine/threonine residues, particularly in the *C*-terminal tail and intracellular loops (Luttrell, 2008). Receptor phosphorylation is an important regulator to prevent the excessive stimulation of the persistent ligand-bound receptor or repeated challenge as desensitisation can be blocked by removal of phosphorylation sites (Bouvier *et al.*, 1988; Hausdorff *et al.*, 1989). Phosphorylation events are regulated by two important protein kinase classes: the second messenger kinases and G-protein coupled receptor kinases (GRKs). The second messenger kinases such as PKC and PKA are able to phosphorylate either ligand-bound GPCRs leading to homologous desensitisation or GPCRs that are not occupied by ligand resulting in heterologous desensitisation (Pierce *et al.*, 2002). GRKs specifically phosphorylate agonist-occupied receptors and hence induce homologous desensitisation (Pierce *et al.*, 2002). Seven GRK subtypes (GRK 1- 7) have been identified and are grouped into three classes according to their function and sequence: GRK1/7, GRK2/3 and GRK4/5/6 (Pitcher *et al.*, 1998; Premont *et al.*, 2007). GRK2/3 and GRK5/6 are distributed widely in the body while GRK1/7 and GRK4 are restricted in the visual region (rod and cone cells) and testis respectively (Rajagopal *et al.*, 2018). GRK-mediated phosphorylation of receptors leads to the recruitment of arrestins to the receptor, resulting in the uncoupling from G-proteins and thereby promoting desensitisation (Luttrell, 2008). There are four subtypes of arrestins (1 - 4). Two (arrestin 1 and arrestin 4) are expressed in the retina (visual and cone arrestins) whilst arrestin 2 and arrestin 3 are ubiquitously distributed (Ferguson, 2001; Luttrell *et al.*, 2002) **(Figure 1.8)**.

Recently, biased agonism has been identified at GPCRs in which a specific ligand selectively regulates one or more signalling pathways that may differ to that of other ligands. Such observations may provide novel opportunities to the development of drugs,

targeting specific pathways that might lead to better therapeutic outcomes with lower unwanted effects (Rajagopal *et al.*, 2010b; Wisler *et al.*, 2018). An example of bias is that different ligands can have distinct behaviours toward G-protein activation and arrestins recruitment. Thus, some ligands can preferentially activate G-proteins compared to arrestins, whilst for other ligands the reverse can be true. In another example, ligands can selectively activate specific subtypes of G-proteins or may differentially regulate the functions of the arrestins, promoting arrestins signalling rather than desensitisation. This highlights that different patterns of desensitisation might emerge with different ligands (Kahsai *et al.*, 2011; Rajagopal *et al.*, 2011; Whalen *et al.*, 2011; Rajagopal *et al.*, 2018). The precise mechanisms underlying bias remain to be fully defined but are likely to involve the stabilisation of different conformational states of the receptor. This may result in, for example, different patterns of receptor phosphorylation and, as a consequence of this or the different conformations, the recruitment of different proteins. Different patterns of receptor phosphorylation could occur through the activation of different kinases (second messenger kinases or GRKs) and/or the presentation of different residues. For example, of the thirteen phosphorylation sites mapped in the $\beta_2$ adrenoceptor, all were phosphorylated by GRK2 and GRK6 in response to isoproterenol. By contrast, carvedilol, which is a β adrenoceptor blocker but functions as inverse agonist, mediates phosphorylation of the receptors at only two sites by GRK6 (Nobles *et al.*, 2011b). Activation of the angiotensin II type 1 receptor results in its phosphorylation by either GRK5 or GRK6, which mediates phosphorylation and activation of ERK while GRK2 or GRK3 phosphorylation of the receptor causes internalisation (Kim *et al.*, 2005). Such studies have led to the concept of the phosphorylation barcode in which the receptor can phosphorylate at different sites, potentially by different kinases depending on the ligand bound. This may alter the outcomes in terms of both signalling receptor regulation (Butcher *et al.*, 2011; Nobles *et al.*, 2011b; Yang *et al.*, 2015; Rajagopal *et al.*, 2018).

A number of potential phosphorylation sites have been identified in NMU1 and NMU2. In-silico identification provides information which relate only to kinases with clear consensus sites such as PKC and PKA whilst there are no consensus sites for GRKs. These sites include serine and threonine residues which are located in the *C*-terminal tail in addition to the second and third intracellular loops of both receptors (Brighton *et al.*, 2004b) **(Figure 6.4)**. Although potential phosphorylation sites for the second messenger kinases have been identified, it is not possible to identify sites for GRK-dependent

phosphorylation and it remains to be established both if and where NMU1 and NMU2 are phosphorylated by one or more members of this family of kinases.

#### 1.4.2.4.2 GPCR internalisation and redistribution

Following ligand occupation, GPCRs are removed from the cell surface and this phenomenon represents a critical point for receptor desensitisation, re-sensitisation and down regulation. Currently, it would seem that for the vast majority of GPCRs, ligand binding results in receptor phosphorylation by GRKs or PKC and/or PKA and when this is GRK-mediated this leads to the binding of arrestins to the ligand-bound receptor. This then initiates receptor desensitisation and internalisation by the recruitment of molecules involved in endocytosis (Claing *et al.*, 2002). Thus, arrestins act as a scaffolding platform, recruiting adaptor protein (AP2) and clathrin heavy chain (Ferguson, 2001; Shenoy *et al.*, 2011; Pavlos *et al.*, 2017). These components are considered the backbone for clathrin-coated formation in which the ligand-bound receptor and arrestins are associated allowing this complex to be internalised by cutting the neck of endocytic vesicles from plasma membrane with the GTPase, dynamin, thus contributes in receptor internalisation (Claing *et al.*, 2000b; Moore *et al.*, 2007; Antonny *et al.*, 2016). These vesicles fuse with endosomes which are tubulovesicular organelles. These endosomes carry the ligand and receptor and transport them to different intracellular destinations (Maxfield, 2014). Endosomes are acidic in nature and acidification plays a critical role in maturation of endosomes. In early endosome, the pH ranges from 5.6 - 6 while mature endosomes (late endosome) more acidic (pH 5 - 5.5) (Maxfield, 2014). Following stopping the fusion with newly formed endocytic vesicles, the early endosomes maturate to late endosomes which provide acidic environment for lysosomal activity (Yamashiro *et al.*, 1987). Although the vast majority of GPCRs appear to follow this general scheme of receptor internalisation and are therefore arrestin-dependent manner, there are other pathways that are arrestin-independent including clathrin- and dynamin-related mechanisms along with a number of potential mechanisms (Paing *et al.*, 2002; Chen *et al.*, 2004c) **(Figure 1.8)**.

NMU1 and NMU2 internalisation has been explored using a fluorescent-tagged version of porcine NmU-8, Cy3B-pNmU-8, and either NMU1 or NMU2 with *C*-terminal eGFP tags. Here, ligand and receptor were co-internalised following ligand binding (Brighton *et al.*, 2004b; Alhosaini *et al.*, 2018). This was attenuated by concanavalin A, suggesting a role for clathrin-coated pits (Yu *et al.*, 1993; Budd *et al.*, 1999; Kramer *et al.*, 2000; Trincavelli *et al.*, 2000). The temporal profiles of NMU2 internalisation in response to

either hNmU-25 or hNmS-33 were also investigated in a cell line expressing NMU2-tagged GFP. In this study, these ligands caused similar patterns and extent of internalisation when the receptors continuously exposed to ligand (Alhosaini *et al.*, 2018).

#### 1.4.2.4.3 GPCR intracellular trafficking and resensitisation

Apart from the role of arrestins in desensitisation and internalisation of GPCRs, it has also been shown to play a critical role in the regulation of intracellular signalling through its ability to recruit and activate a variety of signalling proteins. This can result in a new wave of signals that are independent of G-protein and which lead to different responses (Shenoy *et al.*, 2011; Shukla *et al.*, 2011a; Lefkowitz, 2013; Smith *et al.*, 2016). Among the GPCRs there are differences in the affinity for arrestins, leading to classification into two classes; A and B (Lefkowitz, 1998; Oakley *et al.*, 2000). Class A GPCRs, such as $\beta_2$ adrenoceptors, bind to arrestins with low affinity, resulting in dissociation of receptor-arrestin complexes at the plasma membrane. The receptors then immediately undergo recycling to the cell surface (Oakley *et al.*, 2000). In contrast, class B GPCRs such as parathyroid hormone receptors (PTHR) have a stronger affinity for arrestin binding and remain as a complex with arrestins within endosomes for a longer period of time (often hours) (Wehbi *et al.*, 2013).

In addition to arrestins, a range of proteins regulate GPCR trafficking and sorting. These include Rab-4 and Rab-5 which are members of Rab GTPases family (Mohan *et al.*, 2012). Thus, for example, $\beta_2$ adrenoceptor resensitisation was blocked in HEK293 expressing dominant negative Rab-4, pointing to impairment of receptor recycling by preventing receptor-bearing endosomes approaching the plasma membrane (Seachrist *et al.*, 2000). In contrast, cells expressing dominant negative Rab-5 impaired receptor internalisation and caused retention of vesicles containing $\beta_2$ adrenoceptors at the cell surface (Seachrist *et al.*, 2000). Recently, an endosomal binding protein, sorting nexin (SNX27), has also been shown to play a critical role in directing the recycling of endosomes containing receptors, including $\beta_1$ adrenoceptor and PTHR. In these studies, inhibition of SNX27 resulted in impairment of receptor recycling and directing them to degradation (Nakagawa *et al.*, 2013; Chan *et al.*, 2016; McGarvey *et al.*, 2016). Furthermore, apart from the phosphorylation of GPCRs, another post-translational modification event, ubiquitination, has also been shown to play a critical role in determining the fate of receptors (Shenoy *et al.*, 2001). Ubiquitination of GPCRs also

regulates receptor trafficking, including directing the receptor for recycling and resensitisation, when the receptor becomes deubiquitinated by deubiquitinating enzymes (Marchese *et al.*, 2013). Alternatively, the receptor remains ubiquitinated and becomes a target for Ubiquitin-dependent lysosomal degradation (Marchese *et al.*, 2001; Busillo *et al.*, 2010; Marchese *et al.*, 2013). The ubiquitination of arrestins is also integral to their regulation by promoting a tight association with activated and phosphorylated receptors (Tian *et al.*, 2016). For example, it has been demonstrated that ubiquitination of arrestin 3 results in sustained interaction between arrestin 3 and the $\beta_2$ adrenoceptor within endosomes, promoting lysosomal degradation (Shenoy *et al.*, 2008; Han *et al.*, 2013).

Following internalisation, receptors are either recycled back to the cell membrane for a new round of stimulation or are degraded within lysosomes (Oakley *et al.*, 1999; Oakley *et al.*, 2000; Moore *et al.*, 2007) **(Figure 1.8)**.

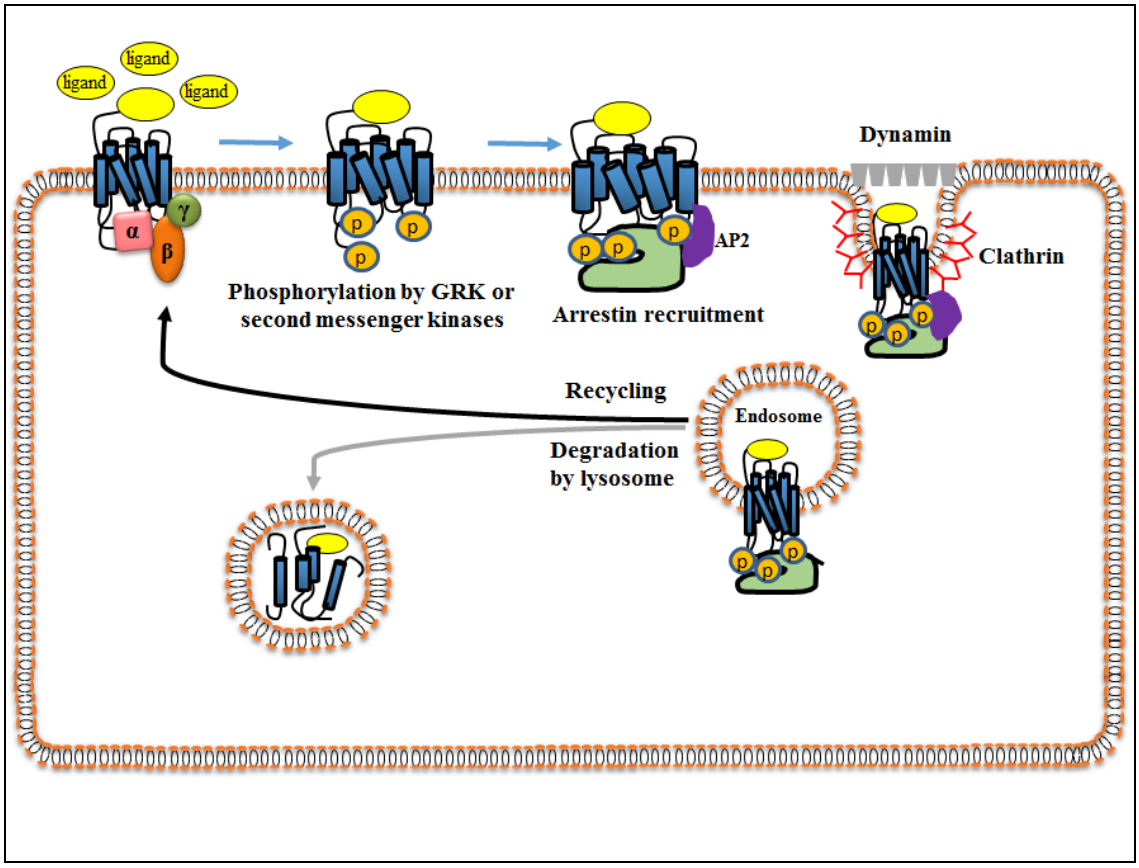


**Figure 1.8 General scheme of GPCR regulation**

Ligand-triggered receptor activation stimulates G-protein-dependent signalling. Upon activation, the receptor is phosphorylated by second messenger kinases or GRKs. Phosphorylation by GRKs leads to recruitment of arrestins to the phosphorylated receptor. This complex (ligand-receptor-arrestin) then, interacts with components of the endocytic pathway, clathrin and AP2, thereby promoting receptor internalisation. Ultimately, the complex either recycles back the membrane or subjects to lysosomal degradation.

#### 1.4.2.4.4 Arrestin-dependent GPCR signalling

Apart from the role of arrestins in facilitating receptor desensitisation and internalisation, it is now well established that arrestins play an important role in regulating a variety of cellular signalling events that are independent of G-proteins (Luttrell *et al.*, 1999a). The spatio-temporal profiles of signalling mediated by arrestins can be different from those of G-protein signalling, resulting in specific biological responses (Smith *et al.*, 2016). Although GPCR signalling may subject to a rapid desensitisation, the presence of internalised receptor with arrestins might form stable complex generating sustained signalling (Bahouth *et al.*, 2017). Arrestin-mediated signalling can arise as consequences of their ability to act as scaffold proteins, binding various intracellular signalling proteins such as MAPKs (Gurevich *et al.*, 2018b).

The presence of a dynamic network of endosomes through the cytosol can cause GPCR to signal in various intracellular compartments which might be critical in determination of specific biological responses (Thomsen *et al.*, 2018). Phosphorylation of GPCR following ligand binding plays a critical role in mediating different conformations of arrestins which influence their functions (Yang *et al.*, 2015; Nuber *et al.*, 2016). It has been reported that specific arrestin conformations with specific receptor phosphorylation barcode are emerged in which seven binding sites on arrestin 2 were replaced by unnatural amino acids and from which 1, 4, 6 and 7 phospho-acceptor sites were responsible for binding to GPCR domain and caused a specific conformation for clathrin recruitment. In contrast, binding of phosphates on GPCR to (1- 5) phospho-acceptor sites of arrestin 2 resulted in a conformation that led to activation of c-Src signalling (Yang *et al.*, 2015).

Existence of GPCR signalling from endosomal compartments has been shown. This was after examinations of functions of arrestins, particularly arrestin-mediated ERK activation (Eichel *et al.*, 2018). Indeed, inhibition of $\beta_2$ adrenoceptor internalisation by dominant -negative versions of both arrestin 2 and dynamin decreased ligand-dependent ERK activation (Daaka *et al.*, 1998). Furthermore, activation of protease-activated receptor 2 (PAR2) led to formation of a complex of arrestin 2, Raf-1 and activated ERK (DeFea *et al.*, 2000a). However, G-protein signalling has been shown to be involved in arrestin-dependent signalling from internalised receptor in a number of GPCRs and the arresin can generate sustained G-protein rather than its inhibited effect on G-protein (Thomsen *et al.*, 2016). Different conformations of arrestin mediated by ligand-activated

receptor might affect coupling of G-protein to the receptor (Jean-Charles *et al.*, 2017). Studies on $G\alpha_s$-coupled receptors such as PTH1R and vasopressin 2 receptor showed existence of sustained G-protein and cAMP activation in early endosome (Vilardaga *et al.*, 2012; Feinstein *et al.*, 2013; Irannejad *et al.*, 2013; Wehbi *et al.*, 2013). Using cryo-electron microscope and BRET assay, megaplexes, which are complexes consisting of activated receptor, arrestin, Gα and Gβγ, are determined (Thomsen *et al.*, 2016). For example, formation of ternary complex including PTH1R, arrestin and Gβγ in endosome following activation of receptor with PTH (1-34) (Wehbi *et al.*, 2013). Another study showed that $G\alpha_i/G\alpha_q$-coupled receptor, sphingosine-1-phosphate receptor 1 (S1P1) generated sustained $G\alpha_i$ signalling but not $G\alpha_q$ that persists for hours following ligand removal as revealed by inhibition of forskolin-mediated cAMP activation. This inhibition was ligand-specific by immunomodulator drug FTY720 as the natural ligand failed to do so (Mullershausen *et al.*, 2009). Furthermore, stimulation of vasopressin 2 receptor with vasopressin but not oxytocin causes arrestin recruitment to the endosome and promotes persistent cAMP signalling in endosome (Feinstein *et al.*, 2013)

Very little is currently known about the interaction of arrestins and either NMU1 or NMU2 although recent study has showed that activation of NMU2 by hNmS-33 resulted in arrestin 3 recruitment in a recombinant system (Sampson *et al.*, 2018).

#### 1.4.2.4.5 GPCR dephosphorylation

After activating and phosphorylating the GPCR, arrestins bind to the receptor and mediate internalisation. Internalised receptor undergoes either degradation or dephosphorylation in the endosomal vesicles by phosphatases to be recycled back to cell membrane for further stimulation (Kelly, 2006). Therefore, dephosphorylation considers a critical event subsequent to the receptor resensitisation.

GPCR dephosphorylation has received less attention than phosphorylation although it is known to be involved in resensitisation/recycling. In addition, such aspects, for example, the molecular mechanisms, potential regulation and functional consequences are also less clear (Gupta *et al.*, 2018). There is evidence that dephosphorylation by protein phosphatases can be regulated, thereby modulating GPCRs signalling consequences (Iyer *et al.*, 2006; Kelly, 2006; Gupta *et al.*, 2018). Furthermore, the hypothesis of phosphorylation barcode has added a layer of complexity in which different serine/threonine phosphorylation of the receptor can be read differently by arresins thereby promoting different GPCRs signalling outcomes (Tobin *et al.*, 2008; Butcher *et al.*, 2011; Nobles *et al.*, 2011b; Prihandoko *et al.*, 2016b). It is likely that serine/threonine phosphorylation barcode might have an influence on the interaction with protein phosphatases.

A family of thirteen protein phosphatases is identified and has a critical role in dephosphorylation of serine/threonine in eukaryotic cells (Kliewer *et al.*, 2017). It has been demonstrated that the dephosphorylation of $\beta_2$ adrenoceptor by PP2A (a member of protein phosphatases family) can occur in the acidified endosomes because disruption of dephosphorylation by ammonium chloride treatment suggests that dephosphorylation occurs in endosomes (Krueger *et al.*, 1997). Subsequent studies showed that dephosphorylation of the $\beta_2$ adrenoceptor can also happen at the plasma membrane as inhibition of internalisation by dynamin mutants and hypertonic sucrose did not block dephosphorylation suggesting that these distinct molecular mechanisms of receptor dephosphorylation may initiate at different phosphorylation sites of the activated receptor (Iyer *et al.*, 2006; Kelly, 2006; Tran *et al.*, 2007). There are a large number of studies that describe the selectivity and specificity of protein phosphatases interaction. For example, PP1β was responsible for dephosphorylation of $T_{353}$-T-E-T-Q-R-$T_{359}$ pattern in the *C*-terminal side chain of somatostatin type 2 receptor (SST2). These sites were phosphorylated by GRK2 and GRK3 and resulted in arrestin binding and ERK1/2

signalling as PP1β knockdown resulted in an increase in arrestin-mediated ERK1/2 activation (Poll *et al.*, 2010; Poll *et al.*, 2011). In addition, heterologous phosphorylation of SST2 by stimulation of the epidermal growth factor receptor (EGF) or alternatively genetic inhibition of PP1α or PP1γ in HEK-293 expressing SST2 did not affect arrestin-mediated ERK1/2 activation, suggesting a specific and selective role of PP1β in mediating dephosphorylation of SST2. Such dephosphorylation is thought to be responsible for the dissociation of the receptor-arrestin complex, leading to the inhibition of arrestin-mediated ERK1/2 signalling (Poll *et al.*, 2011).

Another study showed PP1γ dephosphorylation of the mu opioid receptor (MOP) near the plasma membrane at T370 and S375 residues following a few minutes of ligand removal. This dephosphorylation promoted receptor recycling as the genetic deletion of PP1γ attenuated the receptor recycling to the plasma membrane (Doll *et al.*, 2012). Further, in that study, ligand-specific patterns of phosphorylation were demonstrated that resulted in the recruitment of different GRKs, highlighting biased signalling (Doll *et al.*, 2012).

Research to date has not yet determined phosphorylation and dephosphorylation profiles of NMU1 or NMU2 in response to either hNmU-25 or hNmS-33 which are endogenous agonists for these receptors. Given that a recent study (Alhosaini *et al.*, 2018) has shown a different behaviour in NMU2 signalling and resensitisation profiles in response to hNmU-25 and hNmS-33 raising a question in which do hNmU-25 and hNmS-33 regulate NMU2 similarly?

## 1.5 Aims and objectives

hNmU-25 and hNmS-33 are endogenous neuropeptides that mediate their effects via two Family A G-protein coupled receptors, NMU1 and NMU2. These receptors couple preferentially to $G\alpha_{q/11}$ leading to $Ca^{2+}$ mobilisation but may also couple to $G\alpha_{i/o}$ to reduce cAMP. Central expression of NMU2 is responsible for the regulation of a variety of effects including the suppression of feeding behaviour and energy expenditure highlighting a potential anti-obesity target. Therefore, understanding NMU2 signalling and regulation in response to hNmU or hNmS-33 is of particular importance

Previous studies in our laboratory have identified signalling pathways mediated by recombinant NMU2 including $Ca^{2+}$ signalling and ERK1/2 activation. They reported previously that there are different resensitisation patterns in response to hNmU-25 and hNmS-33, most likely as a consequence of receptors recycling at different rates in the presence of the different ligands. These were apparent only following brief ligand exposure. Short-term exposure to the ligand may be more similar to the transient *in vivo* stimulation as it is likely that would be released sporadically and then removed by degradation and uptake. It has also been found that the brief ligand exposure, the two ligands activate ERK1/2 measured at five minutes of stimulation, which then reduces back to the basal levels after three hours but was sustained following hNmS-33. The difference in the rates of NMU2 resensitisation and ERK signalling between hNmU-25 and hNmS-33 could result from different types or temporal profiles of arrestins recruitment. Given that arrestins recruitment is generally a consequence of receptor phosphorylation, one of the key aims of this project was to investigate arrestins recruitment and identify the possible kinases and phosphorylation sites which are responsible for receptor phosphorylation and arrestins recruitment. Furthermore, given that phosphorylation and arrestins recruitment drive internalisation of GPCRs and that internalised receptors can signal in both G-protein dependent and G-protein independent (arrestin-dependent) pathways, this project aimed to study NMU2 phosphorylation in response to hNmU-25 and hNmS-33 as the arrestin recruitment is a consequences of receptor phosphorylation following agonist activation. Furthermore, it was to examine the potential ligand specificity of phosphorylation of NMU2, for example, the temporal profile of receptor phosphorylation because it could be possible that different phosphorylation patterns could drive different signalling outcomes. Moreover, it was important to identify the responsible kinases such as second messenger kinases, PKC and

PKA that could phosphorylate NMU2 and any possible differences upon stimulation with hNmU-25 and hNmS-33.

Identification of the phosphorylation sites was another aim of interest as it would be possible that hNmU-25 and hNmS-33 could mediate NMU2 phosphorylation at different sites. Given the mapping of NMU2 phosphorylation sites and side-directed mutagenesis, which is a further aim, were added to address the effect of investigated phosphorylation sites on NMU2 phosphorylation status following agonist stimulation to consider the functional consequences.

To study the receptor phosphorylation, we need to immunprecipitate the receptor by using a specific antibody. Therefore, we generate epitope-tagged receptors using HA tag which is incorporated into *C*-terminal end of the NMU2 (NMU2-HA). This strategy has been used to study receptor phosphorylation in previous studies.

Therefore, the first part of the project is to confirm that the tagged version NMU2-HA behaves similar to the untagged version NMU2 wild-type.

# 2 Chapter two: Materials and methods

## 2.1 Materials

### 2.1.1 Growth media, chemicals, peptides and radioactive substances

Dulbecco's modified Eagle's medium (DMEM) GlutaMax, minimum essential medium (MEM), Opti-MEM reduced serum media, fetal bovine serum (FBS), Dulbecco's phosphate buffered saline (DPBS), simply safestain-1L, L-glutamine and Geneticin (G418) were from Life Technologies (Paisley, UK). Penicillin/streptomycin solution (5000 units / ml), Hanks' balanced salt solution (HBSS) , trypsin/EDTA solution (1 X, composition: 0.05 % trypsin, 0.53 mM EDTA), MOPS SDS running buffer (50 mM MOPS; 50 mM Tris base; 0.1 % SDS; 1 mM EDTA; pH 7.7), cell culture 10 ml dish and fluo-4-acetoxymethylester (fluo-4-AM) and Glu-C Endoproteinase were from Fisher Scientific Ltd (Loughborough, UK). Dithiothreitol (DTT), poly-D-lysine hydrobromide, bovine serum albumin (BSA), phosphostop tablets, complete mini EDTA-free 25 tablets, IGEPAL CA-630, anti-HA affinity matrix, Carestream Kodak biomax intensifying screen and Carestream Kodak biomax film were supplied by Sigma-Aldrich (Poole, UK). ELISA microplates (96-well plate) transparent for $Ca^{2+}$ measurement or white bottomed for BRET assays, 24- and 6-well plates were purchased from Greiner Bio-One (Gloucestershire, UK). Human neuromedin U (hNmU-25) and human neuromedin S (hNmS-33) were from Cambridge Bioscience (Cambridge, UK). Tissue culture pipettes, falcon cell culture flasks (175 $cm^2$) were supplied from VWR international (Lutterworth, UK). Phosphorus-32 radionuclide 5 mCi ($^{32}$P-orthophosphate) was supplied from PerkinElmer LAS (UK) (Buckinghamshire, UK). Ro 31-8220 and KT5720 were supplied by Santa Cruz Biotechnology (Heidelberg, Germany). PKC 20-28 inhibitor, PKA inhibitor 14-22 amide and H89 dihydrochloride hydrate were from Merk Chemicals (Dorset, UK). Polyethylenimine HCl max was supplied by Polysciences Europe (Germany).

### 2.1.2 Western blot reagents

Acrylamide (30%) was from National Diagnostics (Hessle, UK), polyvinylidene fluoride (PVDF) transfer membrane was from Milipore (Brecillia, USA). PageRuler pre-stained protein ladder was purchased from Generon (Berkshire, UK). Amersham ECL Western blotting detection reagent was supplied from GE Healthcare Life Sciences (Buckinghamshire, UK). Rabbit monoclonal phospho-p42/44 MAPK (Thr202, Tyr204) (catalogue no.4377S), rabbit monoclonal phospho-SAPK/JNK (Thr183, Tyr185)

(catalogue no.4668S), phospho-P38 MAPK (Thr180, Tyr182) (catalogue no.9211S), S6 ribosomal protein (5G10) (catalogue no.2217S) and HRP-linked anti-rabbit IgG secondary antibodies (catalogue no.7074S) were obtained from New England Biolabs (Hertfordshire, UK). Anti-HA high affinity, rat monoclonal antibody (clone 3F10) (catalogue no.11867423001) was from Roche (Mannheim, Germany). Anti-Rat IgG (whole molecule)-peroxidase antibody produced in goat (catalogue no.A9037-1ML) was from Sigma-Aldrich (Missouri, USA). X-Ray film 18 x 24 cm was from Scientific lab Supplies (East Yorkshire, UK).

### 2.1.3 Cell lines

Cell lines were supplied from Dr. Gary B. Willars Laboratory (Molecular and Cell Biology, University of Leicester, UK) including human embryonic kidney cells (HEK-293) which either wild-type (HEK293-WT) or stably expressing NMU2 (HEK293-NMU2). The cell line expressing NMU2 have been described previously (Brighton *et al.*, 2004b).

### 2.1.4 Materials used for generation of NMU2 with either a *C*-terminal HA or nLUC tag, arrestin 2 and arrestin 3 with either a *C*-terminal YFP or RLuc sequence

High fidelity DNA polymerase, restriction enzymes (XhoI, XbaI, HindIII, KpnI, NheI and NotI), T4 DNA ligase and buffers were purchased from New England Biolab (Hitchin, UK). DNA ladder (200 bp - 10,037 bp) was from Bioline (London, UK). DNA gel purification kit and maxiprep kit were from QIAGEN (Crawley, UK). Primers, miniprep kit and LB broth powder were obtained from Sigma-Aldrich (Poole, UK). DH5α cells and super optimal broth S.O.C medium were from Invitrogen (Paisley, UK). Ethidium bromide was provided from National Diagnostics (Hessle, UK).

### 2.1.5 Plasmids used in the study

pcDNA 3.1+ (empty vector) and plasmid encoding NMU2 were in-house. Plasmids including pcDNA 3.1+ containing the nLUC sequence, pcDNA5 FRT containing either YFP or RLuc were kindly provided by Dr. Adrian Butcher (MRC Toxicology Unit, University of Leicester). Plasmids encoding arrestin 2 and arrestin 3 were purchased from the cDNA Resource Centre (www.cdna.org).

## 2.2 Methodology

### 2.2.1 Culture and maintenance of cell lines

All HEK-293 cell lines were cultured in DMEM GlutaMax provided with, Earl's salts, FBS (10 %), penicillin/streptomycin and non-essential amino acids. The cells were cultured on 10 ml dishes or flasks (175 $cm^2$) at 37 $C^o$ in $CO_2$ 5 % and 95 % humidified air. For sub-culturing, the growth medium was removed from the 10 ml dish and the cell monolayer washed with DPBS (5 ml). The cells were detached using trypsin-EDTA (1 ml) followed by neutralization with growth medium (9 ml). The cell suspension was centrifuged at 750 xg for 3 min and the pellet then reconstituted with growth medium (10ml). The re-suspended cells were then placed at a ratio 1:5 (v:v) in a dish or prepared for experimentation.

### 2.2.2 Freezing and resuscitation of Cell lines

To freeze the cells for storage, they were first sub-cultured as described **(Section 2.2.1)** and cultured until ~ 80 % confluency. Cells were then harvested, centrifuged and the pellet re-suspended in 1 ml of freezing medium (10 % dimethyl sulfoxide (DMSO) in FBS). The cell suspension was transferred into a 2 ml cryogenic vial which was then placed into a freezing container at - 80 °C for 3 - 4 h. The cryogenic vial was either stored for short-term (6 month) at - 80 °C or long-term at liquid nitrogen until use.

Cell defrosting was performed by rabid thawing of the cryogenic vial containing cells at 37 °C. The cell suspension was then transferred into a sterile 15 ml tube containing fresh growth medium and centrifuged at 750 xg for 3 min. Following removal of the supernatant, the pellet was re-suspended with 1ml of growth medium and transferred into a dish containing 9 ml of fresh growth medium. Cells were then cultured under standard conditions until use.

### 2.2.3 Buffer used for experiments with cells

Cells were maintained in Krebs-HEPES buffer containing BSA (KHB) during the time of the experiment unless otherwise stated. The buffer composition was: HEPES, 10 mM; $NaHCO_3$, 4.2 mM; glucose, 11.7 mM; $MgSO_4$, 1.18 mM; KCl, 4.7 mM; NaCl, 118 mM; $KH_2PO_4$, 1.2 mM and $CaCl_2$. $2H_2O$, 1.29 mM, pH 7.4. Ligands and test agents were also prepared in this buffer unless otherwise stated.

### 2.2.4 Coating plasticware with poly-D-lysine

Poly-D-lysine hydrobromide was used to coat 6-, 24-, or 96-well plates where needed. To coat the wells, poly-D-lysine 0.1 % w/v was added for 10 - 20 min. The plate was then washed twice with an appropriate volume of DPBS and left to dry inside a tissue culture hood until use.

### 2.2.5 Cells number counting

Cells were counted using a haemocytometer. Cells were sub-cultured and harvested as described **(Section, 2.3.1)**. The pellet was re-suspended in 10 ml of fresh growth medium. Following re-constitution, 10 µl of the cell suspension was added to the haemocytometer (Neubauer improved, with 0.0025 $mm^2$ area and 0.100 mm depth, Sigma-Aldrich, Poole, UK). Cells were counted in the large four squares and the total number of cells was divided by four to obtain the average cells number per square. The average number of cells was multiplied by 10000 to obtain the total cells number per 1 ml of the cell suspension.

### 2.2.6 Generation of NMU2-HA, NMU2-nLUC, arrestin 2-YFP, arrestin 3-YFP, arrestin 2-RLuc and arrestin 3-RLuc

#### 2.2.6.1 Primer design

The primers, forward and reverse were designed as appropriate **(see Chapter, 3.2.1, 5.2.1, 5.2.2, 5.2.3)**. The forward primer contained important positions including restriction sites for enzymes, a start codon, and a Kozak sequence inserted before the gene of interest to promote ribosomal translation (De Angioletti *et al.*, 2004). The reverse primers included the restriction sites, a stop codon, followed by some of the sequence of the gene of interest **(Figure 2.1)**.

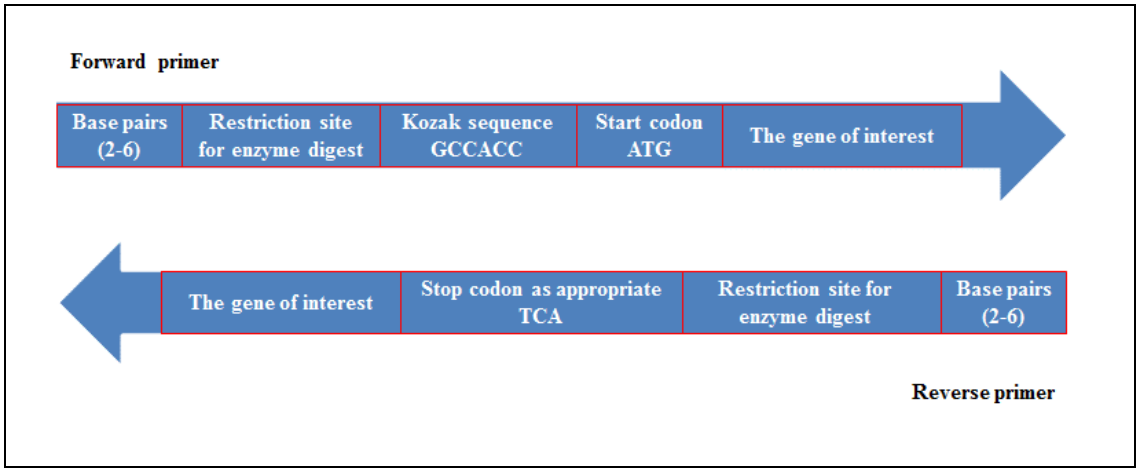

**Figure 2.1 General design of primers for generation of NMU2-HA, NMU2-nLUC, arrestin 2-YFP, arrestin 3-YFP, arrestin 2-RLuc and arrestin 3-RLuc**

Two primers were designed to generate each construct. The forward primer contained a restriction site for enzyme digest, a Kozak sequence and a start codon before the gene of interest. The reverse primer contained a restriction site and a stop codon that was inserted as appropriate before the gene of interest. The full details are provided elsewhere.

### 2.2.6.2 Amplification of gene using polymerase chain reaction (PCR)

Each gene was amplified by PCR from a vector containing an untagged version of the same gene using a thermocycler, Techne Progene (Cambridge, UK). The general PCR programme for amplification of the constructs in the study included 27 cycles as follow:

**First cycle**

Denaturation step for 1 min at 95 °C

**25 cycles of three steps**

1. Denaturation for 30 s at 95 °C
2. Annealing for 1 min at 53 °C for NMU2-HA or NMU2 and 58 °C for arrestin 2 or arrestin 3
3. Extension for 3 min at 72 °C

**The last cycle involved**

1- Denaturation for 30 s at 95 °C

2- Annealing for 1 min at 53 °C for NMU2-HA or NMU2 and 58 °C for arrestin 2 or arrestin 3

3- Extension for 10 min at 72 °C

Finally, the thermocycler was set to hold at 4 °C to maintain the samples at the end of programme. Samples were either processed immediately or maintained at - 20 °C until use. The PCR reaction volume in each flat cap PCR tube was 50 µl and set-up on ice as follows: reaction buffer (5 X, 10 µl), dNTPs (10 mM, 1 µl), forward and reverse primers (0.5 µg), template DNA vectors (0.5 µg), high-fidelity DNA polymerase (2000 U / ml, 1 µl) and nuclease-free water (to 50 µl). The reaction in each PCR tube was mixed by pipetting up and down and centrifuged briefly in a bench-top microfuge for 2 - 3 s and then subjected to the PCR cycles using a thermocycler.

### 2.2.6.3 Detection of constructs using agarose gel electrophoresis

Following the PCR reaction, the PCR products were detected by agarose gel electrophoresis (1%). Agarose (0.5 g) was dissolved in Tris-acetate-EDTA buffer [TAE: Tris acetate, 0.4 M; EDTA, 0.01 M, pH 8.3, 50 ml]. The mixture was heated for 1 min in

a microwave to dissolve the agarose powder and then allowed to cool to 50 - 60 °C. Ethidium bromide was added at a concentration of 0.5 µg / ml [a stock solution of 10 mg / ml] to allow visualization. The solution was poured into a casting tray with a 9-well comb and allowed to solidify at RT for 20 - 30 min. The comb was then removed and the casting tray transferred into a running tank containing 250 ml of 1 X TAE buffer. The samples were then mixed with DNA loading buffer (Bioline Reagents Ltd, London, UK) at a ratio 1 : 4 loading buffer to sample and loaded into the wells of the agarose gel. Electrophoresis was performed by exposing the gel to 85 V for 60 - 90 min. Finally, the gel was removed from the tank and viewed on a UV light box.

#### 2.2.6.4 DNA extraction and purification

After visualization of the PCR products under UV light, each DNA fragment was excised from the agarose gel with a clean scalpel and transferred into an autoclaved, pre-weighted 1.5 ml Eppendorf tube. DNA purification from the gel was performed using a QIAquick Gel Extraction Kit. In brief, a 3 X volume of QG buffer was added to the gel slice and then incubated at 50 °C in a water bath for 10 min with vortexing every 2 - 3 min until the gel dissolved completely. Isopropanol was added to the mixture with continuous mixing and then the mixture was loaded to a QIAquick column in a 2 ml tube and centrifuged at 16000 xg for 1 min. The flow-through was discarded and the QIAquick columns placed in the same tube. An additional 500 µl of QG buffer was added and the tube centrifuged again. QIAquick columns were washed with 750 µl of PE buffer and left to stand for 5 min before centrifugation at 16000 xg for 1 min. The columns were transferred into clean, autoclaved 1.5 ml Eppendorf tubes. The DNA was then eluted by adding 30 µl of water and letting the column to stand for 1 min before centrifugation. The eluted DNA was stored at - 20 °C for future use.

#### 2.2.6.5 Double digestion using restriction enzymes for sub-cloning

The purified PCR products (inserts) were digested by appropriate enzymes to form two sticky ends ready for ligation into the desired plasmid which was also subjected to the same digest conditions. Each reaction was set up in a 50 µl volume, including the purified PCR products (approximately 20 µl; calculated by dividing 1000 by ng of PCR product measured by nanodrop) in a PCR tube. Cutsmart buffer, compatible with the two restriction enzymes at the same temperature according to the manufacturer's instructions (10 X, 5 µl) was added. The appropriate restriction enzymes (1 µl) were added followed by DNase/RNase-free water up to 50 µl. The components of each PCR tube were mixed

by pipetting up and down and then spun down at 16000 xg for 3 s. The PCR tubes containing the mixture were incubated at 37 °C overnight using a thermocycler. The digested PCR products were purified using the method described **(Section 2.2.6.4)** and stored at - 20 °C until use.

### 2.2.6.6 Ligation of PCR product into the vector

The digested PCR product (insert) was ligated into the appropriate vector which was subjected to the same double digest using the restriction enzymes that were used to digest the PCR product **(Section 2.2.6.5)**. For a 20 µl reaction, the quantity of insert used for the ligation step was calculated by the amount of vector to be used in the ligation in ng (100 ng) / X multiply by 3, where X = length of vector / length of insert in an optimal molar ratio 3:1 insert to vector. Following determination of the desired amount of both insert and vector, they were added to a sterile PCR tube. T4 DNA ligase buffer (10 X, 2 µl) was added followed by DNase/RNase-free water up to 19 µl. Finally, T4 DNA ligase (1 µl) was added to the mixture with gentle mixing which was then spun down briefly at 16000 xg for 3 s. The samples were then incubated at 16 °C overnight using a thermocycler. The ligated plasmids were then amplified by transforming into DH5α competent cells.

### 2.2.6.7 Transformation of the ligated construct into the DH5α competent cells

Following ligation, the new construct was amplified to generate a sufficient quantity by transforming into DH5α competent cells. Briefly, the competent cells (50 µl aliquots stored at - 80 °C) were thawed on ice for 10 min before transformation. The ligated construct (1 - 5 µl) was then added to an Eppendorf tube containing competent cells and placed on ice for 30 min. Subsequently, the mixture was exposed to heat shock (42 °C) for 45 s using a water bath and then placed promptly on ice for 2 min. The cells were mixed with S.O.C medium (yeast extract, 0.5 % w / v; trypton 2 % w / v; NaCl, 10 mM; KCl, 2.5 mM; $MgCl_2$, 10 mM; $MgSO_4$, 10 mM and; glucose, 20 mM) (950 µl) and incubated at 37 °C for 1 h with continuous shaking at 250 rpm. Following incubation, the mixture was centrifuged at 6000 xg for 1 min. The supernatant (900 µl) was then removed and the remaining cell suspension (100 µl) resuspended and spread in different dilutions (10 µl, 20 µl or 50 µl) on Lysogeny broth (LB) agar plates (composition: (yeast extract, 0.5 % w / v; tryptone 1 % w / v and NaCl 0.5 % w / v) (Bibby Sterilin, Staffs, UK). The agar contained ampicillin (286.2 µM) as the plasmids carried the ampicillin-resistant gene conferring resistance for bacteria carrying the plasmids. The cultured plates were then

incubated at 37 °C overnight in a bacterial incubator. Plates were then collected, sealed with parafilm and stored at 4 °C in an inverted position prior to selection of the positive colonies.

#### 2.2.6.8 Preparation of plasmid from transformed colonies

The transformed colonies, which carried the DNA plasmid of interest, were used to start cultures for preparation of plasmids for transfection of cells. Depending on the required quantity of the plasmid, there were three scales of DNA plasmid purification: miniprep (DNA < 20 µg); midiprep (DNA up to 100 µg) and; maxiprep (DNA < 500 µg).

#### 2.2.6.9 DNA preparation using miniprep

Initially, a small scale of DNA plasmid was prepared to enable confirmation that the newly synthesised plasmid was correct at the expected molecular size and not, for example, mutated using double digests with restriction enzymes or DNA sequencing, which was supplied by PNACL (Protein and Nucleic acid Characterisation Laboratory, University of Leicester). Before performing the miniprep, six colonies were inoculated from each plate carrying the appropriate DNA plasmid and transferred into six 50 ml Falcon tubes containing 2 ml of LB broth medium and 2 µl of ampicillin (286.2 mM). The Falcon tubes were then incubated overnight at 37 °C with shaking (250 rpm) using a bacterial incubator. The next day, each culture was used in a miniprep using a Sigma GeneElute plasmid miniprep kit. In brief, each overnight transformed culture solution (1 ml) was transferred into an autoclaved 1.5 ml Eppendorf tube and the remaining volume was made as glycerol stock and stored at - 80 °C. The tubes were centrifuged at 12000 xg for 1 min. The supernatant was decanted and the pellet re-suspended by adding 200 µl of re-suspension buffer. The re-suspended cells were then lysed by adding 200 µl of lysis solution with inverting 6 - 8 times. The mixture was then neutralized by adding 350 µl of neutralization solution with gentle shaking 4 - 6 times. The components were then centrifuged at 16500 xg for 10 min to pellet the cell debris. The GeneElute column was assembled and 500 µl of column preparation buffer added. The column was then centrifuged at 12000 xg for 1 min and the liquid at the bottom of the tube discarded. The supernatant from the cells was then transferred into the prepared column, centrifuged at 12000 xg for 1 min and the flow-through discarded. The column was washed by adding 750 µl of diluted wash solution, centrifuged at 12000 xg for 1 min and the liquid flow-through discarded again. The column was re-centrifuged at maximum speed for 2 min and transferred into an autoclaved Eppendorf tube. DNA was eluted into this tube by

adding 30 µl of TE buffer (Tris-base, 10 mM; EDTA 1 mM, pH, 8) into the column and then centrifugation at 12000 xg for 1 min. The concentration and purity of eluted DNA was then assessed using a nanodrop ND-1000 spectrophotometer, Nanodrop Technologies (Wilmington, USA) prior to immediate use or stored at - 20 °C for future use.

#### 2.2.6.10 Restriction enzyme digest test of DNA plasmids

Following preparation of a small quantity of the DNA plasmid, double digests were performed in a 25 µl reaction. Briefly, DNA plasmid (0.5 µg / µl, 1 µl) was incubated with CutSmart buffer (10 X, 2.5 µl), which was compatible with the appropriate enzymes according to manufacturer's instructions. The restriction enzymes were added (0.5 µl) followed by DNase/RNase-free water up to 25 µl. The reaction was incubated at 37 Cº for 1 h and then run on 1 % gel agarose stained with ethidium bromide. The gel was then visualised under UV light.

#### 2.2.6.11 DNA sequencing

Further confirmation of the prepared plasmids was performed in which the DNA sequences of the gene of interest were sequenced by PNACL, University of Leicester. The primers used to sequence the gene of interest within the vector were explored in **Table 2.1**

**Table 2.1 Primers used for sequencing the gene of interest after cloning into the vector**

| DNA plasmid | Forward primer | Reverse primer |
|---|---|---|
| pcDNA 3.1+ | 5' AATACGACTCACTATAGGG 3' | 5' TAGAAGGCACAGTCGAGG 3' |
| pcDNA5 FRT | 5' CGCAAATGGGCGGTAGGCGTG 3' | 5' TAGAAGGCACAGTCGAGG 3' |
| pLEICS-12 | 5' GGAGACCCAAGCTTGGTACC 3' | 5' AAGGCACAGTCGAGGCTGA 3' |

#### 2.2.6.12 Preparation of large quantities of DNA plasmid using maxiprep

Following confirmation that the synthesised gene of interest cloned into the appropriate DNA plasmid was at the correct molecular size and the sequence was correct, it was necessary to prepare a sufficient amount of plasmid for transfection into mammalian cells using the QIAGEN plasmid maxi kit. From the appropriate glycerol stock, a sample was taken using a sterile disposable plastic loop and spread on an agar plate containing ampicillin. The agar plate was then incubated overnight at 37 °C in a bacterial incubator. A single colony was then picked and transferred into a 50 ml Falcon tube containing 2 ml of LB broth and 2 µl of ampicillin (286.2 mM). The tube was then incubated for 8 h at 37 °C with continuous shaking (250 rpm). The bacterial culture suspension was then transferred into an autoclaved 1 L flask containing 250 ml of LB broth and 250 µl of ampicillin (286.2 mM stock). The flask was then incubated overnight at 37 °C with shaking (250 rpm). The next day, plasmids were prepared by maxiprep. Briefly, the cells were centrifuged at 6000 xg at 4 °C for 15 min. The supernatant was then discarded and the pellet re-suspended by adding 10 ml of P1 buffer (Tris-HCl, 50 mM; EDTA, 10 mM; pH, 8.0 and RNase A, 100 µg / ml). Re-suspended cells were then lysed with 10 ml of P2 buffer (NaOH, 200 mM and 1 % SDS w/v) by inverting 4 - 6 times and incubated for 5 min at RT. The mixture was then neutralized by adding 10 ml of pre-cooled P3 (potassium acetate, 3 M, pH, 5.5) and mixed by inverting 4 - 6 times followed by incubation for 20 min on ice. The components were centrifuged at 20000 xg for 30 min at 4 °C and re-centrifuged for 15 min at the same speed. Before centrifugation was completed, a QIAGEN tip was equilibrated by adding 10 ml of QBT buffer (NaCl, 750 mM; MOPS, 50 mM, pH 7; isopropanol, 15 % v/v and Triton X-100, 0.15 % v/v) that was allowed to drain-through under gravity. The supernatant resulting from the centrifugation step was applied to the equilibrated QIAGEN tip and allowed to drain by gravity. The QIAGEN tip was then washed twice by adding 30 ml of QC buffer (NaCl, 1 M; MOPS, 50 mM, pH 7 and isopropanol, 15 % v/v). The DNA was then eluted into an autoclaved 50 ml tube by adding 15 ml of QF buffer (NaCl, 1.25 M; Tris.HCl, 50 mM, pH 8.5 and isopropanol, 15 % v/v). The DNA was then precipitated by adding 10.5 ml of isopropanol with mixing and then centrifuged (20000 xg for 30 min at 4 °C). The supernatant was removed carefully and the DNA pellet washed with 5 ml of 70 % ethanol. The washed DNA was centrifuged at 20000 xg for 10 min and supernatant was discarded. Finally, the DNA pellet was allowed to dry for 5 - 10 min and then re-suspended using TE buffer

(150 µl; Tris.HCl, 10 mM, pH 8 and EDTA, 1 mM). The DNA was then stored at - 20 °C until use.

#### 2.2.6.13 Glycerol stock preparation for transformed bacterial culture

Glycerol stocks for storing the plasmid of interest were prepared. Equal volumes of glycerol and water were mixed and autoclaved. This was then stored at RT for future use. For each bacterial glycerol stock, 500 µl of glycerol (50%) was added to 500 µl of transformed bacterial culture solution in a cryotube which was then mixed gently and stored at - 80 °C.

### 2.2.7 Transient transfection of mammalian cells

Transfection was performed on wild type HEK-293 cells using JetPRIME® DNA transfection kit (Polyplus, USA) or PEI MAX (Polysciences, Inc., USA). For the JetPRIME transfection reagent, the transient transfection was carried out according to the manufacturer's instructions. Briefly, cells were seeded at 60% - 80% confluency in 6-well plates with serum-containing media before the day of transfection. JetPRIME buffer (200 µl) was added to an autoclaved 1.5 ml Eppendorf tube followed by addition of the appropriate construct(s) (2 µg). The mixture was then mixed by vortexing for 10 s and centrifuged briefly. The jetPRIME® reagent (4 µl) was then added at a ratio 1:2 (w:v) (for example, 1 µg of DNA requires adding 2µl of the jetPRIME® reagent) followed by vortexing for 10 s. Following incubation for 10 min at RT, the mixture was then added to the cells drop by drop and incubated at 37 °C. It was preferable that the media was replaced after 4 h to reduce cell toxicity. Following 2 days, the transfected cells were used to measure gene expression and function. For transfection with the PEI MAX reagent, cells were cultured in 6-well plates to 70 % confluency for 24 h (2.7 ml of media per well). On the day of the transfection, PEI MAX (1 mg / ml, 9 µl) was diluted with Opti-MEM (150 µl) in an autoclaved Eppendorf tube. An appropriate construct (2 µg) was diluted with Opti-MEM (150 µl) in another Eppendorf tube. The diluted PEI MAX was added to the diluted construct and mixed by pipetting up and down. The mixture was then added to cells drop by drop and the plate then incubated at 37 °C. For both transfection methods, cells were assessed for protein expression or function after 48 h.

### 2.2.8 Generation and maintenance of stable cell lines

Cell lines with a stable expression of the gene of interest were established by transfecting HEK-293 cells with the appropriate construct using either JetPRIME transfection kit or

PEI MAX transfection reagent as described in **Section 2.2.7**. After 48 h, the transfected cells were treated with the selection antibiotic, Geneticin (G418) (1 mg / ml; stock, 50 mg / ml). The media was replaced every three days. After three weeks of treatment, the surviving cells were highly diluted (1, 2, 4, 6, 8, 10, 15 or 20 µl per 10 ml) to obtain a number of single cells which were then grown into single colonies under continued selection. The surviving colonies under Geneticin treatment were selected under a light microscope and transferred into a 24-well plate using autoclaved 200 µl yellow tips. Colonies were then left to grow to ~ 90 % confluence. Immunoblotting was then used to quantify the levels of protein and identify positive clones using an anti-HA antibody to recognise HA-tagged receptors. Following selection of the successful clones, they were expanded to either make stocks or used for experimentation.

### 2.2.9 Measurement of $Ca^{2+}$ signalling on a population of cells using a Fluo-4-AM

Fluo-4-AM is a cell permeable, $Ca^{2+}$-sensitive dye, which is widely used as $Ca^{2+}$ indicator to measure the free intracellular $Ca^{2+}$ concentration. Following excitation at a wavelength 480 nm, fluorescence is collected at emission 525 nm. The fluorescent intensity increases as [$Ca^{2+}$] increases, resulting in greater binding of $Ca^{2+}$ to the dye (Chen *et al.*, 2010; Alhosaini *et al.*, 2018). Cells were seeded on a 96-well plate at ~ 95 % confluency which consisted of strips, each strip contained 8-wells. These strips were coated with poly-D-lysine before plating the cells. Next day, the growth media was removed from confluent monolayers which were then washed twice with KHB. Cells were loaded with Fluo-4-AM (2 µM) by incubating at 37 °C for 45 min in the dark. Following incubation, the cells were washed once using KHB and 100 µl of KHB added to each well. Fluorescence changes were measured as an index of changes in $[Ca^{2+}]_i$ in response to agonist using a NOVOstar microplate reader (BMG LABTECH, Germany). The plate reader was set to add 20 µl of the ligand from a separate reagent plate at a speed of 230 µl / s and record the fluorescence every 0.5 s for 1 min. Fluorescence intensity was monitored at excitation 480 nm and emission 525 nm. For re-sensitisation experiments, HEK-NMU2 or HEK-NMU2-HA were plated at 96-well plates before the day of the experiment as mentioned above. On the day of the experiment, cells were washed twice with KHB and left in the incubator for 30 min to equilibrate. Cells were then manually challenged with either hNmU-25 or hNmS-33 (30 nM) for 5 min followed by washing of cell monolayers with KHB. Cells were then allowed to recover in either KHB (without ligand) for 1 or 3 h or serum-free media for 6 h. Fluo-4-AM was then loaded for the final 45 min of the recovery

period. Cells were washed with KHB, left 5 min in the incubator and then stimulated with the same ligand (30 nM) using a plate reader.

### 2.2.10 Immunoblotting

Immunoblotting can be used for the identification and quantification of a protein of interest in a mixture of proteins in cell lysates (Towbin *et al.*, 1979). Briefly this depends on separating proteins in a sample containing a mixture of proteins by polyacrylamide gel electrophoresis. Resolved proteins are then transferred electrophoretically onto a membrane of, for example, nitrocellulose or PVDF. The membrane is then incubated with a primary antibody against the protein of interest. Following washing of membrane, a secondary antibody, which is an antibody that is often conjugated with for example horse reddish peroxidase (which is an enzyme used for protein detection) or is fluorescent allowing direct visualisation following addition of compatible substrates, for example, chemiluminescent substrate (ECL). Bands of the protein of interest are then detected (Alegria-Schaffer *et al.*, 2009).

#### 2.2.10.1 Stimulation and preparation of the cell monolayers

Cells were cultured on 24-well plates coated with poly-D-lysine before serum-starving overnight. On the day of the experiment, the growth media was removed and the cell monolayers washed twice with KHB followed by the addition of 500 µl of KHB added to each well. At the appropriate time, the cells were washed once with PBS or KHB and lysed using cold, 2X sample buffer (Tris-base, 125 mM, pH 6.8; SDS 4 % w/v; glycerol 20 % v/v; bromophenol 0.01 % w/v; dithiothreitol, 250 mM (freshly prepared on experiment day)) for 5 min on ice. The lysed cells were then heated for 5 min at 95 °C using a block heater and then put on ice or stored at - 20 °C until use.

#### 2.2.10.2 Polyacrylamide gel electrophoresis

Electrophoresis was performed using a resolving gel of 10 % which was prepared as follows for a 10 ml total volume: polyacrylamide, 30 % v/v, 3.3 ml; Tris-HCl, 1.5 M, 2.5 ml, pH 8.8; sodium dodecyl sulfate (SDS), 10 % w/v, 0.1 ml; ammonium persulfate, 10 % w/v, 0.1 ml; N, N, N', N' tetramethylethylenediamne (TEMED), 0.004 ml and; $H_2O$, 4ml. After gentle mixing, the solution was poured into the space between two glass plates fixed by two spacers (1.5 mm) of a Mini-BioRad electrophoresis system (Bio-Rad, Hemel Hempestead, UK). Isopropanol was then added to the top layer to make a sharp edge. The resolving gel was left for 15-20 min to solidify and then washed with water to remove the isopropanol. The stacking gel (5 %) was then prepared as follows: for 8 ml total

volume acrylamide, 30 % v/v, 1.3 ml; Tris-HCl, 1 M, 1 ml, pH 6.8; SDS, 10 % w/v, 0.08 ml; ammonium persulfate, 10 % w/v, 0.08 ml; N, N, N', N' tetramethylethylenediamne (TEMED), 0.008 ml and; $H_2O$, 5.5 ml. The components were mixed, poured onto the top of the resolving gel and a comb (usually 15-well) was inserted into the stacking gel to form the loading lanes. The gel was then left for 20 - 25 min to solidify. The comb was then removed and the gel was immersed in the electrophoresis tank. The tank was filled with running buffer (Tris-HCl, 25 mM; glycine, 192 mM; SDS, 0.1 w/v, pH 8.3). The samples were heated at 95 °C for 5 min, spun down for 1 min at 16000 xg and then loaded into each lane (20 µl per lane).The first lane was loaded with a pre-stained protein ladder (5 µl). Using a POWER PAC 300 (Bio-Rad, Hemel Hempestead, UK), the electrophoresis was performed at 180 V for 50 min until the samples reached the bottom of the gel by using the ladder as indicator.

#### 2.2.10.3 Semi-dry blocking to transfer proteins onto membranes

The PVDF transfer membrane and filter papers were prepared by cutting to a size corresponded to the resolving gel (8.5 cm x 5 cm). PVDF membrane was then immersed in methanol for 30 s and then transferred into distilled water for 2 min. The membrane and filter papers were then placed in transfer buffer (composition: Tris, 48 mM; SDS, 0.0375 % w/v; glycine, 40 mM and; methanol 20 % v/v) for 10 min. Following gel electrophoresis, the stacking gel was removed and the resolving gel was placed in transfer buffer. The semi-dry transfer was performed by putting three filter papers on the positive plate of the semi-dry blotter followed by transfer membrane. The resolving gel was then placed on the membrane followed by a further three filter papers. The negative cover was then placed carefully and the transfer performed at 15 V for 30 min using a POWER PAC 300 (Bio-Rad, Hemel Hempestead, UK).

#### 2.2.10.4 Membrane blocking and antibody incubation

After semi-dry electrophoresis was completed, the membrane was blocked for 1 h at RT with continuous rocking using a blocking buffer containing 5% fat-free milk. (TBST:) Tris-base, 50 mM, pH 7.5; NaCl, 150 mM; Tween 20, 0.05 % v/v). The membrane was then washed for 1 min three times and incubated at 4 °C overnight with an appropriate primary antibody in TBST and 5 % BSA with continuous rolling **(Table 2.2)**. Next day, the membrane was washed three times for 8 min with TBST followed by incubation with an appropriate secondary antibody in TBST containing 5 % fat-free milk for 1 h at RT with continuous shaking **(Table 2.2)**. The membrane was then washed as above and

immunoreactive bands detected using ECL Western blotting detection reagent which consists of two reagents (reagent 1 and reagent 2) that used at a ratio 1:1 (1 ml per membrane) followed by exposure to X-ray film. The exposure time was optimised according to the signal intensity (5 - 60 s).

**Table 2.2 Dilution of primary and secondary antibodies used**

| Primary antibody | Secondary antibody |
|---|---|
| Rabbit monoclonal phospho p42/44 MAPK<br>Dilution factor, 1 : 1000 | HRP-linked anti-rabbit IgG<br>Dilution factor, 1 : 2000 |
| Rabbit monoclonal phospho-SAPK/JNK<br>Dilution factor, 1 : 1000 | HRP-linked anti-rabbit IgG<br>Dilution factor, 1 : 2000 |
| phospho-P38 MAPK<br>Dilution factor, 1 : 1000 | HRP-linked anti-rabbit IgG<br>Dilution factor, 1 : 2000 |
| Rabbit monoclonal S6 ribosomal protein<br>Dilution factor, 1 : 20000 | HRP-linked anti-rabbit IgG<br>Dilution factor, 1 : 2000 |
| Anti-HA high affinity, rat monoclonal antibody (clone 3F10) 100 ng / ml | Anti-Rat IgG (whole molecule)-peroxidase<br>Dilution factor, 1 : 5000 |

All sources of the antibodies with catalogue numbers are found in **Section 2.1.2**

### 2.2.11 Determination of receptor phosphorylation

Phosphorylation of NMU2 or mutants of this, each containing a *C*-terminal HA-tag was determined as previously described (Prihandoko *et al.*, 2015a). HA-tag was included in the construct to allow immunoprecipitation of the receptor using an anti-HA antibody. The principle of this technique in brief is that cells expressing the receptor are metabolically labelled with $^{32}$P-orthophosphate before stimulation with the ligand of interest. Following stimulation, cells are solubilised and the HA-tagged receptors purified using anti-HA antibody beads. Immunoprecipitated receptors are resolved by gel electrophoresis and viewed by autoradiography **(Figure 2.2)**.

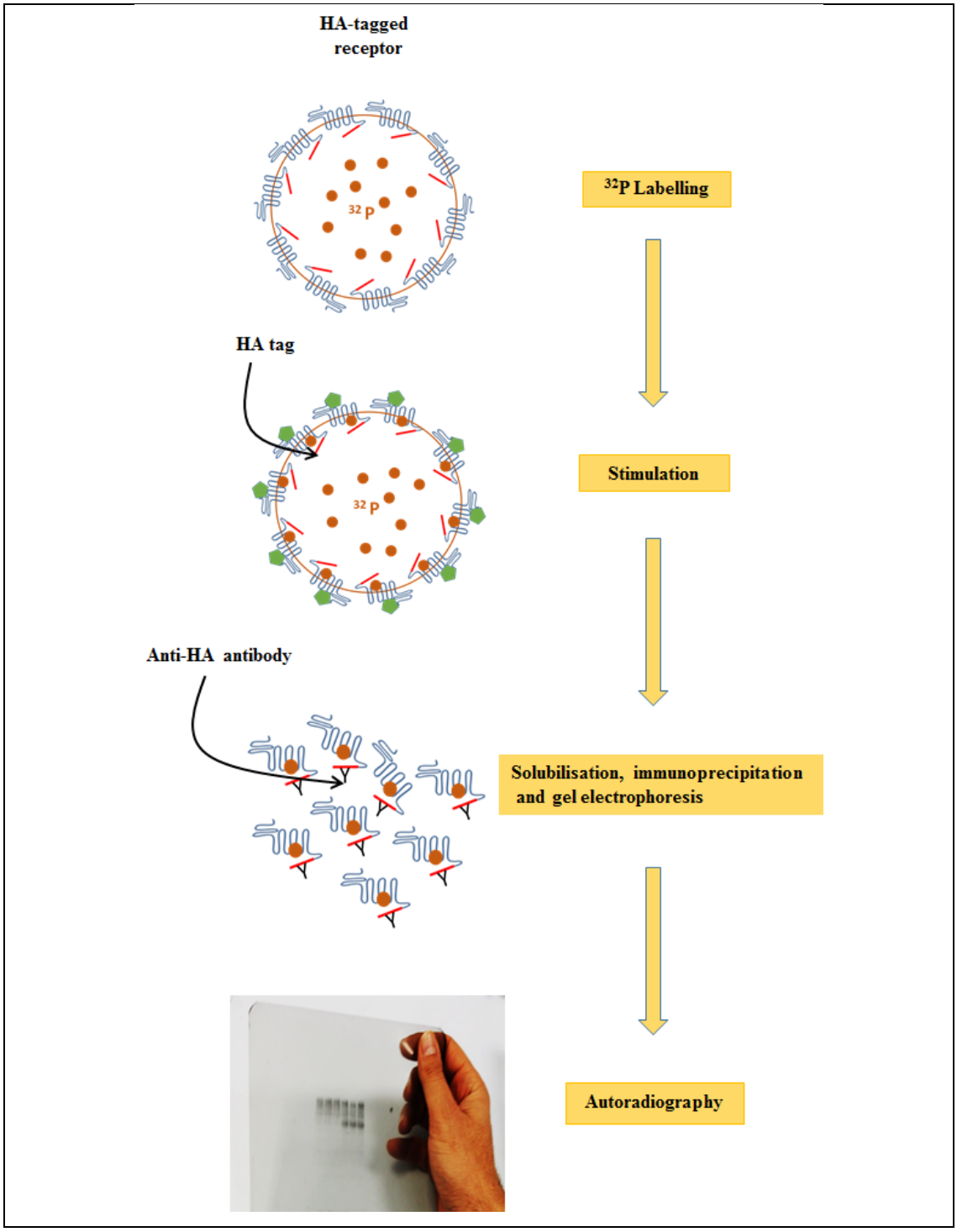


**Figure 2.2 Experimental principles of Receptor phosphorylation**

A schematic diagram showing the protocol for studying receptor phosphorylation. HA-tagged receptor were labelled with $^{32}$P-orthophosphate prior to challenge with the ligand. Following stimulation, the reaction was terminated by addition of lysis buffer. HA-tagged receptors were immunopurified using anti-HA antibody conjugated beads. Immunoprecipitated receptors were resolved by gel electrophoresis and visualised by autoradiography.

#### 2.2.11.1 NMU2-HA phosphorylation

Cells expressing NMU2-HA or mutants were used to study receptor phosphorylation.

#### 2.2.11.2 Metabolic labelling with $^{32}P$, ligand stimulation, purification and autoradiography

Cells in ploy-D-lysine coated 6-well plates were cultured to ~ 95 % confluency per well over a 24 h period before the experiment. Cells were washed twice with 1 ml phosphate-free KHB (HEPES, 10 mM; $NaHCO_3$, 4.2 mM; glucose, 11.7 mM; $MgSO_4$, 1.18 mM; KCl, 4.7 mM; NaCl, 118 mM and; $CaCl_2.2H_2O$, 1.29 mM; pH 7.4). Following equilibration at 37 °C for 30 min, cells were labelled by incubating with the $^{32}P$-orthophosphate (50 µCi / ml) for 1 h. Cells were challenged with ligand in the required concentration for the required time. Reactions were terminated by aspiration of the buffer followed by addition of 0.5 ml of ice-cold lysis buffer (composition: Tris HCl, 20 mM, pH 7.4; NaCl, 150 mM; EDTA, 3 mM; IGEPAL CA-630, 1 %; sodium deoxycholate, 25 %) containing protease and phosphatase inhibitors for 30 min on ice. Cell lysates were transferred to 1.5 ml Eppendorf tubes and the samples centrifuged at maximum speed (16000 xg) for 20 min at 4 °C to remove the debris. To purify the HA-tagged receptor from the cell lysates, the supernatants were transferred into clean Eppendorf tubes and incubated with 40 µl anti-HA tag-conjugated beads at 4 °C for 3 h or overnight using end-over-end rotor. The beads were then washed 3 - 4 times with 1 ml ice-cold lysis buffer. Following the last wash, 50 µl of 2X sample buffer (Tris-base, 125 mM, pH 6.8; SDS 4 % w/v; glycerol 20 % v/v; bromophenol 0.01 % w/v; dithiothreitol, 250 mM (freshly prepared on the day of experiment)) was added. Samples were then heated for 5 min at 50 °C using a heat block to dissociate the immunocomplexes. The samples were mixed by vortexing and centrifuged at 16000 xg for 2 min. The purified HA-tagged receptors were resolved using 10 % SDS gel electrophoresis. In brief, 40 µl of each sample was loaded per lane and electrophoresis performed at 100V for 2 h until the blue line reached the bottom of the gel using a POWER PAC 300. The gel was transferred into a tray and incubated with fixing buffer (composition: methanol, 50 % v/v; acetic acid 10 % v/v and; $H_2O$ 40 % v/v) for 15 min using a platform shaker. The gel was put on a piece of filter paper, covered with plastic wrap film and dried at 80 °C for 1 h using a gel dryer with a vacuum pump (SCIE-PLAS, UK). The dried gel was removed from the gel dryer, covered with a plastic wrap film and fixed on the X-ray hypercassette with an appropriate tape. X-ray film was put over the gel inside the X-ray hypercassette and incubated at - 80

°C for 3 h, 6 h or 1 day according to the signal intensity of the phosphorylation bands. These bands were calculated by densitometry and represented as densitometric units.

### 2.2.12 Bioluminescence resonance energy transfer (BRET) assay

BRET is a natural phenomenon that is seen in some sea animals. It is characterised by transferring the energy following oxidation of the enzyme substrate from a luminescence donor enzyme to the adjacent acceptor molecule when they are in a close proximity. This transfer of energy between two molecules is inversely proportional to the $6^{th}$ power of the distance between the interacting molecules providing a powerful assay for assessment of protein-protein interaction (Pfleger *et al.*, 2006).

#### 2.2.12.1 BRET assay requirements

To study the interaction between two proteins using BRET, there are a number of requirements. For example, one of the proteins must be genetically engineered to contain an enzyme donor such as nanoluciferase (nLUC) or renilla luciferase (RLuc). The other protein must be fused with an acceptor fluorescent protein such as yellow fluorescence protein (YFP). A substrate such as coelenterazine h then needs to be provided to allow the enzyme (nLUC or Rluc) to oxidise it, resulting in emission of light that excite the fluorescent protein such as YFP which, in turn, emits yellow light. Light intensities of both donor (nLUC or Rluc) and acceptor (YFP) can be recorded using a ClarioStar microplate reader (BMG Labtech; Offenburg, DE). The acceptor : donor ratio can be calculated and represents BRET ratio **(Figure 2.3)**. To use as a cell-based assay, cells must be transfected with and express these constructs. The present study was conducted to study the interaction between NMU2 and the arrestins, either arrestin 2 or arrestin 3. To allow this, the following three constructs were generated: NMU2 tagged with nLUC (NMU2-nLUC); arrestin 2 tagged with YFP and; arrestin 3 tagged with YFP **(see Chapter 5; Sections, 5.2.1, 5.2.2, 5.2.3)**. In this assay, cells were transfected with the appropriate constructs and 48 h later stimulated with ligands. Coelenterazine h was added for the last 10 min of the experiment and BRET signals detected at 535 nm (YFP) or 465 nm (nLUC) **(Figure 2.3)**.

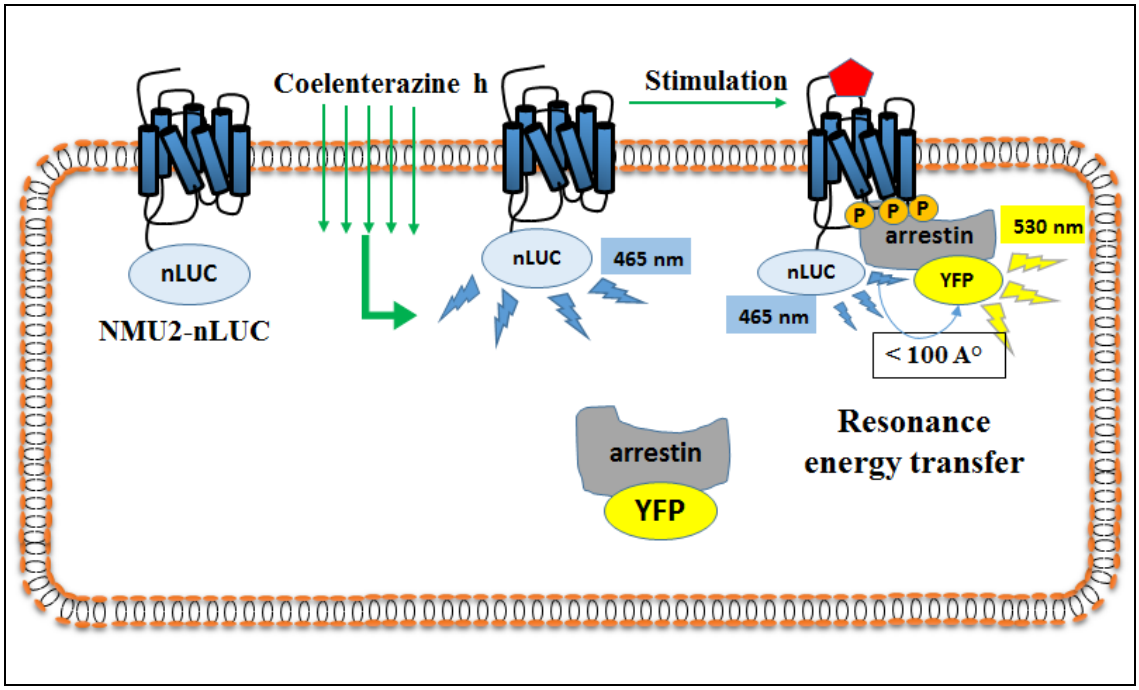


**Figure 2.3 BRET assay principle**

The scheme shows that addition of coelenteraxine h (substrate) to cells expressing donor (nLUC-tagged receptor) and acceptor (YFP-tagged arrestin), mediates its oxidisation by nLUC-tagged receptors thereby causing emission of light at wavelength 465 nm. Upon ligand binding, nLUC-tagged receptors are activated and phosphorylated, resulting in desensitisation and recruitment of YFP-tagged arrestin. If the two molecules (donor and acceptor) in a close proximity, the light emitted from the donor will be captured by the acceptor, resulting in energy transfer and excitation of acceptor. The excited acceptor then emits a light at wavelength 530 nm (YFP). The BRET ratio can be measured by quantification of the amount of YFP light divided by the amount of the nLUC light.

### 2.2.12.2 Saturation BRET assay

To study the interaction between NMU2 and the arrestins, a titration assay was performed in which a fixed amount of the donor (NMU2-nLUC) was added with an increasing quantity of the acceptor (arrestin 2- or 3-YFP). This assay was designed to determine the optimal amount of the acceptor that achieves a maximal interaction between NMU2-nLUC and either arrestin 2- or 3-YFP following stimulation compared to the unstimulated group (control). To do this, HEK-293 were cultured in 6-well plates (250,000 cell per well) for 24 h to ~ 60 - 70 % confluence and then transfected with a constant amount of the appropriate donor (NMU2-nLUC, 50 ng) and increasing amounts of acceptor (arrestin 2-YFP or arrestin 3-YFP; 0, 100, 200, 300, 400, 500, 600, 700, 800, 900, 1000, 1200 ng per well) **(Figure 2.4, a)**. The transfection was performed using PEI MAX reagent.

PEI MAX was prepared at 1 mg / ml stock. For 6-well plates, 9 µg of this stock (9 µl) was diluted with 150 µl of Opti-MEM in a sterile 1.5 ml Eppendorf tube. X ng of each of the appropriate constructs were diluted with 150 µl of Opti-MEM in another sterile 1.5 ml Eppendorf tube. The diluted PEI MAX was added to the diluted constructs followed by gentle pipetting up and down. The mixture was left to stand for 30 min at RT, then added drop by drop into the well and the plate was return back to the incubator for a further 24 h. after 24 h post-transfection, cells were detached with 100 µl of PBS/ EDTA (1mM) per well and re-suspended in 900 µl of DMEM GlutaMax medium. Cells were then sub-cultured on a poly-D-lysine coated white-bottomed 96-well microplate (in this case, each well of a 6-well plate was sufficient to plate one strip of a 96-well plate; 100 µl / well) **(Figure 2.4, b)**. The plate was returned to the incubator for a further 24 h. Cells were then washed twice with HBSS buffer and 80 µl of the same buffer added into each well. Following equilibration for 30 min at 37 °C, fluorescence background was measured at 535 ± 20 nm using a ClarioStar microplate reader (BMG Labtech; Offenburg, DE). The BRET assay was performed by incubating with coelenterazine h (substrate) (Nanolight Technology, USA) at a final concentration of 5 µM for the last 10 min of the experiment. During the last 5 min of the substrate incubation, the ligand or buffer (vehicle control) was added at the required concentration and the signals were measured at 535 ± 20 nm and 465 ± 20 nm **(Figure 2.4, b)**. The BRET signal was calculated using the following equation:

**BRET signal** = [acceptor emission / donor emission] – [acceptor emission / donor emission in the cells transfected with donor only].

Thus, the data are presented as a ratio of the acceptor over the donor (BRET ratio) on the Y-axis while the acceptor over the donor expression ratio was represented on the X-axis **(Figure 2.4, c)**. Data were fitted with a one site binding hyperbola using GraphPad Prism. The maximal BRET (BRET max) is defined as the maximal interaction between the donor and acceptor while the $BRET_{50}$ represents the acceptor over donor expression ratio that gives 50 % of the maximal BRET ratio **(Figure 2.4, c)**.

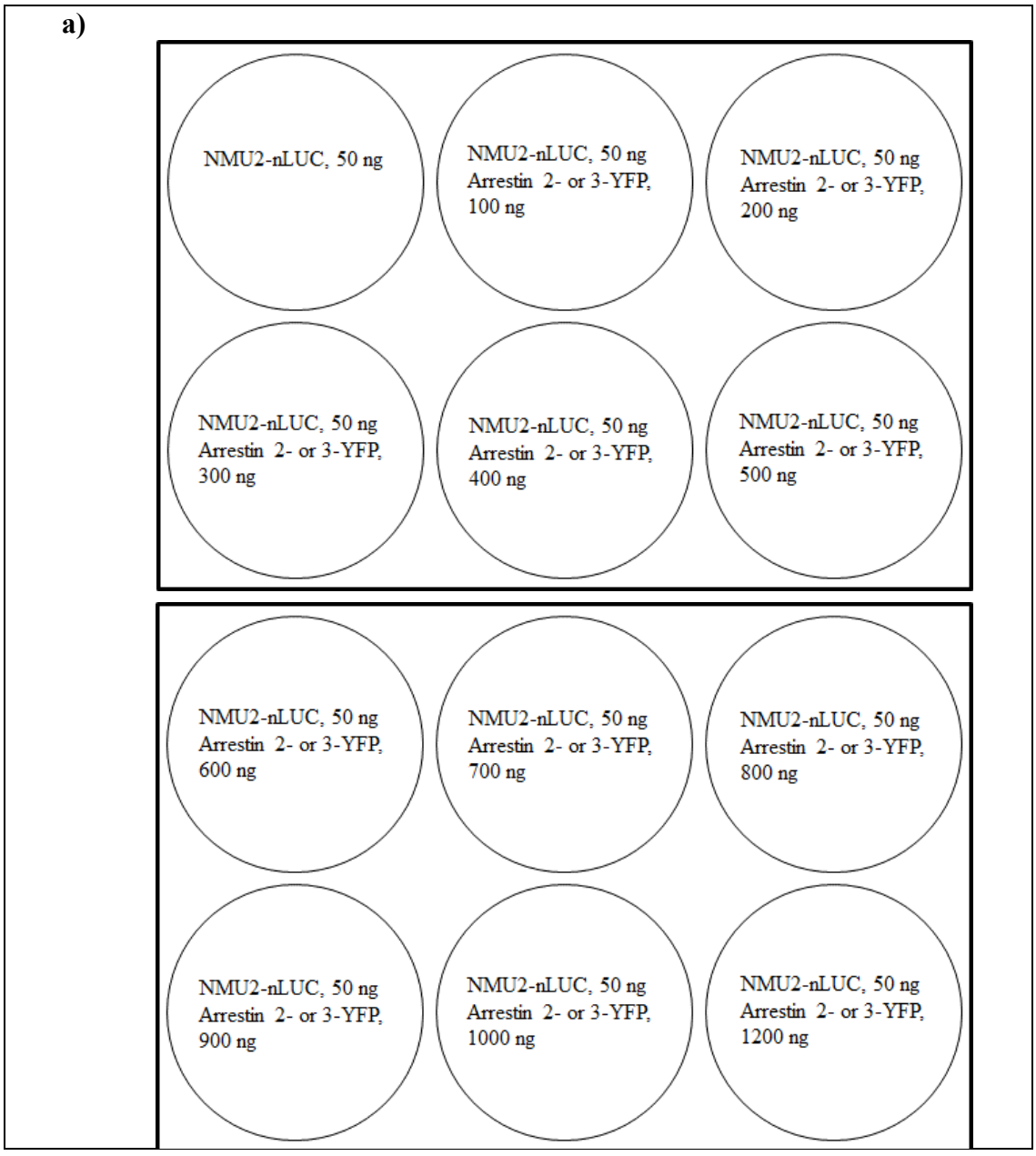

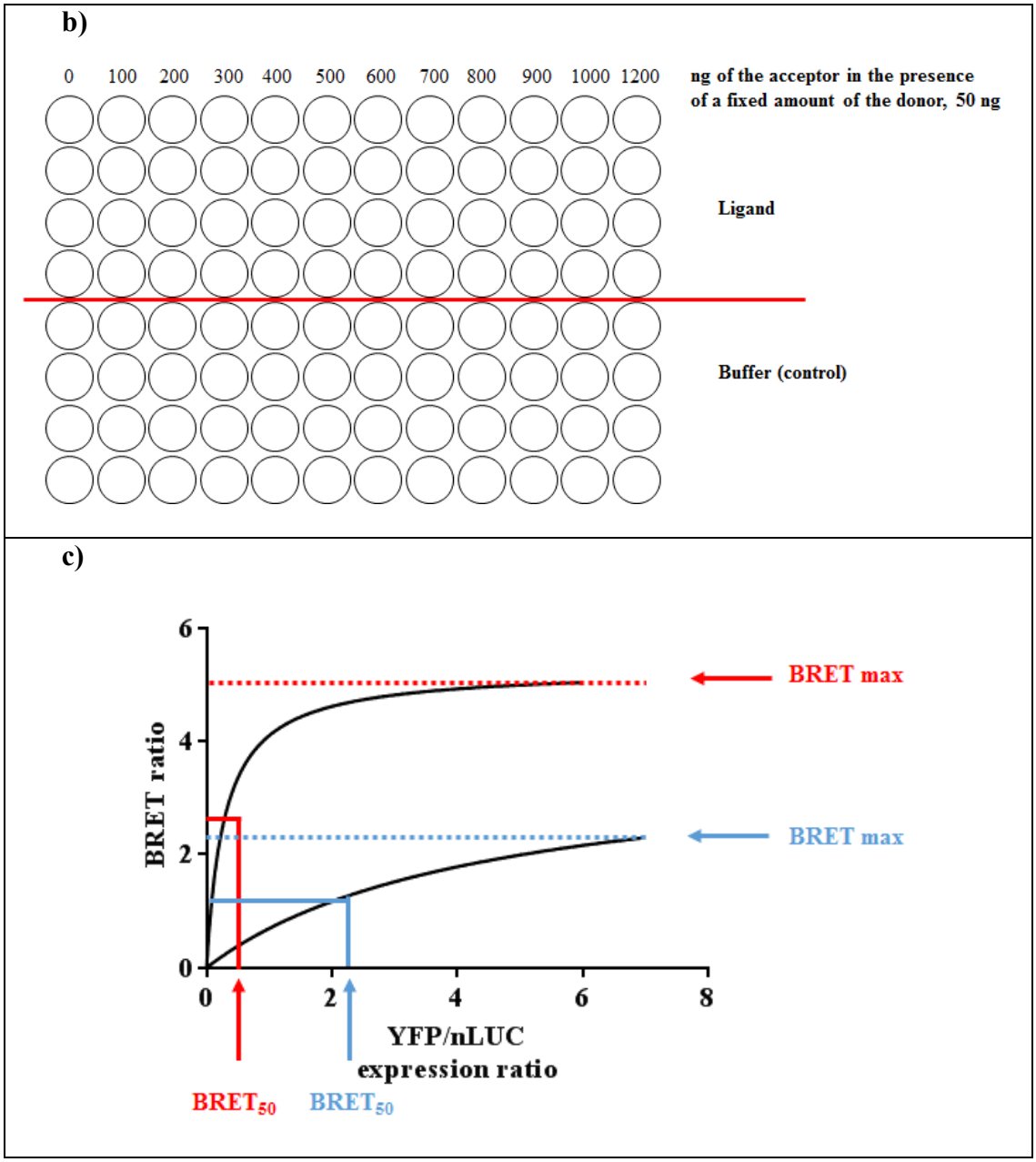


**Figure 2.4 Experiment design and hyperbolic curve used for saturation assay**

a) Experimental design using 6-well plates in which the cells were cultured and transfected with a constant amount of the donor with an increasing amount of the acceptor as indicated. b) White-bottomed 96-well plate in which the co-transfected cells were cultured. In each well of the each strip contains a fixed amount of the donor and indicated amount of the acceptor. c) Hyperbolic curve showing the maximal interaction between the donor and acceptor (BRET max) (dotted lines) while the $BRET_{50}$ refers to the acceptor over the donor expression ratio that gives half of the BRET max (solid lines).

#### 2.2.12.3 Generation of concentration-response curves for NMU2-nLUC interaction with arrestins

After generation of the saturation BRET assay for arresten 2-YFP or arrestin 3-YFP interaction with the NMU2-nLUC in response to the ligand, concentration-response relationships were generated using the optimal quantity of arrestin 2- or 3-YFP (acceptor) obtained **(Chapter 5; Section 5.3)**. HEK-293 were grown in 10 ml dishes (1250000 cell per dish, 9.5 ml media) for 24 h to 60 - 70 % confluence. Two dishes were needed; one was co-transfected with NMU2-nLUC (donor) and either arrestin 2-YFP or arrestin 3-YFP and another dish was transfected with NMU2-nLUC only using the PEI Max transfection reagent as follows:

Following growing the cells in a 10 ml dish, the transfection reagent was prepared by dilution of PEI MAX (1 mg / ml stock, 21 µl) with Opti-MEM (250 µl) in a sterile 1.5 ml Eppendorf tube for each dish. Two sterile 1.5 ml Eppendorf tubes containing Opti-MEM (250 µl) were also prepared in which NMU2-nLUC construct (250 ng) was diluted into the first and NMU2-nLUC (250 ng) and either arrestin 2-YFP (6 µg) or arrestin 3-YFP (4 µg) were diluted into the second one. The diluted PEI MAX was added to the diluted constructs followed by gentle pipetting up and down. The mixtures were left to stand for 30 min at RT and added drop by drop into the dished which were then returned to the incubator for a further 24 h. Cells were then detached with 1 ml of PBS/ EDTA (1mM) followed by re-suspension in 9 ml of DMEM GlutaMax medium. The cell suspension containing only NMU2-nLUC was sub-cultured on the first strip of a poly-D-lysine coated white-bottomed 96-well microplate while NMU2-nLUC with either arrestin 2- or 3-YFP was plated into the rest of the strips (100 µl / well) for a further 24 h **(Figure 2.5)**. On the day of the experiment, cells were washed twice with HBSS buffer and 80 µl of the same buffer added into each well. Fluorescence background was measured at 535 ± 20 nm using a ClarioStar microplate reader (BMG Labtech; Offenburg, DE) to assess the efficiency of transfection and expression of the constructs. Cells were pre-incubated with the substrate, coelenterazine h (5 µM), for the last 10 min of the experiment. During the last 5 min of the substrate incubation, different concentrations of ligand were added and the signals were measured as described **(Section 2.2.12.2)**. Concentration-response curves were fitted with a four parameter logarithmic equation using Graphpad Prism in which the Y axis represents the BRET ratio and X axis is concentrations of the ligand.

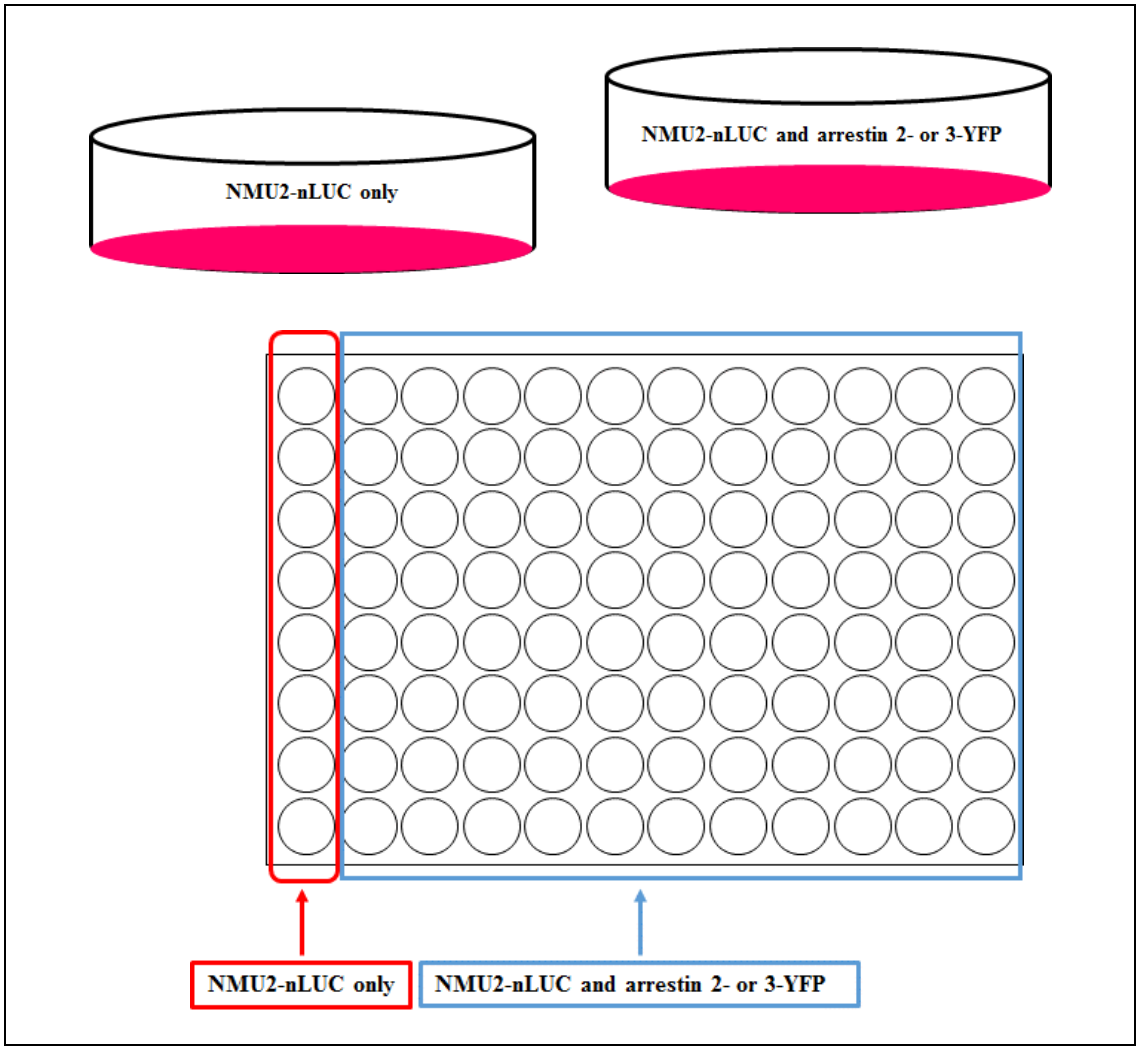


**Figure 2.5 Strategy for the plating of cells to study the concentration-response relationships**

### 2.2.13 Detection of NMU2 phosphorylation sites by mass spectrometry

Mass spectrometry is a powerful tool that has been used to study the phosphorylation sites for a number of GPCRs such as free fatty acid and chemokine receptors (Busillo *et al.*, 2010; Chen *et al.*, 2013; Butcher *et al.*, 2014). This approach was exploited to analyse the NMU2 phosphorylation sites following stimulation with ligand. This technique also requires efficient purification of the receptor from the cell lysates making the use of the HA-tagged NMU2 construct ideal. The steps for the determination of the sites of NMU2 phosphorylation are summarised in **Figure 2.6**.

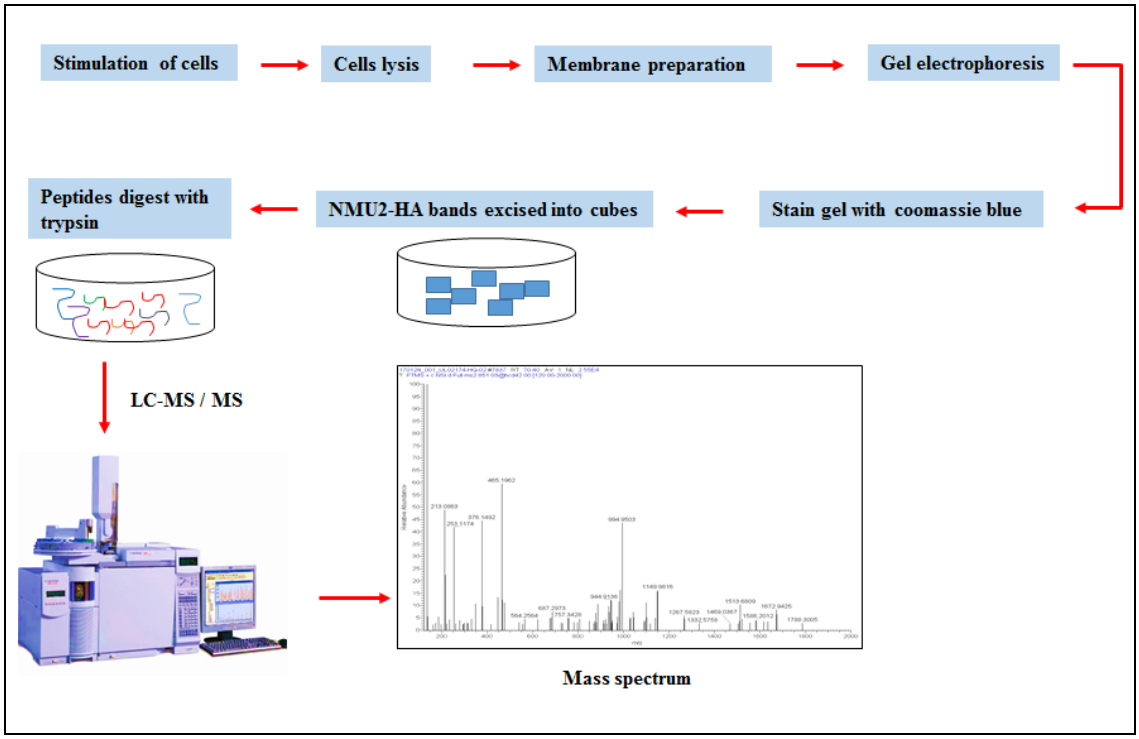


**Figure 2.6 Schematic diagram exploring the brief protocol for identification of phosphorylation sites**

The scheme represents a series of methods for identification of the sites of phosphorylation using mass spectrometry. After growing the cells to ~ 95 % confluence, they were then stimulated with ligand or vehicle control. Cells were lysed by appropriate lysis buffer and membranes prepared. After immunoprecipitation of HA-tagged receptors using anti-HA-conjugated beads, they washed and a sample buffer added. HA-tagged receptors were resolved by gel electrophoresis and stained with coomassie dye. HA-tagged receptors bands were cut in cubes and sent for analysis supplied by PNACL.

#### 2.2.13.1 Stimulation and membranes preparation for assessing the phosphorylation of NMU2 by mass spectrometry

HEK-NMU2-HA were grown in 175cm$^2$ flasks (10 flasks) to ~ 95 % confluency. On the day of the experiment, cells in each flask were washed twice with KHB buffer and detached using DPBS / 1mM EDTA, 5 ml, pH 7.4. Detached cells were transferred into a 50 ml Falcon tube and centrifuged at 750 xg for 5 min. Following removal of the supernatant, cells were gently re-suspended in KHB and incubated at 37 °C for 1 h with continuous shaking every 10 min to avoid the cells from becoming attached. Cells were stimulated with hNmU-25 (1µM), hNmS-33 (1 µM) or KHB for 5 min followed by removal of the buffer and addition of 10 ml of ice-cold TE buffer (Tris-HCl, 10 mM; EDTA, 1 mM, pH 7.4) containing protease and phosphatase inhibitors (Phosphostop tablets, Complete mini EDTA-free tablets; one tablet per 10 ml). Cell lysates were lysed by applying pluses three times every 10 s at 4 °C using homogeniser. The sample was transferred into a centrifuge tube and centrifuged at 40000 xg for 1 h at 4 °C. The supernatant was removed and the membrane pellets stored at - 80 °C until use.

#### 2.2.13.2 Gel preparation for mass spectrometry

Membrane pellets were re-constituted with 5 ml of the buffer (PBS containing EDTA, 1 mM; IGEPAL CA-630 1 %, Phosphostop tablets, Complete mini EDTA-free tablets; one tablet per 10 ml) and incubated on ice for 1 h. The sample (5 ml) was divided into 1.5 ml Eppendorf tubes (1 ml per tube) and membrane preparations centrifuged at 16000 xg for 20 min at 4 °C to pellet any insoluble material. The supernatant was collected in a 15 ml centrifuge tube and diluted at ratio 1 : 1 by addition of an equal volume of PBS / EDTA. Anti-HA antibody conjugated beads (300 µl) were added to the diluted supernatant and incubated overnight at 4 °C with continuous rolling using a platform roller. Immunocomplexes were then collected by centrifugation at 1000 xg for 1 min at 4 °C and washed four times with buffer (PBS containing EDTA, 1 mM; IGEPAL CA- 630, 0.5 %, 10 ml). Following a last wash with (PBS; EDTA, 1 mM; IGEPAL CA- 630, 0.5 %; NaCl, 500 mM), the supernatant was removed carefully and 150 µl of 2X sample buffer (Tris-base, 125 mM, pH 6.8; SDS 4 % w/v; glycerol 20 % v/v; bromophenol 0.01 % w/v; dithiothreitol, 100 mM) added. Immunocomplexes were heated for 5 min at 65 °C using a heat block followed by vortexing and centrifugation at 1000 xg for 1 min. The purified NMU2-HA receptors were resolved using 10 % SDS-PAGE. In brief, the samples were loaded on a gel (Eurogenic, Belgium) and run at 100 V for 2 h until the

blue dye moved out of the gel. The stacking gel was then removed followed by transferring resolving gel from the glass plate onto a tray. The gel was washed three times with $H_2O$ every 15 min using a platform shaker. The gel was then incubated with coomassie blue stain (Simply Safestain-1L, Life Technologies, Paisley, UK) for 1 h at RT in a volume that covered the gel. The gel was then washed with water for 1 h and NMU2-HA bands were excised in small pieces using a scalpel blade. The gel pieces were then transferred into a clean Eppendorf tube and submitted to Protein Nucleic Acid Chemistry Laboratory (PNACL), (University of Leicester, UK) for identification of phosphorylation sites using LC-MS / MS analysis. The data were received as Excel sheets indicating the peptide fragments that were detected by mass spectrometry (including the number of times the peptide fragment was detected and the number of times a phosphorylated serine/threonine residue was observed within the peptide fragment). The number of times for both the detected peptide fragment and those residues assigned as phosphorylated was manually calculated for each experiment. The total number of times represents the number of observations in the three experimental repeats for each group **(See Figure 6.3)**.

### 2.2.14 Generation of mutants and establishment of cell lines with a stable expression of these mutants

After identification of sites of NMU2 phosphorylation **(Section; 6.1)**, three mutants of NMU2-HA were generated each containing a number of serine/threonine to alanine mutations. One mutant (NMU2-HA-M1) included mutations of five phosphorylation sites detected by mass spectrometry, the second (NMU2-HA-M2) contained mutations of seven potential phosphorylation sites, which were not covered by mass spectrometry. The third mutant (NMU2-HA-M3) contained mutations of fourteen phosphorylation sites including five phosphorylation sites that had been detected by mass spectrometry, seven potential phosphorylation sites (not covered by mass spectrometry) and two potential phosphorylation sites (detected by mass spectrometry but not phosphorylated). Two fragments were generated to form each mutant. The first fragment started from the start codon of NMU2 sequence and ended in an AfeI restriction site present within the NMU2 sequence (1 - 421 bp). This was generated by PROTEX Services (University of Leicester). The second fragment containing the mutations were synthesised by Eurofins (Wolverhampton, UK) and started from AfeI restriction site to XbaI (421 - 1267 bp), further details are provided elsewhere **(Section; 6.3.1)**. These fragments were cloned into

pEX-A128 vectors. Both fragments, 1 and 2 were then amplified and joined using appropriate forward and reverse primers and cloned into pLEICS-12 vector by PROTEX Services (University of Leicester) **(Section; 6.3.1)**. Further details are provided elsewhere **(Chapter six)**.

### 2.2.15 Statistics

All data were analysed by Graphpad Prism 7 Software (San Diego, CA, USA) and presented as mean ± sem, $n \geq 3$ unless otherwise stated. Concentration-response relationships were fitted with a four parameter logarithmic equation using Graphpad Prism 7. A four parameter fit was used as no assumptions were made regarding the slope factor as these were functional experiments. Slope factors were not included in the tables of concentration-responses curves as they provide little interpretive value for such functional assays. For multiple comparisons, one- or two-way analysis of variance (ANOVA) tests followed by Bonferroni's test were performed. Bonferroni's adjustment is a post-hoc multiple comparison test that limits the type I error rate in a conservative manner, thereby reducing the likelihood of false positive results. For the BRET saturation assay, curves were fitted with a one site binding hyperbolic equation. Statistical significance was accepted at $P < 0.05$. The statistical analyses used are described in the figure legends.

# 3 Chapter three: Generation and characterisation of HEK-293 cells expressing NMU2 with a *C*-terminal HA tag (NMU2-HA)

## 3.1 Introduction

NMU1 and NMU2 are Family A, G-protein coupled receptors that mediate the actions of distinct but structurally related neuropeptides, NmU and NmS. Both receptors couple preferentially to $G\alpha_{q/11}$ leading to $Ca^{2+}$ mobilisation by activation of the phospholipase C pathway ($IP_3$-$Ca^{2+}$-PKC axis) (Aiyar *et al.*, 2004; Brighton *et al.*, 2004b). Differential distribution of both receptors and ligands suggests divergent biological responses **(Section 1.2.2, 1.3.2)**. It is now well established from a variety of studies that central expression of the NMU2 is responsible for regulation of a variety of effects, particularly the suppression of feeding behaviour and enhancement of energy expenditure highlighting a potential anti-obesity target (Hosoya *et al.*, 2000; Howard *et al.*, 2000; Shan *et al.*, 2000; Mitchell *et al.*, 2009). It has been reported that NMU2 knockout mice were hungry and showed an increase in food intake (Egecioglu *et al.*, 2009). NmU appears to be scattered in different regions of the brain; thus showing low mRNA levels in the whole brain while NmS is restricted centrally, particularly in the suprachiasmatic nuclei of hypothalamic tissue (Mori *et al.*, 2008; Mitchell *et al.*, 2009). Both ligands mediate a myriad of functions, particularly the suppression of feeding-related behaviour with some reports suggesting that NmS mediates these effects more persistently than NmU, therefore, characterisation of NMU2 signalling in response to NmU or NmS was of particular interest (Ida *et al.*, 2005). Previous reports have shown cell signalling mediated by recombinant NMU2 including $Ca^{2+}$ signalling, ERK and P38 activation. In addition, NMU2 was shown to resensitise (on the basis of $Ca^{2+}$ signalling) at a faster rate following desensitisation by hNmU-25 compared to hNmS-33. One explanation for this is that there are ligand-dependent differences in the rates of receptor recycling (Alhosaini *et al.*, 2018). Furthermore, although the patterns of ERK and P38 activation were identical (sustained) in the continued presence of either hNmU-25 or hNmS-33, this was not true with brief ligand exposure, which may more accurately reflect the situation *in vivo*. Thus, under these circumstances, activation of ERK and P38 were more sustained in response to NmS than NmU (Alhosaini *et al.*, 2018). The difference in the rates of NMU2 resensitisation and MAP kinases signalling between NmU and NmS may be a consequence of different types or temporal profiles of receptor-arrestins interaction (Yang *et al.*, 2017). Given that arrestin recruitment is generally a consequence of receptor

phosphorylation (Tobin *et al.*, 2008), this study therefore set out to assess NMU2 phosphorylation and arrestin recruitment in response to either hNmU-25 or hNmS-33. To study receptor phosphorylation, a critical requirement was to be able to immunoprecipitate NMU2. Given the lack of appropriate antibodies, the first challenge was to generate an epitope-tagged NMU2 which could then be used to immunoprecipitate the receptor.

Different epitopes along with their specific antibodies, are commercially available and used for a variety of purposes, particularly GPCR purification and studies of expression and trafficking (Huang *et al.*, 2011). In this study, a hemagglutinin (HA) tag was selected and fused with NMU2 at *C*-terminus (NMU2-HA). This tag has been used previously in a variety of GPCRS to study receptor phosphorylation without influencing signalling functions (Butcher *et al.*, 2011; Prihandoko *et al.*, 2016b; Zindel *et al.*, 2016). Therefore, work described in this chapter aimed to generate a cell line with stable expression of NMU2-HA. Furthermore, different functional assays were employed to compare the newly generated cell line that expresses the tagged version (NMU2-HA) with an untagged version of the NMU2 that had been previously characterised (Brighton *et al.*, 2004b; Alhosaini *et al.*, 2018) to ensure the tag had not impacted on NMU2 functions.

## 3.2 Results

### 3.2.1 Generation of NMU2-HA construct

NMU2-HA was generated by PCR using forward and reverse primers with an existing untagged version of the receptor as the template. The forward primer contained a restriction site for XhoI at the beginning that was to be used for the sub-cloning step, a Kozak sequence to promote the translation process and a start codon before the NMU2 sequence **(Figure 3.1)**. The reverse primer contained an HA tag sequence followed by a stop codon and a restriction site for XbaI after the NMU2 sequence **(Figure 3.1)**. The generation of NMU2-HA was by PCR amplification and the resulting PCR products were resolved by agarose gel electrophoresis. The bands were then viewed under UV light to validate the expected fragment size of NMU2-HA (~ 1.26 kb) before the sub-cloning step **(Figure 3.2; a)**. Two restriction sites for XhoI and XbaI in the forward and reverse primers respectively were used to sub-clone NMU2-HA into pcDNA 3.1+ as indicated **(Figure 3.2; b)**. Both NMU2-HA (insert) and pcDNA 3.1+ (vector) were double digested using XhoI and XbaI to generate two sticky ends which were then joined to form the final construct as indicated **(Figure 3.2; b)**. After ligation and transformation of the ligated NMU2-HA construct, at least six colonies were randomly selected and examined on agarose gel electrophoresis following XhoI and XbaI digests. Data showed that the running of resulting NMU2-HA construct in the absence of restriction enzymes resulted in a circular plasmid (supercoiled). Digestion with either XhoI or XbaI resulted in linear constructs running at the predicted sizes of (~ 6.69 kb). Two fragments of the expected sizes were separated following the double digests with XhoI and XbaI. These fragments were NMU2-HA (~ 1.26 kb) and the linear pcDNA 3.1+ vector (~ 5.43 kb) **(Figure 3.2; c)**. The resulting NMU2-HA construct was also validated via DNA sequencing (PNACL; University of Leicester) **(Figure 3.2; d, e)**.

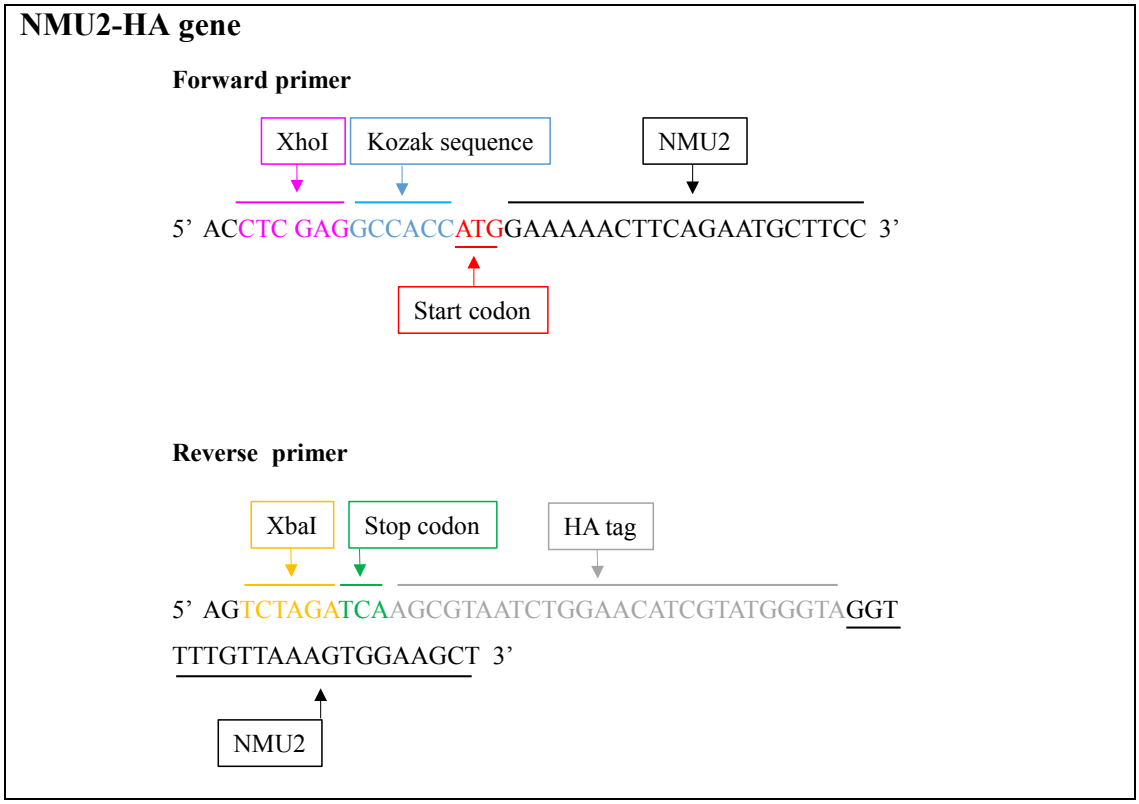


**Figure 3.1. Primer design of NMU2-HA**

Two primers were designed to generate the NMU2-HA gene. The forward primer contained a restriction site for XhoI (purple), a Kozak sequence (blue) and a start codon (red) before the primary sequence for NMU2 (black). The reverse primer contained a restriction site for XbaI (orange) and a stop codon (green) before the HA sequence (grey).

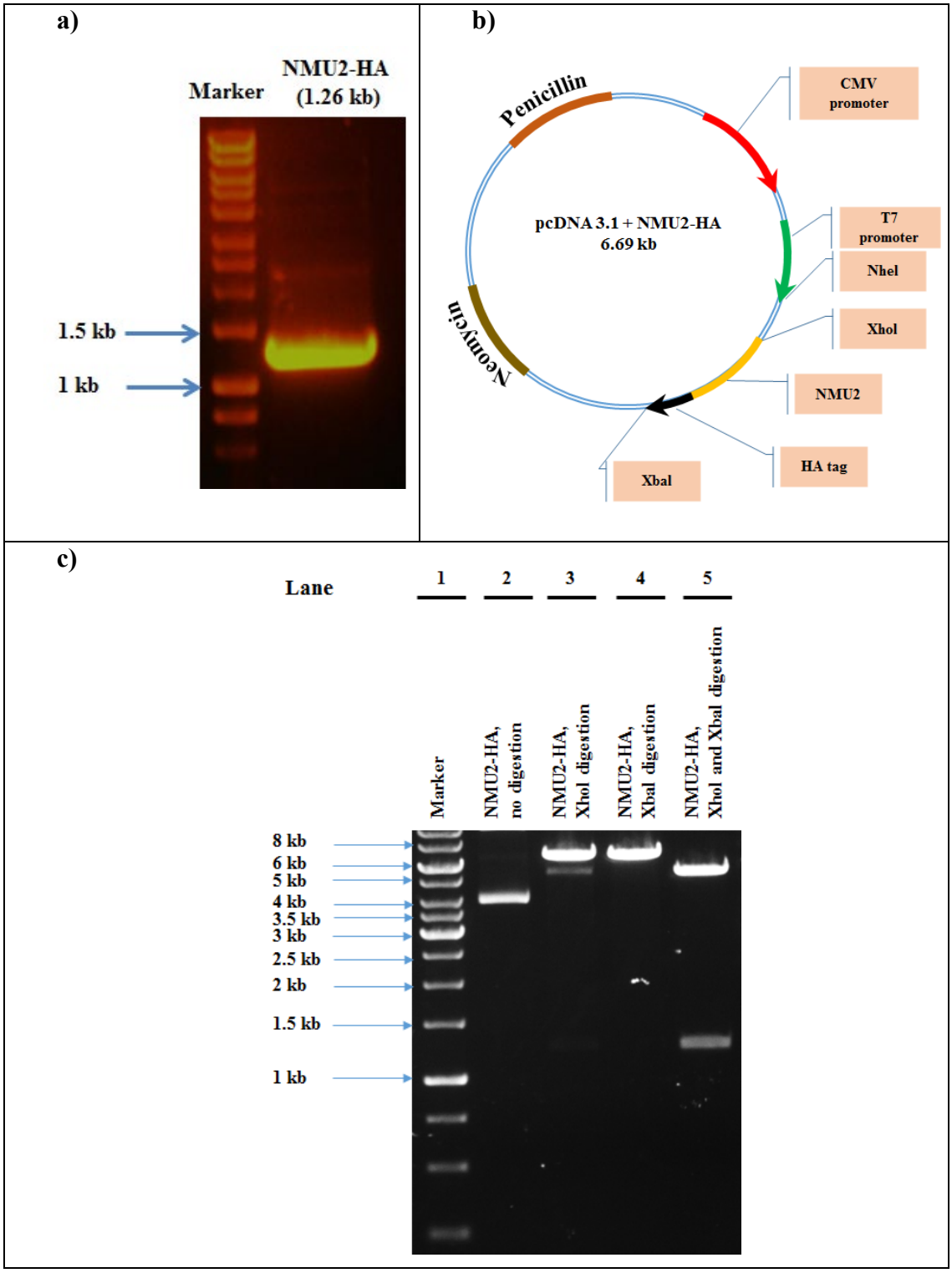
a)
Marker
NMU2-HA
(1.26 kb)
1.5 kb
1 kb
b)
Penicillin
Neomycin
pcDNA 3.1 + NMU2-HA
6.69 kb
CMV
promoter
T7
promoter
NheI
XhoI
NMU2
HA tag
XbaI
c)
Lane
1
2
3
4
5
Marker
NMU2-HA,
no digestion
NMU2-HA,
XhoI digestion
NMU2-HA,
XbaI digestion
NMU2-HA,
XhoI and XbaI digestion
8 kb
6 kb
5 kb
4 kb
3.5 kb
3 kb
2.5 kb
2 kb
1.5 kb
1 kb

**d)** NMU2-HA forward sequencing

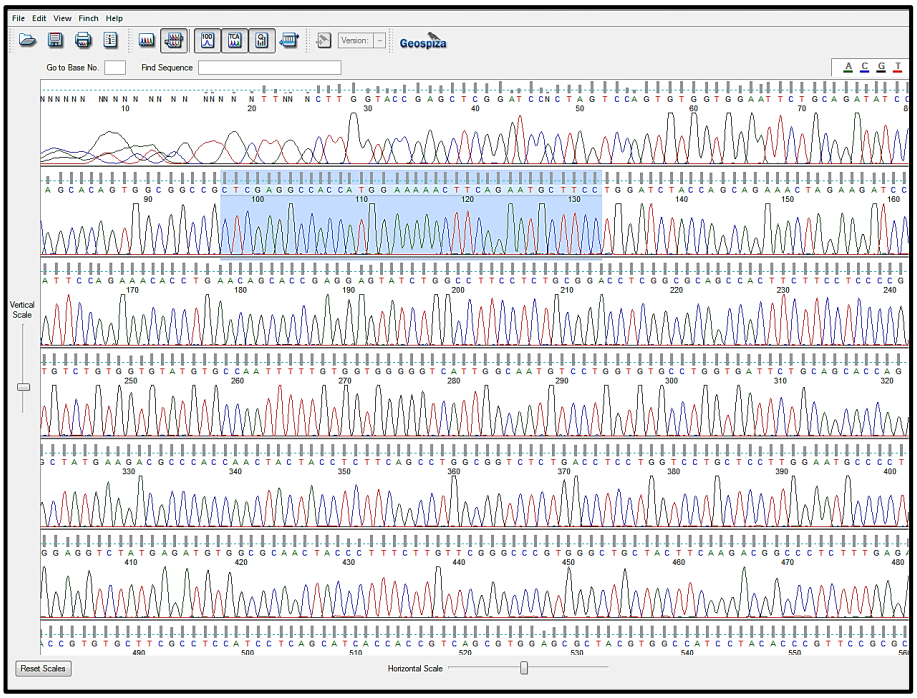


**e)** NMU2-HA reverse sequencing

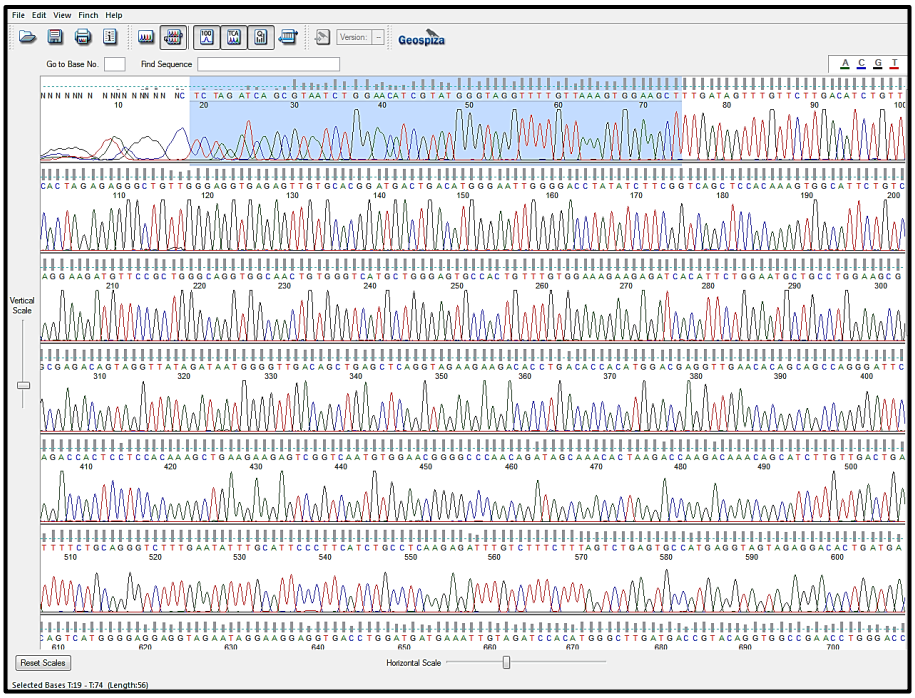


**Figure 3.2. PCR amplification, map of NMU2-HA construct and validation restriction digest of NMU2-HA**

The NMU2-HA sequence was generated by PCR amplification from a vector containing an untagged version of the receptor using the primers indicated in **(Figure 3.1)**. The PCR products were then separated using agarose gel electrophoresis and detected under UV light (a). The map showing NMU2-HA in pcDNA 3.1+ (b).The NMU2-HA construct

generated from ligation of the PCR product (a) into pcDNA 3.1+ was validated using XhoI and XbaI restriction enzymes (c). The lanes were: a size marker (lane 1); circular construct (no digestion) (lane 2); construct digested with either XhoI (lane 3) or XbaI (lane 4) or double digestion with XhoI and XbaI (lane 5).

### 3.2.2 Transient and stable expression of NMU-HA in HEK-293: Establishment of HEK-293 with stable expression of NMU2-HA

After generation and validation of the NMU2-HA construct **(section 3.2.1)**, the next step was to examine the transient and stable expression of NMU2-HA in HEK-293 using immunoblotting with an anti-HA antibody to detect the receptor. HEK-293 cells were transfected with pcDNA 3.1+ containing NMU2-HA using JetPrime transfection kit **(see Methods)**. After 48 h, cells were either immediately solubilised for immunoblotting with anti-HA antibody (transient transfection) or treated with Geneticin (G418) to establish stable cell lines. Cells surviving under antibiotic selection were sub-cultured in high dilutions to obtain single cells, which were then grown into single colonies. Cells were selected, expanded and screened by immunoblotting with an anti-HA antibody. Immunoblots of the transient expression showed multi-bands located lower than 55 kDa and an indistinct band at ~ 80 kDa **(Figure 3.3; a)**. Immunoblotting of cell lysates from the colonies surviving under antibiotic selection showed a variety of immunoreactive patterns. For instance, of 48 colonies selected, some did not show any immunoreactivity including colonies 6, 9, 18 and 21 **(Figure 3.3; b)**. Colony 2 and 12 showed two faint bands; one band was broad at ~ 80 kDa and another was more narrow at ~ 47 kDa. Four colonies showed high levels of immunoreactivity with a large, intense band at ~80 kDa. A narrow band also detected in those colonies that was ~ 47 kDa **(Figure 3.3; b)**. Depending on the molecular mass of NMU2-HA that based on its sequence; ~ 47 kDa and the predicted glycosylated form; ~ 80 kDa which is a typical for GPCRs and represents the glycosylated version of the receptor (Li *et al.*, 2017a), one of the four intensively positive colonies was selected (colony 20) for further experimentations. The efficiency of immunoprecipitation using anti-HA conjugated beads was then determined. This is critical for the study of the receptor phosphorylation. Colony 20 was harvested and exposed to either immunoblotting with anti-HA antibody or immunoprecipitation using anti-HA conjugated beads. The immunoprecipitated NMU2-HA was then immunoblotted with an anti-HA antibody. The results showed clear immunoreactivity for both conditions and included two immunoreactive bands (~ 47 kDa based on the NMU2-HA sequence and ~ 80 kDa, consistent with the glycosylated form of the receptor (**Figure 3.4; a, b)**.

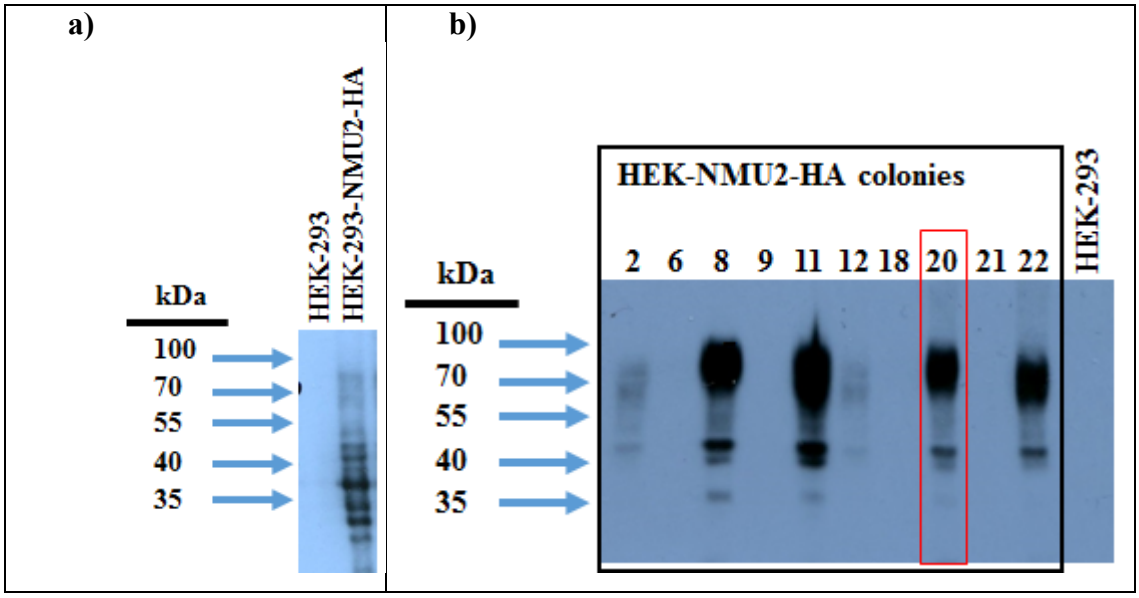


**Figure 3.3. Transient and stable expression of NMU2-HA**

HEK-293 cells in 6-well plates were transiently transfected with NMU2-HA. After 48 h, cells were washed twice with PBS and solubilised (a). (b) Stable cell line colonies generated by transfecting the HEK-293 with NMU2-HA and treating with geneticin. After three weeks of treatment, the survived cells were then sub-cultured in high dilutions to get single cells. The surviving cells were selected and allowed to grow up into colonies. Each selected colony was sub-cultured and plated in 24-well plates for 24 h. Cells were washed twice with PBS and solubilised. The samples from transiently transfected (a) or selected stable cell lines (b) were resolved by gel electrophoresis and immunoblotted with an anti-HA tag antibody **(see Methods)**. Colony 20 was selected and expanded to be used for experiments (red box). Untransfected HEK-293 cells was used as negative controls.

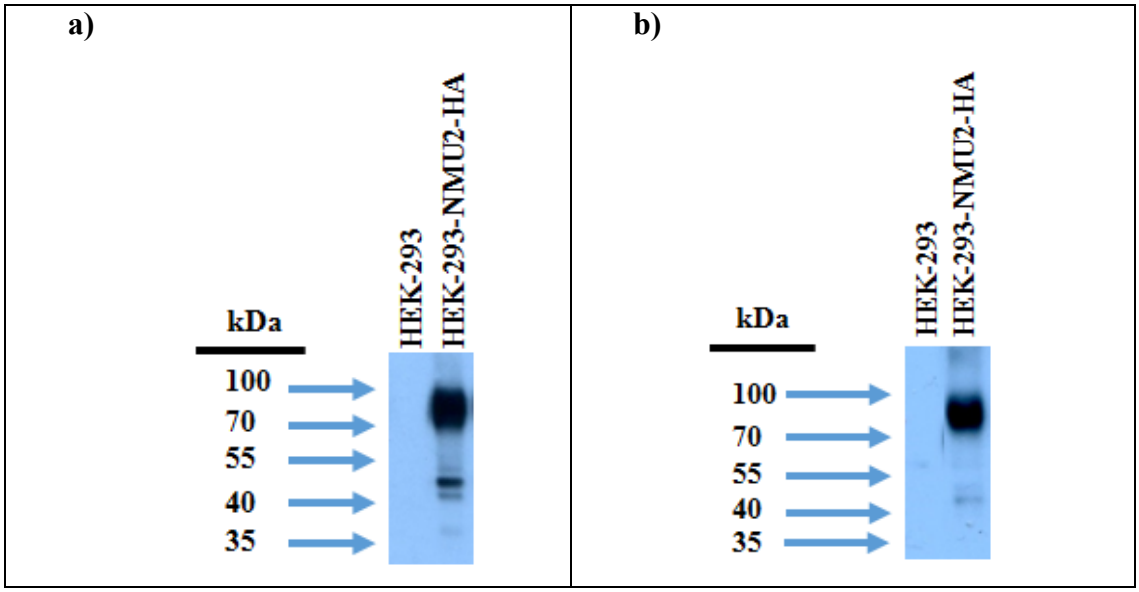


**Figure 3.4. Immunoblotting of either cell lysates or immunoprecipitated NMU2-HA with an anti-HA antibody**

HEK-293 cells with stable expression of NMU2-HA (colony 20) were washed twice with PBS and then solubilised. Cell lysates were resolved by gel electrophoresis and immunoblotted with anti-HA tag antibody (a). Cell lysates were immunoprecipitated using anti-HA tag conjugated beads and the NMU2-HA was then immunoblotted with an anti-HA tag antibody (b). Data are representative immunoblots of three independent experiments. Untransfected HEK-293 cells were used as negative controls.

### 3.2.3 Signalling characteristics of HEK-293 cells with stable expression of either NMU2 (HEK-NMU2) or NMU2 with a *C*-terminal HA tag (HEK-NMU2-HA)

#### 3.2.3.1 Concentration-response relationships of hNmU-25- and hNmS-33-mediated $Ca^{2+}$ signalling

$Ca^{2+}$ signalling was measured in HEK-NMU2 and HEK-NMU2-HA loaded with fluo-4-AM using different concentrations of hNmU-25 and hNmS-33. Both ligands caused concentration-dependent $Ca^{2+}$ increases in fluorescence as an index of increases in $[Ca^{2+}]_i$. Following addition of the ligand at 11s, a rapid peak was observed, particularly at higher agonist concentrations, followed by a gradual decline over the period of recording (approximately 40 - 45 s following challenge) **(Figure 3.5; A and $B_{i-ii}$)**. For instance, 100 nM of either hNmU-25 or hNmS-33 increased $Ca^{2+}$ responses that peaked at 4.0 ± 0.2 s and 4.9 ± 0.3 s respectively while at low concentrations, 1 nM of the ligands evoked increases that reached to the peak at 18.0 ± 0.9 s and 18.0 ± 0.7 s respectively **(Figure 3.5; $A_{iv}$, $B_{iv}$)**. Concentration-response relationships were similar for both ligands in the two cell lines with maximum changes at 30 nM (**Figure 3.5; $A_{iii}$, $B_{iii}$)**. Maximum changes in fluorescence were employed to generate concentration-response curves. The $pEC_{50}$ values for both ligands in the two cell lines are shown in **Table 3.1**. There were no significant differences between hNmU-25 and hNmS-33 in either untagged or HA-tagged versions of the receptor.

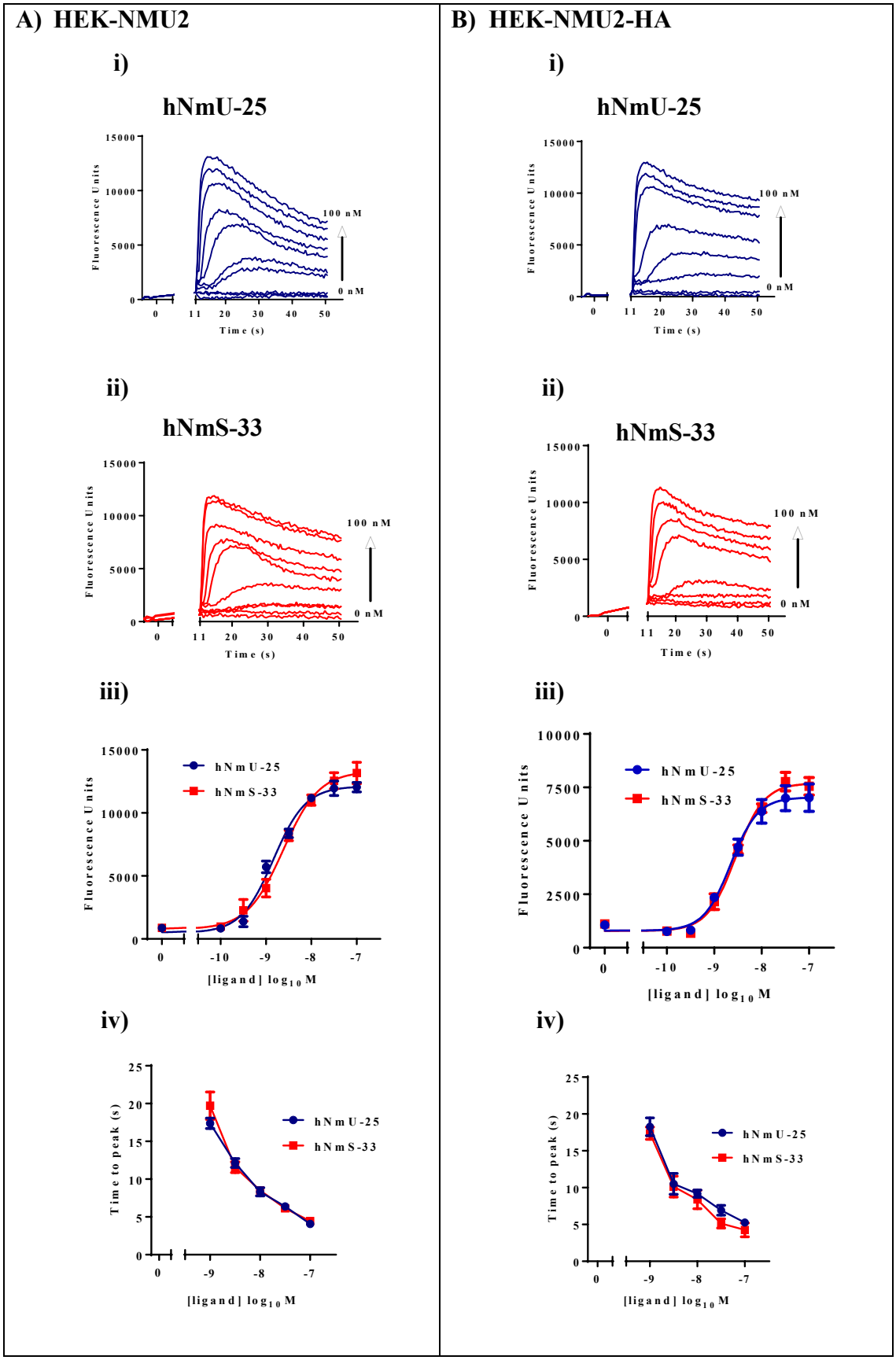


**Figure 3.5. $Ca^{2+}$ responses to hNmU-25 and hNmS-33 in HEK-NMU2 and HEK-NMU2-HA**

HEK-NMU2 (A) or HEK-NMU2-HA (B) in 96-well plates were loaded with fluo-4-AM and then stimulated with either hNmU-25 or hNmS-33 at the required concentration using a microplate reader (NOVOstar). Fluorescence changes were measured as an index of changes in $[Ca^{2+}]_i$ (A $_{i-ii}$, B $_{i-ii}$). The maximum cytosolic fluorescence changes were used to generate concentration-response curves (A $_{iii}$, B $_{iii}$). Time-to-peak graphs were derived by plotting the concentrations against the time required to reach the maximum response (A $_{iv}$, B $_{iv}$). Data are either representative of n ≥ 3 (A and B $_{i-iii}$) or mean ± sem, n ≥ 3 (A and B $_{iii-iv}$).

**Table 3.1. $pEC_{50}$ values for hNmU-25- and hNmS-33-mediated $Ca^{2+}$ responses in HEK-NMU2 and HEK-NMU2-HA**

Concentration-response curves were derived by plotting the concentrations of the agonist against the responses and then fitted with a log (agonist) versus (response). The model used to fit the curves was four parameter logistic fit using Graphpad Prism. Data are mean ± sem, n = ≥ 3.

| Ligand | HEK-NMU2 | HEK-NMU2-HA |
|---|---|---|
| | $pEC_{50}$ | $pEC_{50}$ |
| **hNmU-25** | 8.84 ± 0.07 | 8.62 ± 0.10 |
| **hNmS-33** | 8.66 ± 0.10 | 8.51 ± 0.07 |

### 3.2.3.2 Time-course of re-sensitisation of hNmU-25-and hNmS-33-mediated $Ca^{2+}$ signalling

Previously, data from the laboratory demonstrated the desensitisation and re-sensitisation profiles of both hNmU-25 and hNmS-33 in HEK-NMU2. These data showed that challenge of cells with either hNmU-25 or hNmS-33 for 5 min followed by a wash with KHB (pH 7.4) and a 5 min period of recovery caused reductions in $Ca^{2+}$ responses to a subsequent re-challenge. However, the events following desensitisation in response to either hNmU-25 or hNmS-33 were different. They showed that the rate of re-sensitisation was slower with hNmS-33 than hNmU-25 (Alhosaini *et al.*, 2018) .

The present experiments assessed the re-sensitisation profiles of $Ca^{2+}$ response for both ligands in HEK-NMU2 and HEK-NMU2-HA. Following pre-treatment with maximal concentrations of either hNmU-25 or hNmS-33 (30 nM) for 5 min, NMU2 re-sensitisation mediated by both ligands was determined by re-challenge with maximal concentration of the same ligand at the required time **(Figure 3.6; A)**. $Ca^{2+}$ responses to re-challenge increased with increasing periods of recovery. However, different re-sensitisation patterns were observed for hNmU-25 and hNmS-33 in both cell lines. For example, following 6 h recovery time, the $Ca^{2+}$ response has fully recovered following desensitisation caused by hNmU-25. However, the $Ca^{2+}$ response was not fully recovered, reaching only 60 % of the maximal response following desensitisation mediated by hNmS-33 **(Figure 3.6; B, C)**. Similar results were obtained in both cell lines.

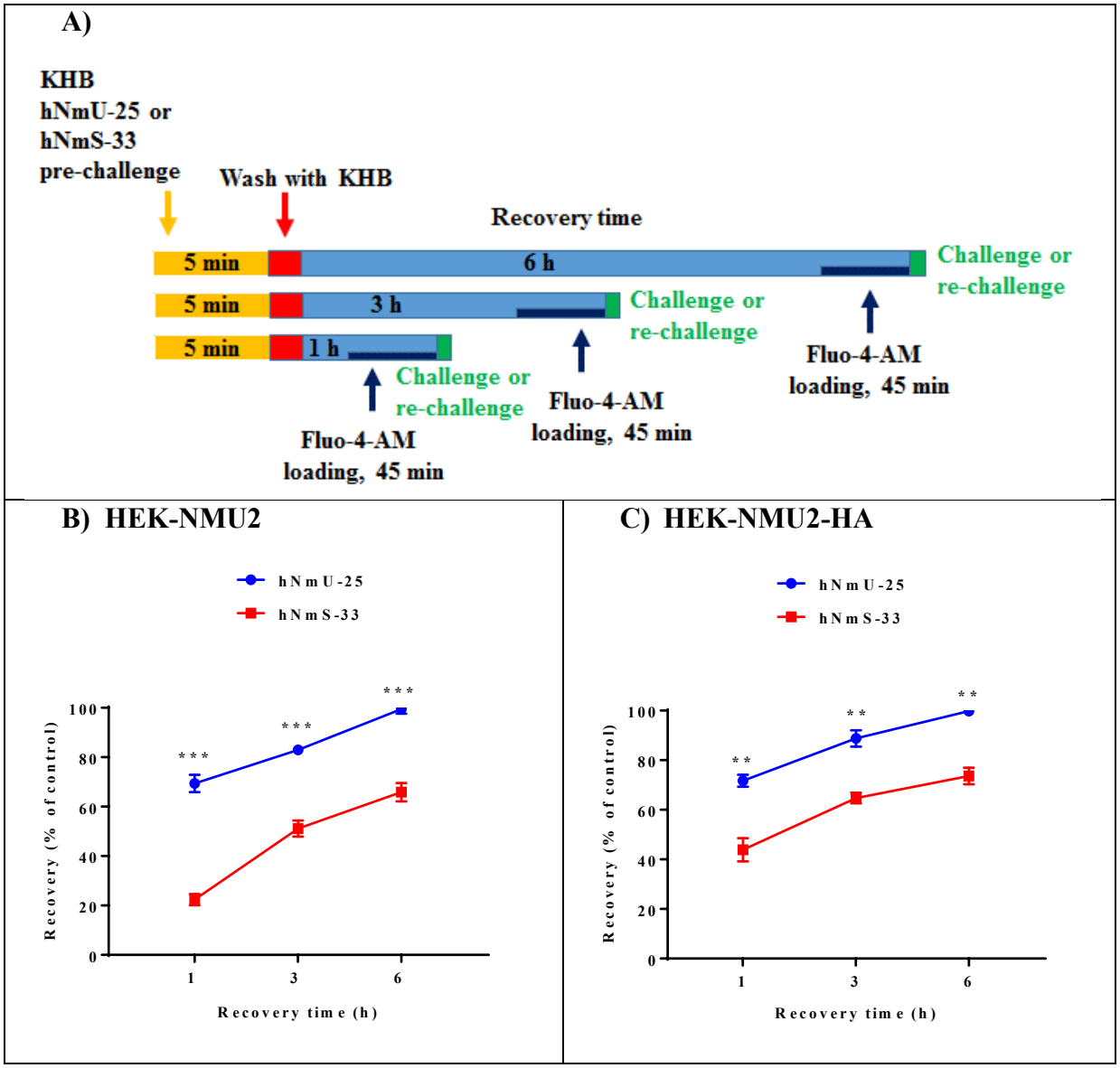


**Figure 3.6. Time-course of re-sensitisation of hNmU-25- and hNmS-33-mediated $Ca^{2+}$ signalling in HEK-NMU2 and HEK-NMU2-HA**

Cells in poly-D-lysine coated plates were stimulated with either hNmU-25 (30 nM) or hNmS-33 (30 nM) for 5 min followed by two brief washes with KHB at pH 7.4 and left in KHB for either 1 or 3 h or in serum-free media for 6 h to recover. In the last 45 min of the recovery period, cells were loaded with fluo-4-AM and then challenged with hNmU-25 (30 nM) or hNmS-33 (30 nM) or alternatively re-challenged with the same ligand (30 nM) used for the initial stimulation using a microplate reader (NOVOstar) (A). Fluorescence changes were measured as an index of changes in $[Ca^{2+}]_i$ and are represented as the percentage of the maximum response in controls (cells without pre-stimulation) (B, C). Data are expressed as mean ± sem, n = 3, and analysed using two-

way ANOVA followed by Bonferroni's multiple comparison test: $^{**}P < 0.01$, $^{***}P < 0.001$ for hNmU-25 versus hNmS-33.

### 3.2.4 hNmU-25- and hNmS-33-mediated MAP kinase activation in HEK-NMU2 and HEK-NMU2-HA

#### 3.2.4.1 Time-course of hNmU-25- and hNmS-33-mediated ERK activation in HEK-NMU2 and HEK-NMU2-HA

The temporal profiles of either hNmU-25- or hNmS-33-mediated ERK activation in both cell lines were determined by exposing the cells to either ligand at maximal concentration for the required times (5, 30, 60, 90, 180 min). Both ligands showed increases in the levels of ERK activity determined by immunoblotting of pERK **(Figure 3.7; A and $B_{i-ii}$)**. The pattern here is predominantly a rapid increase by 5 min that was largely, then sustained with some evidence of a fall at later time periods **(Figure 3.7; $A_{iii}$, $B_{iii}$)**. No significant differences were observed between hNmU-25 and hNmS-33 in either untagged or HA-tagged version of the receptor.

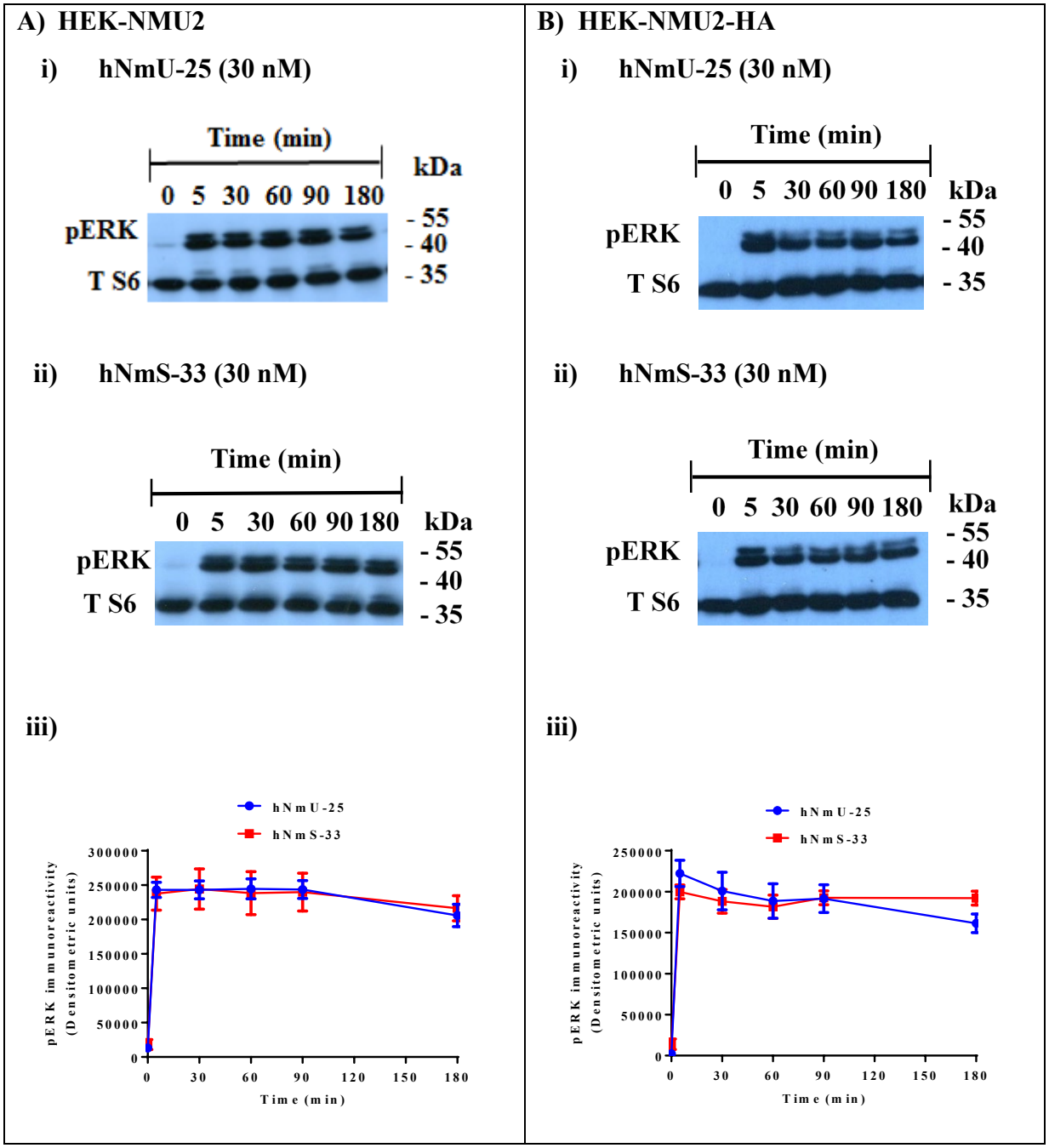


**Figure 3.7. Time course of hNmU-25- and hNmS-33-mediated ERK activation in HEK-NMU2 and HEK-NMU2-HA**

Cells were grown on poly-D-lysine coated 24-well plates for 24 h and serum-starved overnight. Cells were then stimulated with either hNmU-25 (30 nM) or hNmS-33 (30 nM) for the required time before assessment of ERK activity by immunoblotting of pERK in HEK-NMU2 (A) or HEK-NMU2-HA (B). Total ribosomal S6 (T S6) was used as loading control. The immunoblots were quantified by densitometry using Image J software (A $_{iii}$, B $_{iii}$). Data are either representative immunoblots of $n \geq 3$ (A and B $_{i-ii}$) or mean ± sem, $n \geq 3$ (A $_{iii}$, B $_{iii}$).

#### 3.2.4.2 Concentration-dependent ERK activation by hNmU-25 and hNmS-33 in HEK-NMU2 and HEK-NMU2-HA

Concentration-response curves for ERK activation were generated in HEK-NMU2 and HEK-NMU2-HA. The potency of each ligand was determined by incubating the cells with different concentrations before the assessment of ERK activity **(Figure 3.8 A and $B_{i - ii}$)**. The increases in ERK activity were concentration-dependent with the levels of activated ERK increased gradually and peaked at the concentration of 30 nM **(Figure 3.8; $A_{iii}$, $B_{iii}$)**. Both ligands showed equivalent potency for ERK activation in both cell lines. The maximum concentrations of both ligands were employed to graph concentration-response curves. The $pEC_{50}$ values for hNmU-25 and hNmS-33 on both cell lines are shown in **Table 3.2**

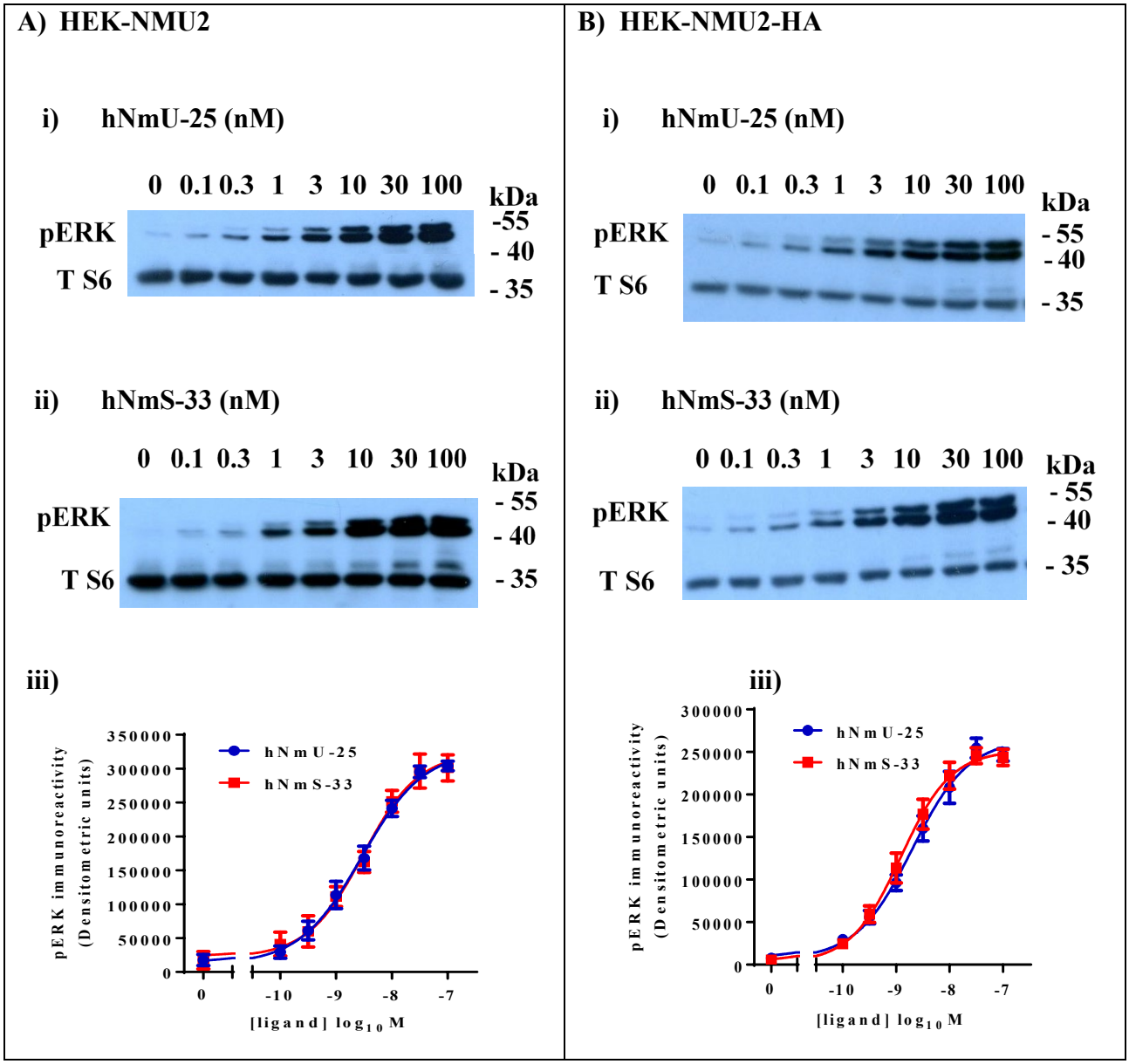


**Figure 3.8. Concentration-dependent activation of ERK by hNmU-25 and hNmS-33 in HEK-NMU2 and HEK-NMU2-HA**

Cells were cultured in poly-D-lysine coated 24-well plates for 24 h and serum-starved overnight. HEK-NMU2 (A) or HEK-NMU2-HA (B) were challenged for 5 min at the required concentrations with either hNmU-25 or hNmS-33. ERK activity was assessed by immunoblotting of pERK and quantified by densitometric analysis using Image J software (A $_{iii}$, B $_{iii}$). Data are either representative blots of n ≥ 3 (A and B $_{i-ii}$) or mean ± sem, n ≥ 3. Total ribosomal S6 (T S6) was used as a loading control.

**Table 3.2 $pEC_{50}$ values for hNmU-25-and hNmS-33-mediated ERK activation in HEK-NMU2 and HEK-NMU2-HA**

Concentration-response curves were derived by plotting the concentrations of the agonist against the responses and then fitting with a log (agonist) versus (response). The model used to fit the curves was four parameter logistic fit using Graphpad Prism. Data are mean ± sem, n = ≥ 3.

| Ligand | HEK-NMU2 | HEK-NMU2-HA |
|---|---|---|
| | $pEC_{50}$ | $pEC_{50}$ |
| **hNmU-25** | 8.56 ± 0.08 | 8.75 ± 0.08 |
| **hNmS-33** | 8.52 ± 0.11 | 8.87 ± 0.19 |

### 3.2.4.3 Time-course of hNmU-25- and hNmS-33-mediated P38 activation in HEK-NMU2 and HEK-NMU2-HA

Activation of P38 in both cell lines was assessed by challenging the cells with either hNmU-25 or hNmS-33 at maximal concentration for the required times. Data showed marked increases in P38 activity mediated by both ligands in the two cell lines **(Figure 3.9; A and B$_{i - ii}$)**. Using a maximal concentration of either hNmU-25 or hNmS-33 (30 nM) demonstrated that P38 activity increased in a time-dependent manner and reached a maximal when the cells exposed to either ligand for 180 min **(Figure 3.9; A$_{iii}$, B$_{iii}$)**. A slight drop in P38 activity was observed between 30 and 60 min for both ligands in NMU2-HA cells, although this subsequently recovered **(Figure 3.9; B$_{iii}$)**. No significant differences were seen between hNmU-25 and hNmS-33 in the two cell lines **(Figure 3.9; A$_{iii}$, B$_{iii}$)**.

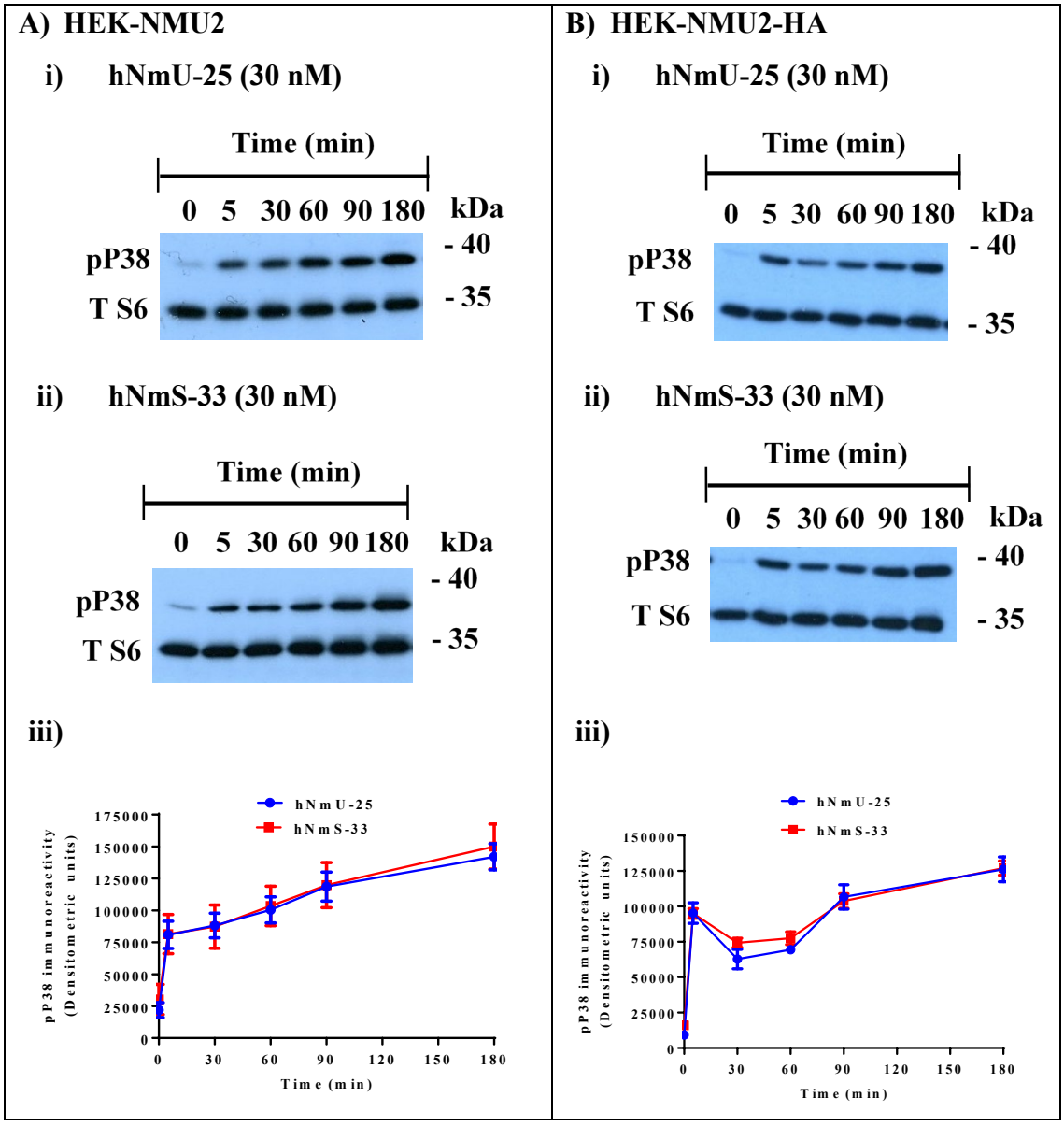


**Figure 3.9. Time course of hNmU-25- and hNmS-33-mediated P38 activation in HEK-NMU2 and NMU2-HA**

Cells were cultured in poly-D-lysine coated 24-well plates for 24 h and serum-starved overnight. HEK-NMU2 (A) or HEK-NMU2-HA (B) were challenged with either hNmU-25 (30 nM) or hNmS-33 (30 nM) for the indicated times. The pP38 was measured as an index of P38 activation using Western blotting (A and B $_{i-ii}$). Total S6 (T S6) was used as a loading control. The blots were quantified by densitometric analysis using Image J software (A $_{iii}$, B $_{iii}$). Data are either representative blots of $n \geq 3$ (A and B $_{i-ii}$) or mean ± sem, $n \geq 3$ (A $_{iii}$, B $_{iii}$).

#### 3.2.4.4 Concentration-response relationships of hNmU-25- and hNmS-33-mediated P38 activation in HEK-NMU2 and HEK-NMU2-HA

To generate concentration-response curves in both lines, cells were exposed to either hNmU-25 or hNmS-33 for 5min using different concentrations as indicated **(Figure 3.10; A and B$_{i - ii}$)**. Both ligands caused considerable increases in P38 activity which were concentration-dependent. These increases in immunoreactivity were maximal at 100 nM. The maximal concentrations were used to graph the curves and determine the potencies of hNmU-25 and hNmS-33 in the two cell lines **(Figure 3.10; A$_{iii}$, B$_{iii}$)**. The $pEC_{50}$ values for hNmU-25 and hNmS-33 in the two cell lines are showed in **Table 3.3**. hNmU-25 and hNmS-33 showed equivalent potency in both cell lines **(Figure 3.10; A$_{iii}$, B$_{iii}$)**.

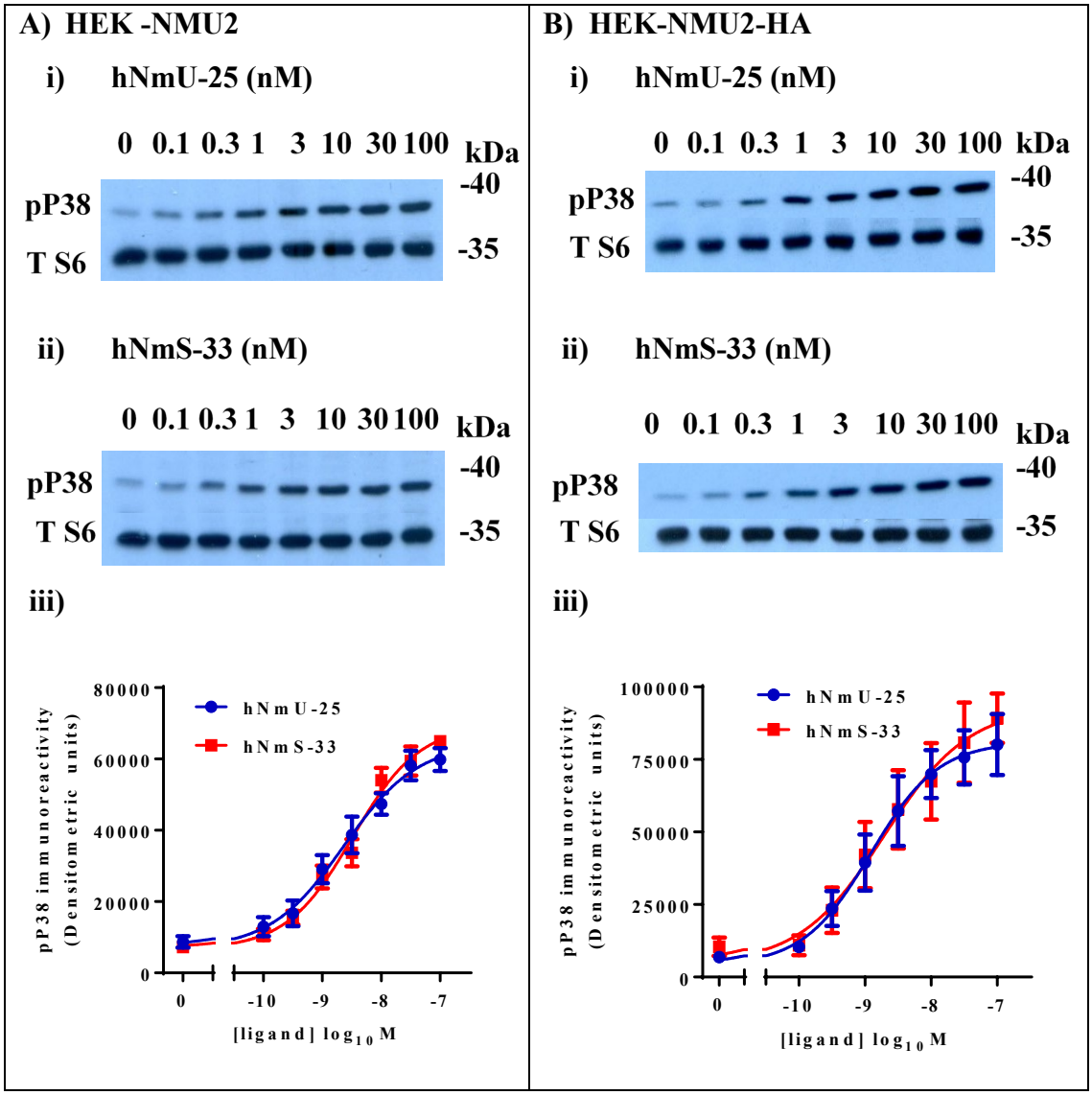


**Figure 3.10. Concentration-response relationships for hNmU-25- and hNmS-33-mediated P38 activation in HEK-NMU2 and HEK-NMU2-HA**

Cells were cultured in poly-D-lysine coated 24-well plates for 24 h and serum-starved overnight. HEK-NMU2 (A) or HEK-NMU2-HA (B) were challenged for 5 min at the required concentrations of either hNmU-25 or hNmS-33. The pP38 was measured by Western blotting as an index of P38 activation (A and B $_{i-ii}$). T S6 was used as a loading control. The immunoblots were quantified by densitometric analysis using Image J software (A, $_{iii}$, B$_{iii}$). Data are either representative immunoblots of n ≥ 3 (A and B $_{i-ii}$) or mean ± sem, n ≥ 3 (A, $_{iii}$, B$_{iii}$).

**Table 3.3. $pEC_{50}$ values for hNmU-25- and hNmS-33-mediated P38 activation in HEK-NMU2 and HEK-NMU2-HA**

Concentration-response curves were derived by plotting the concentrations of the agonist against the responses and then fitted with a log (agonist) versus (response). The model used to fit the curves was four parameter logistic fit using Graphpad Prism. Data are mean ± sem, n = ≥ 3.

| Ligand | HEK-NMU2 | HEK-NMU2-HA |
|---|---|---|
| | $pEC_{50}$ | $pEC_{50}$ |
| **hNmU-25** | 8.64 ± 0.12 | 8.68 ± 0.21 |
| **hNmS-33** | 8.51 + 0.09 | 8.85 ± 0.15 |

#### 3.2.4.5 Time-course of hNmU-25- and hNmS-33-mediated JNK activation in HEK-NMU2 and HEK-NMU2-HA

The activation of JNK in both cell lines was determined by assessment of pJNK activity. The temporal profiles of either hNmU-25 or hNmS-33 were generated by challenging the cells with the ligands for the required times at maximal concentration. Both ligands resulted in marked increases in JNK activity that were peaked at 30 min of incubation period with the ligand. **(Figure 3.11; A and B$_{i-ii}$)**. Subsequently, these levels were then decreased gradually at later time periods to reach the minimal levels at 3 h of incubation period. No significant differences between hNmU-25 and hNmS-33 in activation of JNK were seen in the two cell lines **(Figure 3.11; A$_{iii}$, B$_{iii}$)**.

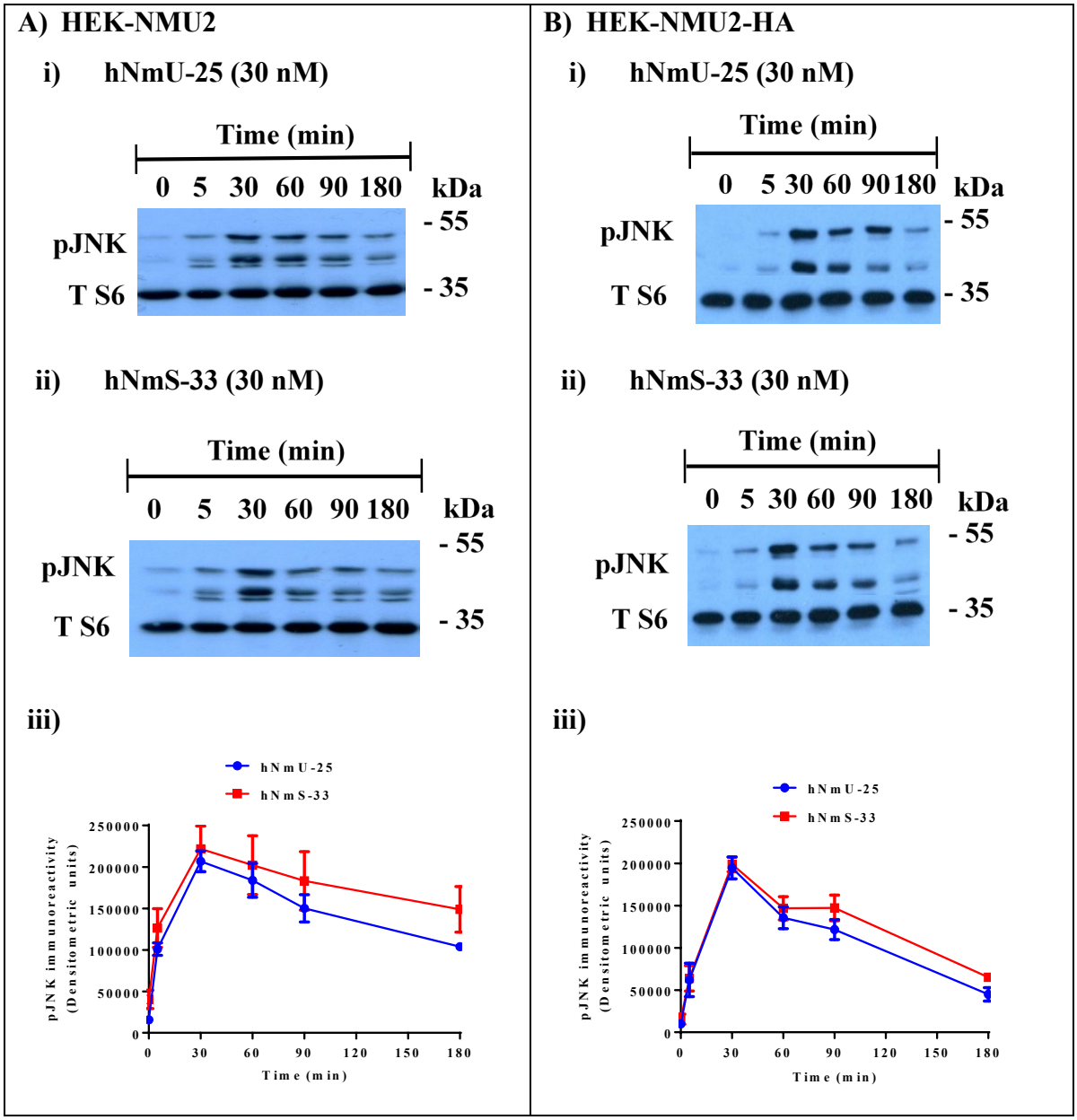


**Figure 3.11. Time course of hNmU-25- and hNmS-33-mediated JNK activation in HEK-NMU2 and HEK-NMU2-HA**

Cells were cultured in poly-D-lysine coated 24-well plates for 24 h and serum-starved overnight. HEK-NMU2 (A) or HEK-NMU2-HA (B) were stimulated with either hNmU-25 (30 nM) or hNmS-33 (30 nM) for the indicated times. The pJNK was measured by Western blotting as an index of JNK activation (A and B $_{i-ii}$). T S6 was used as loading control. The density of the immunoblots were quantified by densitometric analysis using Image J software (A $_{iii}$, B $_{iii}$). Data are either representative blots of $n \geq 3$ (A and B $_{i-ii}$) or mean ± sem, $n \geq 3$ (A $_{iii}$, B $_{iii}$).

### 3.2.5 Time-course of hNmU-25- and hNmS-33-mediated MAP kinases activation in HEK-NMU2 and HEK-NMU2-HA following brief ligand exposure

In contrast to similar MAP kinases response between hNmU-25 and hNmS-33, previous studies in the laboratory on HEK-NMU2 identified different temporal patterns mediated by those ligands, particularly in ERK activation. These differences were apparent only when the ligand was removed following stimulation for 5 min (brief ligand exposure). This protocol of brief ligand stimulation may be more similar to the *in vivo* situation as it is likely that such ligands would be released sporadically and then removed quickly by degradation and uptake. In these experiments, it reported that ERK signalling was sustained over 3 h of recovery following 5 min stimulation with hNmS-33 and ligand removal. In contrast, ERK activation returned to basal levels following a similar protocol using hNmU-25 challenge. Using this ligand removal protocol, experiments were performed on HEK-NMU2-HA to confirm if they behave in a similar way to HEK-NMU2. Furthermore, the study was expanded to include other members of MAP kinases family including P38 and JNK.

#### 3.2.5.1 Time-course of hNmU-25- and hNmS-33 mediated ERK activation in HEK-NMU2 and HEK-NMU2-HA following brief ligand exposure

The temporal profiles of ERK activation following brief ligand exposure to either hNmU-25 or hNmS-33 were generated in both cell lines by assessment of pERK activity. Challenge of cells with either hNmU-25 or hNmS-33 for 5 min evoked significant increases in ERK activity **(Figure 3.13; A and $B_{i-ii}$)**. However, following the 5 min stimulation and removal of hNmU-25 **(Figure 3.12)**, the levels of activated ERK decreased gradually to reach basal levels over the 3 h of recovery **(Figure 3.13; $A_i$, $B_i$)**. In contrast, ERK signalling was sustained over 3 h following brief exposure to hNmS-33 **(Figure 3.13; $A_{ii}$, $B_{ii}$)**. For example, following 3 h of recovery time in the absence of ligand, ERK levels following the brief hNmS-33 exposure were 42.8 % ± 6.5 and 39.3 % ± 4.8 of the response at 5 min of stimulation HEK-NMU2 and HEK-NMU2-HA respectively. By contrast following 3 h of recovery, only 3.0 % ± 1.2 and 4.9 % ± 3.1 of the response to hNmU-25 were observed in HEK-NMU2 and HEK-NMU2-HA respectively. The two cell lines showed similar behaviour in the brief ligand exposure protocol (**Figure 3.13; $A_{iii}$, $B_{iii}$)**.

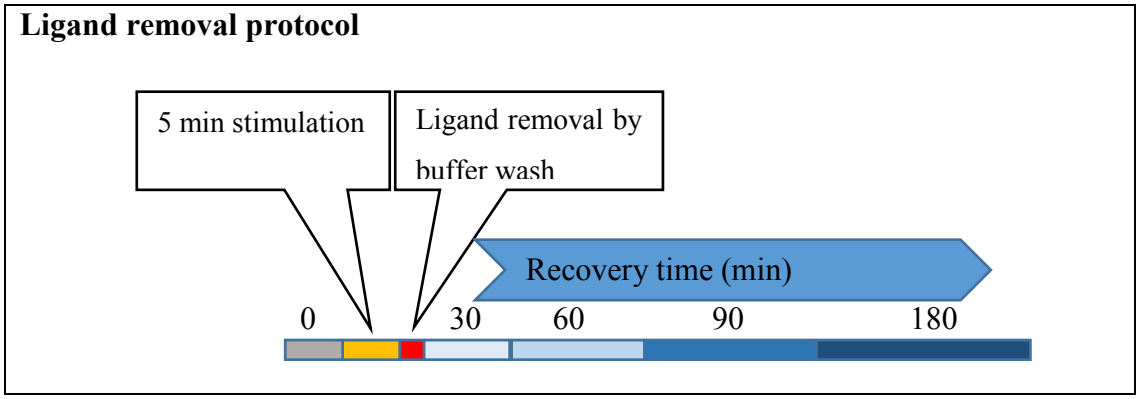


**Figure 3.12. Ligand removal protocol**

Schematic diagram showing the brief ligand exposure protocol. In this protocol, cells were incubated with the ligand for 5 min followed by washing with KHB to remove the free extracellular ligand. Cells were then left in KHB for the indicated times before determination of MAPK (ERK, P38, JNK) activity.

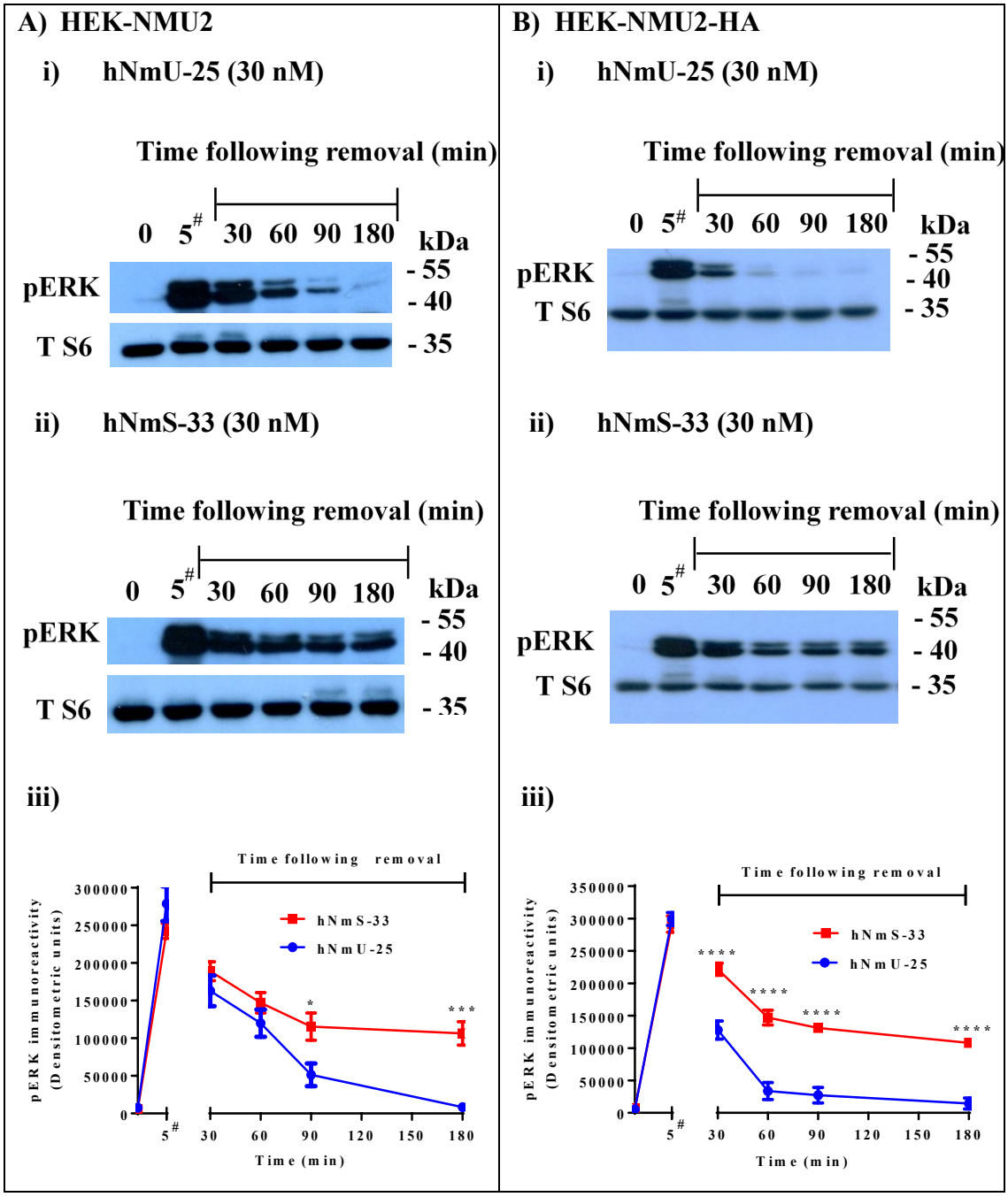


**Figure 3.13. Time-course of hNmU-25- and hNmS-33-mediated ERK activation in HEK-NMU2 and HEK-NMU2-HA following brief ligand exposure**

Cells were cultured in poly-D-lysine coated 24-well plates for 24 h and serum-starved overnight. HEK-NMU2 (A) or HEK-NMU2-HA (B) were challenged with either hNmU-25 (30 nM) or hNmS-33(30 nM) for 5 min. Following ligand removal and washing of the cell monolayers, cells were left in KHB to recover for 30 - 180 min before the determination of pERK by immunoblotting as an index of ERK activation (A and B i - ii). 0 and 5# represent the start and finish of the ligand stimulation period. T S6 was used as a loading control. The immunoblots were then quantified by densitometric analysis using

Image J software (A $_{iii}$, B $_{iii}$). Statistical analysis was performed using two way ANOVA followed by Bonferroni's test: $^{*}P < 0.05$; $^{***}P < 0.001$; $^{****}P < 0.0001$ for hNmU-25 versus hNmS-33. Data are either representative immunoblots of $n \geq 3$ (A and B $_{i\text{ - }ii}$) or mean ± sem, $n \geq 3$ (A $_{iii}$, B $_{iii}$). The split pieces of blots were in the same gel but different exposures (A $_{i\text{ -}ii}$).

#### 3.2.5.2 Time-course of hNmU-25- and hNmS-33-mediated P38 activation in HEK-NMU2 and HEK-NMU2-HA following brief ligand exposure

P38 activation was assessed following brief exposure to either hNmU-25 or hNmS-33 in both cell lines. In these experiments, the cells were challenged with either hNmU-25 or hNmS-33 for 5 min followed by ligand removal and determination of pP38 at various times during the recovery period. Challenge for 5 min provoked marked increases in the levels of activated P38 **(Figure 3.14; A and $B_{i-ii}$)**. Following ligand removal, levels reduced gradually over the subsequent 3 h recovery period following the challenge with hNmU-25 **(Figure 3.14; $A_i$, $B_i$)** In contrast, levels of pP38 were sustained over 3 h after hNmS-33 stimulation despite ligand removal **(Figure 3.14; $A_{ii}$, $B_{ii}$)**. The two cell lines showed similar behaviour **(Figure 3.14; $A_{iii}$, $B_{iii}$)**.

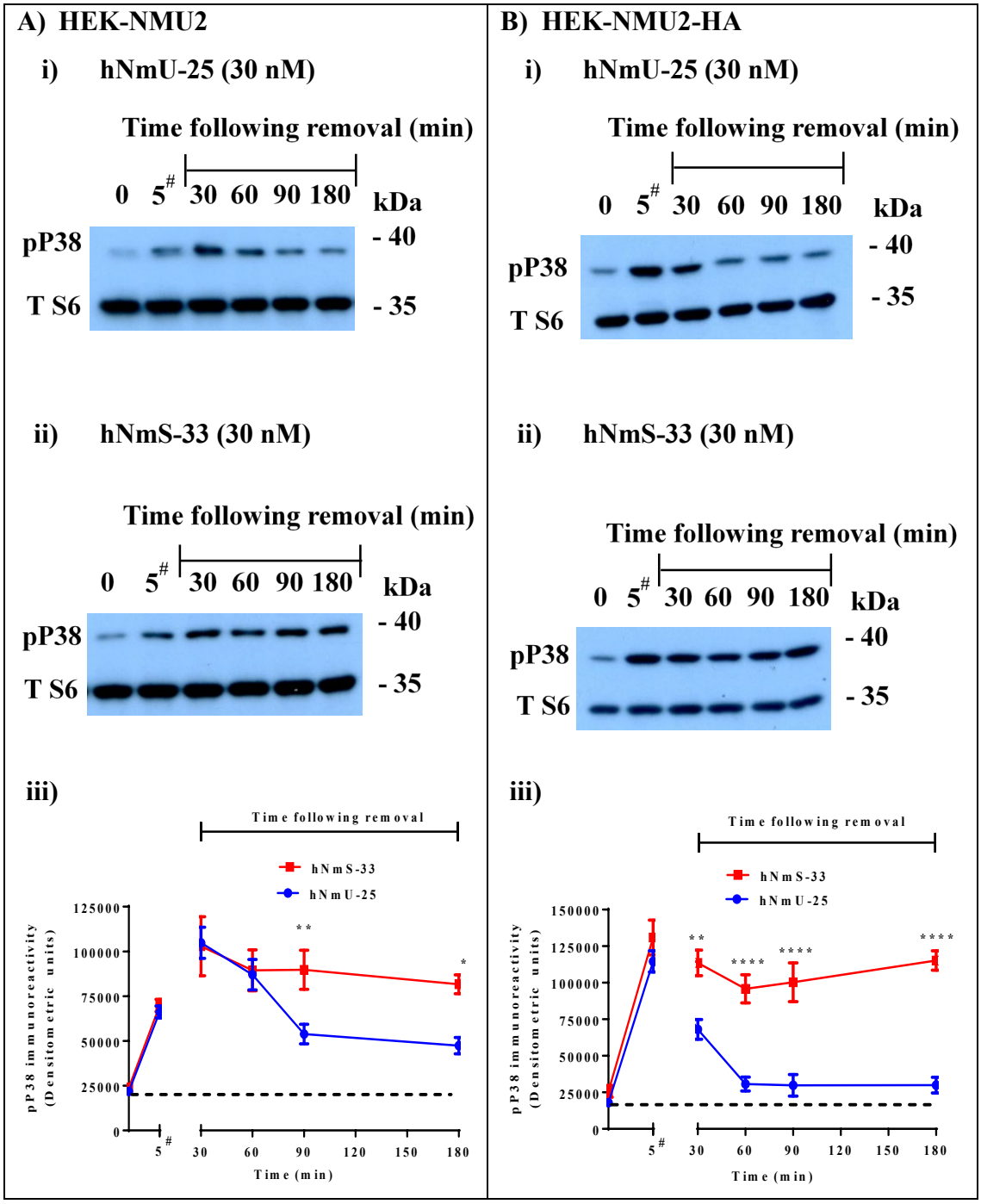


**Figure 3.14. Time-course of hNmU-25- and hNmS-33-mediated P38 activation in HEK-NMU2 and HEK-NMU2-HA following a brief ligand exposure**

Cells were cultured in poly-D-lysine coated 24-well plates for 24 h and serum-starved overnight. HEK-NMU2 (A) or HEK-NMU2-HA (B) were challenged with either hNmU-25 (30 nM) or hNmS-33(30 nM) for 5 min. Following ligand removal and washing of the cell monolayers, cells were left in KHB to recover for 30 - 180 min before the determination of pP38 by immunoblotting as an index of P38 activation (A and B i - ii). 0 and 5# represent the start and finish of the ligand stimulation period. T S6 was used as a

loading control. Immunoblots were quantified by densitometric analysis using Image J software (A $_{iii}$, B $_{iii}$). Statistical analysis were performed using two way ANOVA followed by Bonferroni's test: $^{*}P < 0.05$; $^{**}P < 0.01$; $^{****}P < 0.0001$ for hNmU-25 versus hNmS-33. Data are either representative blots of n ≥ 3 (A and B $_{i - ii}$) or mean ± sem, n ≥ 3 (A $_{iii}$, B $_{iii}$).

#### 3.2.5.3 Time-course of hNmU-25- and hNmS-33-mediated JNK activation in HEK-NMU2 and HEK-NMU2-HA following brief ligand exposure

Challenge of cells for 5 min with either hNmU-25 (30 nM) or hNmS-33 (30 nM) caused activation of JNK as assessed by immunoblotting of pJNK **(Figure 3.15; A and B$_{i - ii}$)**. Following ligand removal after 5 min, immunoblotting showed JNK activity to be further and markedly increased at 30 min in ligand-free buffer **(Figure 3.15; A$_{iii}$, B$_{iii}$)**. In both cell lines, HEK-NMU2 and HEK-NMU2-HA, the activity of JNK was significantly greater at this time point following challenge and removal of hNmS-33 compared to hNmU-25. With increasing the periods of recovery in ligand-free buffer, there were reductions in pJNK toward basal levels. However, in most instances, JNK activity remained higher following brief stimulation with hNmS-33 compared to hNmU-25. The pattern in the HEK-NMU2-HA was slightly different, particularly for hNmS-33 and seemed to fall quicker than in HEK-NMU2. However, the general pattern was similar **(Figure 3.15; A$_{iii}$, B$_{iii}$)**.

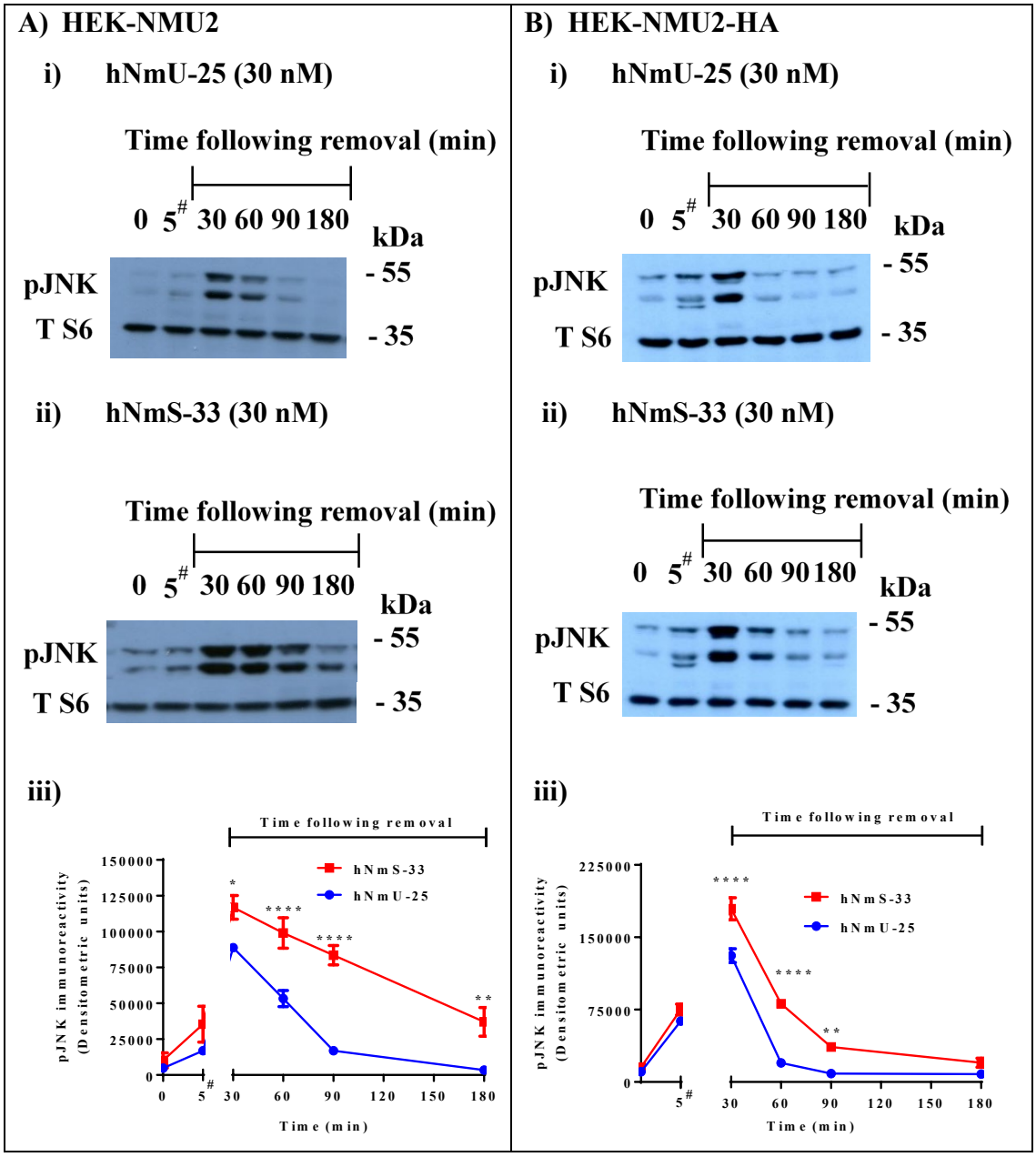


**Figure 3.15. Time-course ofhNmU-25- and hNmS-33-mediated JNK activation in HEK-NMU2 and HEK-NMU2-HA following a brief ligand exposure**

Cells were cultured in poly-D-lysine coated 24-well plates for 24 h and serum-starved overnight. HEK-NMU2 (A) or HEK-NMU2-HA (B) were challenged with either hNmU-25 (30 nM) or hNmS-33(30 nM) for 5 min. Following ligand removal and washing of the cell monolayers, cells were left in KHB to recover for 30 - 180 min. The pJNK was determined by Western blotting as an index of JNK activation (A and B i - ii). 0 and 5# represent the start and finish of the ligand stimulation period. TS6 was used as a loading control. The immunoblots were quantified by densitometric analysis using Image J software (A iii, B iii). Statistical analysis was performed using two way ANOVA followed

by Bonferroni's test: $^{**}P < 0.01$; $^{***}P < 0.001$; $^{****}P < 0.0001$ for hNmU-25 versus hNmS-33. Data are either representative blots of n ≥ 3 (A and B $_{\mathbf{i-ii}}$) or mean ± sem, n ≥ 3 (A $_{\mathbf{iii}}$, B $_{\mathbf{iii}}$).

## 3.3 Discussion

In this chapter, an epitope-tagged receptor was generated in which an HA tag was fused to the *C*-terminus of NMU2. This construct was then transfected into HEK-293 cells to establish a cell line with stable expression of NMU2-HA.

The results of immunoblotting of cell lysates from HEK-293 with a stable expression of NMU2-HA showed two intense immunoreactive bands at ~ 47 kDa and ~ 80 kDa. These bands may point to a newly synthesised receptor in the endoplasmic reticulum (ER) (band at ~ 47 kDa) and a mature version of the receptor after post-translation modification that might be exported to the cell surface (band at ~ 80 kDa). These results are consistent with studies with other GPCRs. For example, immunoblotting of HEK-293 expressing a GFP-tagged human vasopressin 2 receptor with anti-GFP antibody showed two immunoreactive bands at ~ 55 kDa and ~ 75 kDa corresponding to immature and mature glycosylated forms of the receptor respectively (Wuller *et al.*, 2004). Furthermore, immunoblotting of cell lysate from HEK-293 expressing GLP-1 receptors tagged with either HA or GFP also resulted in two immunoreactive bands (high and lower bands). In that study, pre-treatment of lysates with endoglycosidase H, to remove mannose high oligosaccharides that are linked to the *N*-terminal side chain of the receptor within the ER, reduced the intensity of the lower band without affecting the higher band, confirming that the lower molecular weight version represents the immature version of the receptor within the ER. In contrast, pre-incubation of these lysates with peptide N-glycosidase F, which removes both mannose high oligosaccharides and complex oligosaccharides (the latter being added after conjugation of mannose high oligosaccharides in the ER), reduced the intensity of both higher and lower molecular weight bands indicating the higher band might represent the mature glycosylated form of the receptor (Huang *et al.*, 2010). In contrast, the transient expression of NMU2-HA did not show these two intensive bands but rather generated bands at different molecular sizes compared to the stable cell line, suggesting different processing of the receptor. This is in agreement with transient transfection in which the exogenous DNA does not integrate into the genome, leading to high level of expression that persists for a short time, while in the stable expression condition, the transfected DNA is incorporated into the genomic DNA of the cell resulting in sustained gene expression (Kaufman, 1990). Thus, transient transfection of NMU2 may generate a high level of expression that accumulates in the ER thereby affecting receptor maturation by blocking the post-translational modification events or

there may be insufficient time for full processing, consistent with angiotensin type 2 receptor (Jiang *et al.*, 2012). Another explanation for this might be the processing systems could just be overwhelmed leading to an excess of proteins that have not been fully processed.

The life cycle of a GPCR starts in the ER where the receptor is produced, folded and structured. In the ER, which is like a quality control checkpoint, the correctly folded receptor is packed in ER-derived vesicles, sorting the receptor to the Golgi apparatus. The receptor is then transported to the trans-Golgi network where it undergoes post-translation modification such as glycosylation, conferring the mature form of the receptor (Duvernay *et al.*, 2005). Trafficking of the receptor from the ER to the plasma membrane is an essential step for cell surface expression and function (Conn *et al.*, 2010).

*N*-glycosylation is a crucial step in the post-translation modification of GPCRs as this modulates trafficking of the receptor to plasma membrane. However, this process regulates receptor trafficking differently amongst GPCR families (Dong *et al.*, 2007). Mutations of *N*-glycosylation sites of the angiotensin type 1 receptor, melanocortin 2 receptor (MC2R), dopamine 3 (D3) receptor and follicle stimulating hormone receptor (FSHR) inhibit trafficking to the plasma membrane and result in aggregation of these receptors around the nucleus, suggesting critical roles in cell surface expression (Davis *et al.*, 1995; Deslauriers *et al.*, 1999; Jayadev *et al.*, 1999; Perron *et al.*, 2010; Min *et al.*, 2015). However, cell surface expression of other receptors such as the histamine H1, muscarinic (M2) receptor and alpha 1 adrenoceptor ($\alpha_1$ AR) are not affected by *N*-glycosylation (Sawutz *et al.*, 1987; van Koppen *et al.*, 1990; Fukushima *et al.*, 1995). NMU2 has three putative sites of *N*-glycosylation; two sites in the *N*-terminus and one site in the second extracellular loop (Brighton *et al.*, 2004a). However, the full role of these sites in the synthesis, trafficking and function of NMU2 remains to be elucidated.

Functional characterisation of NMU2-HA was performed using hNmU-25 and hNmS-33 as ligands to allow a comparison between tagged and untagged versions of the receptor. The results of the functional assays show that hNmU-25 and hNmS-33 evoke equivalent $Ca^{2+}$ maximal responses and have equivalent potency and that these are similar in the two cell lines. The elevation of $[Ca^{2+}]_i$ is consistent with several reports showing that elevated levels of $[Ca^{2+}]_i$ are mediated by NMU2 by either hNmU-25 or hNmS-33 in recombinant cell lines and cells with endogenous expression of the receptor (Shan *et al.*, 2000; Funes

*et al.*, 2002; Aiyar *et al.*, 2004; Brighton *et al.*, 2004b; Brighton *et al.*, 2008; Meng *et al.*, 2008; Alhosaini *et al.*, 2018). The mechanism that underlies the rapid phase of $[Ca^{2+}]_i$ elevation by this receptor is probably due to $G\alpha_{q/11}$ coupling and subsequent activation of PLC. This activation is responsible for the hydrolysis of the plasma membrane phospholipid, $PIP_2$ to $IP_3$ and DAG. The binding of $IP_3$ to the $IP_3R$ that resides in the ER causes release of $Ca^{2+}$ from the ER to the cytoplasm, thereby increasing $[Ca^{2+}]_i$ . The increased level of intracellular $Ca^{2+}$ is followed by activation of $Ca^{2+}$ release activated $Ca^{2+}$ channels and store operated channels (SOC) in the plasma membrane. This increased level of $Ca^{2+}$ is followed by activation of the sarcoplasmic/endoplasmic reticular ATP-dependent $Ca^{2+}$ pump (SERCA) to refill intracellular stores and activation of the plasma membrane $Ca^{2+}$ ATPase resulting in removal of intracellular $Ca^{2+}$. In the continued presence of PLC activity, $[Ca^{2+}]_i$ then reaches the plateau phase, the level of which will depend on $Ca^{2+}$ entry and removal from the cytosol (Kiselyov *et al.*, 2003). A role for intracellular stores in the ER in the $Ca^{2+}$ response has been demonstrated by the ability of thapsigargin, an irreversible inhibitor of the SERCA, to reduce NmU-mediated increases in $[Ca^{2+}]_i$ (Brighton *et al.*, 2004b). Removal of extracellular $Ca^{2+}$ also reduces the plateau phase of $Ca^{2+}$ signalling, highlighting a role for $Ca^{2+}$ influx from the extracellular environment (Brighton *et al.*, 2004b). This is presumably capacitive $Ca^{2+}$ entry in response to the NmU-mediated depletion of intracellular stores.

It has been shown previously that a 5 min exposure to either hNmU-25 or hNmS-33 causes desensitisation of subsequent $Ca^{2+}$ responses of NMU2 (Alhosaini *et al.*, 2018). Desensitisation is a regulatory process in which the cell reduces the signalling arising from continuous or repetitive stimulation of the receptor. This phenomenon can occur rapidly (short-term) and is thought to be mediated predominantly by receptor phosphorylation and the subsequent recruitment of arrestins **(Section 1.4.2.4.1)** (Rajagopal *et al.*, 2018). Given that hNmU-25 and hmS-33 bind essentially irreversibly to NMU2, studying receptor resensitisation in the absence of continued ligand binding is difficult. Therefore, an acid wash protocol was used to allow a subsequent assessment of the receptor desensitisation on ligand re-addition without the complication of ligand remaining bound to the receptor from the desensitising challenge (Brighton *et al.*, 2008; Alhosaini *et al.*, 2018). This short acid wash showed no impact on NMU2 responses or cell viability (Alhosaini *et al.*, 2018).

In the current study, an acid wash was not used but a buffer wash at physiological pH (7.4) was employed **(Figure 3.6)**. Although, this would not remove the ligand from the receptor, it would remove free ligand and this might reflect more accurately the situation *in vivo*. Thus, peptides are often released in a pulsatile fashion and are then removed by dilution and degradation. This allows a more realistic assessment of receptor resensitisation, including any possible role of the ligand. The current study shows that a brief exposure of NMU2 to ligand causes desensitisation of $Ca^{2+}$ signalling followed by resensitisation (the time frame is 6 h for recovery following hNmU-25 and more than 6 h following hNmS-33). This slow rate of NMU2 resensitisation in response to either ligand matches rates observed in studies with some other GPCRs. For example, $Ca^{2+}$ responses mediated by either the GLP-1 receptor or neurokinin 1 receptor need ~ 3 h to recover (Schmidlin *et al.*, 2001; Lu *et al.*, 2019). Furthermore, $Ca^{2+}$ responses of the calcitonin receptor like receptor (CCLR) to calcitonin gene-related peptide (CGRP) require 4 - 6 h to recover (Padilla *et al.*, 2007). The rate of recovery of NMU2-mediated $Ca^{2+}$ signalling following brief exposure to hNmU-25 in HEK-NMU2 and HEK-NMU2-HA was fast compared to hNmS-33. While $Ca^{2+}$ response mediated by hNmU-25 required ~ 6 h to recover, hNmS-33 was not fully recovered (~ 60 % of the maximal response), suggesting that the rate of resensitisation is ligand-dependent. Different factors affect the temporal profile of receptor resensitisation and recycling including, for example, the strength of ligand- -receptor-arrestin binding where arrestin represents an essential regulator in receptor desensitisation, internalisation and receptor trafficking **(Figure 1.8)** (Pierce *et al.*, 2001). Differences in arrestin binding between receptors has been observed leading to the classification of receptors into two classes; A and B according to the differential affinity to arrestins. Class A GPCRs have a higher affinity for arrestin 3 binding than arrestin 2and arrestin rapidly dissociates either at the plasma membrane or shortly after internalisation, thereby promoting a rapid recycling (Oakley *et al.*, 2000). By contrast, class B GPCRs interact with arrestin 2 and arrestin 3 with high affinity, therefore the receptor and arrestin may form a stable complex in the endosome that may dissociate slowly, leading to resensitisation at a slower rate (Ferguson, 2001; Luttrell, 2008). The current findings suggest that NMU2 may be a class B GPCR because it requires a long time to recycle back to cell membrane, assuming that resensitisation is related to recycling. This is likely as NMU2 shows significant ligand-dependent internalisation (Alhosaini *et al.*, 2018) indicating that recycling would be required, at least as a component of resensitisation.

Some GPCRs such as the angiotensin II type 1 receptor, oxytocin receptor and neurotensin 1 receptor can form stable complexes with arrestins, thus resulting in slow recycling and resensitisation (Oakley *et al.*, 2001). The stable complexes are dependent on clusters of serine/threonine residues in the *C*-terminal of these receptors, which are sites of ligand-induced receptor phosphorylation (Oakley *et al.*, 2001). The presence of potential phosphorylation sites in the *C*-terminus of NMU2 (Brighton *et al.*, 2004a) highlights a possible role of these sites in mediating arrestin binding to the phosphorylated receptor. However, it is currently unknown if and where NMU2 is phosphorylated. Therefore, NMU2 phosphorylation will be explored in subsequent chapters.

Data presented above show that the HA-tagged NMU2 (HEK-NMU2-HA) behaves identically to the untagged version (HEK-NMU2), confirming that the HA-tag version does not influence $Ca^{2+}$ signalling in response to either ligand.

The two endogenous ligands (hNmU-25 and hNmS-33) cause different resensitisation profiles of NMU2. If this results from, for example, differences in the duration of association between the receptor and partners such as the arrestins, then it might be possible that some signalling events differ between the two ligands. One possibility might be in the activation of MAPK signalling, as in some circumstances MAPK signalling occurs due to scaffolding of signalling proteins on arrestins that are bound to activated receptors (Gurevich *et al.*, 2018b).

The current study shows that hNmU-25 and hNmS-33 are equally potent in the activation of ERK1/2 signalling in either the HEK-NMU2 or HEK-NMU2-HA cell lines and that there are no differences between cell lines regarding ligand potencies and maximal responses. Although the temporal profiles and magnitude of ERK1/2 activation were similar for both ligands in both cell lines (in the continued presence of ligand), distinct ligand-dependent profiles emerged following brief exposure to either hNmU-25 or hNmS-33. Thus, the level of activated ERK1/2 was more sustained over 3 h following brief stimulation with hNmS-33 compared to hNmU-25. This occurred in both cell lines, providing further evidence of similarity between tagged and untagged versions of the receptor. Given that hNmU-25 and hNmS-33 bind to NMU2 essentially irreversibly (Brighton *et al.*, 2008), these differences may be related to roles of the ligand on aspects such as receptor internalisation, recycling and resensitisation (Brighton *et al.*, 2004b;

Alhosaini *et al.*, 2018). It is possible that hNmS-33 limits one of the processes required for receptor trafficking leading to both slower resensitisation of $Ca^{2+}$ signalling and more sustained ERK1/2 activation compared to events following hNmU-25 stimulation. Recent research suggests that ECE-1 plays a role in the degradation of hNmU-25 but not hNmS-33, thereby contributing to the different temporal profiles of ERK1/2 activation (Alhosaini *et al.*, 2018). Definition of the precise mechanisms underlying such differences are, however, unclear, particularly as the mechanisms by which NMU2 mediates ERK1/2 activation by any ligand are not fully understood. The two possible overarching mechanisms include G-protein-dependent signalling and G-protein-independent signalling, both of which have been reported for a number of other receptors. For example, the PTH1R induces ERK1/2 activation with an early phase (5 min) shown to be PKA- and PKC-dependent and a late phase (30 - 60 min) that was arrestin dependent (Gesty-Palmer *et al.*, 2006) thereby supporting the notion of both G-protein-dependent and arrestin-dependent mechanisms. The arrestin-dependent pathway of ERK1/2 activation persisted for a long time in comparison to the G-protein-dependent mechanism that was rapid but relatively transient. Similarly, the activated angiotensin II type 1 receptor mediates acute ERK1/2 activation (2 min) by G-protein-dependent mechanisms whereas arrestin-dependent signalling resulted in ERK1/2 activation that peaked between 5 min and 10 min, and lasted for 90 min (Ahn *et al.*, 2004; Lefkowitz *et al.*, 2005) although arrestin-independent mechanisms also exist. For example, while the overexpression of an arrestin dominant negative mutant did not influence internalisation of some receptors such as the endothelin type B receptor and vasoactive intestinal peptide type 1 receptor, overexpression of a dominant negative mutant of dynamin resulted in inhibition of receptor endocytosis, suggesting alternative mechanisms such as the caveolae pathway may play a role in receptor trafficking and signalling (Teixeira *et al.*, 1999; Claing *et al.*, 2000a). For the CCK receptor expressed in CHO cells 20 % of the ligand-dependent internalisation was by the caveolae pathway and 80 % through clathrin-coated pits (Roettger *et al.*, 1995). However, inhibition of the latter pathway resulted in full receptor endocytosis, suggesting the first pathway can also fully support the internalisation of the CCK receptor in the absence of the other pathway (Roettger *et al.*, 1995). It might be possible that either hNmU-25 or hNmS-33 engages receptor with different endocytosis pathways thereby affecting receptor trafficking and signalling.

The role of arrestins in receptor internalisation and trafficking depends on their recruitment to receptors activated by agonist and phosphorylated by one or more GRKs (Tobin *et al.*, 2008). It is possible that different ligands stabilise the receptor in different conformations thereby causing different functional consequences. One such aspect might be different extents or patterns of receptor phosphorylation, including the possibility that the receptor may be phosphorylated by different GRKs. For example, the chemokine receptor 7 (CCR7) has two native ligands, CCL19 and CCL21. These ligands have equivalent potency on the $Ca^{2+}$ response and ERK1/2 activation but CCL19 induces strong receptor phosphorylation via GRK3 and GRK6 resulting in a strong arrestin recruitment. In contrast, CCL21 promotes only GRK6-mediated phosphorylation thereby recruiting less arrestin to the receptor (Zidar *et al.*, 2009). It is possible to hypothesise that NMU2 is phosphorylated differently by hNmU-25 and hNmS-33 which might affect one or more aspects of receptor signalling, desensitisation, internalisation, trafficking, recycling and resensitisation. Having established that NMU2-HA behaves similarly to NMU2 in relation to the functional characterisation including $Ca^{2+}$ signalling, ERK1/2 activation and receptor resensitisation, this study sought to extend observations of NMU2-mediated MAPK regulation to P38 and JNK. P38 plays a vital role in regulating of a variety of cellular responses **(Section 1.4.2.2)**. The present study shows that hNmU-25 and hNmS-33 activate P38 with equivalent potency in either of the cell lines and that there is no difference in potencies between the two cell lines. These data indicate that hNmU-25 and hNmS-33 are equipotent and that the HA tag added to NMU2 does not affect P38 signalling. Although similar temporal profiles of P38 activation in the continued presence of ligands were obtained, ligand removal uncovered different temporal patterns of NMU2-mediated P38 activation. Thus, P38 activation was more sustained following brief challenge with hNmS-33 compared to hNmU-25. A number of studies have also examined GPCR-mediated P38 activation. For example, carbachol caused P38 activation by the $G_{\alpha q/11}$ -coupled M1 muscarinic receptor which was maximal at ~ 10 min (Yamauchi *et al.*, 1997). Furthermore, transfection of $G_{\alpha o}$ to remove the free $G\beta\gamma$ dimer resulted in partial (~ 50 %) inhibition of muscarinic M1 receptor-mediated P38 activation. This suggests that M1 muscarinic receptors mediate P38 activation at least to some extent by $G_{\alpha q/11}$ . In another study, a biphasic activation of P38 was observed in response to isoproterenol stimulation of the $\beta_2$-adrenoceptor in which the early phase of activation (peaking at ~ 10 min and reducing to basal at ~ 60 min) was mediated by arrestin 2 but not arrestin 3 while the late phase of activation (starting at ~ 90 min and

lasting for 6 h) was mediated by the $G_{\alpha s}$-cAMP-PKA-P38 axis highlighting G-protein dependent and independent signalling respectively (Gong *et al.*, 2008). Recently, evidence has emerged pointing to the ability of GPCRs to continue signalling from endosomal vesicles and such signalling can be related to either G-protein-dependent or arrestin-dependent pathways (Thomsen *et al.*, 2018). For example, endosomal neurokinin 1 receptor mediates a sustained $G_{\alpha q}$ signalling thereby causing PKC and nuclear ERK1/2 activation leading to neuronal excitation and nociception (Jensen *et al.*, 2017). In the present study, the differences in the activation profiles between hNmU-25- and hNmS-33-mediated P38 activation might be a consequence of hNmS-33 driving the formation of a stable complex between NMU2 and the arrestins for a prolonged period of time. This could lead to prolonged G-protein-independent signalling (Wei *et al.*, 2003; Shenoy *et al.*, 2006). Such differences may arise through differences in ligand processing or receptor conformations as discussed. For example, recently, it has been shown that ECE-1 is a critical determinant in NMU2 trafficking following hNmU-25 but not hNmS-33. Thus, brief ligand exposure resulted in P38 activation by either ligand but activation was more sustained following hNmS-33 than hNmU-25. Inhibition of ECE-1 potentiated P38 signalling following hNmU-25 but not hNmS-33 suggesting that the nature of ligand might be critical factor in determining receptor trafficking and signalling profiles (Alhosaini *et al.*, 2018). Alternatively, the more sustained P38 activation in response to hNmS-33 could arise from sustained G-protein-dependent signalling (as opposed to sustained G-protein-independent signalling) either from the plasma membrane or intracellular sites. Again, differences in, for example, ligand processing, receptor conformations and/or desensitisation may account for this. Further work is required to define the mechanisms of P38 following brief exposure to the two different ligands.

In addition to ERK1/2 and P38, the present study also determined the effects of hNmU-25 and hNmS-33 on the temporal profile of NMU2-mediated JNK activation. The JNK signalling pathway is a key player in a variety of responses such as inflammation, proliferation and apoptosis (Ip *et al.*, 1998). Here, both hNmU-25 and hNmS-33 mediated JNK activation which peaked at 30 min with similar patterns between the two ligands in both cell lines and no difference in activation between the two cell lines. Although there were similar temporal profiles of JNK activation in the persistent presence of ligands, similar to the other MAPKs (ERK and P38), there was a more sustained JNK activation in response to hNmS-33 compared to hNmU-25 following brief ligand exposure. A

number of possibilities for the activation of JNK exist including signalling through G-protein-dependent pathways. For example, stimulation of CHO cells expressing the $G_{\alpha q}$-coupled muscarinic M3 receptor resulted in JNK activation which was maximal at ~ 40 min (Hirshman *et al.*, 1999). Furthermore intracellular depletion of $Ca^{2+}$ inhibited JNK activation by more than 50 %. Moreover, pre-treatment of cells with PTX reduced M3 receptor-mediated JNK signalling suggesting that both $G_{\alpha q}$ and $G_{\alpha i}$ subunits are involved (Hirshman *et al.*, 1999). In the current study, the mechanisms and consequences of NMU2-mediated JNK activation are not known but clearly require exploring and defining. A previous study has shown that NMU2 is able to signal through both $G_{\alpha q}$ and $G_{\alpha i}$ (Brighton *et al.*, 2004b) thereby providing possible links to JNK activation. Arrestins play a critical role in the recruitment of variety of signalling proteins to receptors and this provides a G-protein-independent mechanism or the activation of signalling pathways **(See 1.4.2.2)**. For example, arrestin 2 is involved in c-Src recruitment (non-receptor tyrosine kinase) to the $\beta_2$ adrenoceptor following stimulation with isoproterenol (Luttrell *et al.*, 1999b). Arrestin also appears as a scaffolding protein in the JNK cascade. Thus, arrestin 3 acts as a scaffold for JNK3 and ASK1 (component of MAPKKK) resulting in JNK3 signalling following activation of the angiotensin II type I receptor (McDonald *et al.*, 2000). This scaffold consisting of JNK3, arrestin and receptor has been found to co-localise to the intracellular vesicles (McDonald *et al.*, 2000). It has also been shown that stimulation of the MOP receptor with fentanyl also results in JNK2 activation which is GRK3/arrestin 3 dependent (Kuhar *et al.*, 2015). The precise mechanisms for ligand-dependent differences in the profile of JNK activation following brief exposure to either hNmU-25 or hNmS-33 are also unclear but again may align with the mechanisms discussed above for ligand-dependent differences in the temporal activation profiles of the other MAPKs.

In conclusion, this chapter shows that both HEK-NMU2 and the newly generated HEK-NMU2-HA behave similarly in response to hNmU-25 and hNmS-33. Activation of either receptor type demonstrates that hNmU-25 and hNmS-33 elevate $[Ca^{2+}]_i$, and activate a number of MAPKs with equivalent potency. However, both hNmU-25 and hNmS-33 generate distinct patterns of receptor resensitisation and differences in MAPK signalling profiles following brief ligand exposure. Thus, the rate of $Ca^{2+}$ resensitisation was slower and the temporal profiles of signalling by a number of MAPKs were more sustained following brief exposure to hNmS-33 compared to hNmU-25. Such differences could be

crucial in the development of drugs for the treatment of obesity and indeed when targeting other conditions and receptors where ligand-specific signalling may exist. Interestingly ICV administration of hNmS-33 in rats causes a more sustained inhibition of signalling compared to hNmU-25 (Ida *et al.*, 2005; Miyazato *et al.*, 2008) and whilst this might have been assumed to be a consequence of differential susceptibilities to extracellular protease degradation, the present study suggests that signalling differences could be responsible, thereby emphasising the relevance to drug development. Although the current study shows a clear difference between hNmU-25 and hNmS-33 in the signalling of NMU2 in recombinant system, further work needs to be done to establish whether NMU2 signalling difference between the two ligands can be observed in the hypothalamus tissue where NMU2 is expressed.

As discussed, ligand-dependent differences in the recruitment of arrestin and receptor desensitisation could contribute to ligand-dependent signalling. Thus, next chapter will explore ligand-dependent NMU2 phosphorylation.

# 4 Chapter four: Study of NMU2 phosphorylation

## 4.1 Introduction

GPCRs are well-known to regulate a variety of cellular signalling via two main pathways including G-protein-dependent and arrestin-dependent mechanisms (Pierce *et al.*, 2002; Shukla *et al.*, 2011a). Stimulation of GPCRs with a cognate ligand mediates G-protein activation that regulates signalling via several effector proteins. However, this activation needs to be switched off and this can be done by phosphorylation of the receptor by GRKs or second messenger kinases such as PKC and PKA. When the receptor is phosphorylated by GRK, this promotes arrestins recruitment to the ligand activated and phosphorylated receptor that prevents access of further G-proteins resulting in receptor desensitisation, internalisation and initiation of G-protein-independent but arrestin-dependent signalling (Pitcher *et al.*, 1998). Receptor phosphorylation appears to play a critical role not only in receptor desensitisation but also in regulation of several aspects of GPCRs signalling. It has been reported that phosphorylation of $\beta_2$ adrenoceptor by PKA inhibits its binding to $G_{\alpha s}$ and promotes coupling to $G_{\alpha i}$ (Daaka *et al.*, 1997b; Lefkowitz *et al.*, 2002). Furthermore, phosphorylation of receptors by GRKs recruits arrestins which, in turn, can initiate a second wave of signalling through scaffolding with many signalling proteins such as Src, Raf-1, protein kinase B (Akt) and ERK1/2 (Yang *et al.*, 2017). Indeed, activation of angiotensin II type 1 receptor recruits a list of signalling proteins (> 220) that have been found assembled in complexes with the receptor and arrestins (Xiao *et al.*, 2010). GPCRs are phosphorylated at multiple sites in their intracellular regions and the specific pattern could be important for arrestins recruitment and the mediation of specific signalling responses (Tobin, 2008). Indeed, there is a large number of studies that describe the importance of receptor phosphorylation in the regulation of signalling. They have shown that ligands of the same receptor can generate ligand-dependent different phosphorylation profiles that lead to different signalling consequences (Jean-Charles *et al.*, 2016a; Peterhans *et al.*, 2016; Latorraca *et al.*, 2017a).

Data in chapter three have shown that different patterns of some signalling and resensitisation between hNmU-25 and hNmS-33 in the cell line expressing NMU2. Thus, the rate of resensitisation of NMU2 was slower in response to hNmS-33 than hNmU-25. Furthermore, more sustained activation of MAPKs was observed in response to hNmS-33 compared to hNmU25. These differences could be a consequence of a difference in the temporal profiles and types of arrestins that are recruited to the activated receptor.

Given that arrestins recruitment is a consequence of receptor phosphorylation, the aim of experiments described in this chapter were to address if NMU2 is phosphorylated in response to hNmU-25 or hNmS-3 and to investigate the potential kinases that could be involved. Moreover, the temporal profiles of NMU2 dephosphorylation following brief ligand exposure were determined to see if there is a ligand-dependent link between the receptor phosphorylation/dephosphorylation profile and sustained MAPKs signalling.

### 4.1.1 NMU2-HA phosphorylation in transiently transfected HEK-293

The study of NMU2-HA phosphorylation was firstly performed on HEK-293 with transient expression of NMU2-HA. In these experiments, NMU2-HA was transfected into HEK-293 using the JetPrime transfection kit **(see Methods)**. After 48 h, the cells were labelled with $^{32}P$ orthophosphate and stimulated with either hNmU-25 or hNmS-33 for 5 min. The autoradiographs of the immunoprecipitated NMU2-HA showed three non-specific phosphorylation bands in which the first was ~ 110 kDa, second > 80 kDa and third ~ 60 kDa. The intensities and positions of the bands were similar whether cells had been untreated (control) or stimulated with hNmU-25 or hNmS-33 **(Figure 4.1; $a_i$)**. Immunoblotting of immunoprecipitated NMU2-HA with an anti-HA antibody showed a large band ~ 47 kDa which is the predicted molecular size of NMU2-HA. A faint band ~ 80 kDa was also observed which is the higher molecular weight band that would be consistent with that of a glycosylated form of the receptor that has been observed with many other GPCRs (Li *et al.*, 2017a) **(Figure 4.1; $a_{ii}$)**. No significant differences were seen in response to either hNmU-25 or hNmS-33 compared to the control group **(Figure 4.1; b)**.

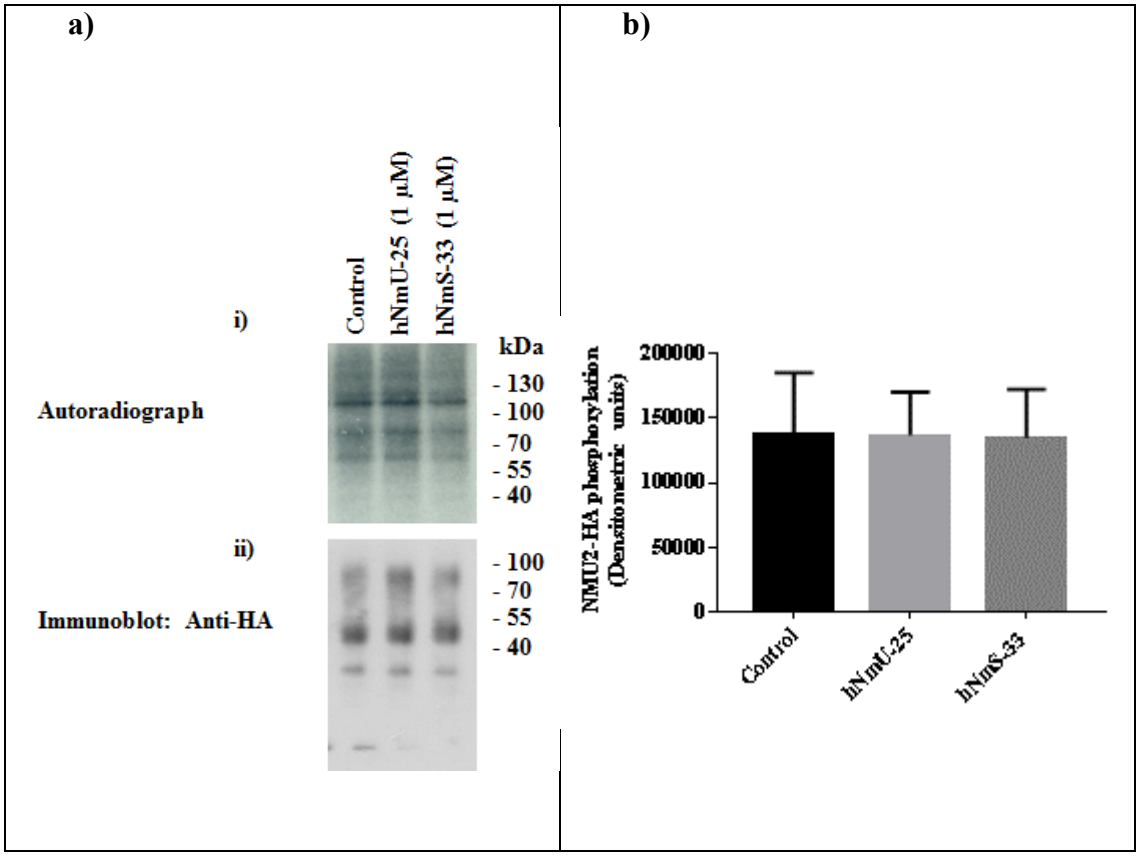


**Figure 4.1. hNmU-25 and hNmS-33 did not induce changes in the levels of phosphorylation of transiently transfected NMU2-HA**

HEK-293 cells were grown on poly-D-lysine coated 6-well plates for 24 h. Cells were then transfected with NMU2-HA **(see Methods)**. After 48 h, cells were washed twice with phosphate-free KHB and labelled with $^{32}P$ orthophosphate for 1 h. Cells were then stimulated with hNmU-25 (1 µM), hNmS-33 (1 µM) or control (KHB) for 5 min. Following solubilisation of the cell monolayer, NMU2-HA was immunoprecipitated and resolved by gel electrophoresis. The gel was then dried and visualised by autoradiography ($a_i$). Immunoblotting of the immunoprecipitates with an anti-HA antibody was used as a loading control of NMU2-HA ($a_{ii}$). Data are either representative autoradiographs or blots of n = 2 or mean ± sd, n = 2 (b).

### 4.1.2 hNmU-25- and hNmS-33-mediated NMU2-HA phosphorylation in HEK-NMU2-HA

After generation and characterisation of HEK-NMU2-HA and comparison of its signalling characteristics to those of HEK-NMU2 in **Chapter 3**, HEK-NMU2-HA were used to study agonist-mediated NMU2 phosphorylation. Agonist-induced NMU2-HA phosphorylation was determined by exposing the cells to either hNmU-25 or hNmS-33 (1 μM) for 5 min. Stimulation of HEK-NMU2-HA with either ligand resulted in a robust increase in phosphorylation (> 11 fold) compared to unstimulated controls **(Figure 4.2; $a_i$, $b_i$)**. The increased phosphorylation was apparent in a band at ~ 80 kDa, which is coincident with the major immunoreactive band in the immunoblot of the cell extracts. Notably, the amount of NMU2-HA immunoprecipitated was equivalent between the different conditions, demonstrating that neither receptor activation nor phosphorylation affected the immunoprecipitation **(Figure 4.2; $a_{ii}$, $b_{ii}$)**. Both ligands induced similar levels of phosphorylation after 5 min challenge **(Figure 4.2; c)**.

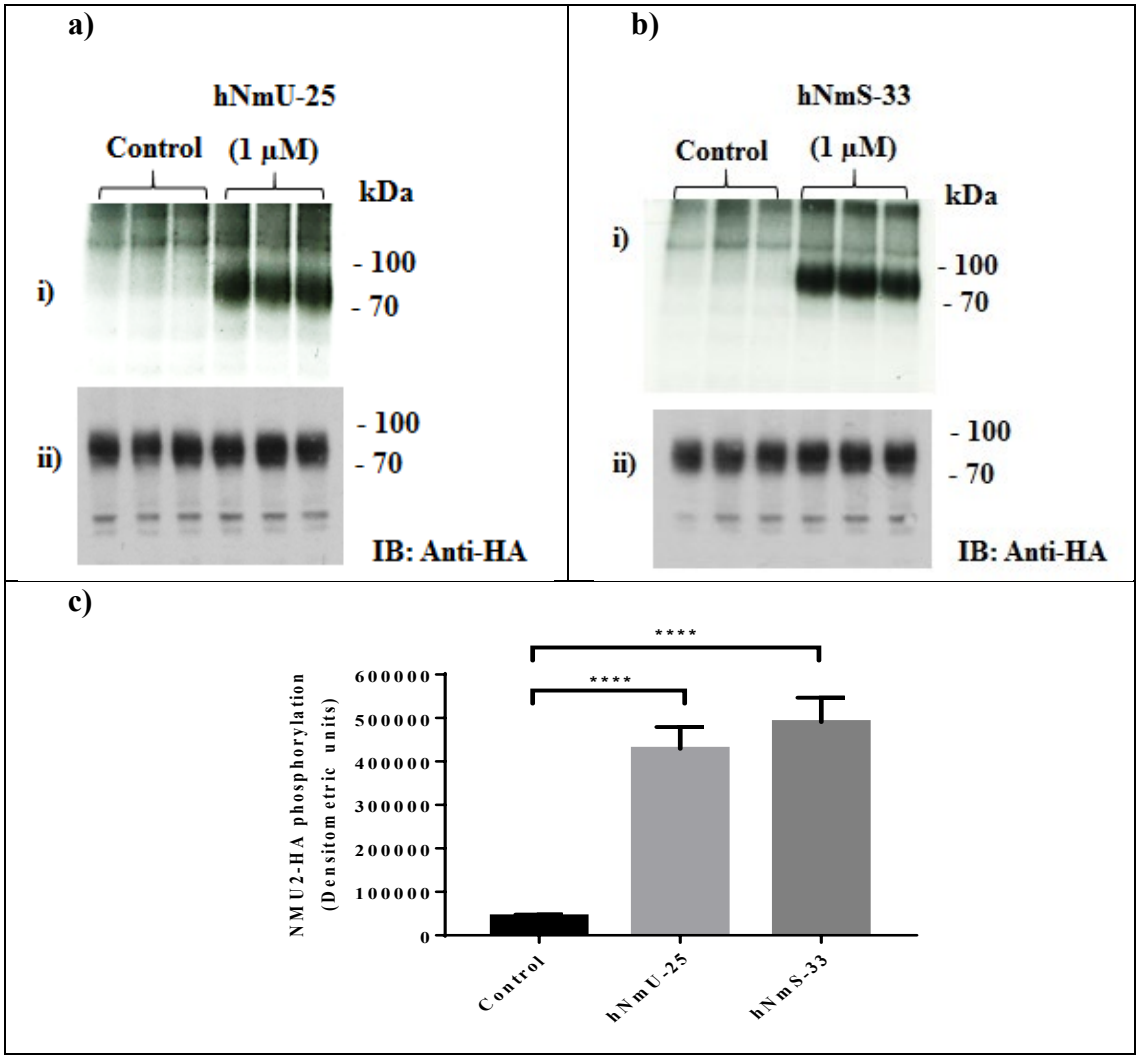


**Figure 4.2. hNmU-25- and hNmS-33-mediated phosphorylation of NMU2-HA in cells with stable transfection**

HEK-NMU2-HA were grown on poly-D-lysine coated 6-well plates for 24 h. Cells were washed twice with phosphate-free KHB and labelled with $^{32}$P orthophosphate for 1 h. Cells were then stimulated with hNmU-25 (1 µM), hNmS-33 (1 µM) or control (KHB) for 5 min as indicated (a, b). Following solubilisation of the cell monolayer, NMU2-HA was immunoprecipitated and resolved by gel electrophoresis. The gel was then dried and visualised by autoradiography ($a_i$, $b_i$). Immunoblotting of the immunoprecipitates with an anti-HA antibody was used as a loading control of NMU2-HA (IB; $a_{ii}$, $b_{ii}$). The phosphorylation bands were quantified by densitometric analysis using Image J software (c). Data are either representative autoradiographs or blots of n = 3 (a, b) or mean ± sem, n = 3 (c). Statistical analysis was performed using a one way ANOVA followed by Bonferroni's test: $^{****}P < 0.0001$.

### 4.1.3 NMU2-HA phosphorylation induced by 300 nM and 1 μM of the ligands

The levels of NMU2-HA phosphorylation following challenge with either hNmU-25 or hNmS-33 were assessed at either 300 nM or 1μM to assess if the concentration of 1 μM was maximal. $^{32}P$ labelled cells were challenged with either hNmU-25 or hNmS-33 at either 300 nm or μM for 5 min. NMU2-HA was immunoprecipitated and $^{32}P$ incorporation visualised by autoradiography. Stimulation for 5 min with either 300 nM or 1 μM resulted in similar levels of NMU2-HA phosphorylation for each ligand **(Figure 4.3; $a_i$, $b_i$)**. Furthermore, levels of phosphorylation were similar between hNmU-25 and hNmS-33 **(Figure 4.3; c, d)**.

.

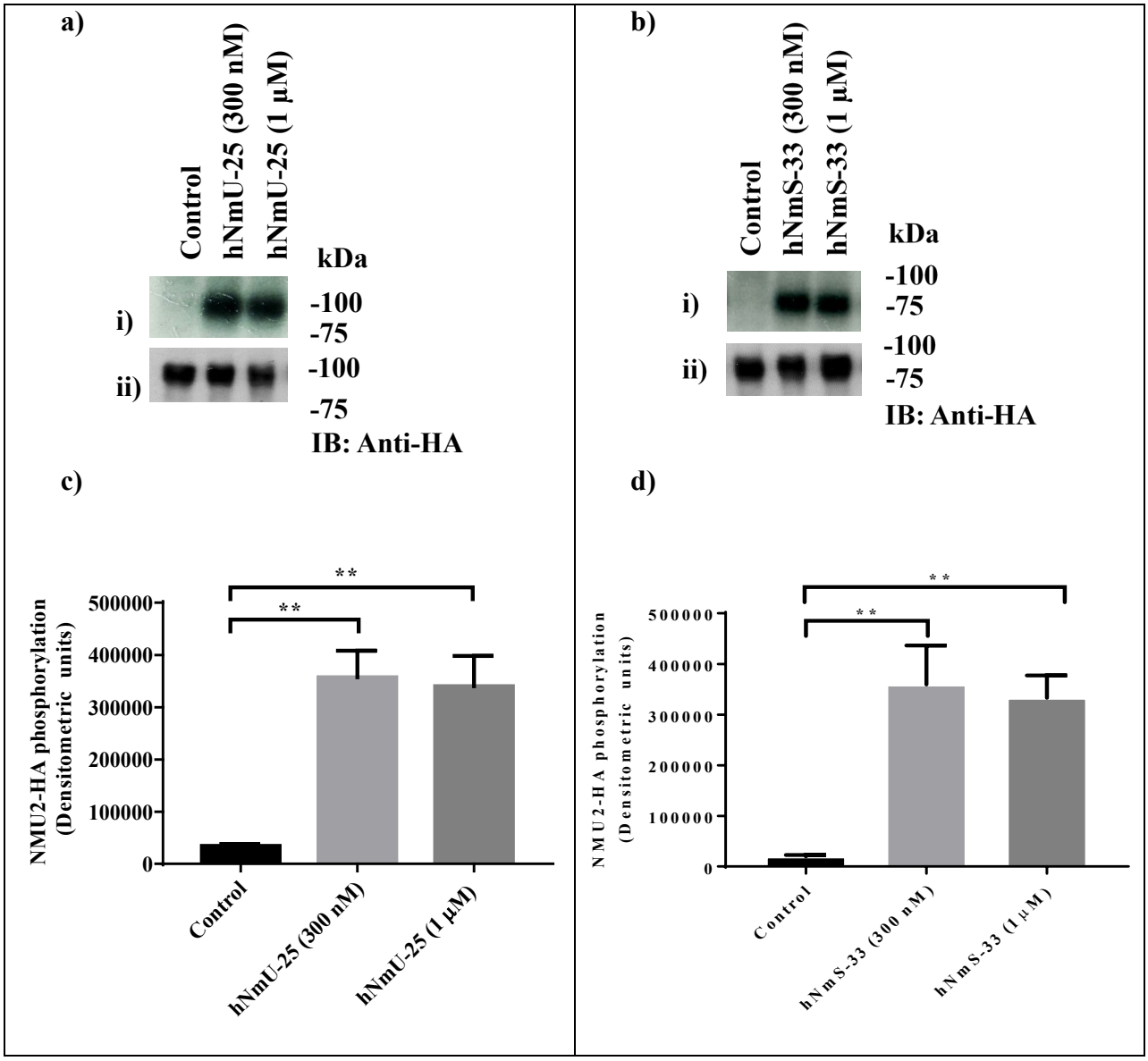


**Figure 4.3. hNmU-25- and hNmS-33-mediated similar levels of NMU2-HA phosphorylation at 300 nM and 1 µM.**

HEK-NMU2-HA cells were plated in poly-D-lysine coated 6-well plates for 24 h. Cells were washed twice with phosphate-free KHB and labelled with $^{32}P$ orthophosphate for 1 h. Cells were then challenged with either hNmU-25 or hNmS-33 at either 300 nM or 1 µM for 5 min. Cells were then solubilized and NMU2-HA was immunoprecipitated and resolved by gel electrophoresis. The gel was then dried and visualised by autoradiography ($a_i$, $b_i$). Immunoblotting of the immunoprecipitates with an anti-HA antibody was used as a loading control for NMU2-HA (IB; $a_{ii}$, $b_{ii}$). The phosphorylation bands were quantified by densitometric analysis using Image J software (c, d). Data are either representative autoradiographs or blots of n = 3 (a, b) or mean ± sem, n = 3 (c, d). Statistical analysis

was performed using a one way ANOVA followed by Bonferroni's test: $^{**}P < 0.01$. (Control = KHB buffer).

## 4.2 Role of second messenger-dependent kinases (PKC and PKA) in phosphorylation of NMU2-HA

### 4.2.1 Effect of direct PKC activation on ERK activation in HEK-NMU2-HA

The present experiments were generated on HEK-NMU2-HA to assess 1) if NMU2-HA is a substrate for PKC and 2) if PKC is involved in agonist-mediated NMU2-HA phosphorylation. Firstly to assess the ability of PDBu to activate PKC and the ability of PKC inhibitors (Ro 31-8220, GF109203X, or PKC 20-28 inhibitor peptide) to inhibit PKC in these cells, ERK activation was examined as it is often driven by PKC activation (Cisse *et al.*, 2011). Exposing the cells to PDBu for 5 min caused a robust increase in ERK activity determined by immunoblotting of pERK **(Figure 4.4; b)**. Levels of PDBu-induced ERK activation were significantly decreased when the cells pre-incubated with the PKC inhibitors (Ro 318220 and GF109203X) **(Figure 4.4; a, c)**. In contrast, PKC 20-28 showed no effect on the levels of ERK activity in response to challenge of the cells with PDBu **(Figure 4.4; c)**.

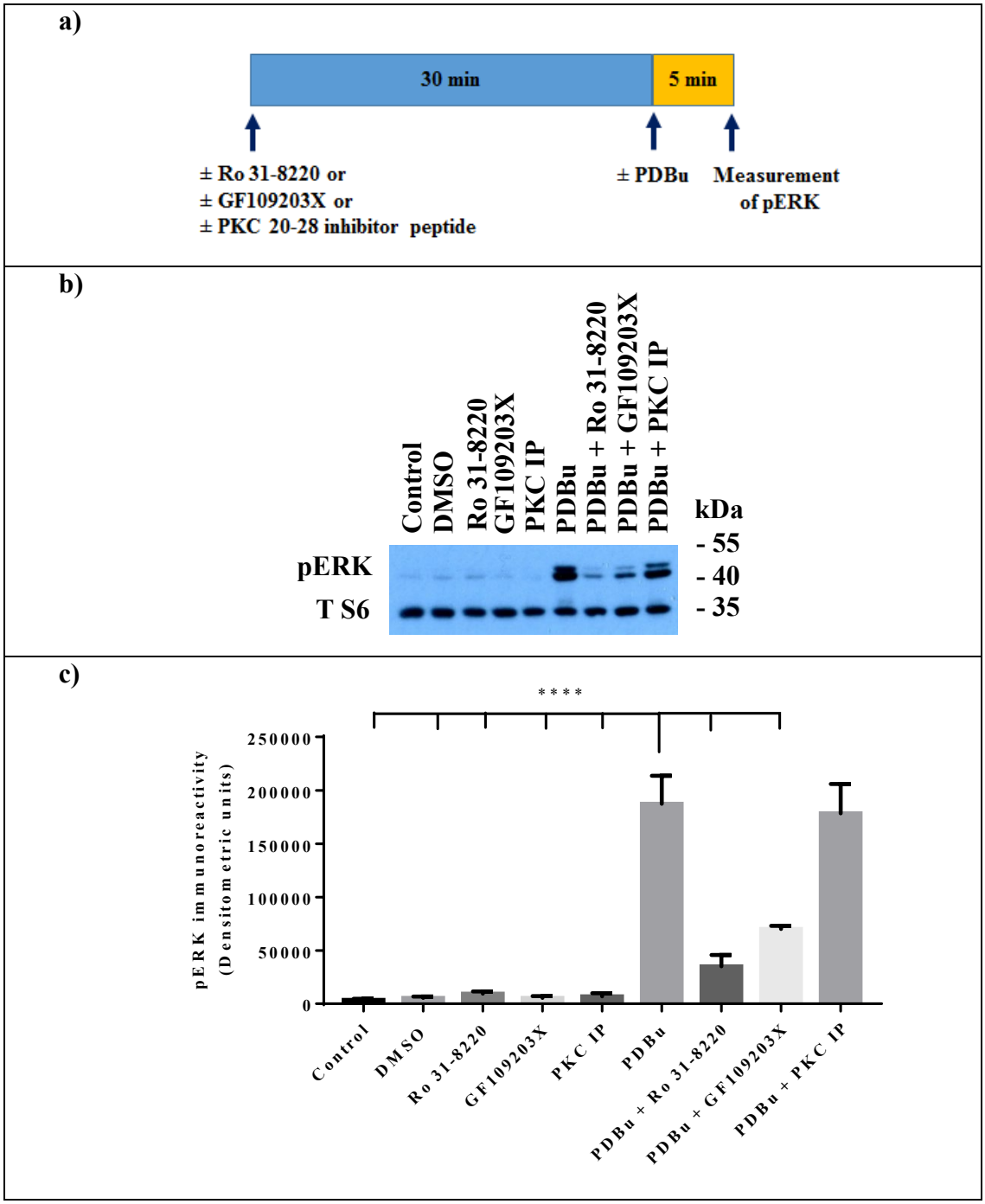


**Figure 4.4. PDBu-mediated ERK activation in HEK-NMU2-HA.**

Cells were plated on poly-D-lysine coated 24 well plates for 24 h and serum-starved overnight. Cells were pre-treated with Ro 31-8220 (5 µM, 30 min), GF109203X (1 µM, 30 min), PKC 20-28 inhibitor peptide (PKC IP; 50 µM, 30 min), DMSO (vehicle), control (buffer). Cell were then challenged with PDBu (1 µM, 5 min) or left without further treatment (a) as indicated (b). Following solubilisation, the samples were resolved by gel electrophoresis and the pERK was measured as an index of ERK activation using Western blotting. The blots were then quantified by densitometric analysis using Image J software

(c). Statistical analysis was performed using a one way ANOVA followed by Bonferroni's test: $^{****}$, $P < 0.0001$ for PDBu versus other groups as indicated. Data are either representative immunoblots of n = ≥ 3 (b) or mean ± sem, n = ≥ 3 (c). T S6 was used as a loading control. Control = KHB buffer, DMSO = vehicle control for Ro 31-8220 and GF109203X.

### 4.2.2 Effect of direct PKC activation on phosphorylation of NMU2-HA

After demonstrating that PDBu provoked ERK activation by its direct PKC activation and the levels of ERK activity induced by PDBu were impaired in the presence of Ro 318220 or GF109203X in HEK-NMU2-HA **(Section 4.2.1)**, PDBu was then used to determine if NMU2-HA is a substrate for PKC. In addition, the ability of Ro 318220 to inhibit PDBu-mediated phosphorylation of NMU2-HA was determined to confirm the ability of this inhibitor to inhibit any PKC-mediated NMU2-HA phosphorylation. In HEK-NMU2-HA, challenge with PDBu for 5 min provoked a marked increase in NMU2-HA phosphorylation (6.9 ± 1.3 fold over basal levels) **(Figure 4.5; $a_i$)**. After pre-incubation with Ro 31-8220, PDBu-mediated NMU2-HA phosphorylation was significantly reduced **(Figure 4.5; b)**.

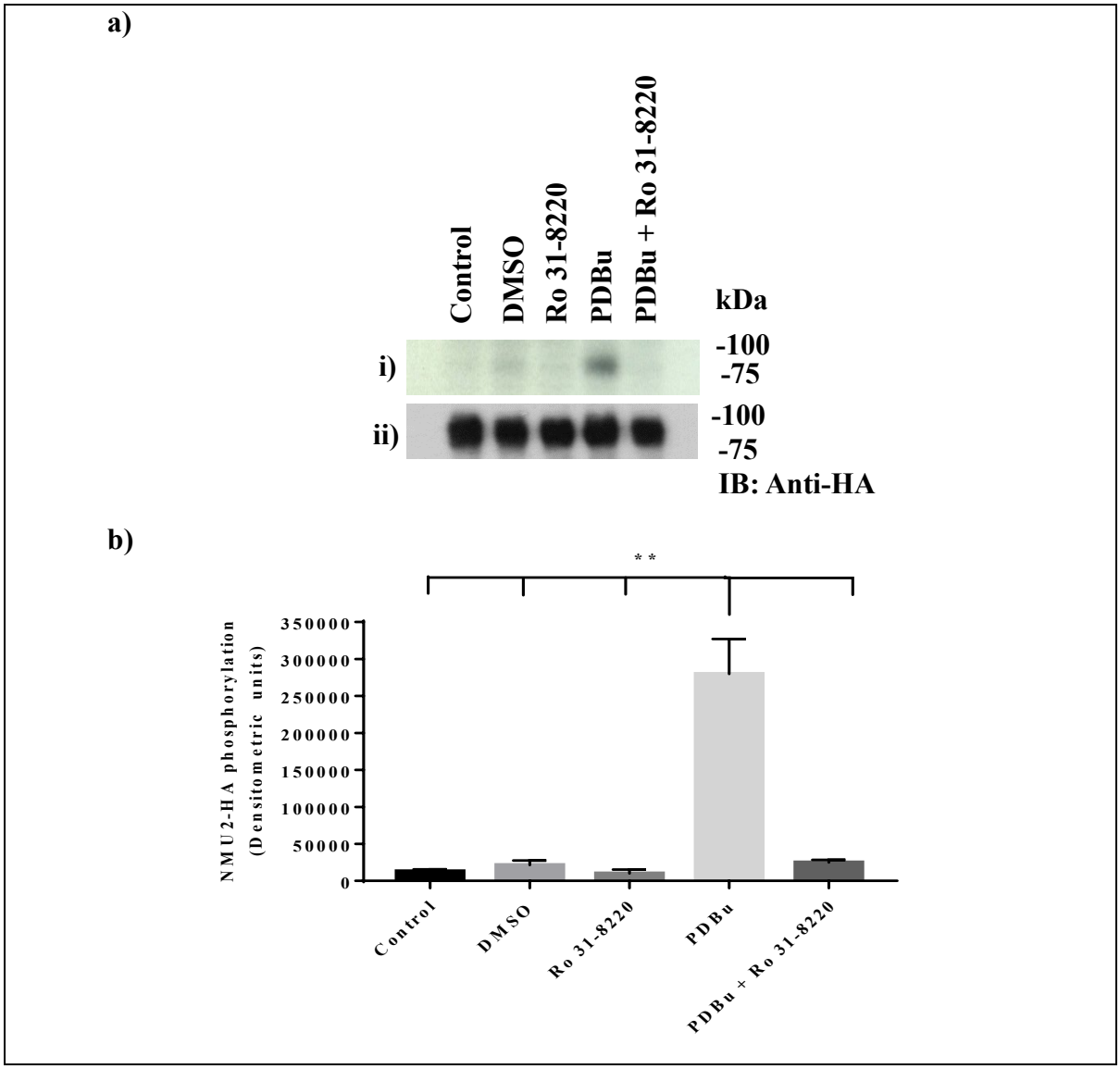


**Figure 4.5. Direct activation of PKC causes phosphorylation of NMU2-HA**

HEK-NMU2-HA cells were grown on poly-D-lysine coated 6-well plates for 24 h. Cells were washed twice with phosphate-free KHB and labelled with $^{32}P$ orthophosphate for 1 h. Cells were then pre-incubated with or without Ro 31-8220 (5 μM, 30 min) and then challenged with PDBu (1 μM, 5 min) where required as indicated (b). Cells were then solubilized and NMU2-HA was immunoprecipitated and resolved by gel electrophoresis. The gel was dried and visualised by autoradiography ($a_i$). Immunoblotting of the immunoprecipitates with an anti-HA antibody was used as a loading control for NMU2-HA (IB; $a_{ii}$). The phosphorylated bands were quantified by densitometry using Image J software (b). Data are either representative autoradiographs or blots of n = 3 (a) or mean ± sem, n = 3 (b). Statistical analysis was performed using a one way ANOVA followed

by Bonferroni's test: **, $P < 0.01$ for PDBu versus all other groups. Control = KHB buffer, DMSO = vehicle control for Ro 31-8220.

### 4.2.3 Effect of PKA activation on CREB signalling in HRK-NMU2-HA

Experiments were performed to confirm that forskolin (FSK), a direct activator of adenylyl cyclase, is able to induce PKA activation in HEK-NMU2-HA. this was carried out by examining phosphorylation of cAMP response element binding protein (CREB), which is a substrate for PKA in some circumstances (Li *et al.*, 2017c). Furthermore, the ability of PKA inhibitors (KT5720 and H89) to inhibit the forskolin-mediated PKA activation was also determined. Isobutyl-1-methylxanthine (IBMX) was used to inhibit phosphodiesterase activity and to therefore potentially increase FSK-mediated increases in cellular cAMP levels. Stimulation of cells with FSK for 5 min caused a significant increase in CREB activity, assessed by immunoblotting of phospho-CREB (pCREB). At this point, the levels of activated CREB increased (8.7 ± 1.1 fold over basal levels) **(Figure 4.6; b)**. Following pre-incubation of cells with H89 and stimulation with FSK in the presence of IBMX as indicated **(Figure 4.6; a)**, CREB activity was significantly reduced by H89 only 35.9 % ± 0.5 of the response to FSK. By contrast, KT5720 had no effect on levels of activated CREB **(Figure 4.6; c)**.

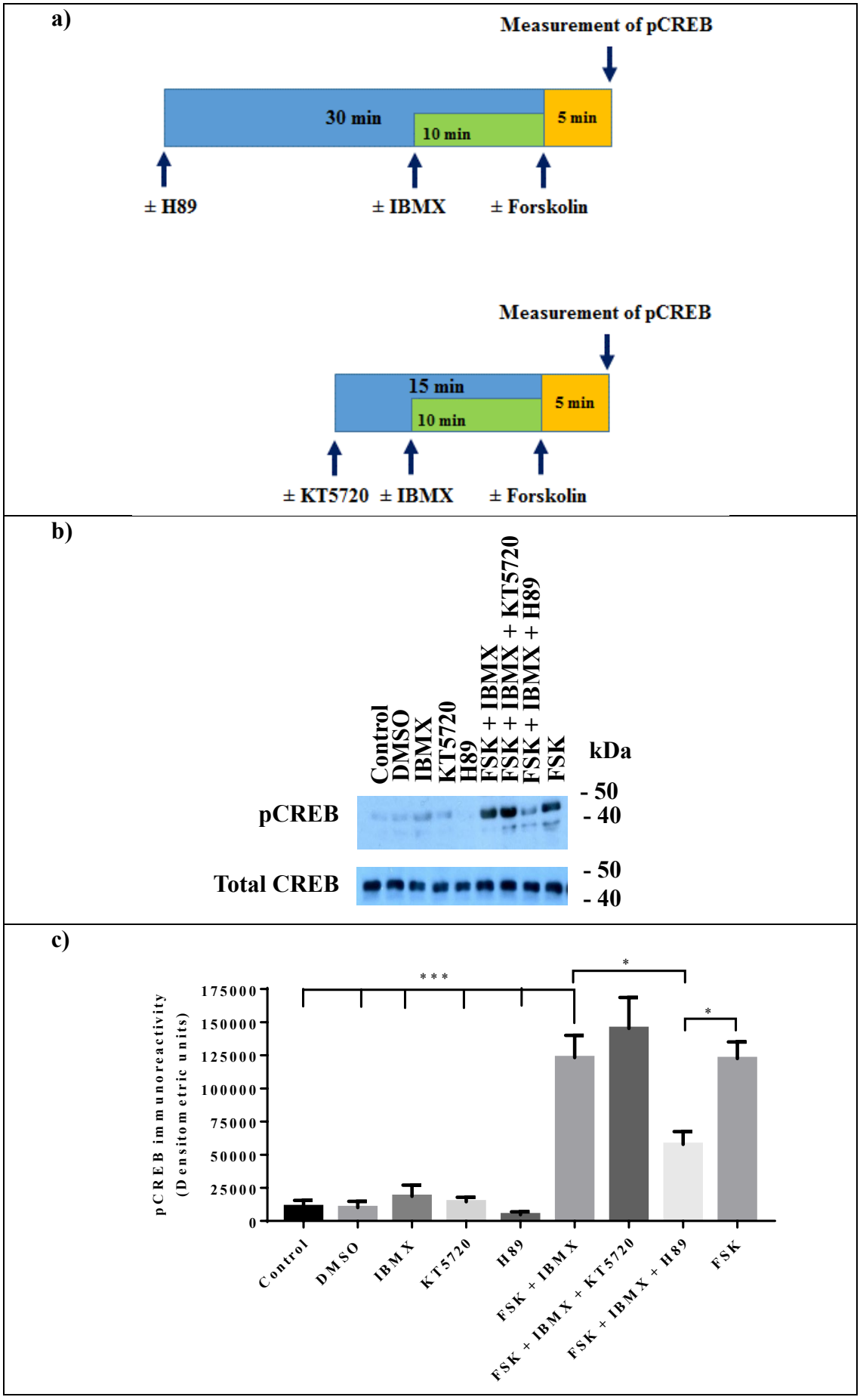
a)
Measurement of pCREB
30 min
10 min
5 min
± H89
± IBMX
± Forskolin
Measurement of pCREB
15 min
10 min
5 min
± KT5720
± IBMX
± Forskolin
b)
Control
DMSO
IBMX
KT5720
H89
FSK + IBMX
FSK + IBMX + KT5720
FSK + IBMX + H89
FSK
kDa
pCREB
- 50
- 40
Total CREB
- 50
- 40
c)
pCREB immunoreactivity (Densitometric units)
175000
150000
125000
100000
75000
50000
25000
0
***
*
*
Control
DMSO
IBMX
KT5720
H89
FSK + IBMX
FSK + IBMX + KT5720
FSK + IBMX + H89
FSK

**Figure 4.6. FSK-mediated CREB activation in HEK-NMU2-HA.**

Cells were grown on poly-D-lysine coated 24-well plates for 24 h and serum-starved overnight. Cells were pre-incubated with or without the PKA inhibitors H89 (10 μM, 30 min), KT5720 (1 μM, 15 min). The phosphodiesterase inhibitor, IBMX , was then added if required (as indicated) for the final 10 min of the pre-incubation period before cells were challenged where required with FSK (100 μM, 5 min) (a) as indicated (b). Following solubilisation, pCREB was determined as an index of CREB activation using Western blotting. The density of immunoblots was determined using Image J software (c). Statistical analysis was performed using a one way ANOVA followed by Bonferroni's test: $^{*}P < 0.05$, $^{***}$, $P < 0.001$ for FSK +IBMX versus other groups as indicated. Data are either representative immunoblots of n = 3 (b) or mean ± sem, n = 3 (c). Immunoblotting of total CREB was used as a loading control. Control = KHB buffer, DMSO = vehicle control for KT5720, H89 and IBMX.

### 4.2.4 Effect of PKA activation on NMU2-HA phosphorylation

The levels of NMU2-HA phosphorylation were assessed using forskolin as a direct PKA activator to confirm that NMU2-HA is a potential substrate for PKA. To address this, cells were pre-incubated with IBMX before challenge with forskolin for 5 min **(Figure 4.7; a)**. Stimulation with hNmU-25 was used as a positive control for NMU2-HA phosphorylation which markedly increased the levels of NMU2-HA phosphorylation (7.8 ± 0.8 fold over basal levels) **(Figure 4.7; $b_i$)**. None of the other conditions enhanced the phosphorylation levels of NMU2-HA, including challenge with forskolin in the presence of IBMX **(Figure 4.7; c)**.

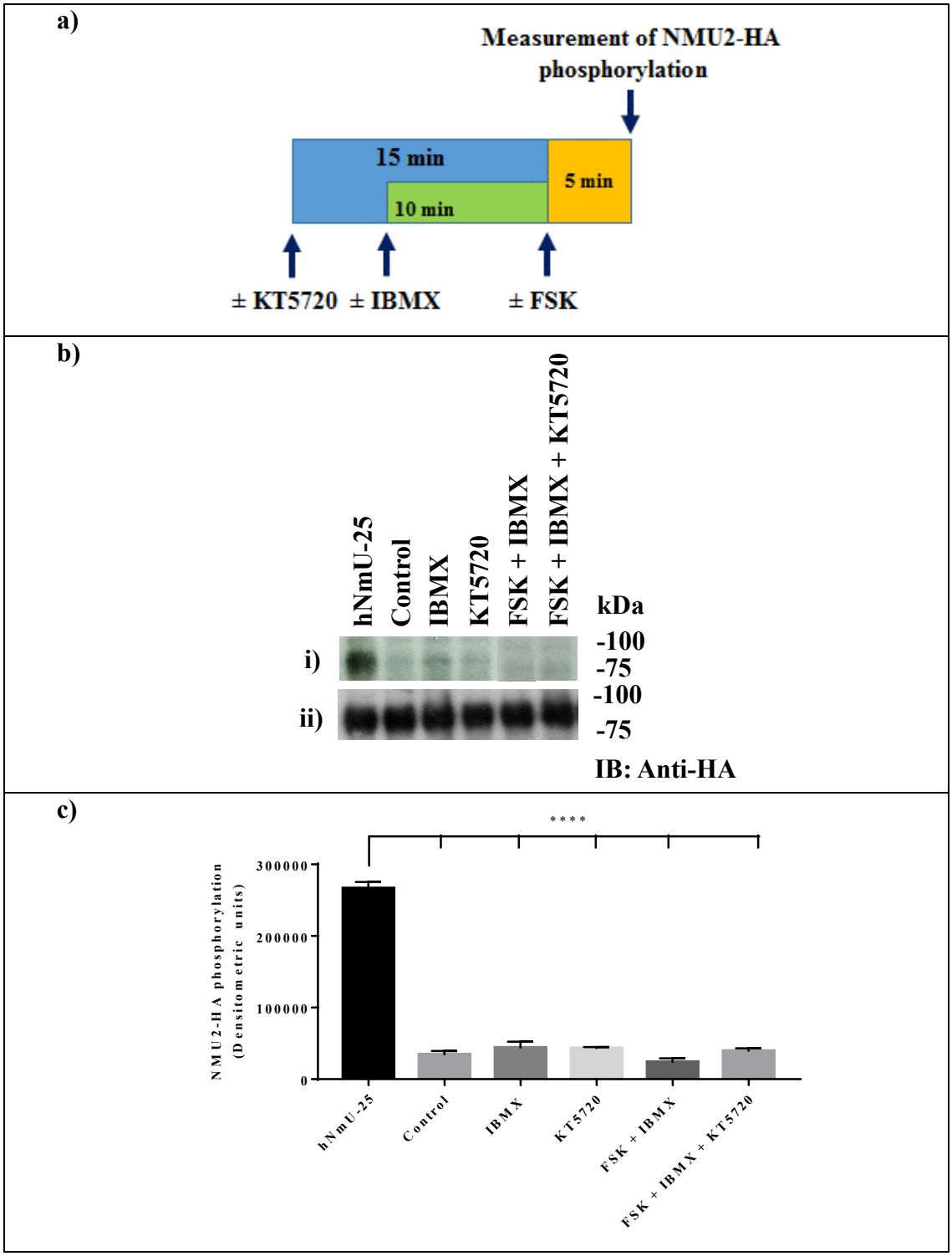


**Figure 4.7. Effect of PKA activation on NMU2-HA phosphorylation.**

HEK-NMU2-HA cells were grown on poly-D-lysine coated 6-well plates for 24 h. Cells were washed twice with phosphate-free KHB and labelled with $^{32}P$ orthophosphate for 1 h. Cells were pre-incubated with or without KT5720 (1 µM, 15 min) before addition of IBMX (500 µM, 10 min) and then forskolin (100 µM, 5 min) as required. As a positive control, cells were challenged with hNmU-25 (1 µM, 5 min) or vehicle (DMSO; control)

for 5 min (a) as indicated (b). Following solubilisation of cell monolayers, NMU2-HA was immunoprecipitated and resolved by gel electrophoresis. The gel was then dried and visualised by autoradiography (bi). Immunoblotting of the immunoprecipitates with an anti-HA antibody was used as a loading control for NMU2-HA (IB; $b_{ii}$). The phosphorylated bands were quantified by densitometry using Image J software (c). Data are either representative autoradiographs or blots of n = 3 (b) or mean ± sem, n = 3 (c). Statistical analysis was performed using a one way ANOVA followed by Bonferroni's test: $^{****}$, $P < 0.0001$ for hNmU-25 versus all other groups.

## 4.3 Exploring potential heterologous phosphorylation of HEK-NMU2-HA

Heterologous phosphorylation by the second messenger kinases PKC and PKA is an essential phenomenon, generally resulting in desensitisation, that commonly occurs in either active or inactive states of GPCRs to avoid the cells from being overstimulated by long-term exposure to ligands (Rajagopal *et al.*, 2018). Here, experiments were performed on HEK-NMU2-HA to investigate the potential role of heterologous phosphorylation by PKC or PKA following activation of $G_{\alpha q}$-coupled muscarinic M3 receptors and $G_s$-coupled $\beta_2$ adrenoceptors that are endogenously expressed in HEK-293. These receptors will activate PKC and PKA respectively upon ligand binding (Daaka *et al.*, 1997a; Luo *et al.*, 2008b) and the muscarinic M3 receptor is therefore of particular interest given the work described earlier that demonstrated that NMU2-HA is a substrate for PKC.

Carbachol was used to confirm that HEK-NMU2-HA express muscarinic receptors by examining ERK activity in response to challenge. Activation of $G_{\alpha q}$-coupled muscarinic receptors will result in PKC activation leading to activation of ERK (Kim *et al.*, 1999). Challenge of cells with hNmU-25, hNmS-33 or carbachol for 5 min induced ERK activation which was assessed by immunoblotting of pERK (37.6 ± 6.5, 38.7 ± 6.3 and 21.5 ± 3.2 fold over basal levels respectively) **(Figure 4.8; a)**. ERK activity in response to hNmU-25 and hNmS-33 was significantly greater than that induced by carbachol **(Figure 4.8; b)**.

Experiments were also performed to confirm that the $\beta_2$ adrenoceptor is endogenously expressed in HEK-NMU2-HA by determining the activation of CREB in response to isoprenaline. Activation of CREB is a downstream consequence of PKA activation (Bird *et al.*, 2010; Pearce *et al.*, 2017). Cells were stimulated with isoprenaline for 5 min and the CREB activity was determined by immunoblotting of pCREB. Data showed a marked increase in CREB activity (8.9 ± 0.6 fold over basal levels) **(Figure 4.9; b)**. Isoprenaline-mediated CREB activation was significantly decreased following pre-treatment with the PKA inhibitor, H89. In contrast, KT5720 did not influence the levels of activated CREB **(Figure 4.9; c)**.

After confirmation that $G_{\alpha q}$-coupled muscarinic receptors and $G_{\alpha s}$-coupled β adrenoceptors were endogenously expressed on HEK-NMU2-HA, the potential

heterologous phosphorylation of NMU2-HA was assessed by incubating the $^{32}P$ labelled cells with hNmU-25 (positive control), carbachol (1 mM) or isoprenaline (1 μM) for 5 min. Autoradiographs of $^{32}$ P-incorporated NMU2-HA showed that hNmU-25 significantly increased NMU2-HA phosphorylation (10.7 ± 1.7 fold over basal levels). However, neither carbachol nor isoprenaline caused increases in NMU2-HA phosphorylation following 5 min exposure **(Figure 4.10; b)**. Moreover, no changes were observed in the levels of NMU2-HA phosphorylation following pre-treatment with either Ro 31-8220 or KT5720 alone or following challenge with either carbachol or isoprenaline respectively **(Figure 4.10; a, c)**.

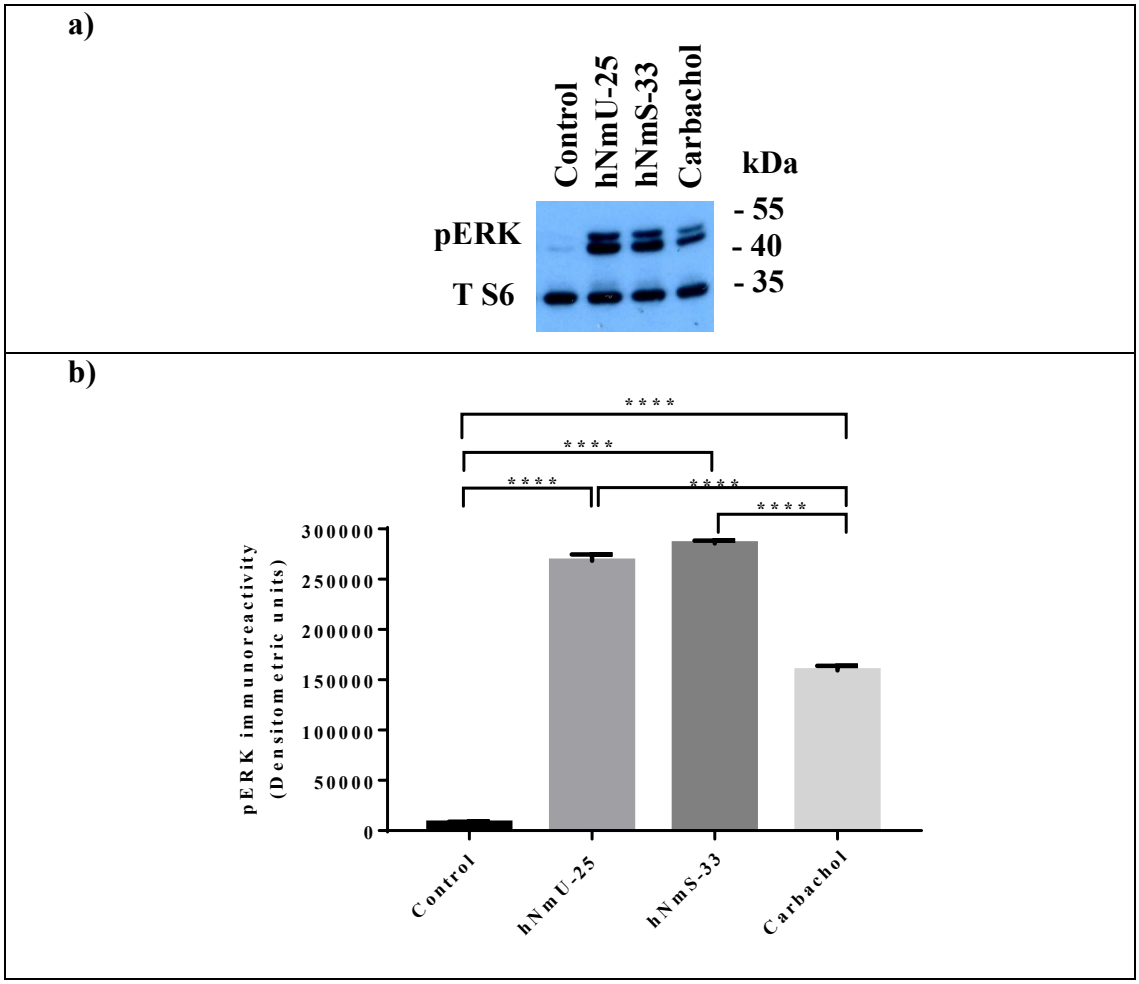


**Figure 4.8. hNmU-25-, hNmS-33- and carbachol-mediated ERK activation in HEK-NMU2-HA.**

Cells were grown on poly-D-lysine coated 24-well plates for 24 h and serum-starved overnight. Cells were challenged with hNmU-25 (30 nM), hNmS-33 (30 nM) or carbachol (1 mM) for 5 min before solubilisation. The pERK activation was determined as an index of ERK activation using Western blotting. The immunoblots were quantified by densitometric analysis using Image J software (b). Statistical comparison was performed using a one way ANOVA followed by Bonferroni's test: $^{****}P < 0.0001$. Data are either representative immunoblots of n ≥ 3 (a) or mean ± sem, n ≥ 3 (b). T S6 was used as loading control.

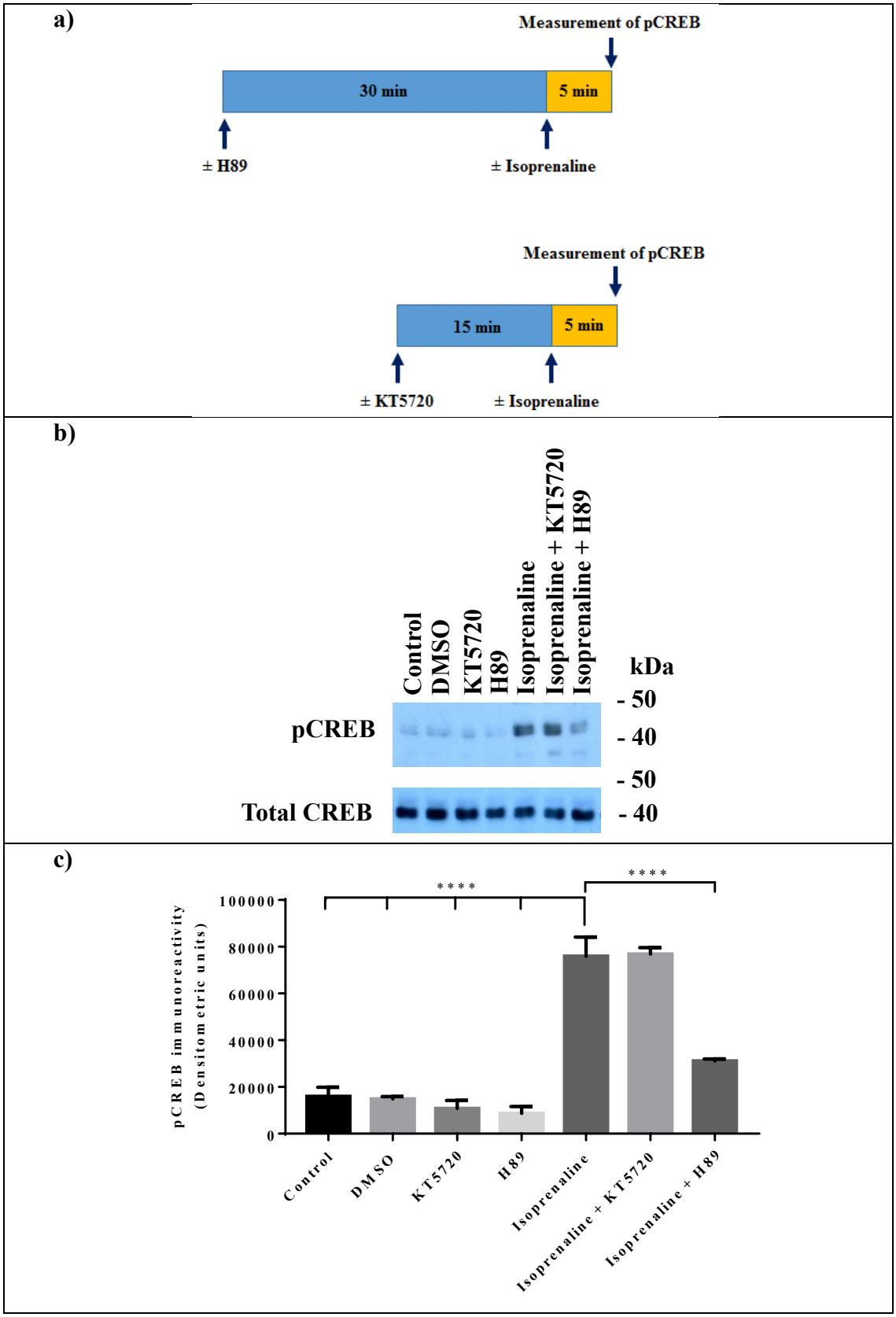


**Figure 4.9. Isoprenaline-mediated CREB activation in HEK-NMU2-HA.**

Cells were cultured in poly-D-lysine coated 24-well plates for 24 h and serum-starved overnight. Cells were pre-treated with or without H89 (10 µM, 30 min), KT5720 (1 µM,

15 min) and then challenged with isoprenaline (1 μM, 5 min) as required (a, b). Cells were solubilised and pCREB determined as an index of CREB activation using Western blotting. Immunoblotting of total CREB was used as a loading control. The signal density of immunoblots was calculated using Image J software (c). Statistical analysis was performed using a one way ANOVA followed by Bonferroni's test: $^{****}$, $P < 0.0001$ for isoprenaline versus other groups as indicated. Data are either representative immunoblots of n = 3 (b) or mean ± sem, n = 3 (c). Control = KHB buffer, DMSO = vehicle control for KT5720 and H89.

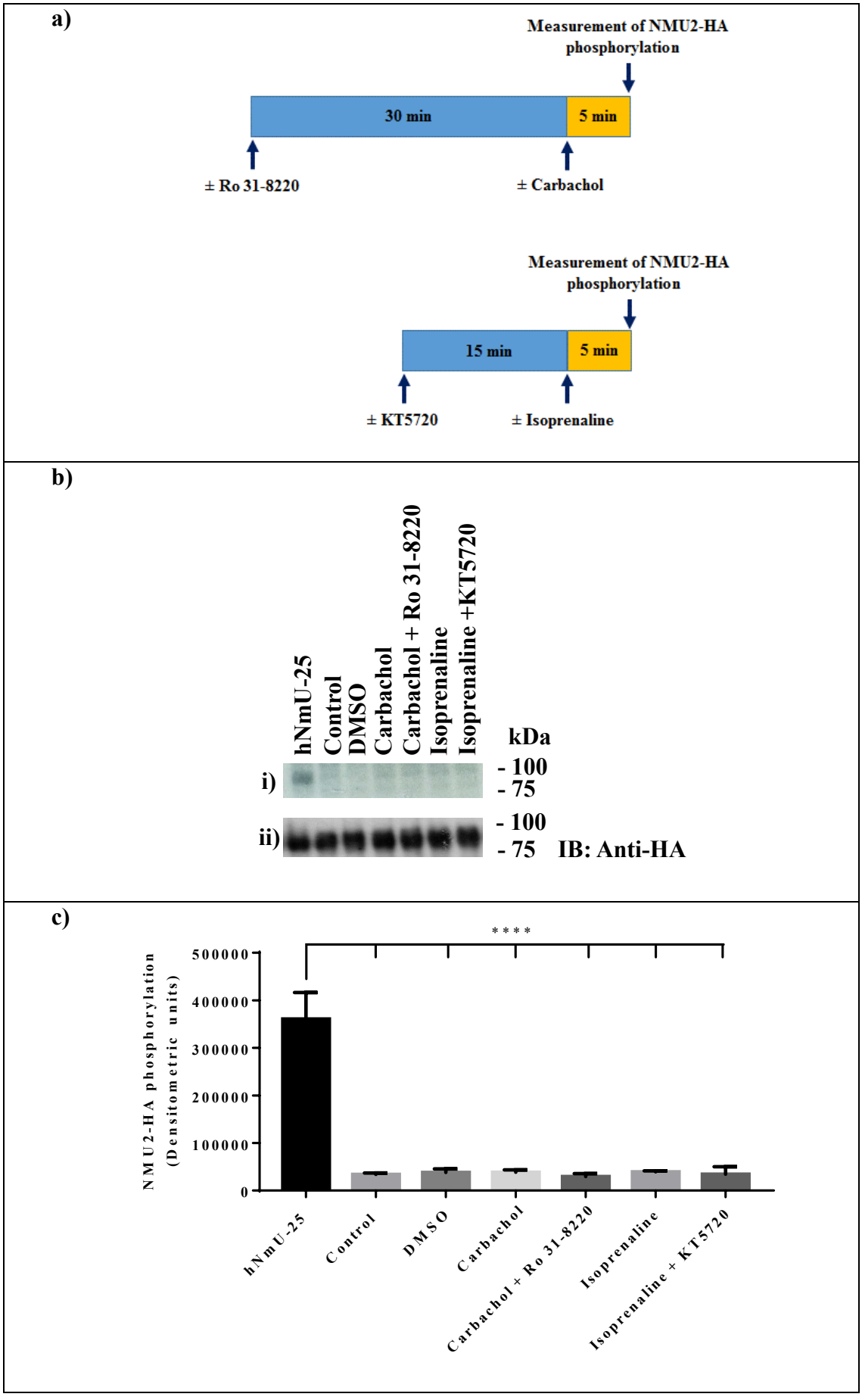
a)
Measurement of NMU2-HA phosphorylation
30 min
5 min
± Ro 31-8220
± Carbachol
Measurement of NMU2-HA phosphorylation
15 min
5 min
± KT5720
± Isoprenaline
b)
hNmU-25
Control
DMSO
Carbachol
Carbachol + Ro 31-8220
Isoprenaline
Isoprenaline +KT5720
kDa
i)
- 100
- 75
ii)
- 100
- 75
IB: Anti-HA
c)
****
NMU2-HA phosphorylation (Densitometric units)
500000
400000
300000
200000
100000
0
hNmU-25
Control
DMSO
Carbachol
Carbachol + Ro 31-8220
Isoprenaline
Isoprenaline + KT5720

**Figure 4.10. Lack of Effect of carbachol or isoprenaline on NMU2-HA phosphorylation.**

HEK-NMU2-HA cells were cultured in poly-D-lysine coated 6-well plates for 24 h. Cells were washed twice with phosphate-free KHB and labelled with $^{32}P$ orthophosphate for 1 h. Cells were pre-incubated within the $^{32}P$ labelling period with or without Ro 31-8220 (5 μM, 30 min), KT5720 (1 μM, 15 min) and then left unchallenged or challenged with either carbachol (1 mM, 5 min) or isoprenaline (1 μM, 5 min) (a, b). hNmU-25 (1 μM, 5 min) was used as a positive control. Following solubilisation, NMU2-HA was immunoprecipitated and resolved by gel electrophoresis. The gel was then dried and visualised by autoradiography ($b_i$). Immunoblotting of the immunoprecipitates with an anti-HA antibody was used as a loading control for NMU2-HA (IB; $b_{ii}$). The phosphorylated bands were quantified by densitometric analysis using Image J software (c). Data are either representative of autoradiographs or blots of n = 3 (b) or mean ± sem, n = 3 (c). Statistical analysis was performed using a one way ANOVA followed by Bonferroni's test: $^{****}$, $P < 0.0001$ for hNmU-25 versus all other groups. Control = KHB buffer, DMSO = vehicle control for Ro 31-8220 and KT5720.

## 4.4 Role of PKC and PKA in agonist-dependent phosphorylation of NMU2-HA

The potential role of PKC or PKA phosphorylation of NMU2-HA following stimulation with either hNmU-25 or hNmS-33 was investigated by pre-incubating the cells with PKC or PKA inhibitors before challenge with the ligands (1μM, 5 min) **(Figure 4.11; a)**. Both ligands markedly increased NMU2-HA phosphorylation **(Figure 4.11; b, c)**. The PKC inhibitor, Ro 31-8220, significantly reduced levels of NMU2-HA phosphorylation in response to both hNmU-25 **(Figure 4.11; d)** and hNmS-33 **(Figure 4.11; e)**. In contrast, a number of different PKA inhibitors did not influence the levels of NMU2-HA phosphorylation in response to either ligand **(Figure 4.11; d, e)**.

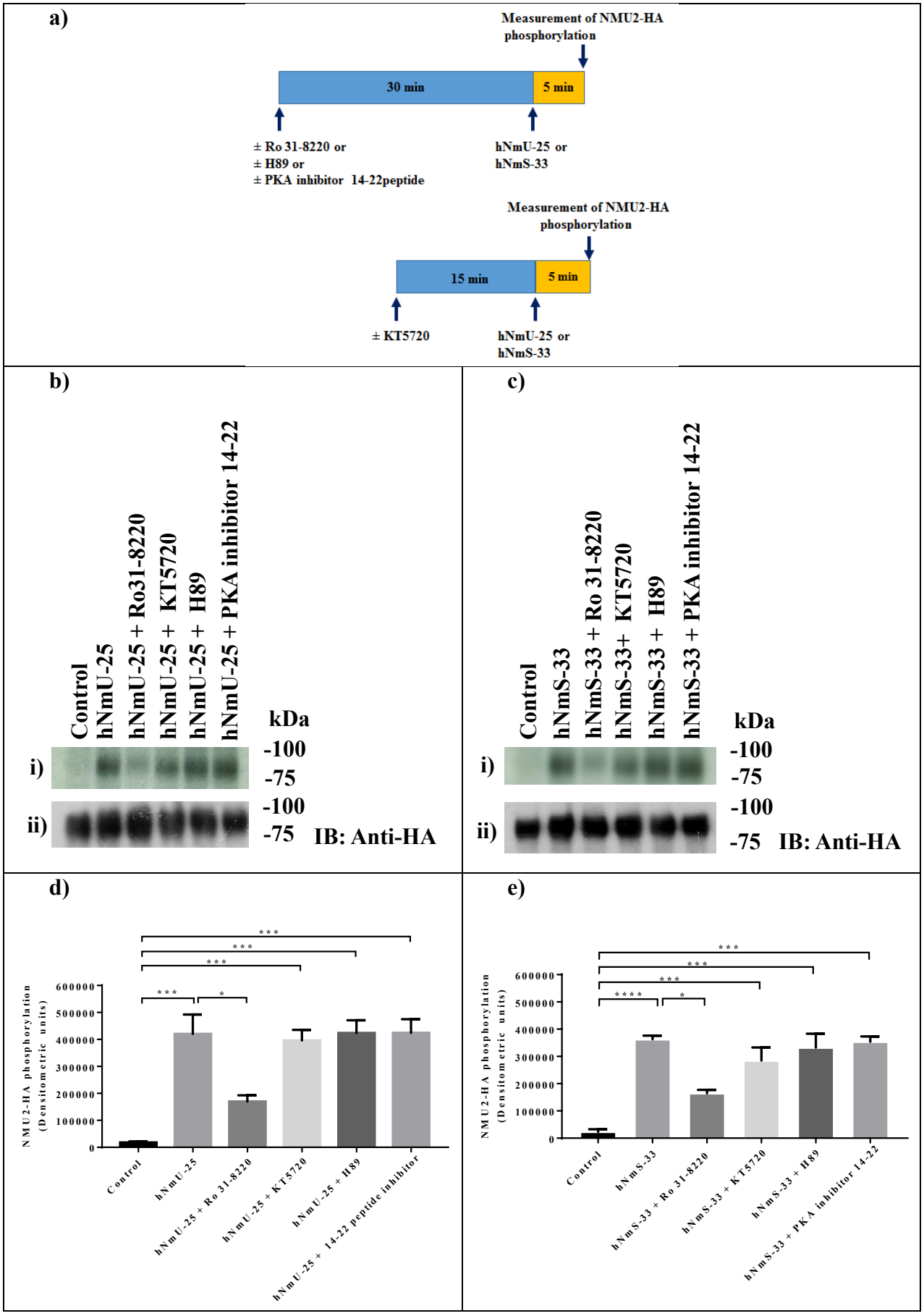
a)
Measurement of NMU2-HA phosphorylation
30 min
5 min
± Ro 31-8220 or
± H89 or
± PKA inhibitor 14-22peptide
hNmU-25 or
hNmS-33
Measurement of NMU2-HA phosphorylation
15 min
5 min
± KT5720
hNmU-25 or
hNmS-33
b)
Control
hNmU-25
hNmU-25 + Ro31-8220
hNmU-25 + KT5720
hNmU-25 + H89
hNmU-25 + PKA inhibitor 14-22
kDa
i)
ii)
-100
-75
-100
-75
IB: Anti-HA
c)
Control
hNmS-33
hNmS-33 + Ro 31-8220
hNmS-33+ KT5720
hNmS-33 + H89
hNmS-33 + PKA inhibitor 14-22
kDa
i)
ii)
-100
-75
-100
-75
IB: Anti-HA
d)
NMU2-HA phosphorylation (Densitometric units)
600000
500000
400000
300000
200000
100000
0
Control
hNmU-25
hNmU-25 + Ro 31-8220
hNmU-25 + KT5720
hNmU-25 + H89
hNmU-25 + 14-22 peptide inhibitor
e)
NMU2-HA phosphorylation (Densitometric units)
600000
500000
400000
300000
200000
100000
0
Control
hNmS-33
hNmS-33 + Ro 31-8220
hNmS-33 + KT5720
hNmS-33 + H89
hNmS-33 + PKA inhibitor 14-22

**Figure 4.11. Effect of PKC and PKA inhibition on agonist-induced NMU2-HA phosphorylation.**

HEK-NMU2-HA were cultured in poly-D-lysine coated 6-well plates for 24 h. Cells were then washed twice with phosphate-free KHB and labelled with $^{32}P$ orthophosphate for 1 h. Cells were pre-incubated with or without Ro 31-8220 (5 μM, 30 min), PKA inhibitors (H89; 10 μM, 30 min, KT5720; 1 μM, 15 min, and PKA inhibitor 14-22 peptide; 5 μM, 30 min) prior to the challenge with either hNmU-25 (1 μM) or hNmS-33 (1 μM) for 5 min (a). Following solubilisation of the cell monolayers, NMU2-HA was separated by immunoprecipitation and resolved by gel electrophoresis. The gel was then dried and visualised by autoradiography ($b_i$, $c_i$). Immunoblotting of the immunoprecipitates with an anti-HA antibody was used as loading control of NMU2-HA (IB; $b_{ii}$, $c_{ii}$). The phosphorylated bands were quantified by densitometric analysis using Image J software (d, e). Data are either representative autoradiographs or blots of n = 3 (b, c) or mean ± sem, n = 3 (d, e). Statistical analysis was performed using a one way ANOVA followed by Bonferroni's test: $^{*}P < 0.05$, $^{***}P < 0.001$, $^{****}P < 0.0001$. Control = KHB buffer.

## 4.5 NMU2-HA dephosphorylation following brief ligand exposure

Data in **Section 3.2.5** demonstrated profiles in the NMU2-mediated activities of MAP kinases that differed in response to hNmU-25 and hNmS-33. These profiles were similar in the continued presence of ligand. In contrast, they were apparently different when the cells were challenged with the ligand for 5 min followed by removal of the free ligand but not receptor-bound ligand (brief ligand exposure) **(Figure 3.12)**. To address further distinct aspects between hNmU-25 and hNmS-33 on NMU2, NMU2 phosphorylation experiments were performed using brief ligand exposure in which HEK-NMU2-HA was exposed briefly to either hNmU-25 or hNmS-33 for 5 min followed by removal of free extracellular ligand. The levels of NMU2-HA phosphorylation were then determined at different time periods of recovery in ligand-free buffer **(Figure 3.12)**. Both ligands provoked equivalent levels of NMU2-HA phosphorylation at 5 min (16.6 ± 3.5 and 19.7 ± 7.7 fold over basal levels for hNmU-25 and hNmS-33 respectively) **(Figure 4.12; $a_i$, $b_i$)** consistent with earlier data **(Section; 4.1.2)**. However, following the removal of hNmU-25 after the initial 5 min exposure, the phosphorylation levels were different and markedly decreased over 60 min and then remained sustained within the basal levels at later time points. In contrast, NMU2-HA phosphorylation was sustained at 30 min recovery and then gradually decreased over subsequent period of the recovery but still greater than basal levels following brief challenge with hNmS-33. For example, at 90 min of recovery time, the levels of NMU2-HA phosphorylation in response to brief hNmS-33 exposure was 59 % ± 3 of the maximum response whilst only 9 % ± 3 of the total response was observed following brief exposure to hNmU-25 (**Figure 4.12; c)**.

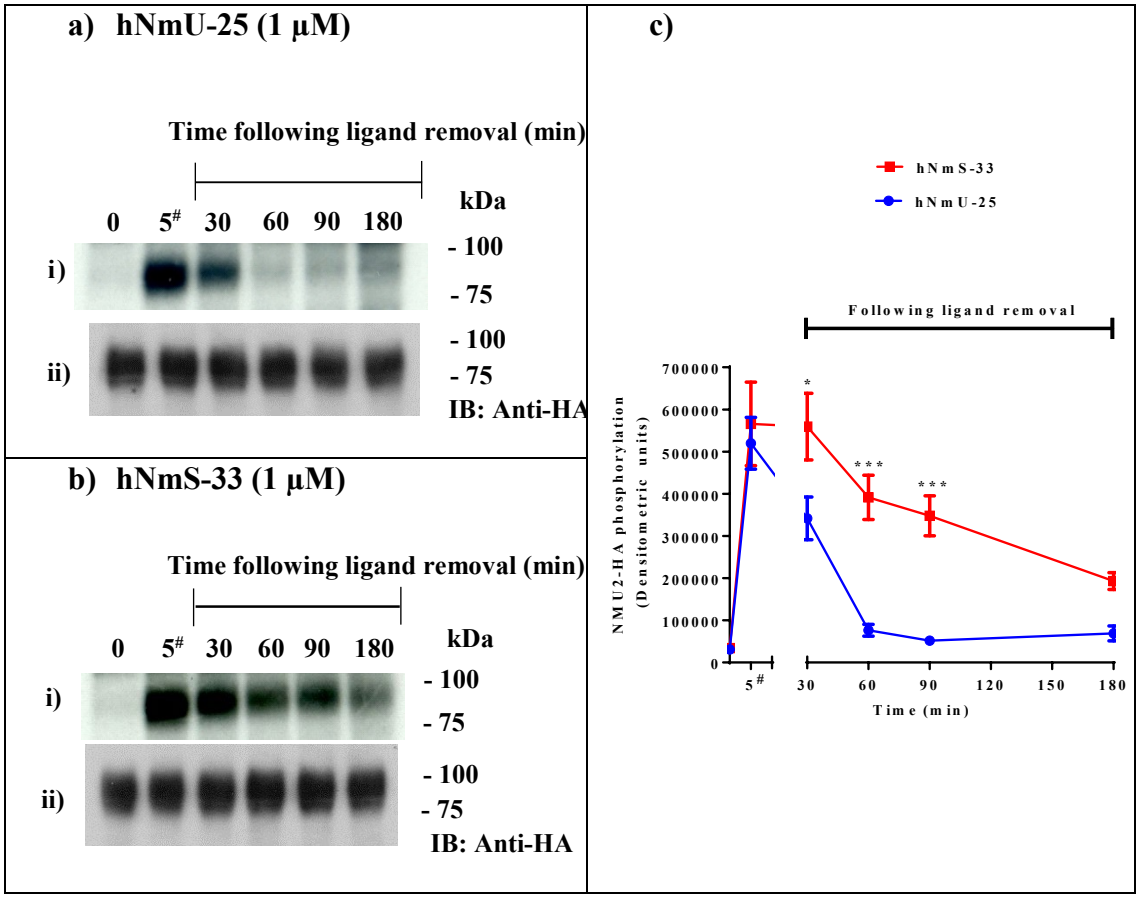


**Figure 4.12. Ligand-dependent dephosphorylation patterns of NMU2-HA following brief ligand exposure.**

HEK-NMU2-HA were grown in poly-D-lysine coated 6-well plates for 24 h. Cells were washed twice with phosphate-free KHB and labelled with $^{32}$P orthophosphate for 1 h. Cells were then challenged with either hNmU-25 (1 µM) or hNmS-33 (1 µM) for 5 min. Following ligand removal and washing of the cell monolayer, cells were allowed to recover in ligand-free buffer for 30 - 180 min. Cells were then solubilized and NMU2-HA was immunoprecipitated and resolved by gel electrophoresis. The gel was dried and visualised by autoradiography ($a_i$, $b_i$). Immunoblotting of the immunoprecipitates with an anti-HA antibody was used as a loading control for NMU2-HA (IB; $a_{ii}$, $b_{ii}$). The phosphorylated bands were quantified by densitometry using Image J software (c). Data are either representative autoradiographs or blots of n = 3 (a, b) or mean ± sem, n = 3 (c). Statistical analysis was performed using two way ANOVA followed by Bonferroni's test: $^{*}P < 0.05$; $^{***}P < 0.001$ for hNmU-25 versus hNmS-33. 0 and 5$^{\#}$ represent the start and finish of the ligand stimulation period.

## 4.6 Effect of PKC inhibition on NMU2-HA phosphorylation following brief exposure

Following brief exposure (5 min) to hNmU-25 and hNmS-33, NMU2-HA phosphorylation was more sustained following hNmS-33 compared to hNmU-25 **(Section; 4.5)**. The results in **Section 4.4** demonstrated that more than 50 % NMU2-HA phosphorylation in response to either hNmU-25 or hNmS-33 at 5 min of stimulation was PKC-dependent. Here, the potential dependence on PKC phosphorylation in response to either hNmU-25 or hNmS-33 was examined during the recovery time following brief ligand exposure to address the potential role of PKC, particularly in the more sustained phosphorylation seen following removal of free extracellular hNmS-33 **(Figure 4.13; a)**.

The potential effect of PKC on the sustained NMU2-HA phosphorylation following brief hNmS-33 exposure was assessed during the recovery time by challenging the cells with either hNmU-25 or hNmS-33 for 5 min followed by removal of free ligand. NMU2-HA phosphorylation was then determined after 1 h recovery in ligand-free buffer **(Figure 4.13; a)**. The level of NMU2-HA phosphorylation at 1 h of the recovery was lower following brief exposure to hNmU-25 compared to hNmS-33 **(Figure 4.13; $b_i$)** consistent with earlier experiments **(Figure 4.12; c)**. Addition of the PKC inhibitor, Ro 31-8220 to the cells during the recovery time, immediately following brief ligand exposure did not significantly affect the levels of NMU2-HA phosphorylation at 1 h recovery following either ligand although there was a numerical reduction following the challenge with hNmU-25 **(Figure 4.13; c)**.

Additional experiments were performed and were consistent with the data that already shown earlier **(Figure 4.5 and Figure 4.11)** to confirm that the PKC inhibitor, Ro 31-8220 is able to inhibit PKC. Challenge of cells for 5 min with either hNmU-25 or hNmS-33 (1 μM) resulted in a marked increase in the levels of NMU2-HA phosphorylation compared to control group **(Figure 4.14; $a_i$)**. In contrast, these levels were significantly decreased when the cells pre-incubated with Ro 31-8220 **(Figure 4.14; b)**.

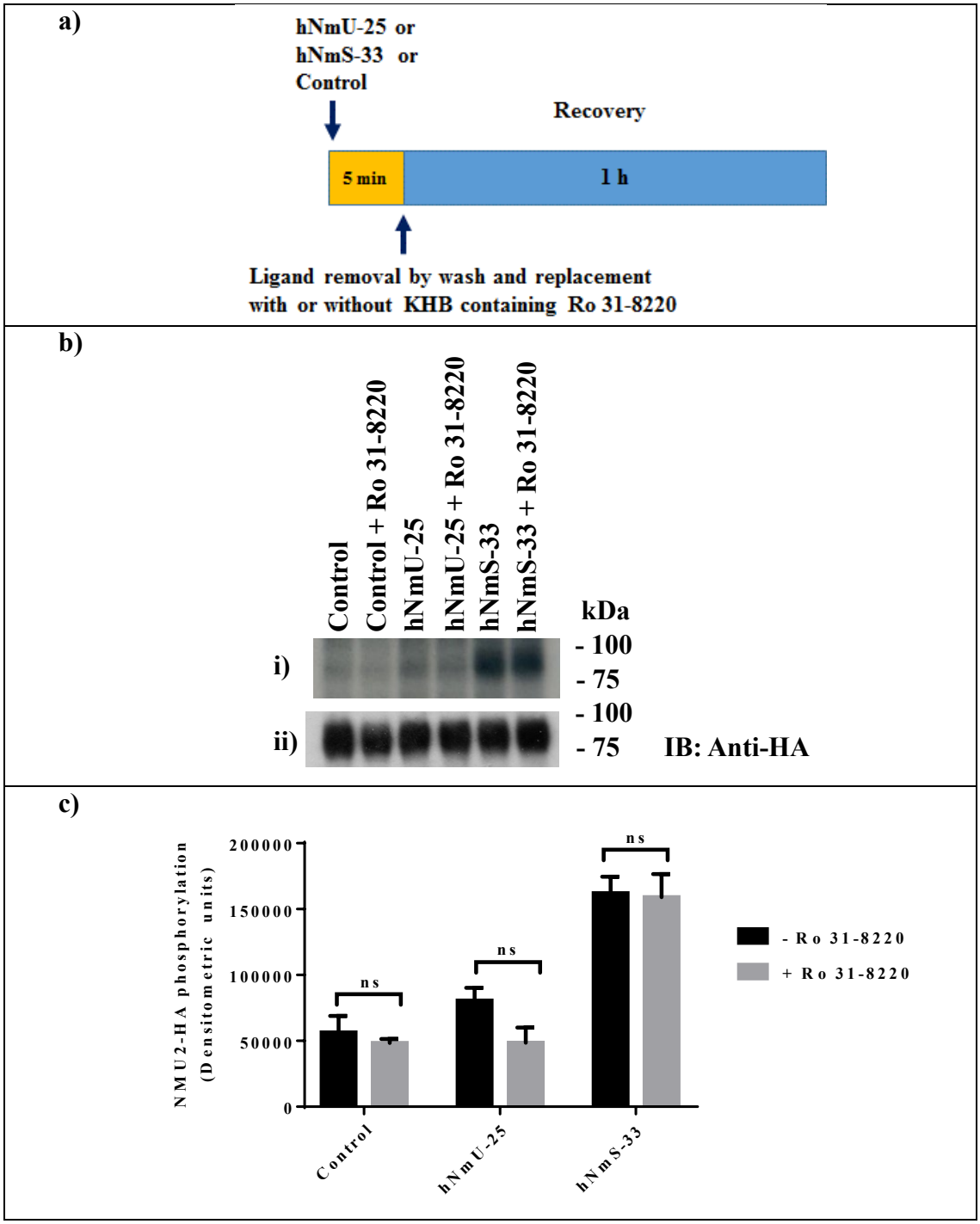


**Figure 4.13. Effect of PKC inhibition during the recovery time on NMU2-HA phosphorylation following brief ligand exposure.**

HEK-NMU2-HA were cultured in poly-D-lysine coated 6-well plates for 24 h. Cells were washed twice with phosphate-free KHB and labelled with $^{32}P$ orthophosphate for 1 h. Cells were then challenged with hNmU-25 (1 µM), hNmS-33 (1 µM) or control (KHB buffer) for 5 min. Following ligand removal and washing of the cell monolayers, KHB with or without Ro 31-8220 (5 µM) was added and the cells were allowed to recover for 1 h in free-ligand buffer (a). Following solubilisation, NMU2-HA was

immunoprecipitated and resolved by gel electrophoresis. The gel was dried and visualised by autoradiography ($b_i$). Immunoblotting of the immunoprecipitates with an anti-HA antibody was used as a loading control for NMU2-HA (IB; $b_{ii}$). The phosphorylated bands were quantified by densitometry using Image J software (c). Data are either representative autoradiographs or blots of $n \geq 3$ (b) or mean ± sem, $n \geq 3$ (c). Statistical analysis was performed using two way ANOVA followed by Bonferroni's test.

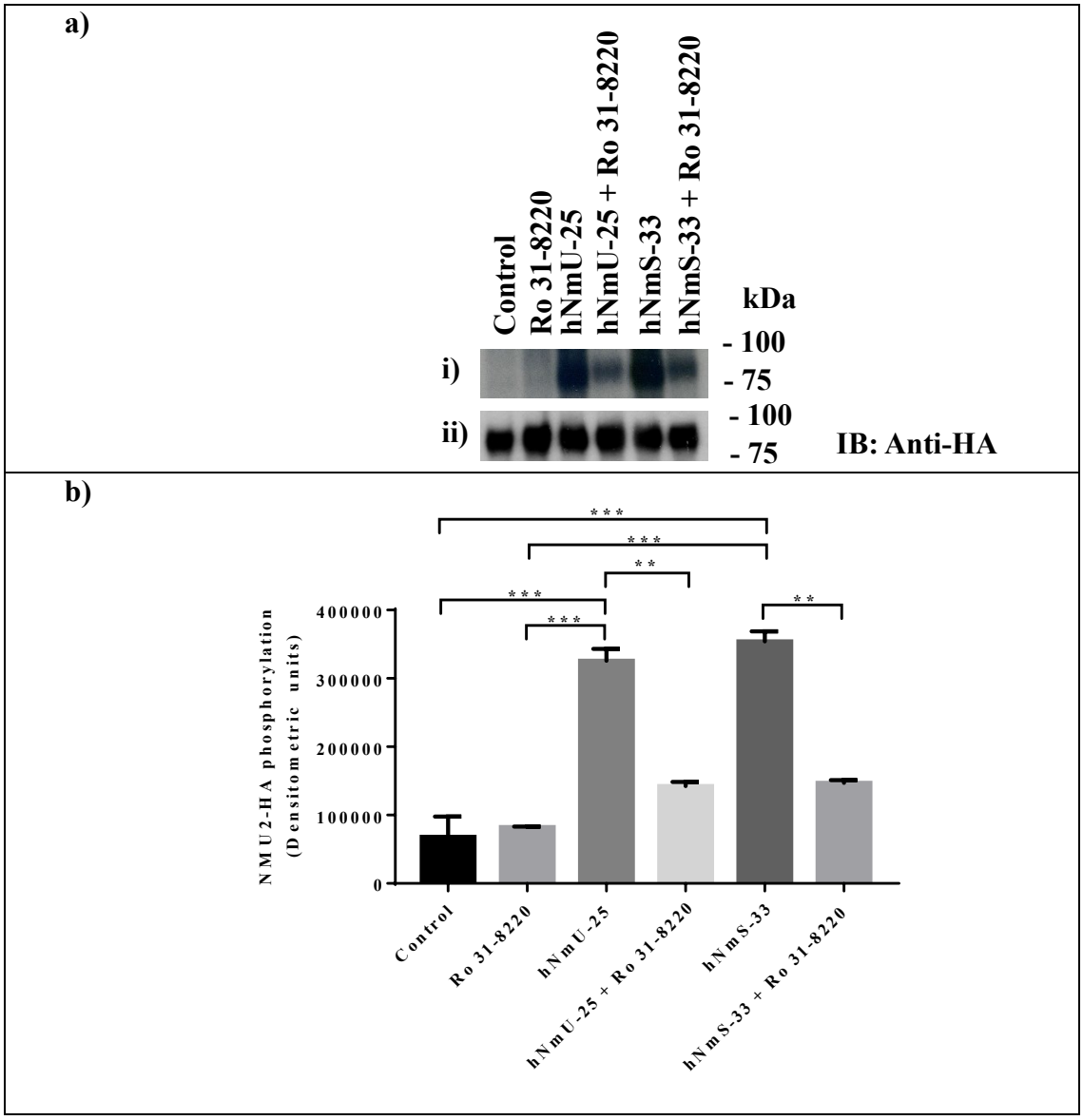


**Figure 4.14. Effect of PKC inhibition on agonist-mediated NMU2-HA phosphorylation.**

HEK-NMU2-HA were cultured in poly-D-lysine coated 6-well plates for 24 h. Cells were washed twice with phosphate-free KHB and labelled $^{32}P$ orthophosphate for 1 h. Cells were pre-incubated with or without Ro 31-8220 (5 μM, 30 min) prior to the challenge with hNmU-25 (1 μM), hNmS-33 (1 μM) or control (KHB buffer) for 5 min. Following solubilisation, NMU2-HA was separated by immunoprecipitation and resolved by gel electrophoresis. The gel was then dried and visualised by autoradiography ($a_i$). Immunoblotting of the immunoprecipitates with an anti-HA antibody was used as a loading control for NMU2-HA (IB; $a_{ii}$). The phosphorylated bands were quantified by densitometric analysis using Image J software (b). Data are either representative of autoradiographs or blots of n = 3 (a) or mean ± sem, n = 3 (b). Statistical analysis was

performed using a one way ANOVA followed by Bonferroni's test: $^{**}P < 0.01$, $^{***}P < 0.001$.

## 4.7 Discussion

After generation of a tagged version of NMU2 (NMU2-HA) **(Chapter three)**, the phosphorylation status of the receptor was investigated in transiently transfected HEK-293 cells. Phosphorylation of NMU2 was not detected when NMU2 was transiently expressed in HEK-293 cells. This may attribute to issues related to the lack of processing of the receptor following synthesis in the ER and the lack of expression at the cell membrane as a mature version **(Discussion 3.3)**. Hence, a stable cell line was generated to study the NMU2 phosphorylation. Using this cell line, data presented in this chapter show for the first time that NMU2 is phosphorylated following stimulation with ligand. Furthermore, hNmU-25 and hNmS-33 induce marked and equivalent NMU2 phosphorylation after 5 min challenge. Since early observations on the $\beta_2$ adrenoceptor, ligand-dependent phosphorylation has been established for growing list of GPCRs coupling to a variety of different G-proteins including, for example, muscarinic M3 receptor, PTH1R, GHSR1a and free fatty acid receptor (FFA4) (Butcher *et al.*, 2011; Nobles *et al.*, 2011a; Bouzo-Lorenzo *et al.*, 2016; Prihandoko *et al.*, 2016a; Zindel *et al.*, 2016). FFA4 receptor is an example of $G_{\alpha q}$-coupled GPCR that is phosphorylated in response to agonist activation. Indeed, stimulation of human or murine FFA4 receptor with α-linolenic acid in recombinant systems for few min results in a robust FFA4 phosphorylation compared to vehicle-treated group (control) (Burns *et al.*, 2010; Hudson *et al.*, 2013; Prihandoko *et al.*, 2016a). It is well-established paradigm for a vast majority of GPCRs that ligand binding to the receptor mediates a rapid receptor phosphorylation thereby promoting arrestin recruitment that blocks further G-protein from coupling to the receptor. Arrestin, in turn, also mediates receptor internalisation which, although initially thought to terminate receptor signalling, is now known to be able to initiate a second wave of signalling which is independent of G-protein (Lefkowitz *et al.*, 2005) **(Section 1.4.2.4.1, 1.4.2.4.2)**.

Two different regulatory processes are responsible for receptor phosphorylation that, in turn, initiates receptor desensitisation to attenuate the repeated responses resulting from further stimulation with ligand (Kelly *et al.*, 2008). These are heterologous desensitisation as a consequence of phosphorylation by second messenger kinases (PKC and PKA) and homologous desensitisation as a consequence of phosphorylation by GRKs (Pierce *et al.*, 2002) **(Section 1.4.2.4)**. To address the potential kinases responsible for NMU2 phosphorylation, either PDBu or FSK were used to challenge cells which are able

to activate PKC and PKA respectively. Although not directly providing information about the kinases responsible for agonist-dependent phosphorylation, such experiments establish if NMU2 is a substrate for these kinases. The activation of ERK1/2 (substrate for PKC) by PDBu and CREB (substrate for PKA) by FSK in HEK-NMU2-HA demonstrated the efficacy of these agents in these cells. Furthermore, ERK and CREB activation were reduced following pre-treatment with PKC and PKA inhibitors respectively **(Section 4.2)** demonstrating the efficacy of these inhibitors.

PDBu induces a marked increase in NMU2 phosphorylation in a ligand-independent manner that is completely abolished by inhibition of PKC. This suggests that NMU2 is a substrate for PKC. A list of many GPCRs that show phosphorylation in response to direct activation of PKC, for example, muscarinic M3 receptor, sphingosine-1-phosphate receptor and chemokine receptor 2 (CXCR2) (Willars *et al.*, 1999; Singh *et al.*, 2014; Martínez-Morales *et al.*, 2018). Indeed, a 5 min stimulation of HEK-293 expressing $G_{\alpha q}$-coupled-angiotensin II type 1 receptor with the activator of PKC, PMA (phorbol 12-myristate 13-acetate), resulted in receptor phosphorylation in the absence of receptor ligand. This phosphorylation was abolished by pre-treatment of cells with staurosporine, a rather non-specific PKC inhibitor (Oppermann *et al.*, 1996). Furthermore, PMA and PDBu induced dopamine $D_2$ receptor phosphorylation in the absence of dopamine that was inhibited by PKC inhibition (Namkung *et al.*, 2004). PMA also induces μ opioid receptor (MOR) phosphorylation, specifically at T370 (Illing *et al.*, 2014). Despite the demonstration that many GPCRs are substrates for PKC (demonstrated by PDBu/PMA), PKC has been shown to play no role or a very limited in agonist-dependent phosphorylation for most/all of these. However, there are examples where PKC does appear to play a role in ligand-dependent receptor phosphorylation such as, CXCR2 and angiotensin II type 2 receptor (Oppermann *et al.*, 1996; Singh *et al.*, 2014)

The data highlight that NMU2 has the potential to be phosphorylated by PKC, opening up the possibility of both homologous ($G_{\alpha q}$-$IP_3$-PKC axis) and heterologous regulation involving PKC. As NMU2 couples to $G_{\alpha q}$-$IP_3$-PKC axis upon ligand binding, thereby mediating PKC activation, (Brighton *et al.*, 2004b), this suggests that PKC activation negatively regulates NMU2 through its phosphorylation. Further support for this by using NetPhos software to predict the potential serine, threonine and tyrosine phosphorylation, multiple sites were predicted to be substrates for PKC phosphorylation. These were in

the *C*-terminus as well as the second and third intracellular loops of NMU2 (Brighton *et al.*, 2004a).

Apart from PKC, PKA was also investigated as a potential kinase for NMU2 phosphorylation. Forskolin stimulated CREB activation in HEK-NMU2-HA and this activation was partially inhibited by the rather non-specific PKA inhibitor, H89. This is consistent with other studies showing forskolin-mediated pCREB activation in HEK-293 cells (Li *et al.*, 2017c), highlighting that forskolin induces PKA activation in HEK-NMU2-HA.

Despite this, forskolin did not induce NMU2 phosphorylation in the absence of the ligand suggesting that PKA activation is not able to phosphorylate NMU2 although multiple potential PKA phosphorylation sites have been predicted (Brighton *et al.*, 2004a). This was consistent with $D_2$ receptor in which the forskolin did not influence its phosphorylation level in HEK-293 transiently expressing $D_2$ receptor although earlier study showed that PKA acts as a negative feedback loop for $D_2$ receptor in the brain tissues (Elazar *et al.*, 1991; Namkung *et al.*, 2004). Further study also showed that angiotensin II type 1 receptor did not phosphorylate following stimulation of HEK-293 expressing the receptor with forskolin for 5 min (Oppermann *et al.*, 1996). In contrast, stimulation of $\beta_2$ adrenoceptor with forskolin for 5 min resulted in marked increase in receptor phosphorylation using a phospho-specific antibody (Tran *et al.*, 2004).

To understand further about the effect of second messenger kinases on the regulation of NMU2 phosphorylation, we examined the effect of activation of receptors other than NMU2 that couple to $G_{\alpha q}$ or $G_{\alpha s}$ on NMU2 phosphorylation. It is known that PKC and PKA are able to induce heterologous desensitisation in which activation of these kinases by agonist-occupied receptors can phosphorylate and desensitise inactive heterologous receptors (Pierce *et al.*, 2002). The data presented confirmed that consistent with other studies (Luo *et al.*, 2008a; Bird *et al.*, 2010), muscarinic M3 receptors and β adrenoceptors are expressed endogenously in HEK-NMU2-HA using pERK1/2 and pCREB as readouts for $G_{\alpha q}$-PKC-ERK and $G_{\alpha s}$-PKA-CREB activation pathways respectively. Similar to other studies, carbachol and isoproterenol were able to activate ERK1/2 and CREB activation respectively (Luo *et al.*, 2008a; Bird *et al.*, 2010), consistent with activation of endogenously expressed muscarinic M3 receptors and β adrenoceptors in HEK-NMU2-HA. However, stimulation of HEK-NMU2-HA with

either carbachol or isoproterenol did not increase the level of NMU2 phosphorylation. Thus, although both potential PKC and PKA phosphorylation sites have been identified in NMU2 (Brighton *et al.*, 2004a) and the receptor is a substrate for PKC (see above), there is no evidence of heterologous phosphorylation of NMU2 in response to activation of these kinases by other GPCRs. It has been demonstrated that direct activation of PKC by PDBu or methacholine mediate muscarinic M3 receptor phosphorylation in CHO cells expressing both muscarinic M3 receptor and bradykinin $B_2$ receptor as indicated by the $^{32}P$ orthophosphate incorporation into muscarinic M3 receptors (phosphorylation band) but do not induce unoccupied bradykinin $B_2$ receptor phosphorylation as revealed by absence of phosphorylation bands of immunoprecipitated bradykinin $B_2$ receptors suggesting PKC-independent phosphorylation (Willars *et al.*, 1999). Another possible explanation for the lack of heterologous phosphorylation of NMU2 observed in the present study could be that the endogenous expression of muscarinic M3 receptors and β adrenoceptors insufficient to induce a marked activation of PKC or PKA. Further studies, possibly with higher expression of these receptors, would be needed to investigate this further.

Agonist binding to a GPCR leads to activation and phosphorylation of that receptor within its intracellular regions and *C*-terminal side chain (Yang *et al.*, 2017). This process is mediated by a variety of kinases including second messenger-dependent kinases (PKC or PKA) and GRKs **(Section 1.4.2.4.1)**. To address the effect of agonist on phosphorylation of NMU2, hNmU-25 and hNmS-33 were used. The present study shows that either hNmU-25 or hNmS-33 induced a robust NMU2 phosphorylation which was partially inhibited following pre-treatment with a PKC inhibitor but not PKA inhibitor. Thus, ~ 50 % of NMU2 phosphorylation was abolished by inhibition of PKC leaving ~ 50 % of NMU2 phosphorylation as dependent on kinases but most likely GRKs, as yet, unidentified. Stimulation of HEK-293 expressing angiotensin II type 2 receptor with angiotensin II for 5 min has also been shown to induce a marked increase in receptor phosphorylation that was significantly reduced (42 %) by staurosporine (Oppermann *et al.*, 1996). Furthermore, in RBL-2H3 cells stably expressing CXCR2, challenge of these cells with CXCL8 induced CXCR2 phosphorylation that was partially decreased by inhibition of PKC with staurosporine (Singh *et al.*, 2014). This is in contrast to other studies that showed, for example, endothelin mediated phosphorylation of both $ET_AR$ and $ET_BR$ in HEK-293 cells expressing either receptor was not affected by PKC

inhibition despite TPA (PKC activator) induced ETR phosphorylation (Freedman *et al.*, 1997). Although stimulation of sphingosine-1-phosphate receptor with sphingosine-1-phosphate (S1P) for 15 min resulted in a robust increase in sphingosine-1-phosphate receptor phosphorylation, inhibition of PKC by bisindolylmaleimide, a rather non-selective PKC inhibitor, did not influence level of sphingosine-1-phosphate receptor phosphorylation (Martínez-Morales *et al.*, 2018).

NMU2 couples to the $G_{\alpha q}$/PLC/PKC pathway with some studies also pointing to $G_{\alpha i}$ participation (Aiyar *et al.*, 2004; Brighton *et al.*, 2004b; Alhosaini *et al.*, 2018). Given that the NMU2 sequence contains potential serine/threonine sites for PKC (Brighton *et al.*, 2004a) and the present study showed NMU2 phosphorylation in response to PDBu, it is possible that PKC plays a role in agonist-dependent NMU2 phosphorylation. However, the present study provides no evidence of NMU2 phosphorylation by PKA. To develop a full picture of potential kinases that could be responsible for PKC-independent phosphorylation, additional studies will be needed in which the remaining NMU2 phosphorylation that is unaffected by inhibiting PKC needs to be investigated to explore which kinases (eg. GRKs) are responsible for agonist-dependent NMU2 phosphorylation.

Earlier results in this thesis (chapter three) demonstrated ligand-specific profiles of NMU2 signalling and resensitisation in which the brief exposure to hNmS-33 using the ligand removal protocol generated more sustained activation of ERK1/2, P38 and JNK compared to brief hNmU-25 exposure. Furthermore, NMU2 resensitisation was slower in response to hNmS-33 compared to hNmU-25. Using this ligand removal protocol, the present study shows that brief exposure generated different dephosphorylation profiles. Thus, NMU2 dephosphorylation following removal of hNmS-33 was more sustained compared to hNmU-25. As ligands bind essentially irreversibly and internalise with the receptor, this might suggest that differences inside the cells, such as ligand processing (Brighton *et al.*, 2004b; Alhosaini *et al.*, 2018), might play a role. Receptor dephosphorylation is considered a requirement for receptor resensitisation but may also regulate other aspects such as the extent/duration of signalling by internalised receptors (Kliewer *et al.*, 2017). Dephosphorylation is controlled spatio-temporally where it can occur immediately following agonist-mediated receptor activation or continue throughout the intracellular pathways, particularly involving the endosomal compartment (Kliewer *et al.*, 2017). Some GPCRs are partially dephosphorylated leaving some of the receptors bound at plasma membrane for a further round of agonist activation while

others undergo internalisation followed by sorting to either return to plasma membrane or be directed to lysosomal degradation (Kliewer *et al.*, 2017). The general paradigm is that agonist binding to GPCRs leads to receptor activation and phosphorylation by GRKs which, in turn, recruit(s) arrestins to activated receptors resulting in receptor desensitisation and internalisation (Luttrell *et al.*, 2010). Arrestins, then can act a protein adapter scaffolding a list of signalling proteins such as members of the MAPK (ERK and JNK3) and Src tyrosine kinase families (Luttrell *et al.*, 2010). This difference in NMU2 dephosphorylation following brief exposure to hNmU-25 and hNMS-33 could be attributed to the formation a stable ligand-receptor-arrestin complex that could be more resistant to dephosphorlytion by phosphatases. This would be consistent with NMU2-mediated sustained signalling to MAPKs and the slower rate of $Ca^{2+}$ resensitisation following hNmS-33 stimulation **(Chapter 3)**. Indeed, different GPCRs such as the angiotensin II type 1 receptor, protease-activated receptor $PAR_2$, vasopressin $V_2$ receptor, and neurokinin 1 receptor form stable complexes with arrestins and activate ERK signalling from within the endosome (DeFea *et al.*, 2000b; Luttrell *et al.*, 2001; Tohgo *et al.*, 2002). A recent study has shown that ECE-1, which is an enzyme responsible for degradation of some peptide ligands and plays a critical role in receptor signalling and trafficking (Padilla *et al.*, 2007; Roosterman *et al.*, 2007; Cottrell *et al.*, 2009; Pelayo *et al.*, 2011; Hasdemir *et al.*, 2012; Lu *et al.*, 2019), underlies at least a component of ligand-specific NMU2 signalling and resensitisation profiles (Alhosaini *et al.*, 2018). Thus, inhibition of ECE-1 by chemical or genetic tools reduced the rate of NMU2 resensitisation as well as causing more sustained ERK and P38 signalling following hNmU-25 but not hNmS-33 (Alhosaini *et al.*, 2018). This suggests that ECE-1 may work differently on hNmU-25 and hNmS-33 or access hNmU-25 but hNmS-33. Another explanation for this might be hNmS-33 dissociates from the receptor slower than hNmU-25 thereby driving this sustained phosphorylation. The precise dissociation rates for the two ligands are unknown, especially during a prolonged period of exposure to agonist-free media. However, it is also clear that internalisation of both receptor and ligand occurs relatively quickly, suggesting that much of the ligand-receptor complexes may be inside the cell where removal of extracellular ligand may have less impact on the generation of ligand-free receptors. It is possible, of course, that dissociation rates of the two ligands differ when the receptor-ligand complexes are being trafficked within the cells. In contrast, the interactions between the arrestins and receptor were dependent on the presence of either ligand and there were no differences in the dissociation of the arrestins

following removal of the two ligands, perhaps providing little evidence for different rates of dissociation. These aspects require further investigation. Agonist-dependent differences in dephosphorylation patterns have been also reported for the SST2A receptor in which two clusters including S341/343 (cluster 1) and T353/354 (cluster 2) were identified in the *C*-terminal to be a substrate for GRK phosphorylation (Ghosh *et al.*, 2011). In that study, treatment of CHO expressing SST2A with SS14 (natural agonist) for 30 min followed by ligand removal, resulted in dephosphorylation of both cluster 1 and cluster 2 by 6.5 min ($t_{1/2}$) and 7.9 min ($t_{1/2}$) respectively. Although cluster 1 dephosphorylation was not influenced by the agonist used, removal of either pasireotide or pansomatostatin (synthetic analogues) after 30 min stimulation resulted in a faster dephosphorylation of the cluster 2 at $t_{1/2}$ 3 min and 2.7 min respectively compared to removal of SS14 highlighting specificity of ligand in regulation of receptor phosphorylation/dephosphorylation (Ghosh *et al.*, 2011). It may be the case therefore that the observed difference between hNmU-25 and hNmS-33 in NMU2 dephosphorylation rate could result from a difference in the potential serine/threonine sites of NMU2 phosphorylation and/or different conformations of the receptor that could mean different phosphatases are involved or that the some phosphatases have different access. There is a concept termed the phosphorylation barcode in which different ligands binding to the same receptor can result in phosphorylation of receptor at different serine/threonine motifs. This may lead to differences in the nature and/or affinity of arrestin binding resulting in different signalling consequences (Tobin *et al.*, 2008). To further characterise the kinases responsible for the more sustained NMU2 phosphorylation following hNmS-33, a PKC inhibitor was used as experiments showed that ~ 50 % of NMU2 phosphorylation at 5 min was PKC-dependent. Inhibition of PKC following brief exposure to either hNmU-25 or hNmS-33, did not significantly affect levels of phosphorylation in response to either ligand after 1 h recovery suggesting that PKC is not responsible for the sustained NMU2 phosphorylation by hNmS-33. This might be suggest that sustained NMU2 phosphorylation following brief hNmS-33 exposure may result from a greater stability of the complex consisting of the phosphorylated receptor and arrestins compared to hNmU-25. This could restrict access of phosphatases. GPCRs can be categorised into two classes in relation to their binding stability to arrestins including class A and class B (Oakley *et al.*, 2000) **(Section 1.4.2.4.3)**. The vasopressin receptor is requires ~ 4 h to recycle and this is attributed to a sustained interaction between the receptor and both arrestins (Oakley *et al.*, 2000; Lefkowitz *et al.*, 2005). The present

study suggests that NMU2 belongs to class B GPCRs that form stable complex with the arrestins and that the strength of binding between receptor and arrestins may influence temporal profile of signalling, rate of resensitisation and receptor phosphorylation. NMU2 may induce recruitment of any arrestin forming a stable complex that is persist for a longer time in response to hNmS-33 compared to hnmU-25.

Although the present study demonstrates that PKC is partially involved in agonist-dependent NMU2 phosphorylation, other kinases (eg. GRKs) may have a critical role in NMU2 phosphorylation as well. Reasons for differences between hNmU-25 and hNmS-33 not entirely clear in addition to also unknown if phosphorylation sites are same or different in response to hNmU-25 and hNmS-33. It is well-established that ligand processing has been shown to play a role in resensitisation and duration of signalling and this may account for ligand specificity, thus its role in regulating phosphorylation/dephosphorylation needs investigating. Therefore, it would be worth investigating the effect of ECE-1 on dephosphorylation pattern of NMU2 following brief hNmU-25 exposure as it plays a critical role in degradation of hNmU-25 within the endosome thereby promoting rapid recycling (Alhosaini *et al.*, 2018). Given different durations of phosphorylation following brief ligand exposure and possible different patterns/sites of phosphorylation, study of arrestins recruitment important.

# 5 Chapter five: Study of NMU2 interaction with the arrestins using BRET assay

## 5.1 Introduction

Agonist binding to a GPCR stabilises an active conformation of the receptor, thereby promoting G-protein binding. G-proteins then become free to interact with a variety of intracellular effectors leading to different downstream responses (Gilman, 1987; Pierce *et al.*, 2002). To prevent overstimulation by repetitive activation, GPCR signalling is attenuated by their phosphorylation by GRKs, promoting arrestins recruitment and leading to receptor desensitisation of G-protein signalling and internalisation through engaging with components of endocytic machinery (Thomsen *et al.*, 2016). Arrestin engages with a variety of protein kinases, thereby mediating alternative signalling (G-protein-independent) via molecular scaffolding (Pierce *et al.*, 2002). For example, ERK1/2, P38 and JNK signalling are activated by phosphorylation of upstream protein kinases that is promoted by arrestins (DeWire *et al.*, 2007; Eichel *et al.*, 2018).

It is clear that arrestins can act as a switch between two different signalling cascades. One is G-protein-dependent signalling from the cell membrane while the second is an arrestin-dependent signalling which initiates when the receptor desensitises and engages in the endocytic pathway (Luttrell *et al.*, 2010). In addition, there is also evidence pointing to the G-protein-dependent signalling by internalised receptors (Vilardaga *et al.*, 2014). It was previously considered that internalised GPCRs were simply either degraded or recycled to plasma membrane for further rounds of activation and that these processes were important in both preventing overstimulated and facilitating resensitisation (Chini, 2019). Recently, other aspects of GPCR signalling have been added in which GPCR signalling can occur from the intracellular compartments through engaging with other signalling proteins which cause sustained signalling arising from endosomes (Eichel *et al.*, 2018). Arrestins are considered a critical player in this process by forming a stable complex with the activated receptor, causing signalling that can differ in time and space to signalling originating at the plasma membrane (Grundmann *et al.*, 2017; Chini, 2019). There is also the concept of biased agonism in which, an agonist has the selective ability to engage their cognate GPCRs with arrestin-dependent pathways in preference to the G-protein-dependent pathway, adding a further layer of complexity to GPCR signalling (Rajagopal *et al.*, 2010a). Moreover, arrestins can mediate different patterns of signalling by adopting different conformations. These multiple conformations of arrestins appear to

be regulated at different levels including the agonist-receptor-arrestin complex, post-translation modifications of the receptor and other factors such as cell-type (Rajagopal *et al.*, 2010a). For example, specific serine residues of chemokine receptor 4 are phosphorylated by GRK2 and GRK6 upon activation and those kinases and arrestin 3 binding are responsible for regulation of $Ca^{2+}$ desensitisation while GRK3, GRK6 and arrestin 2 are critical in activation of ERK1/2 signalling (Busillo *et al.*, 2010). Different patterns of muscarinic M3 receptor phosphorylation, particularly in the *C*-terminus, have been identified following stimulation with different agonists and in different tissues further highlighting functional selectivity in which the ligand can preferentially direct the receptor to one or more signalling pathways (Butcher *et al.*, 2011).

The results in Chapters 3 and 4 showed more sustained patterns of MAPKs signalling and NMU2 dephosphorylation in response to brief exposure to hNmS-33 compared to hNmU-25. These data might suggest that the type of arrestins and/or temporal profiles of their recruitment to NMU2 may be different following activation with hNmU-25 and hNmS-33. Hence, the aim of this chapter is to assess the potential interactions between NMU2 and the arrestins (arrestin 2 and arrestin 3). A BRET assay is used to study the interaction between NMU2 and the arrestins. This is a biophysical technique that has been exploited for studying the interaction between proteins in real time and in intact cells (Pfleger *et al.*, 2006; Lohse *et al.*, 2012) **(see Methods)**.

## 5.2 Generation of constructs for bioluminescence resonance energy transfer (BRET) assay

Data in **Chapter 4** demonstrated time course of NMU2 dephosphorylation different in response to either hNmU-25 or hNmS-33 following removal of the free extracellular ligand (brief ligand exposure) in which one was more sustained following hNmS-33 compared to hNmU-25. Given that arrestins recruitment is generally a consequence of receptor phosphorylation, therefore, the aim here, was to investigate the NMU2 interaction with the arrestins in response to either ligand using BRET assay. To do this, five constructs were generated including NMU2 tagged with nanoluciferase (NMU2-nLUC), arrestin 2 or arrestin 3 tagged with yellow florescence protein (arrestin 2/3-YFP) and arrestin 2 or arrestin 3 tagged with renilla luciferase enzyme (arrestin 2/3-RLuc).

### 5.2.1 Generation of NMU2 sequence and cloning into pcDNA 3.1+ containing nLUC sequence at *C*-terminus

To generate the NMU2 nucleotide sequence, forward and reverse primers were designed. The forward primer contained a restriction site at beginning for HindIII that would be used later for a sub-cloning step. A Kozak sequence and a start codon were inserted next to the HindIII site followed by 21 bases of the primary sequence of NMU2 **(Figure 5.1)**. The reverse primer included a restriction site for KpnI for a subsequent sub-cloning step and a further 36 bases represents the NMU2 sequence **(Figure 5.1)**. Here, the stop codon was removed from the reverse primer encoding NMU2 sequence in order to obtain an expression of the NMU2 with *C*-terminal nLUC.

The NMU2 sequence was then generated by PCR amplification using the primers **(Figure 5.1)** and a vector containing an untagged version of the NMU2 sequence as the template. Following NMU2 amplification, PCR products were resolved by agarose gel electrophoresis and visualised under UV light. Data showed a large band located between 1 - 1.5 kb which is the predicted molecular size of the NMU2 sequence (~ 1.23 kb) **(Figure 5.2; a)**. Two restriction enzymes, HindIII and KpnI, were used to sub-clone the resulting NMU2 into pcDNA 3.1+ containing nLUC at the *C*-terminus (vector) **(Figure 5.2; b)**. To sub-clone, both the insert and vector were double digested using HindIII and KpnI to obtain two sticky ends that were then used to ligate the insert and vector together and generate the NMU2-nLUC construct **(Figure 5.2; b)**. Following ligation, NMU2-nLUC was transformed into DH5 α cells and at least six colonies grown under selection

were then tested using HindIII and KpnI after purification of the transformed plasmid by miniprep kit **(see Methods)**. Upon agarose gel electrophoresis, the NMU2-nLUC showed an intense band in absence of HindIII and KpnI (~ 4.5 kb) that would be consistent with the circular plasmid **(Figure 5.2; c)**. Furthermore, digestion with both HindIII and KpnI showed two fragments; one was the predicted molecular size for NMU2 (~ 1.23 kb) and another fragment at ~ 6 kb which is consistent with pcDNA 3.1+ containing nLUC **(Figure 5.2; c)**. Agarose gel electrophoresis of pcDNA 3.1+ containing nLUC without digestion resulted in a band at ~ 3.5 kb, consistent with the circular plasmid. Digestion of pcDNA 3.1+ containing nLUC with HindIII and KpnI, showed a band at ~ 6 kb, consistent with the linear plasmid **(Figure 5.2; c)**. Following these initial test digests, the resulting NMU2-nLUC sequence was validated by DNA sequencing (PNACL; University of Leicester) (data not shown).

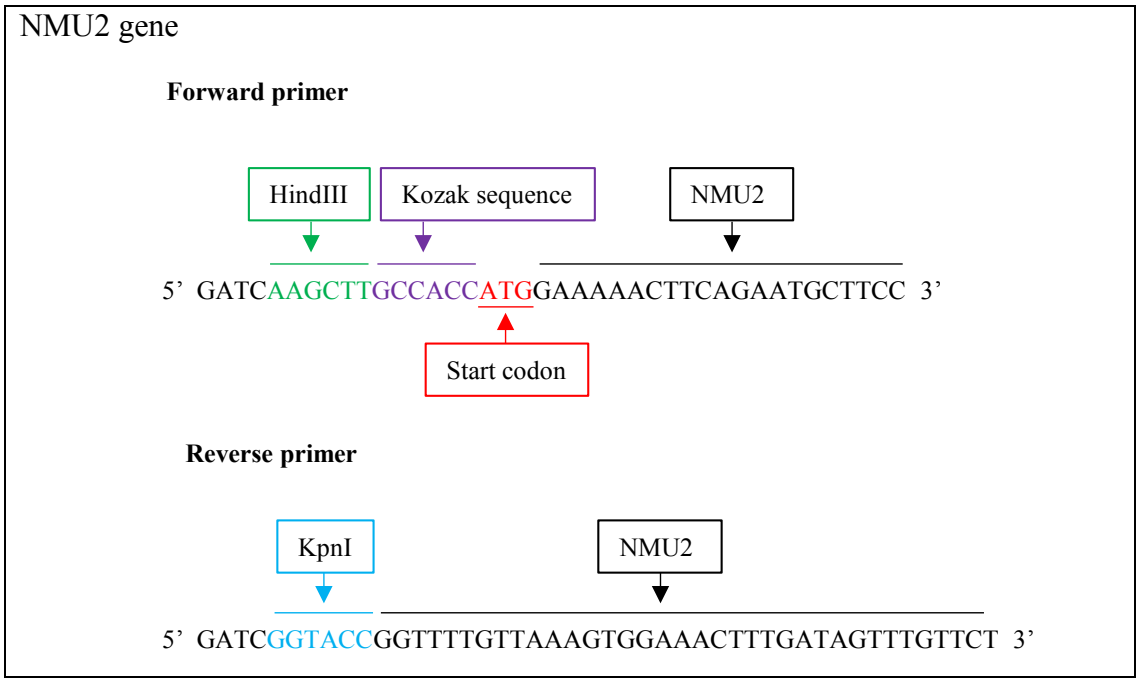


**Figure 5.1. Primer design for PCR generation of NMU2**

Two primers were designed to clone the NMU2-nLUC sequence. The forward primer contained a restriction site for HindIII (green), a Kozak sequence (purple) and a start codon (red) before the sequence of NMU2. The reverse primer included a restriction site for KpnI (blue) before the first 36 bases of the 5' end of NMU2. Following PCR using a vector encoding an untagged version of the NMU2 as the template, the resulting product was sub-cloned into pcDNA 3.1+ containing the sequence for nLUC, resulting in a full-length NMU2 with a *C*-terminal nLUC.

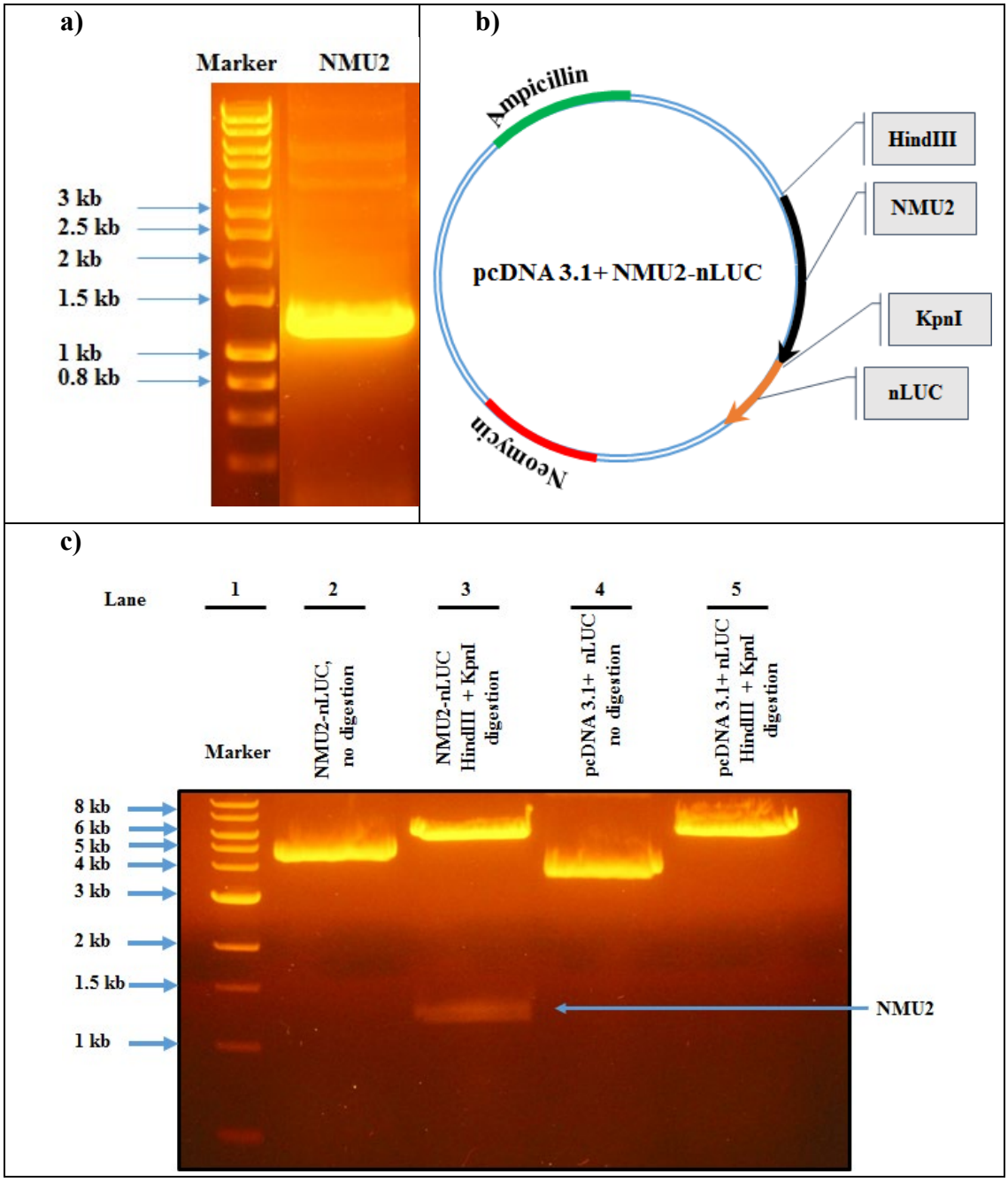


**Figure 5.2. NMU2 amplification, plasmid map and test digests of NMU2-nLUC**

The NMU2 sequence was generated by PCR amplification from a vector containing an untagged version of the receptor using the primers indicated in **Figure 5.1**. The PCR products were separated by agarose gel electrophoresis and viewed under UV light (a). The scheme shows the cloning of the NMU2 sequence into pcDNA 3.1+ containing nLUC using HindIII and KpnI restriction enzymes (b). After cloning the NMU2 sequence into the vector, the resulting construct (NMU2-nLUC) was validated by double digests with HindIII and KpnI (c). The lanes were: 1) a size marker; 2) circular NMU2-nLUC construct; 3) NMU2-nLUC construct exposed to double digestions with HindIII and

KpnI; 4) circular pcDNA 3.1+ with nLUC (no digestion) and; 5) pcDNA 3.1+ with nLUC digested with HindIII and KpnI.

### 5.2.2 Generation of arrestin 2 and arrestin 3 and cloning into pcDNA5 FRT containing the YFP sequence

Generation of human arrestin 2-YFP or arrestin 3-YFP (arrestin 2/3-YFP) was performed using four primers and untagged arrestin 2 or 3 as the template. The forward primers included a restriction site for HindIII for later sub-cloning. A Kozak sequence and a start codon were inserted before the primary sequences of arrestin 2 or 3 **(Figure 5.3; a, b)**. The reverse primers contained a restriction site for NotI before the arrestin 2 or 3 sequences. The stop codon was removed from the reverse primer for expressing of arrestin 2 or 3 with *C*-terminal YFP (**Figure 5.3; a, b)**.

Arrestin 2 and 3 sequences were generated by PCR amplification using these primers and vectors containing untagged versions of arrestin 2 or 3, which were obtained from the cDNA Resource Centre (www.cdna.org). Following amplification and separating the PCR products by agarose gel electrophoresis, a large band was detected for each PCR reaction and located at a molecular size between 1 - 1.5 kb, which is the predicted size of arrestin 2 and arrestin 3 constructs (~ 1.23 kb) **(Figure 5.5; a)**. To generate arrestin 2 or 3-YFP constructs, pcDNA5 FRT containing the YFP sequence (kindly provided by Dr. Adrian Butcher, MRC toxicology, University of Leicester) was used to sub-clone arrestin 2 and 3 generated in **Figure 5.5; a**. HindIII and NotI digests were employed to make two sticky ends. Both arrestin 2 and 3 (inserts) and pcDNA5 FRT containing the YFP sequence (vector) were then ligated to form arrestin 2 or 3-YFP constructs **(Figure 5.5; b)**. Following ligation and transformation, four colonies were selected from each construct and purified by miniprep kit **(see Methods)** to obtain the plasmid. Data showed that agarose gel electrophoresis of arrestin 2 and 3-YFP plasmids following digestion with HindIII and NotI resulted in two fragments. The first fragment was located between 1 - 1.5 kb, which is the predicted molecular size of arrestin 2 and 3 sequences (~ 1.23 kb). The second fragment at ~ 5.79 kb was consistent with the pcDNA5 FRT containing the YFP sequence **(Figure 5.5; d)**. The resulting arrestin 2 and 3-YFP constructs were also validated via DNA sequencing (PNACL; University of Leicester) (data not shown).

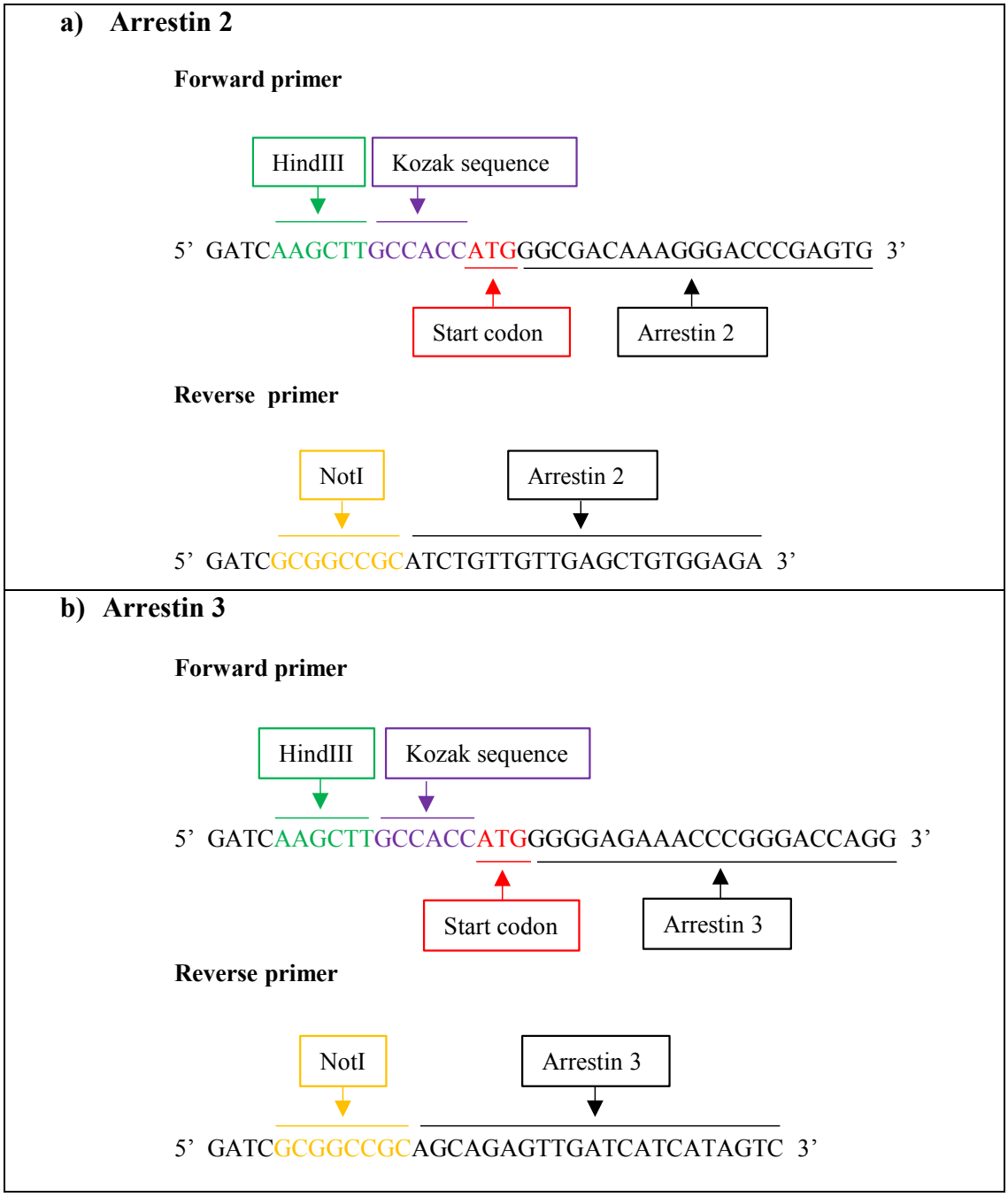


**Figure 5.3. Primer design of arrestin 2 and arrestin 3**

Four primers were designed to generate arrestin 2- or 3 sequences. The forward primers contained a restriction site for HindIII (green), a Kozak sequence (purple) and a start codon (red) before the sequence of arrestin 2- or 3 (a, b). The reverse primers contained a restriction site for NotI (orange) before the arrestin 2- or 3 sequence (a, b).

### 5.2.3 PCR amplification of arrestin 2 and arrestin 3 and cloning into pcDNA5 FRT containing the RLuc sequence

Four primers and untagged versions of arrestin 2 and 3 were used first to generate the arrestin 2 or 3 sequence by PCR. The forward primers contained a restriction site for NheI that was used for the sub-cloning stage, a Kozak sequence and a start codon before the primary sequences of arrestin 2 and 3 **(Figure 5.4; a, b)**. The reverse primers contained a restriction site for HindIII before arrestin 2 or 3 sequences with removal of the stop codon for expressing the arrestin 2 or 3 with *C*-terminal RLuc **(Figure 5.4; a, b)**. Arrestin 2 and 3 sequences were generated by PCR using these primers and plasmids containing untagged versions of the arrestin 2 or 3 sequences (www.cdna.org). Following agarose gel electrophoresis, a large band was detected representing arrestin 2 and 3 **(Figure 5.5; a)**. Arrestin 2 and 3-RLuc plasmids were then generated using pcDNA5 FRT containing a sequence for RLuc (kindly provided by Dr. Adrian Butcher, MRC toxicology, University of Leicester). Both arrestin 2 or 3 and pcDNA5 FRT containing the RLuc sequence were double digested using NheI and HindIII to generate sticky ends that were used for ligation to generate the arrestin 2 and 3-RLuc plasmids **(Figure 5.5; c)**. Following ligation and transformation of the ligated arrestin 2 and 3-RLuc, six colonies of each construct were selected and purified by miniprep kit **(see Methods)** to obtain the DNA plasmids. Digestion of the miniprep DNA plasmids with NheI and HindIII resulted in two fragments in the expected sizes: one from each construct at ~ 1.23 kb which is the predicted size of the arrestin 2 or 3 sequences and another at ~ 6 kb that represented pcDNA5 FRT containing the RLuc sequence **(Figure 5.5; e)**. The resulting arrestin 2 and 3-RLuc constructs were also validated via DNA sequencing (PNACL; University of Leicester) (data not shown).

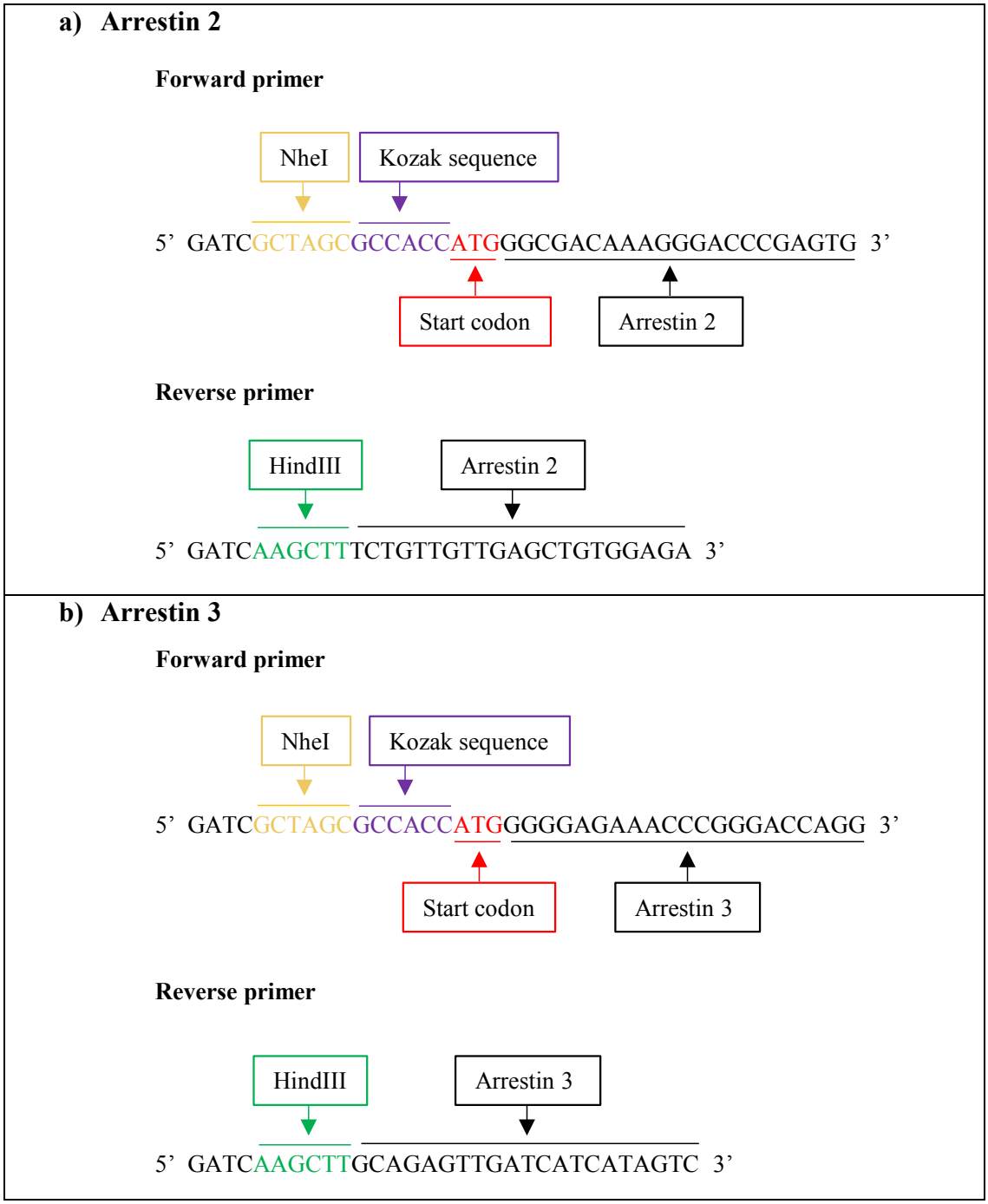


**Figure 5.4. Primer design of arrestin 2 and arrestin 3**

Four primers were designed to generate arrestin 2- or 3 sequences. Forward primers contained a restriction site for NheI (gold), a Kozak sequence (purple) and a start codon (red) before the sequence of arrestin 2- or 3 (a, b). The reverse primers contained a digest site for HindIII (green) before the arrestin 2- or 3 (a, b).

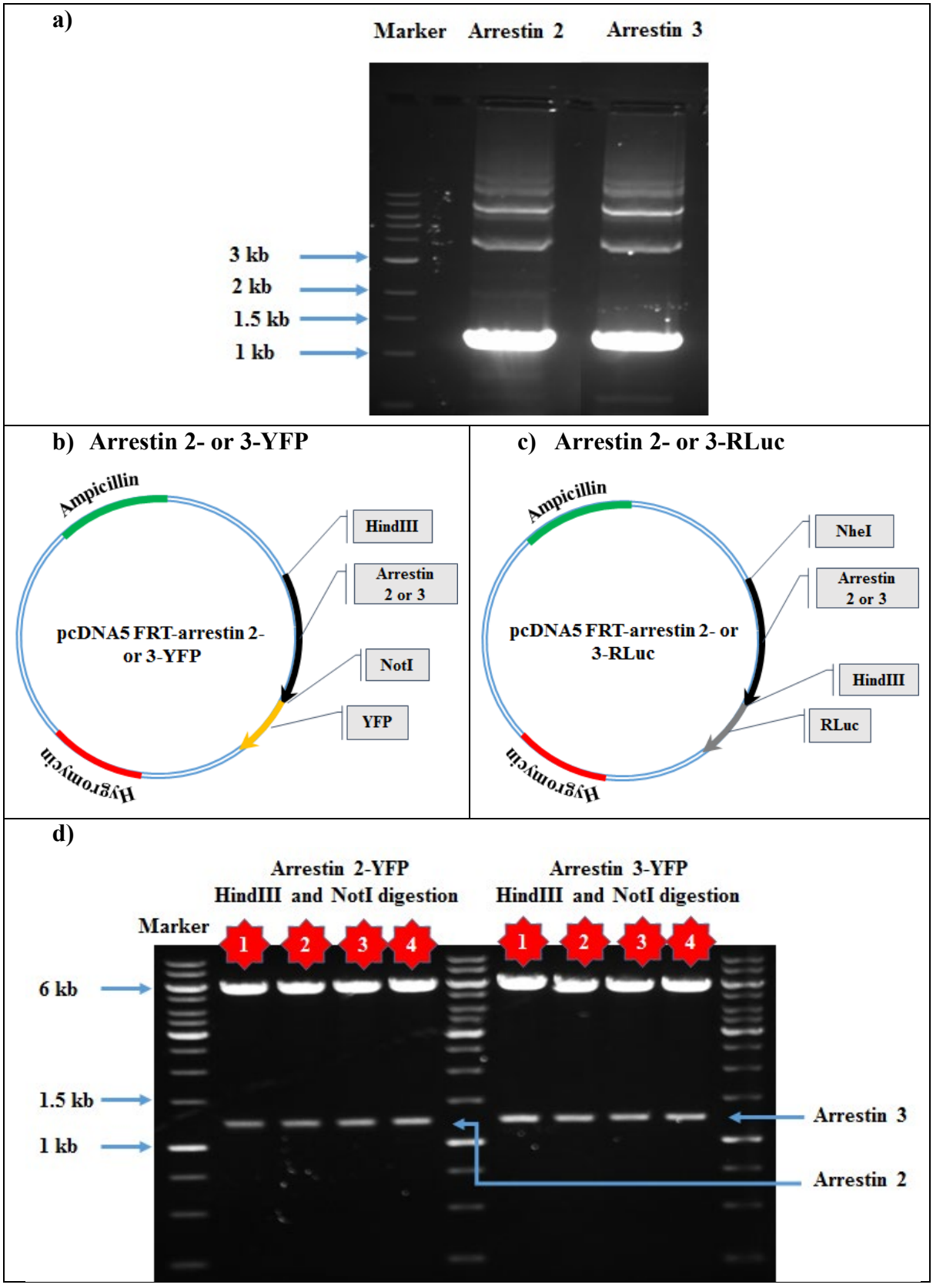
a)
Marker
Arrestin 2
Arrestin 3
3 kb
2 kb
1.5 kb
1 kb
b) Arrestin 2- or 3-YFP
Ampicillin
HindIII
Arrestin 2 or 3
pcDNA5 FRT-arrestin 2- or 3-YFP
NotI
YFP
Hygromycin
c) Arrestin 2- or 3-RLuc
Ampicillin
NheI
Arrestin 2 or 3
pcDNA5 FRT-arrestin 2- or 3-RLuc
HindIII
RLuc
Hygromycin
d)
Arrestin 2-YFP
HindIII and NotI digestion
Arrestin 3-YFP
HindIII and NotI digestion
Marker
1
2
3
4
1
2
3
4
6 kb
1.5 kb
1 kb
Arrestin 3
Arrestin 2

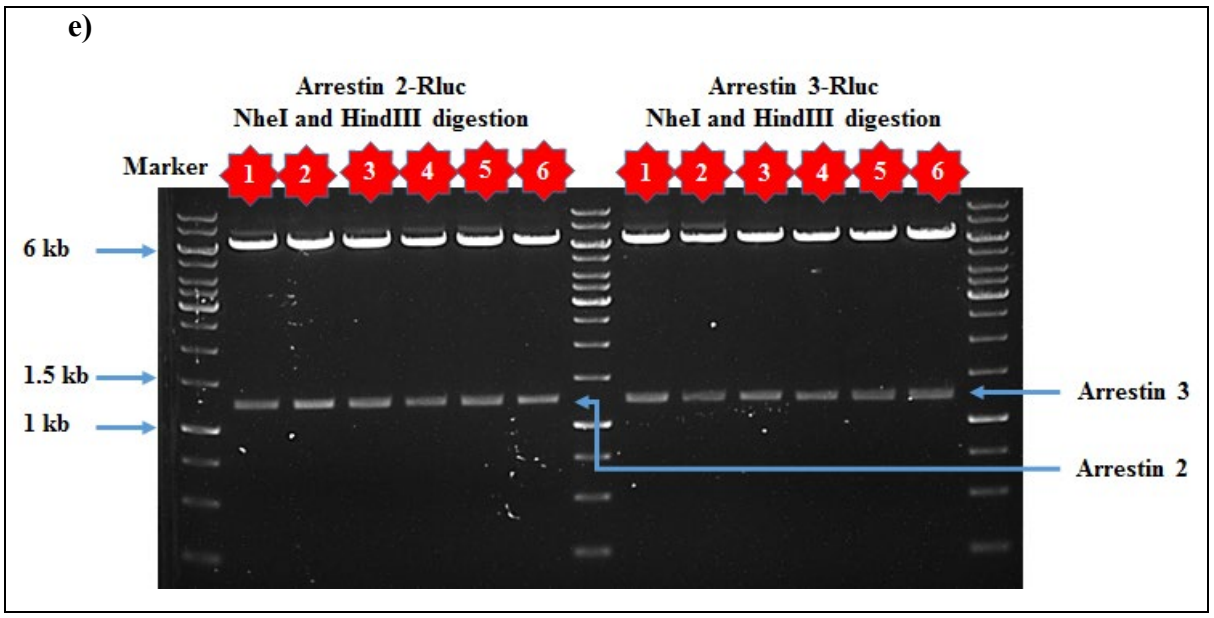


**Figure 5.5. Arrestin 2 and arrestin 3 amplification, plasmid map, and tests of arrestin 2- or 3-YFP and arrestin 2- or 3-RLuc by restriction digest**

The arrestin 2 or arrestin 3 sequences were generated by PCR amplification from vectors containing untagged versions of arrestin 2 arrestin 3. The PCR products were then separated by agarose gel electrophoresis and viewed under UV light (a). The plasmid map shows the arrestin 2 or 3 sequences with restriction sites for HindIII and NotI inserted into pcDNA5 FRT containing the sequence for YFP (b). Diagram (c) represents arrestin 2- or 3-RLuc constructs in which the arrestin 2 or 3 sequences with restriction sites for NheI and HindIII were cloned into the pcDNA5 FRT containing the sequence for RLuc. After cloning the arrestin 2 or 3 into the appropriate plasmids, the resulting constructs; arrestin 2- or 3-YFP (from 4 colonies (d)) and arrestin 2- or 3-RLuc (from 6 colonies (e)) (indicated by the red stars) were randomly selected and examined by double digests with HindIII and NotI for arrestin 2- or 3-YFP (d) or NheI and HindIII for arrestin 2- or 3-RLuc (e).

## 5.3 Examination of NMU2 interaction with arrestin 2-YFP or arrestin 3-YFP by BRET

After generation and verification of NMU2-nLUC, arrestin 2- or 3-YFP and arrestin 2- or 3-RLuc **(Sections; 5.2.1, 5.2.2, 5.2.3)**, NMU2 interaction with arrestins was investigated using a bioluminescence resonance energy transfer assay (BRET). Firstly, to study the interaction between NMU2-nLUC (donor) and arrestin 2- or 3-YFP (acceptor), a saturation BRET assay was performed. In this the amount of donor was fixed and the amount of acceptor was increased to determine the appropriate quantity of acceptor that would allow generation of a maximal BRET window between unstimulated cells and cells stimulated with ligand. The fixed amount of the donor and the optimised quantity of acceptor plasmid would then be used for further experiments.

Following transfection of HEK-293 cells with fixed amounts of NMU2-nLUC and increasing amounts of either arrestin 2-YFP or arrestin 3-YFP, cells were challenged with either hNmU-25 or hNmS-33 (1 μM) for 5 min. This resulted in increased BRET ratio, indicating increased interaction of the NMU2-nLUC with arrestin 2-YFP (1.9 ± 0.2 and 1.7 ± 0.1 fold over basal levels for hNmU-25 and hNmS-33 respectively). The BRET signal increased with increasing the amounts of acceptor and reached a high ratio at acceptor : donor expression ratio greater than 0.03 **(Figure 5.6; a, b)**. The BRET ratio induced by both ligands were used to determine the maximal (BRET max). The quantity of the acceptor derived from the acceptor over the donor expression ratio was used to determine the sub-maximal ($BRET_{50}$) using one site binding hyperbola fit **(Table 5.1)**. Both ligands generated similar BRET windows (ligand-stimulated BRET) that represent the NMU2-nLUC interaction with arrestin 2-YFP in fixed amount of the donor NMU2-nLUC and increasing amount of acceptor arrestin 2-YFP **(Figure 5.6; a, b)**.

Arrestin 3-YFP recruitment to NMU2-nLUC was also investigated by exposing the transfected cells to either hNmU-25 or hNmS-33 for 5 min. Both ligands caused robust increase in BRET signal compared to the control (unstimulated group) at all acceptor : donor expression ratios pointing to the interaction of NMU2-nLUC with arrestin 3-YFP **(Figure 5.7; a, b)**. The BRET signal gradually increased as the acceptor : donor expression ratio increased but tended to saturate at expression ratios greater than 0.04 **(Figure 5.7; a, b)**. BRET max and $BRET_{50}$ were generated for hNmU-25 and hNmS-33

which were showed a similar affinity in the interaction between NMU2-nLUC and arrestin-YFP **(Table 5.1)**.

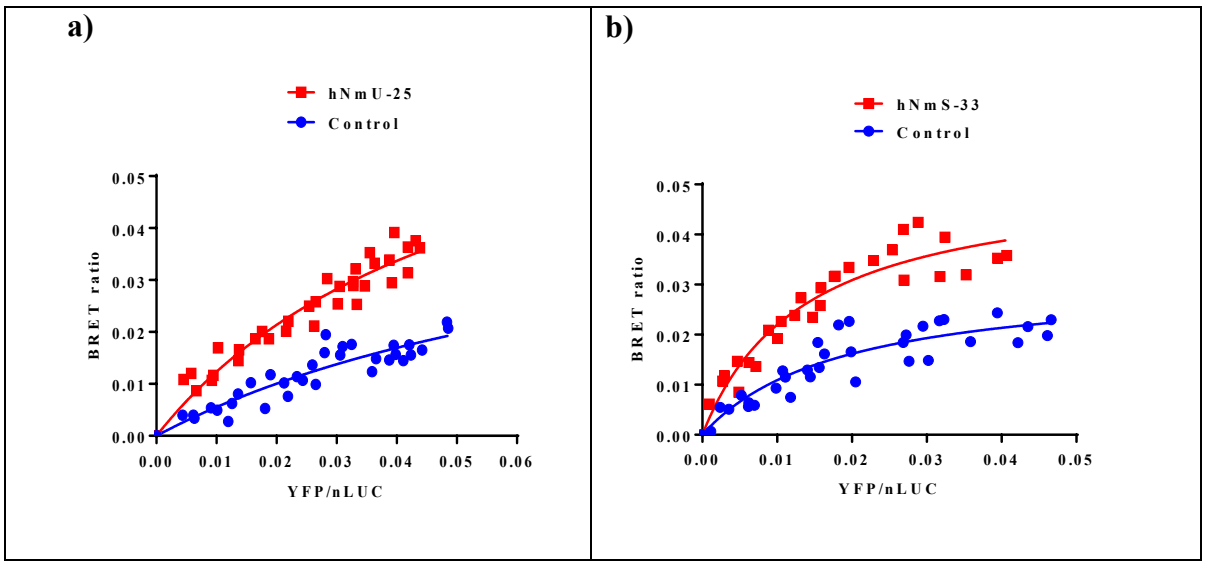


**Figure 5.6. hNmU-25- and hNmS-33-induced interactions between arrestin 2-YFP and NMU2-nLUC in HEK293: BRET saturation assay**

Cells were cultured in 6-well plates (250,000 cells per well) for 24 h before being co-transfected with a constant amount of donor plasmid (NMU2-fused with nanoluciferase (NMU2-nLUC); 50 ng/well) and increasing amounts of acceptor (arrestin 2-fused with YFP (arrestin 2-YFP); 0, 100, 200, 300, 400, 500, 600, 700, 800, 900, 1000, 1200 ng/well). After 24 h, cells were detached and sub-cultured on poly-D-lysine coated 96-well microplates and incubated for a further 24 h. On the day of the experiment, the medium was removed, the cell monolayers were washed twice with HBSS buffer and 80 µl of the same buffer added to each well. Fluorescence background was measured at 535 nm using a ClarioStar microplate reader. Cells were incubated with coelenterazine h (5 µM) for 10 min and either hNmU-25 (1 µM) or hNmS-33 (1 µM) was added for the last 5 min of this. The signal intensity was determined at 535 nm and 465 nm using a ClarioStar microplate reader. The BRET signal was calculated by subtracting the acceptor : donor ratio of the emission from the acceptor : donor ratio in the cells transfected with donor plasmid only **(see Methods)**. Data were fitted with a one site binding hyperbola using GraphPad Prism. The data are representative of three independent experiments carried out in quadruplicate, each showing similar results.

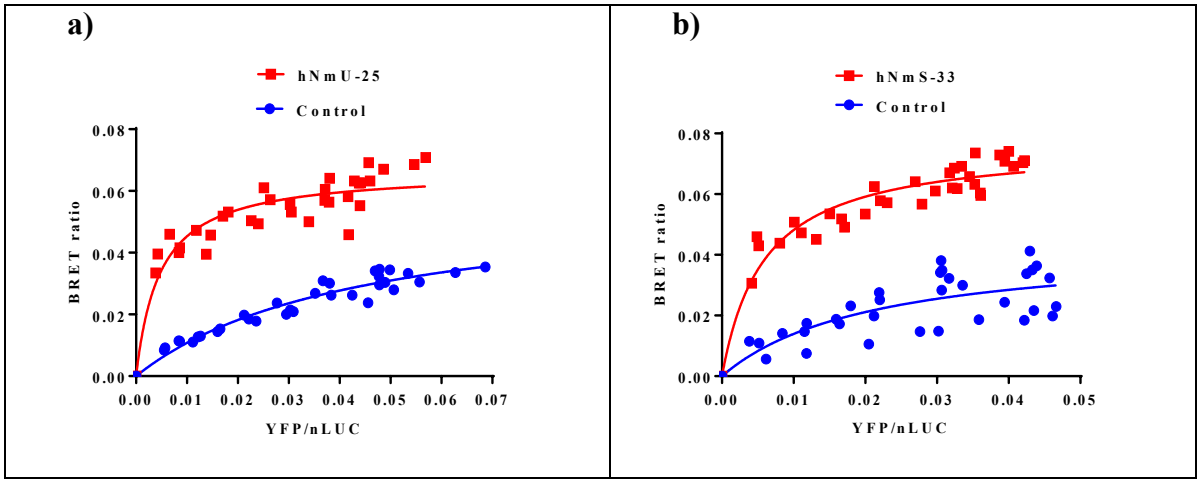


**Figure 5.7. hNmU-25- and hNmS-33-induced interactions between arrestin 3-YFP and NMU2-nLUC in HEK293: BRET saturation assay**

Cells were cultured in 6-well plates (250,000 cells per well) for 24 h before being co-transfected with a constant amount of donor plasmid (NMU2-fused with nanoluciferase (NMU2-nLUC); 50 ng/well) and increasing amounts of acceptor (arrestin 3-fused with YFP (arrestin 3-YFP); 0, 100, 200, 300, 400, 500, 600, 700, 800, 900, 1000, 1200 ng/well). After 24 h, cells were detached and plated on poly-D-lysine coated 96-well plates and incubated for a further 24 h. On the day of the experiment, the cell monolayers were washed twice with HBSS buffer and 80 µl of the same buffer added to each well. Fluorescence background was measured at 535 nm using a ClarioStar microplate reader. Cells were incubated with coelenterazine h (5 µM) for 10 min and either hNmU-25 (1 µM) or hNmS-33 (1 µM) was added for the last 5 min of this. The signals were detected at 535 nm and 465 nm using a ClarioStar microplate reader. The BRET signal was calculated by subtracting the acceptor : donor ratio of the emission from the acceptor : donor ratio in the cells transfected with donor plasmid only **(see Methods)**. Data were fitted with a one site binding hyperbola using GraphPad Prism. The data are representative of three independent experiments carried out in quadruplicate, each showing similar results.

**Table 5.1. BRET max and $BRET_{50}$ values of hNmU-25- and hNmS-33-mediated NMU2 interaction with arrestin 2 or arrestin 3**

The net BRET obtained from donor : acceptor ratio and the BRET value obtained from the ratio of the total expression of acceptor over the donor were fitted with a one site binding hyperbola using GraphPad Prism. The maximal BRET ratio (BRET max) represents the maximal interaction between the donor and acceptor while the $BRET_{50}$ represents the acceptor over the donor expression ratio that gives 50 % of the maximal BRET ratio following stimulation with the ligand. Data are mean ± sem of three individual experiments carried out in quadruplicate. Data taken from the experiments described in **Figure 5.6** and **Figure 5.7**.

| **Interaction NMU2-nLUC** | **hNmU-25** | | **Control** | | **hNmS-33** | | **Control** | |
|---|---|---|---|---|---|---|---|---|
| | **BRET max** | **$BRET_{50}$** | **BRET max** | **$BRET_{50}$** | **BRET max** | **$BRET_{50}$** | **BRET max** | **$BRET_{50}$** |
| **Arrestin 2-YFP** | 0.075 ± 0.008 | 0.050 ± 0.009 | 0.097 ± 0.024 | 0.173 ± 0.072 | 0.089 ± 0.016 | 0.044 ± 0.015 | 0.070 ± 0.0006 | 0.084 ± 0.017 |
| **Arrestin 3-YFP** | 0.066 ± 0.004 | 0.004 ± 0.001 | 0.065 ± 0.003 | 0.053 ± 0.001 | 0.075 ± 0.003 | 0.005 ± 0.001 | 0.071 ± 0.0008 | 0.073 ± 0.019 |

## 5.4 Concentration- dependency of agonist-mediated interactions between NMU2 and the arrestins

Concentration-response curves for arrestin 2-YFP and arrestin 3-YFP recruitment to NMU2-nLUC in response to either hNmU-25 or hNmS-33 were generated by co-transfecting HEK-293 with NMU2-nLUC and either arrestin 2-YFP or arrestin 3-YFP **(see Methods)**. To determine the $pEC_{50}$ for driving the interaction of NMU2 with the arrestins by either ligand, cells were stimulated with either hNmU-25 or hNmS-33 for 5 min using different concentrations as indicated **(Figure 5.8)**. Both ligands caused robust increases in BRET ratio indicating the interaction between NMU2 and either arrestin 2-YFP or arrestin 3-YFP, which were detected by a ClarioStar microplate reader. These increases in ratios were concentration-dependent reaching a maximum at 1 μM ligand **(Figure 5.8; a, b)**. The ligands showed similar potencies ($pEC_{50}$ values) for arrestin 2-YFP or arrestin 3-YFP interactions with NMU2-nLUC **(Table 5.2)**.

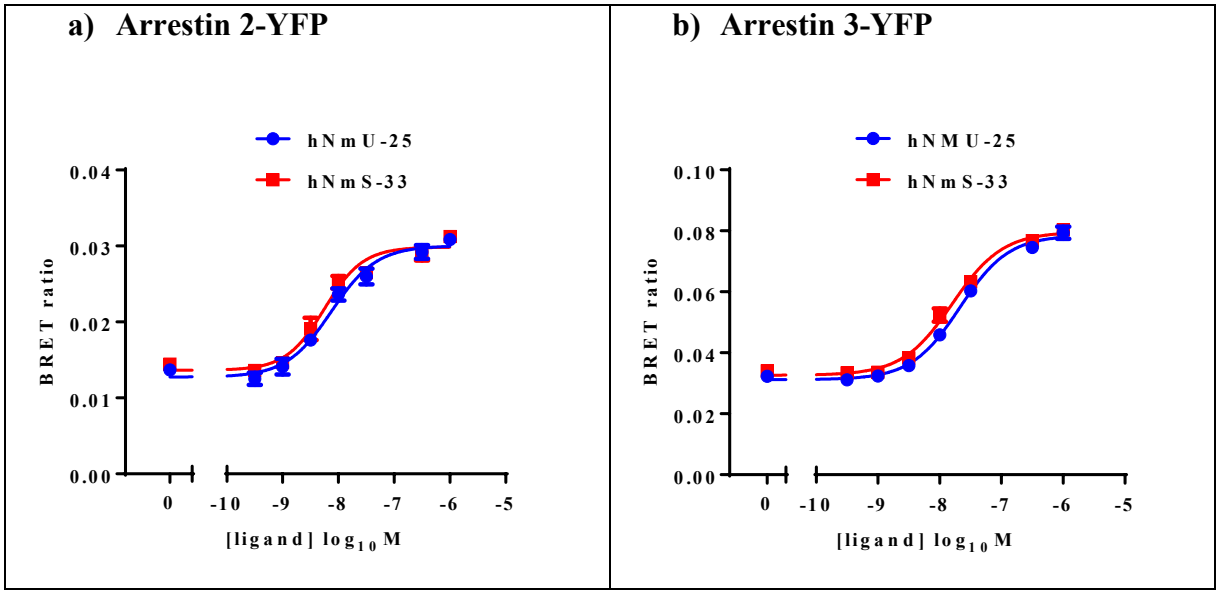


**Figure 5.8. Concentration-dependence of hNmU-25- and hNmS-33-mediated NMU2-arrestin interactions**

Cells were cultured in 10 ml dishes (1,250,000 cells per dish) for 24 h. Cells were then transfected with either: 1) donor (NMU2-nLUC; 250 ng) and acceptor (arrestin 2-YFP; 6 µg); 2) donor (NMU2-nLUC; 250 ng) and acceptor (arrestin 3-YFP; 4 µg) or; 3) NMU2-nLUC (250 ng) only. After 24 h, cells were detached and cells from each transfection sub-cultured on two poly-D-lysine coated 96-well microplates. On the day of the experiment, cells were washed twice with HBSS and 80 µl of the same buffer was added to each well. Cells were incubated with coelenterazine h (5 µM) for 10 min and either hNmU-25 or hNmS-33 was added at the required concentrations for the last 5 min of this. The signals were detected at 535 nm and 465 nm using a ClarioStar microplate reader and the BRET signal was calculated by subtracting the acceptor : donor ratio of the emission from the acceptor : donor ratio in the cells transfected with donor plasmid only. Data are mean ± sem, n > 3 (a, b). $pEC_{50}$ values of hNmU-25 and hNmS-33 in either arretin 2-YFP or arrestin 3-YFP are shown in **Table 5.2**

**Table 5.2. $pEC_{50}$ values of hNmU-25- and hNmS-33-induced NMU2-arrestin interactions**

Concentration-response curves were derived by plotting the concentrations of the agonist against the responses and then fitted with a four parameter logarithmic equation using Graphpad Prism. Data are mean ± sem, n > 3.

| **Interaction** | **hNmU-25** | **hNmS-33** |
|---|---|---|
| | **$pEC_{50}$** | **$pEC_{50}$** |
| **Arrestin 2-YFP** | 8.13 ± 0.02 | 8.24 ± 0.02 |
| **Arrestin 3-YFP** | 7.66 ± 0.05 | 7.79 ± 0.05 |

## 5.5 PTH (1-34) peptide-mediated PTH1R-arrestin interaction in HEK293: BRET saturation assay

Data in **Section 5.3** showed agonist-mediated interactions between the NMU2-nLUC and either arrestin 2-YFP or arrestin 3-YFP. The present experiment was performed to confirm that the BRET assay was working appropriately using a well-established positive control. Parathyroid hormone type 1 receptor (PTH1R), a class B GPCRs that mediates the actions of parathyroid hormone PTH (1-34) was used for arrestins recruitment to determine whether arrestin 2-RLuc and arrestin 3-RLuc are recruited by the receptor upon stimulation with PTH (1-34) as previously reported (Zindel *et al.*, 2016).

HEK-293 were co-transfected with PTH1R-YFP and either arrestin 2-RLuc or arrestin 3-RLuc. After 48 h, exposing the cells to PTH (1-34) for 5 min caused a marked increase in BRET ratio, indicating increased interaction between PTH1R and either arrestin 2-RLuc or arrestin 3-RLuc **(Figure 5.9; a, b)**. These ratios increased with increasing quantities of the acceptor and became saturated in acceptor : donor expression ratios greater than 0.2 and 0.3 for arrestin 2-RLuc and arrestin 3-RLuc respectively **(Figure 5.9, a, b)**. These data are consistent with the published data (Zindel *et al.*, 2016). BRET max and $BRET_{50}$ were determined using one site binding hyperbola **(Table 5.3)**.

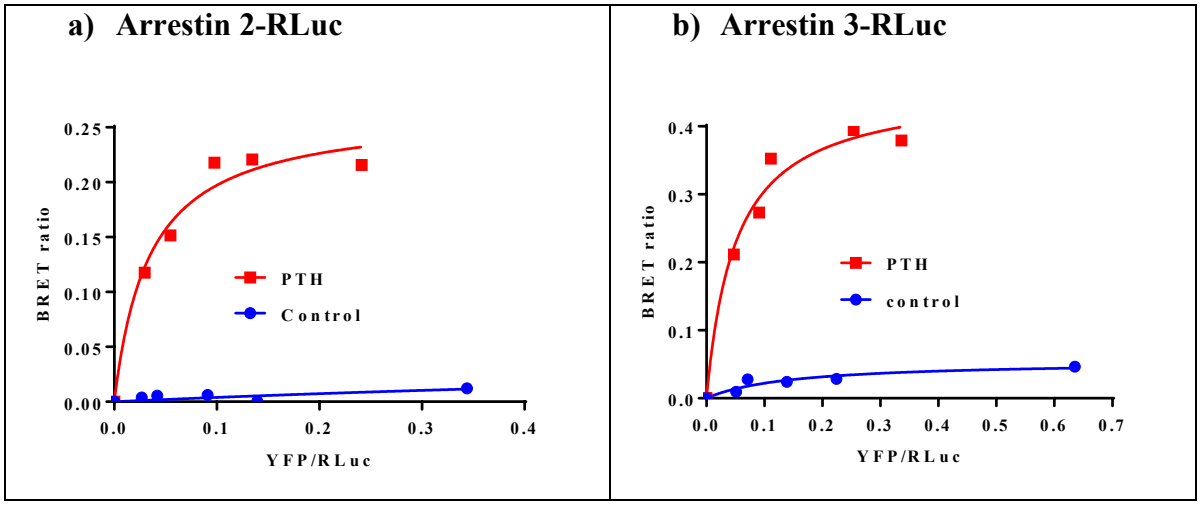


**Figure 5.9. PTH (1-34)-mediated interaction between PTH1R and the arrestins**

Cells were cultured in 6-well plates (250,000 cells per well) for 24 h before being co-transfected with constant amounts of donor plasmid, either a) arrestin 2-RLuc (200 ng/well) or b) arrestin 3-RLuc (200 ng/well) and increasing amounts of acceptor (PTH1R-YFP; 0, 200, 400, 800, 1000, 1600 ng/well). After 24 h, cells were detached and sub-cultured on poly-D-lysine coated 96-well plates and incubated for a further 24 h. On the day of the experiment, cells were washed twice with HBSS and 80 µl of the same buffer was added to each well. The fluorescence intensity was recorded at 535 using a ClarioStar microplate reader. Cells were incubated with coelenterazine h (5 µM) for 10 min and PTH (1-34) (1 µM) was added for the last 5 min of this. The signals were detected at 535 nm and 475 nm using a ClarioStar microreader and the BRET signal was calculated by the subtracting acceptor : donor ratio of the emission from the acceptor: donor ratio in the cells transfected with donor plasmid only. Data were fitted with a one site binding hyperbola using GraphPad Prism. The data show the results of one experiment carried out in quadruplicate.

**Table 5.3. BRET max and $BRET_{50}$ values of PTH (1-34)-mediated PTH1R-arrestin interaction**

The net BRET donor : acceptor ratio and BRET value obtained from the ratio of the total expression of acceptor over the donor were fitted with a one site binding hyperbola using GraphPad Prism. The maximal BRET (BRET max) represents the maximal interaction between the PTH1R and arrestins while the $BRET_{50}$ is the acceptor over the donor expression ratio that gives 50 % of BRET max. Data are from one experiment carried out in quadruplicate. Data are taken from the experiments described in **Figure 5.9**.

| **Interaction PTH1R** | **PTH (1-34)** | | **Control** | |
|---|---|---|---|---|
| | **BRET max** | **$BRET_{50}$** | **BRET max** | **$BRET_{50}$** |
| **Arrestin 2-RLuc** | 0.27 | 0.03 | 0.06 | 1.31 |
| **Arrestin 3-RLuc** | 0.46 | 0.05 | 0.05 | 0.15 |

## 5.6 Temporal profiles of NMU2-arrestin interaction: sustained challenge with the ligand

The time-courses for arrestin 2-YFP and arrestin 3-YFP recruitment to NMU2-nLUC in response to either hNmU-25 or hNmS-33 were generated. HEK-293 were co-transfected with NMU2-nLUC and either arrestin 2-YFP or arrestin 3-YFP before the BRET ratio was measured in response to ligand as index of arrestin recruitment. Sustained challenge of cells with either hNmU-25 or hNmS-33 resulted in marked increases in BRET ratio pointing to increased interaction between the NMU2-nLUC and either arrestin 2-YFP or arrestin 3-YFP **(Figure 5.10; a, b)**. For example, at the first measurement point following ligand addition (5 min), there was an increased BRET ratio compared to untreated controls. Some evidence of small reduction in the continued presence of ligand but generally sustained (**Figure 5.10; a, b)**. Both ligands were similar in mediating sustained arrestin 2-YFP or arrestin 3-YFP recruitment to NMU2-nLUC (sustained challenge) **(Figure 5.10; a, b)**.

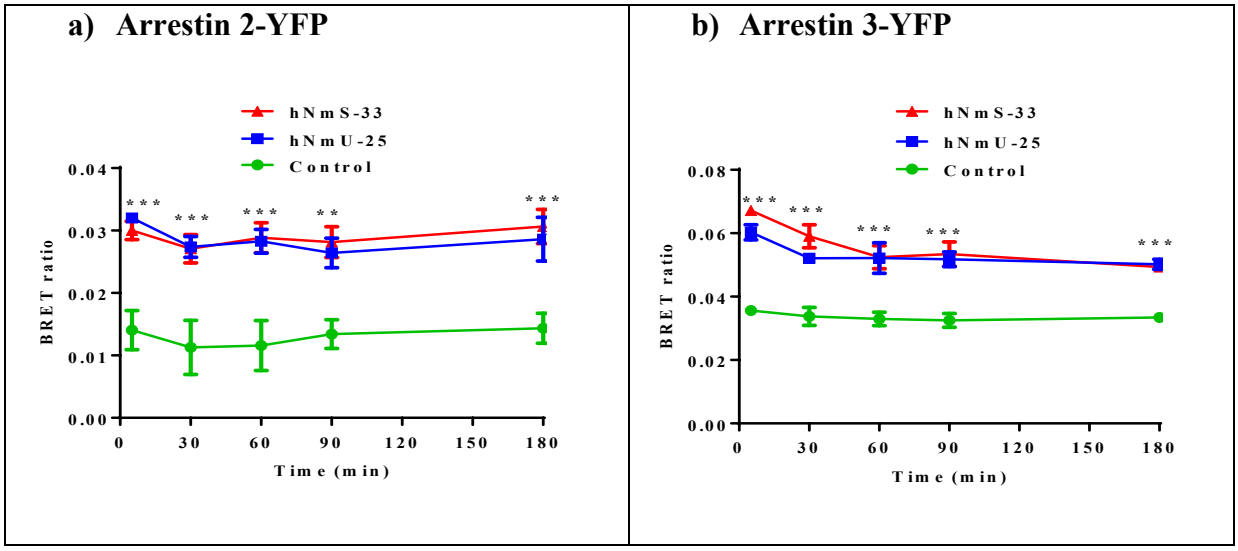


**Figure 5.10. Time course of hNmU-25- or hNmS-33-mediated recruitment of arrestins**

Cells were cultured in 10 ml dishes (1,250,000 cells per dish) for 24 h before being transfected with either: 1) donor (NMU2-nLUC; 250 ng) and acceptor (arrestin 2-YFP; 6 µg); 2) donor (NMU2-nLUC; 250 ng) and acceptor (arrestin 3-YFP; 4 µg) or; 3) donor NMU2-nLUC (250 ng) only. After 24 h, cells were detached and sub-cultured on poly-D-lysine coated 96-well plates and incubated for a further 24 h. On the day of the experiment, cells were washed twice with HBSS and 80 µl of the same buffer was added to each well. Cells were then challenged with either hNmU-25 (1 µM) or hNmS-33 (1 µM) for the required times (0 - 180 min). During the last 10 min of the experiment, cells were incubated with coelenterazine h (5 µM) and the signals were detected at 535 nm and 465 nm using a ClarioStar microplate reader. The BRET signal was calculated by subtracting the acceptor : donor ratio of the emission from the acceptor : donor ratio in the cells transfected with donor plasmid only. Data are mean ± sem, of n = 3 carried out in quadruplicate. Statistical analysis was performed using two way ANOVA followed by Bonferroni's test: $^{**}P < 0.01$; $^{***}P < 0.001$ for both hNmU-25 and hNmS-33 versus nonstimulated group (control). There were no significant differences between hNmU-25 and hNmS-33 responses.

## 5.7 Time-course of NMU2-arrestin interaction following brief exposure to either hNmU-25 or hNmS-33

The time-course of MAP activity and NMU2 phosphorylation following ligand removal after 5 min challenge with either hNmU-25 or hNmS-33 **(Section 3.2.5, 4.5)** showed clear differences between the two ligands in which the pattern in response to hNmS-33 was more sustained compared to hNmU-25. The present experiment was aimed to assess the potential role of arrestins interaction with the NMU2 following brief ligand exposure.

HEK-293 co-transfected for 48 h with NMU2-nLUC and either arrestin 2-YFP or arrestin 3-YFP were challenged for 5 min with either hNmU-25 or hNmS-33. Challenge with either ligand resulted in an increased BRET ratio, pointing to interaction between the NMU2-nLUC and either arrestin 2-YFP or arrestin 3-YFP **(Figure 5.11; a, b)**. Following this initial challenge, removal of the free ligand resulted in decreases in BRET ratio, indicating decreased interaction between NMU2-nLUC and the arrestins (**Figure 5.11; a, b)**. For example, the pattern of interaction of NMU2-nLUC with arrestin 2-YFP in response to either hNmU-25 or hNmS-33 following ligand removal showed a gradual fall at 30 and 60 min recovery with evidence of sustained interactions at later time points **(Figure 5.11; a)**. The pattern generating from the interaction between NMU2-nLUC and the arrestin 3-YFP was slightly different in which the removal of either ligand resulted in rapid decrease in BRET ratio at 30 min recovery and returned to the basal levels at later times of recovery **(Figure 5.11; a)**.

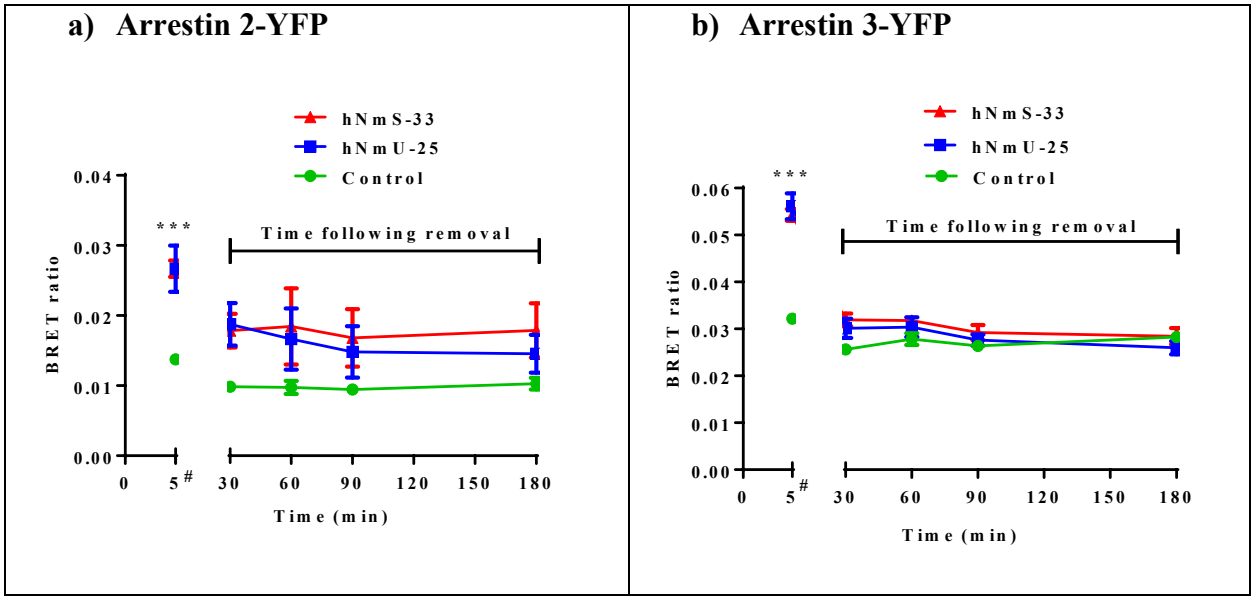


**Figure 5.11. Time-course of NMU2-nLUC-arrestin interaction following brief exposure to either hNmU-25 or hNmS-33**

Cells were cultured on 10 ml dishes (1,250,000 cells per dish) for 24 h before being transfected with either: 1) donor (NMU2-nLUC; 250 ng) and acceptor (arrestin 2-YFP; 6 µg); 2) donor (NMU2-nLUC; 250 ng) and acceptor (arrestin 3-YFP; 4 µg) or; 3) donor (NMU2-nLUC; 250 ng) only. After 24 h, cells were detached and sub-cultured on poly-D-lysine coated 96-well plates and incubated for a further 24 h. On the day of the experiment, cells were washed twice with HBSS and 80 µl of the same buffer was added to each well. Cells were then stimulated with either hNmU-25 (1 µM) or hNmS-33 (1 µM) for 5 min. Following ligand removal and washing the cell monolayers, cells were allowed to recover for 30 – 180 min. Coelenterazine h (5 µM) was added for the last 10 min of the recovery period. The signals were detected at 535 nm and 465 nm using a ClarioStar microplate reader. The BRET signal was calculated by subtracting the acceptor : donor ratio of the emission from the acceptor : donor emission ratio in the cells transfected with donor plasmid only. Data are mean ± sem, of n = 3 carried out in quadruplicate. 0 and $5^{\#}$ represent the start and finish of the ligand stimulation period. Statistical analysis was performed using two way ANOVA followed by Bonferroni's test: $^{***}P < 0.001$ for both hNmU-25 and hNmS-33 versus nonstimulated group (control). There were no significant differences between hNmU-25 and hNmS-33 responses.

## 5.8 Effect of washing the cells with buffer on BRET signal

Data in **Section 5.7** showed a decrease in the association between NMU2-nLUC and arrestins following ligand removal. This ligand removal protocol involved washing the cell monolayer with buffer. To ensure that any changes seen were not a consequence of the wash procedure rather than the ligand removal, further experiments were performed in which HEK-293 co-transfected for 48 h with NMU2-nLUC and arrestin 3-YFP were challenged with either hNmU-25 or hNmS-33 (1 μM), which were then removed, the cell monolayers washed as in the previous experiments but buffer containing the same ligand was then replaced **(Figure 5.12; $a_{ii}$, b)**. In this replacement protocol the BRET signal was sustained in a manner similar to experiments with continued ligand presence **(Figure 5.12; $a_i$, b)**, demonstrating that the wash protocol itself was not responsible for the reduced BRET signal seen on ligand removal.

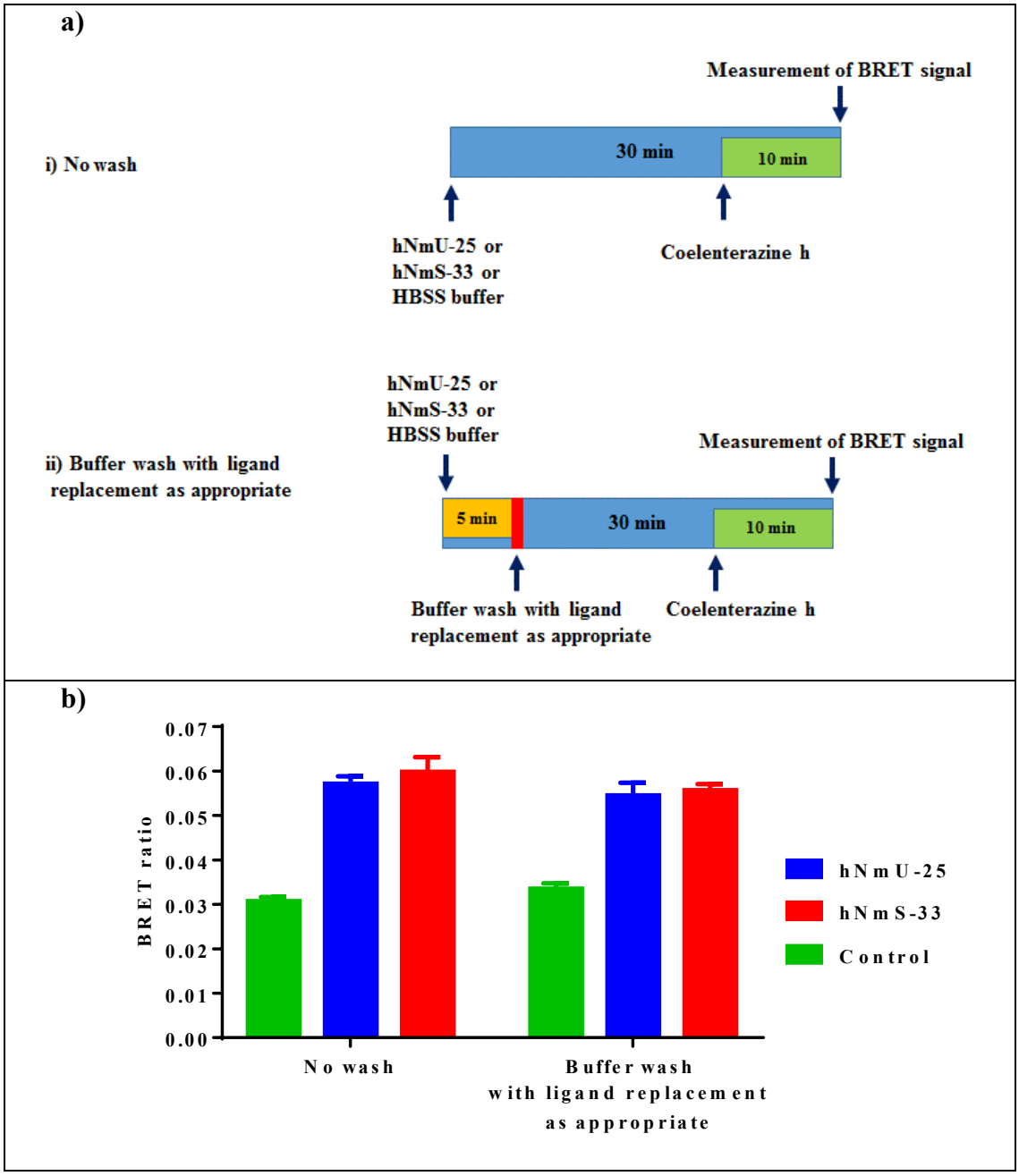


**Figure 5.12. Effect of buffer wash on BRET signal**

Cells were cultured in 10 ml dishes (1,250,000 cells per dish) for 24 h before being transfected with either donor (NMU2-nLUC; 250 ng) only or co-transfected with donor (NMU2-nLUC; 250 ng) and acceptor (arrestin 3-YFP; 4 µg). After 24 h, cells were detached and sub-cultured on poly-D-lysine coated 96-well plates. On the day of the experiment, cells were washed twice with HBSS and then incubated in HBSS. Cells were challenged with either hNmU-25 (1 µM) or hNmS-33 (1 µM) for 5 min followed by either wash and replacement with HBSS containing ligand ($a_{ii}$) or no wash ($a_i$). Cells were then allowed to recover for 30 min. For the last 10 min of the experiment, coelenterazine h (5 µM) was added to the cells and the signals were recorded at 535 nm and 465 nm

using a ClarioStar microplate reader. The BRET signal was calculated by the subtracting acceptor : donor ratio of the emission from the acceptor : donor ratio in the cells transfected with donor plasmid only. Data are mean ± sem of n = 3 carried out in quadruplicate (b).

## 5.9 Effect of PKC activity on the interaction of the arrestins with NMU2

Work described in **Chapter 4** demonstrated that NMU2-HA is a substrate for PKC following direct PKC activation by PDBu and that NMU2-HA phosphorylation induced by either hNmU-25 or hNmS-33 was impaired by PKC inhibition. Here, the potential role of PKC in the recruitment of the arrestins to NMU2 following direct PKC activation by PDBu in the absence of ligand was examined. Furthermore, the potential of PDBu to potentiate agonist-mediated NMU2-arrestins interactions was also assessed. HEK-293 were co-transfected with NMU2-nLUC and either arrestin 2-YFP or arrestin 3-YFP. After 48 h, cells were exposed to PDBu, hNmU-25, hNmS-33 (1 μM) or control (buffer) and PDBu with either hNmU-25 or hNmS-33 for 5 min. Both ligands caused marked increases in BRET signal, indicating increased interaction between NMU2-nLUC and the arrestins **(Figure 5.13; a, b)**. In contrast, following challenge of cells with PDBu, the BRET ratios for NMU2-nLUC and either arrestin 2-YFP or arrestin 3-YFP were not affected and were similar to the non-stimulated group (control) **(Figure 5.13; a, b)**. Addition of PDBu and either hNmU-25 or hNmS-33 simultaneously for 5 min did not influence the BRET ratios compared to those that induced by either hNU-25 or hNmS-33 in the absence of PDBu **(Figure 5.13; a, b)**.

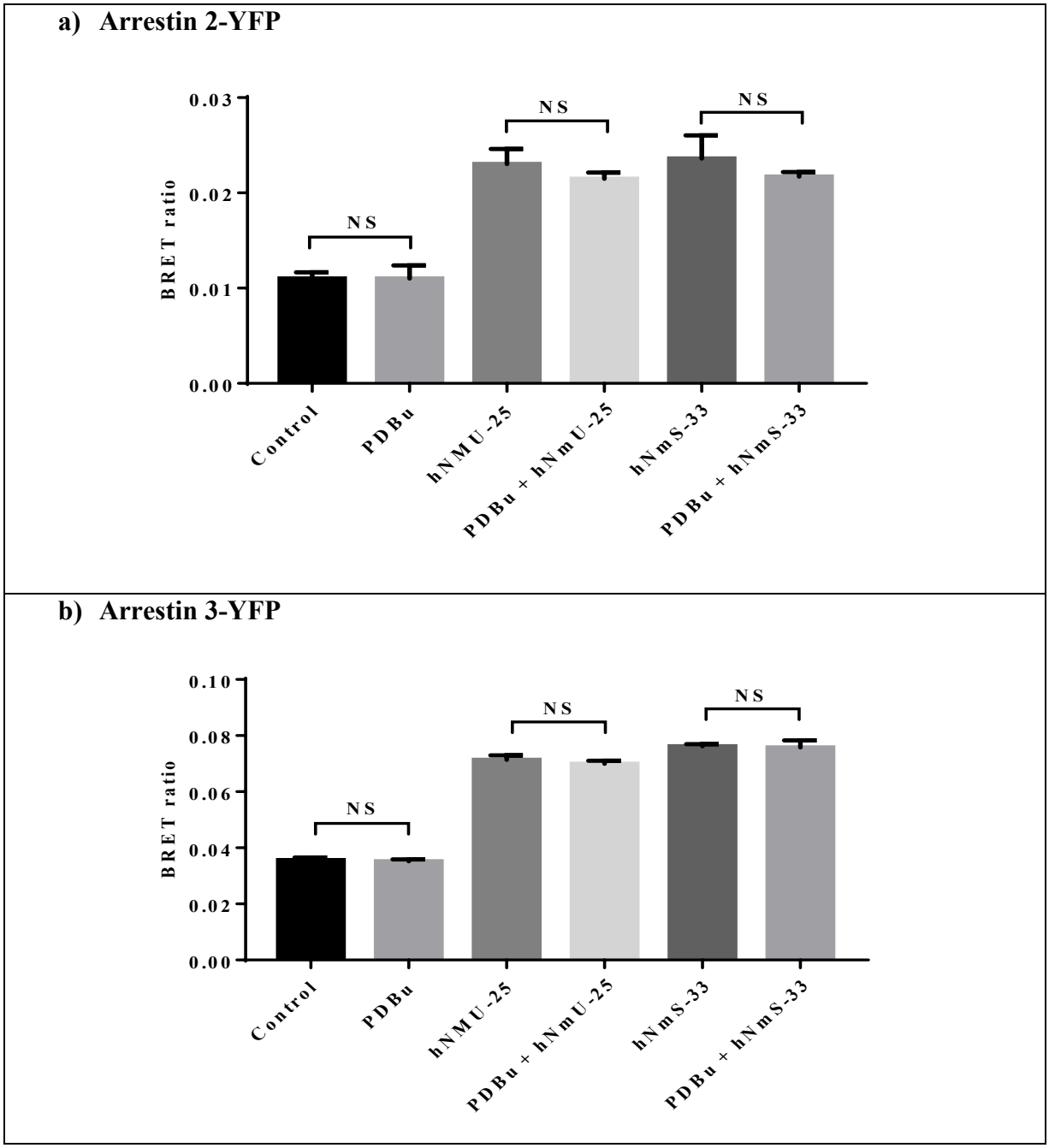


**Figure 5.13. Effect of PDBu on the interaction between NMU2 and the arrestins**

Cells were cultured in 10 ml dishes (1,250,000 cells per dish) for 24 h before being transfected with either: 1) donor NMU2-nLUC (250 ng) and acceptor arrestin 2-YFP (6 µg); 2) donor NMU2-nLUC (250 ng) and acceptor arrestin 3-YFP (4 µg) or; 3) donor (NMU2-nLUC; 250 ng) only. After 24 h, cells were detached and sub-cultured on poly-D-lysine coated 96-well plates. On the day of the experiment, cells were washed twice with HBSS and 80 µl of the same buffer added to each well. Cells were loaded with coelenterazine h (5 µM) for 10 min and PDBu (1 µM), hNmU-25 (1 µM) or hNmS-33 (1 µM) were added for the last 5 min of this. The signals were detected at 535 nm and 465

nm using a ClarioStar microplate reader. The BRET signal was calculated by subtracting the acceptor : donor ratio of the emission from the acceptor : donor ratio emission in the cells transfected with donor plasmid only. Data are mean ± sem, of n = 3 carried out in quadruplicate. Statistical analysis was performed using a one way ANOVA followed by Bonferroni's test. NS; $P > 0.05$, only comparisons ± PDBu for condition are shown for clarity.

## 5.10 Effect of inhibition of PKC on agonist-induced interaction of NMU2 with arrestins

The potential dependence on PKC of the interaction of NMU2 with arrestins following ligand activation was also assessed. HEK-293 were transfected with NMU2-nLUC and either arrestin 2-YFP or arrestin 3-YFP. After 48 h, cells were exposed to the PKC inhibitors, Ro 31-8220 or GF109203X before challenge with the ligand (1 μM, 5 min) **(Figure 5.14; a)**. Both ligands resulted in arrestin 2-YFP and arrestin 3-YFP recruitment to NMU2-nLUC at 5 min challenge as assessed by an increase the BRET ratio using a ClarioStar microplate reader (2.7 ± 0.5, 3.0 ± 0.7 and 2.2 ± 0.04, 2.2 ± 0.06 fold over basal levels for hNmU-25 versus hNmS-33 in arrestin 2-YFP and arrestin 3-YFP respectively) **(Figure 5.14; b, c)**. Following pre-incubation of the cells with Ro 31-8220 and stimulating with either hNmU-25 or hNmS-33, the BRET ratios were significantly increased over the ratios that induced by the ligand only **(Figure 5.14; b, c)**. In contrast, the BRET ratios were not influenced by the presence of GF109203X following 5 min challenge with either ligand compared to the stimulated groups **(Figure 5.14; b, c)**.

a)

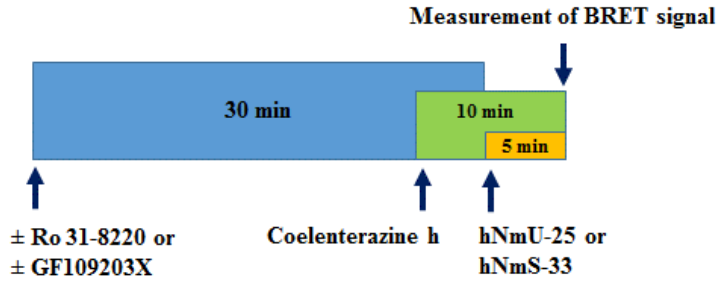


b) Arrestin 2-YFP

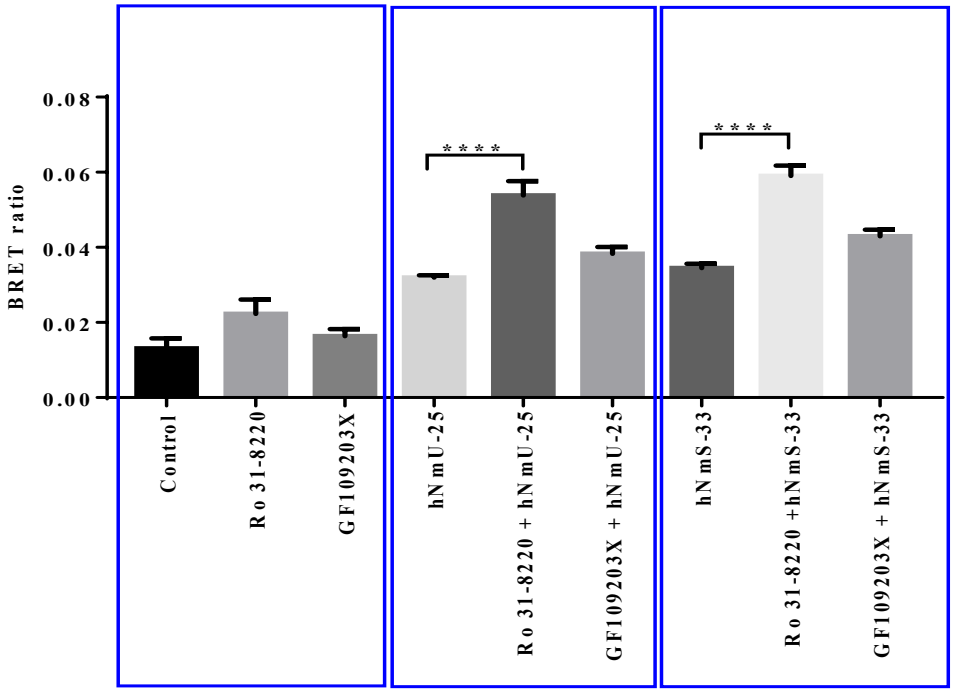


c) Arrestin 3-YFP

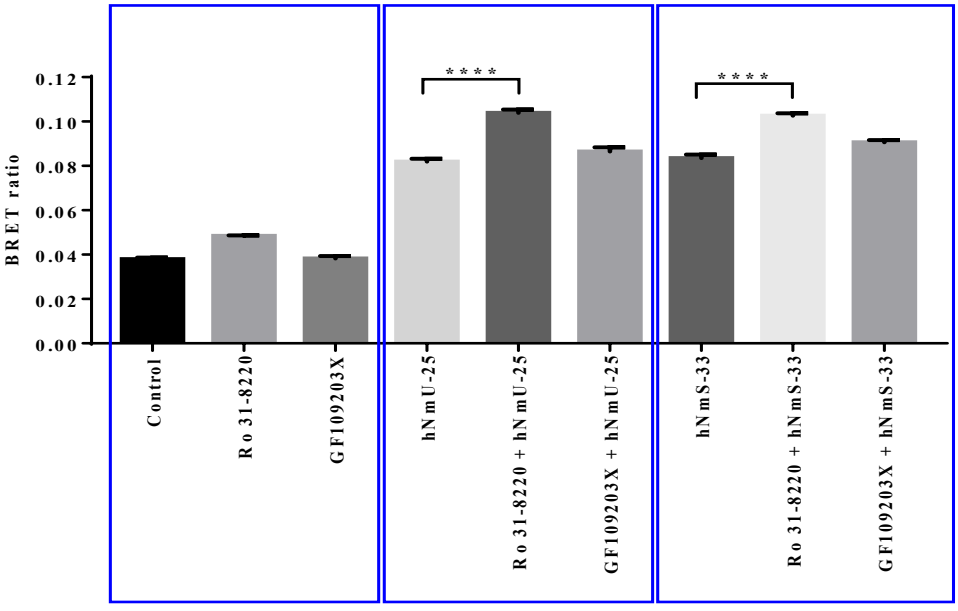

**Figure 5.14. Effect of PKC inhibition on agonist-mediated arrestin recruitment**

Cells were cultured in 10 ml dishes (1,250,000 cells per dish) for 24 h before being transfected with either: 1) donor NMU2-nLUC (250 ng) and acceptor arrestin 2-YFP (6 µg); 2) donor NMU2-nLUC (250 ng) and acceptor arrestin 3-YFP (4 µg) or; 3) donor (NMU2-nLUC; 250 ng) only. After 24 h, cells were detached and sub-cultured on poly-D-lysine coated 96-well plates. On the day of the experiment, cells were washed twice with HBSS and 80 µl of the same buffer added to each well. Cells were pre-treated with or without PKC inhibitors; Ro 31-8220 (5 µM, 30 min) or GF 109203X (1 µM, 30 min). Coelenterazine h (5µM) was added for the last 10 min of this. Cells were challenged with either hNmU-25 (1 µM) or hNmS-33 (1 µM) for the last 5 min of the experiment as indicated (a). The signals were detected at 535 nm and 465 nm using a ClarioStar microplate reader. The BRET signal was calculated by subtracting the acceptor : donor ratio of the emission from the acceptor : donor ratio emission in the cells transfected with donor plasmid only. Data are mean ± sem, of n = 3 carried out in quadruplicate (b, c). Statistical analysis was performed using a one way ANOVA followed by Bonferroni's test: $^{****}P < 0.0001$. Only comparisons of groups treated with a PKC inhibitor versus their respective untreated control are shown for clarity.

## 5.11 Discussion

Constructs encoding NMU2-nLUC, arrestin 2-YFP or arrestin-3YFP were generated to monitor the potential interaction of NMU2 with the arrestins following receptor stimulation. Data in this chapter show that both hNmU-25 and hNmS-33 mediate the interaction between NMU2-nLUC and either arrestin 2-YFP or arrestin 3-YFP. Furthermore, these interactions were dependent upon ligand indicating that ligand-occupation of the receptor is critical in mediating the interaction. These results are in accord with recent studies in other GPCRs. For example, activation of the growth hormone secretagogue receptor (GHSR1a), known to be dually coupled to $G_{\alpha q}$ and $G_{\alpha i}$, results in recruitment of both arrestin 2 and arrestin 3 to the receptor (Bouzo-Lorenzo *et al.*, 2016). Furthermore, $PAR_2$ (protease-activated receptor-2), a $G_{\alpha q}$-coupled receptor, interacts with both arrestin 2 and 3 following stimulation with cognate agonist (Pal *et al.*, 2013).

The present study shows that both ligands mediate NMU2 interaction with the arrestins with $BRET_{50}$ values greater for arrestin 2 than arrestin 3 suggesting that NMU2 may preferentially interact with arrestin 3 compared to arrestin 2. This difference between arrestin 2 and arrestin 3 in mediating the interaction with the receptor is also observed in other GPCRs such as neurokinin 1 receptor and GHSR1a (Salahpour *et al.*, 2012; Pal *et al.*, 2013; Bouzo-Lorenzo *et al.*, 2016). Hence, GPCRs are classified into two classes based on the affinity for arrestins. While class A receptors bind to arrestin 3 preferentially over arrestin 2, class B receptors bind to both arrestin 2 and arrestin 3 with equal affinity (Oakley *et al.*, 2000; Lohse *et al.*, 2012). This classification is based on the affinity of arrestins binding to the receptor and NMU2 may belong to class A GPCRs. However, the data presented in Chapter 3 demonstrated that rate of NMU2 resensitisation following subsequent stimulation with ligand was slow ranging from 6 h and more to fully recover depending on the ligand. The rate of resensitisation represents a marker for the rate of recycling, thereby suggesting that NMU2 recycles slowly and this suggests that NMU2 is classified into class B GPCRs. These paradoxical results may attribute to difference in receptor regulation, for example, following agonist-dependent receptor activation, arrestins recruit and bind to the receptor for a short period of time which then dissociates from the receptor. Following arrestins dissociation, the receptor may engage with other molecules or intracellular compartments and recycle slowly.

As a positive control for the arrestins recruitment to the PTH1R, BRET assay was assessed. This receptor is well-established to show robust arrestins recruitment following agonist occupation (Vilardaga *et al.*, 2002). For these experiments, arrestin 2-Rluc or arrestin 3 Rluc constructs were generated to assess interaction with PTH1R-YFP. Stimulation of PTH1R with PTH (1-34) resulted in a robust interaction between PTH1R and the arrestins (arrestin 2 and arrestin 3), consistent with previous study which showed interaction between PTH1R and arrestin 3 (Zindel *et al.*, 2016). The present study also demonstrated arrestin 2 recruitment to PTH1R in addition to arrestin 3.

Sustained challenge of NMU2 with either hNmU-25 or hNmS-33 mediated a sustained interaction between the receptor and both arrestin 2 and arrestin 3. These results are consistent with results using other GPCRs. For example, sustained challenge of the angiotensin II type 1 receptor for 20 min with angiotensin II resulted in sustained arrestin 3 recruitment. Furthermore, mutations in four serine/threonine phosphorylation sites in the *C*-terminus of this receptor inhibited this interaction, highlighting the critical nature of these residues for the interaction (Wei *et al.*, 2004; Toth *et al.*, 2018). In another example, in which HEK-293 co-transfected with the vasopressin 2 receptor and arrestin 3, stimulation with arginine vasopressin (AVP) generated sustained (50 min) recruitment. Furthermore, in that study, addition of antagonist following stimulation for 10 min inhibited the interaction between the receptor and arrestin 3 which increased over time indicating importance of agonist-bound receptor in recruitment of arrestins and highlighting arrestins dissociation following inhibition of agonist binding to the receptor (Kocan *et al.*, 2009; Kocan *et al.*, 2011). However, the present study investigated the arrestins dissociation by removal of ligand following brief exposure. Many GPCRs have been reported to recruit arrestins on activation (Lefkowitz *et al.*, 2005; Peterson *et al.*, 2017; Mores *et al.*, 2018) and this is an accepted model for GPCR regulation. Arrestins play multiple roles including termination of G-protein signalling by preventing further G-proteins from binding to the receptor thereby mediating receptor desensitisation following phosphorylation by GRKs. Furthermore, it promotes receptor internalisation by engaging it with elements of endocytic machinery. It also has critical roles in the regulation of a variety of intracellular signalling proteins, inducing a list of arrestin-dependent signalling (Shukla *et al.*, 2011b; Bonneterre *et al.*, 2016). The stability of the receptor-arrestin complex may play a critical role in modulation of arrestin-dependent signalling pathways and the regulation of the intracellular trafficking of receptors (Oakley

*et al.*, 2000). The classification of receptors based on the interaction with arrestins **(See Section 1.4.2.4.3)**. Although this classification has focused on the receptor, the nature of the ligand itself may also be important. For example, the chemokine receptor 2 (CCR2)-arrestin complex shows differences following activation with different ligands such as CCL2, CCL7, CCL8 and CCL13 (Berchiche *et al.*, 2011). This suggests that the different ligands by having temporal profiles of receptor-arrestin association/dissociation may confer a functional selectivity or biased agonism. This may lead to ligand-dependent differences in a range of aspects of receptor-function, for example, at the level of desensitisation, resensitisation and arrestin-mediated signalling (Berchiche *et al.*, 2011; Bonneterre *et al.*, 2016). Given that different patterns of NMU2 dephosphorylation were observed following removal of either hNmU-25 or hNmS-33, this could suggest there might be differences in the temporal profile of receptor-arrestin dissociation between the two ligands. Contrary to expectations, the present study did not find a significant difference between hNmU-25 and hNmS-33 responses in the temporal profile of dissociation of either arrestin 2 or arrestin 3 from NMU2 following removal of either hnmU-25 or hNmS-33. This suggests that arrestins are not responsible for ligand-specific profiles of NMU2 dephosphorylation and MAPKs activation. Although the results demonstrated similar patterns of arrestin dissociation from NMU2 following removal of either hNmU-25 or hNmS-33, NMU2 dephosphorylation was significantly slower following removal of hNmS-33 compared to hNmU-25. The more sustained MAPK signalling, slow rate of resensitisation and slow rate of dephosphorylation in response to hnmS-33 do not match with the rate of arrestins dissociation. This inconsistency with arrestins dissociation may be due to differences in engagement of receptor with different molecules, yet to be identified, following arrestins dissociation after removal of either hNmU-25 or hNmS-33 and this might be ligand-specific. For example, differences in the sites of receptor phosphorylation in response to different ligands might play a critical role in the regulation of receptor phosphorylation/dephosphorylation. These differences in the sites of phosphorylation might affect patterns of receptor phosphorylation/dephosphorylation. For example, while some receptors dephosphorylate, others still phosphorylate. The functions of phosphorylation sites of NMU2 following agonist activation are yet to be identified.

The sustained activation of NMU2 with either hNmU-25 or hNmS-33 mediated sustained ERK1/2 activation and arrestin recruitment **(Figure 3.7, Figure 5.10)** which is consistent

with general scheme of GPCRs which suggests that longevity of receptor-arrestin complex is responsible for spatio-temporal profiles of arrestin-dependent signalling. For example, angiotensin II type 1 receptor and vasopressin 2 receptor form stable complexes with arrestin resulting in sustained ERK1/2 activation and engagement in the endocytic vesicles (DeFea *et al.*, 2000b; Oakley *et al.*, 2000; Luttrell *et al.*, 2001; Ahn *et al.*, 2004; Jafri *et al.*, 2006). However, removal of ligand generated ligand-specific NMU2 signalling profiles and receptor phosphorylation in which the brief exposure to hNmS-33 mediated a sustained NMU2-mediated ERK1/2 activation and sustained NMU2 phosphorylation compared to hNmU-25 response although arrestin interaction was dissociated from NMU2 following removal of either hNmU-25 or hNmS-33. A possible explanation for this discrepancy might be that both arrestin 2 and arrestin 3 are responsible for desensitisation of activated and phosphorylated receptor but not internalisation and/or receptor trafficking. This has been suggested for other receptors. For example, urotensin II (UII) activation of the $G\alpha_q$-coupled urotensin receptor (UTR), exerts a long-term effect of vasoconstriction but notably is internalised in a dynamin-dependent but arrestin-independent manner. Co-expression of the UTR with an arrestin 3 mutant, which inhibits targeting of many GPCRs to clathrin-coated pits thereby inhibiting receptor internalisation, does not influence internalisation of the activated UTR. Furthermore, activation of the UTR with UII in mouse embryonic fibroblast lacking both arrestin 2 and arrestin 3 still results in receptor internalisation suggesting that this is arrestin-independent (Giebing *et al.*, 2005). This has also been reported for other GPCRs such as muscarinic M2 receptor, protease activated receptor (PAR1) and prostacyclin receptor (Lee *et al.*, 1998; Smyth *et al.*, 2000; Paing *et al.*, 2002). Agonist binding to a GPCR mediates its activation that is inhibited by a rapid desensitisation following subsequent activation, this process is controlled by different mechanisms including the dissociation of G-proteins, receptor internalisation and downregulation. Receptor internalisation has a critical role in both receptor desensitisation and resensitisation (Yu *et al.*, 1993). GPCR internalisation is generally facilitated by GRKs or second messenger-dependent kinases phosphorylation where the GRKs play a critical role in mediating arrestins recruitment to the receptor facilitating internalisation by interaction of receptor-bound arrestin with the clathrin and AP2 adaptor protein (elements of internalisation) (Pitcher *et al.*, 1998; Ferguson, 2001; Lefkowitz *et al.*, 2005). Recent study showed that NMU2 is significantly internalised following activation with hNmU-25, hNmS-33 or fluorescently labelled pNmU-8, CyB3-pNmU-8 which showed co-

internalisation with GFP-tagged NMU2 suggesting a role for the internalisation in receptor desensitisation, resensitisation and intracellular signalling (Alhosaini *et al.*, 2018). Given that the more sustained phosphorylation of NMU2 following brief hNmS-33 exposure compared to hNmU-25 was PKC-independent, it is possible that GRK phosphorylation might be sustained in response to hNmS-33 but this is independent of arrestin binding. Leukotriene $B_4$ ($LTB_4$) mediates leukotriene receptor (BLT1) internalisation in rat basophil leukaemia cells (RBL-2H3). However, expression of a negative-dominant GRK2 blocked BLT1 internalisation while overexpression of GRK2 enhanced BLT1 internalisation. Although this might suggest a standard phosphorylation- and arrestin-dependent internalisation, expression of negative-dominant arrestin did not influence BLT1 internalisation. Moreover, co-immunoprecipitation showed that BLT1 was not associated with arrestins but was associated with GRK2 suggesting a role of GRK in receptor phosphorylation and internalisation in an arrestin-independent manner (Chen *et al.*, 2004b).

The present study demonstrates that there is no evidence that PKC-dependent phosphorylation of NMU2 is responsible for arrestins recruitment either in the absence or presence of agonist. These results are in agreement with the classic paradigm that suggests that ligand occupied receptor leads to its phosphorylation by GRKs which, in turn, mediate recruitment of arrestins to the receptor resulting in homologous desensitisation by inhibiting a further G-proteins coupling (Pitcher *et al.*, 1992; Tobin *et al.*, 2008; Gurevich *et al.*, 2012). However, evidence from other studies reported a role of PKC-dependent phosphorylation in arrestins recruitment and receptor desensitisation for other GPCRs such as the neurokinin 1 receptor, calcium-sensing receptor and $\alpha_{1B}$ adrenoceptor (Paschke *et al.*, 2007; Murphy *et al.*, 2011; Castillo-Badillo *et al.*, 2015; Toth *et al.*, 2018). Therefore, the present study suggests participation of GRKs in the phosphorylation of NMU2 following stimulation with either hNmU-25 or hNmS-33. Furthermore, the sustained NMU2 phosphorylation following brief exposure to hNmS-33 was PKC-independent at 1 h recovery after removal of hNmS-33 highlighting possible role of GRKs in sustained NMU2 phosphorylation following brief exposure to hNmS-33. The possible role of GRKs in receptor phosphorylation and signalling consequences has been shown for several studies in which the agonist-dependent receptor activation can be differently phosphorylated by different GRK subtypes resulting in distinct consequences. For example, although phosphorylation of $\beta_2$ adrenoceptors following

agonist activation was largely by GRK2, rate of arrestin recruitment was markedly influenced by GRK6 which showed that it phosphorylates the *C*-terminal of $\beta_2$ adrenoceptor at specific residues highlighting the possibility of GRK-mediated different phosphorylation sites of the receptor leading to different signalling consequences (Violin *et al.*, 2006; Tobin *et al.*, 2008). Indeed, activation of angiotensin II type 1 receptors or vasopressin 2 receptors results in their phosphorylation by GRK2 and GRK3 thereby promoting arrestin recruitment and receptor desensitisation while GRK5 and GRK6 are responsible arrestin 3 mediated ERK signalling (Kim *et al.*, 2005; Ren *et al.*, 2005). Furthermore, GRK2 phosphorylation of ligand-bound MOR recruits arrestin 3 and prompts receptor desensitisation in HEK-293 expressing MOR (Chen *et al.*, 2013; Lowe *et al.*, 2015). The differential GRKs activation has also been shown between different endogenous ligands. For example, CCL19 and CCL21, endogenous ligands for CCR7, result in different functional consequences (Zidar *et al.*, 2009). While CCL21 activated CCR7 results in arrestin 3 recruitment by activation of GRK6 only, CCL19 mediates activation of GRK3 and GRK6 by CCR7 resulting in targeting of arrestin 3 to the endocytic vesicles in addition to receptor desensitisation highlighting possible role of biased agonism in driving of distinct consequences (Zidar *et al.*, 2009). In the line of this evidence, NMU2 may differently phosphorylate in response to hNmU-25 and hNmS-33 in terms of phosphorylation sites and GRK subtypes and that may affect phosphorylation pattern of NMU2 following removal of hNmS-33 compared to hNmU-25.

In conclusion, this chapter shows that both hNmU-25 and hNmS-33 induce interaction between NMU2 and the arrestins. Both ligands generate similar temporal profiles of arrestins association and dissociation with NMU2 in either the continued presence of ligand or during and following brief exposure. This suggests that sustained MAPKs activation and NMU2 phosphorylation following brief exposure to hNmS-33 are not related to arrestins recruitment. Furthermore, PKC is not responsible for arrestins recruitment to NMU2. However, whether or not GRKs are involved in arrestins recruitment to NMU2 remains to be explored. To develop a full picture of NMU2 interaction with arrestins and other proteins, additional studies will be needed. For example, it would be worth examining the proteins that associate with NMU2 upon ligand binding, particularly in response to different ligands. This might provide an explanation about the difference between hNmU-25 and hNmS-33 responses in mediating NMU2 phosphorylation, MAPK signalling and resensitisation profile following removal of

ligand highlighting biased agonism. Furthermore, a limitation of this study is that the transient system is used for study of the interaction between NMU2 and the arrestins. This differs from the stably transfected cell line used to investigate NMU2 phosphorylation and results presented earlier demonstrated clear differences in receptor processing and expression in transient compared to stably transfected systems (**Figure 3.3**). Furthermore, ligand-induced receptor phosphorylation was not detectable in transiently transfected cells (**Figure 4.1**). Taken together, these data highlight clear differences between the transiently and stably expressed receptor, This might impact on interpretation and suggests that the investigation of receptor-arrestins interaction in cells with stable expression of NMU2-nLUC should be considered. In addition to such studies, the full mapping of the phosphorylation sites within NMU2 is crucial to address whether or not hNmU-25 and hNmS-33 phosphorylate NMU2 at different sites. Such differences could generate different docking sites for proteins or different conformations of NMU2 in response to different ligands that might lead to different signalling and/or processing consequences.

# 6 Chapter six: Identification of NMU2 phosphorylation sites using mass spectrometry and generation of cell lines expressing NMU2 mutants for the study of phosphorylation

## 6.1 Introduction

It has been known for more than two decades that GPCRs are phosphorylated following agonist activation. This leads to receptor desensitisation and internalisation (Ferguson, 2001; Tobin, 2008) and is additionally involved in coupling the receptors to arrestins, thereby engaging the receptors with alternative G-protein-independent signalling (Lefkowitz *et al.*, 2005; Prihandoko *et al.*, 2015b). There is evidence that some GPCRs might be differently phosphorylated in response to different agonists (Jean-Charles *et al.*, 2016b; Xiao *et al.*, 2016; Yang *et al.*, 2017) highlighting the possibility that different phosphorylation may generate signalling leading to distinct functional outcomes. For example, the activation of CCR7 by either CCL19 or CCL21 (endogenous peptides for CCR7) in HEK-293 cells shows equivalent potency in terms of $Ca^{2+}$ signalling. However, stimulation of receptor with CCL19 resulted in a marked increase in receptor phosphorylation which was mediated by GRK3 and GRK6 resulting in robust recruitment of arrestin 3, receptor desensitisation and redistribution of arrestin 3 to the endocytic vesicles while CCL21 resulted in a small increase in phosphorylation that was mediated by GRK6 (~21 % of CCL19 response) resulting in weak arrestin 3 interaction with no evidence of arrestin trafficking to endocytic vesicles and classical receptor desensitisation (Zidar *et al.*, 2009). Such observations underlie the concept of the phosphorylation barcode that suggests that different ligands are able to drive different patterns of receptor phosphorylation and that this may lead to different biological responses (Tobin *et al.*, 2008; Butcher *et al.*, 2011; Nobles *et al.*, 2011b; Xiao *et al.*, 2016; Latorraca *et al.*, 2017b). For example, two serine residues including $S^{357}$ and $S^{361}$ in the *C*-terminal tail of FFA4 play a critical role in mediating arrestin-dependent receptor internalisation while $T^{347}$, $T^{349}$ and $S^{350}$ were responsible for Akt activation (Prihandoko *et al.*, 2016a). The importance of receptor phosphorylation to physiological responses has been reported in many studies. For example, using transgenic knock-in mice, it was shown that arrestin recruitment to the muscarinic M3 receptor and subsequent receptor internalisation were blocked following removal of phosphorylation sites by mutations without affecting $G_{\alpha q}$-dependent signalling such as $Ca^{2+}$ responses and PKC activation. Furthermore, mice expressing muscarinic M3 receptors lacking phosphorylation sites showed a marked

decrease in a pancreatic insulin release and a deficit in hippocampal learning and memory (Kong *et al.*, 2010; Poulin *et al.*, 2010). Collectively, these studies outline a critical role for receptor phosphorylation in regulation of GPCR signalling and functional outcomes.

Potential phosphorylation sites were predicted within the NMU2 sequence, particularly in the *C*-terminal tail and intracellular loops using NetPhos software (Brighton *et al.*, 2004a) **(Figure 6.4)**. These sites are potential for second messenger kinases (PKC and PKA). As there are no consensus sequences identified for GRKs (Brighton *et al.*, 2004a), GRK sites have not been identified in NMU2.

Site-directed mutagenesis had previously been exploited for determination of potential phosphorylation sites. Recently, different approaches have been developed to facilitate the identification of precise sites of phosphorylation including mass spectrometry and antibodies directed against specific phosphorylated residues within specific proteins. These methods enabled identification of the precise sites of phosphorylation of growing list of GPCRs such as $\beta_2$ adrenoceptor, GHSR1a and MOR (Chen *et al.*, 2013; Yang *et al.*, 2015; Bouzo-Lorenzo *et al.*, 2016).

The aim of this chapter was to identify the precise phosphorylation sites of NMU2 using mass spectrometric analysis. These data were then used to if required to inform mutagenesis, a strategy to determine where receptor phosphorylates in response to agonists and if there are any differences between ligands. Hence, this chapter also includes a study of NMU2 phosphorylation (NMU2 mutants).

## 6.2 Mapping of NMU2 phosphorylation sites using mass spectrometry

Data in **Chapter four,** demonstrated that NMU2 is phosphorylated by hNmU-25 and hNmS-33 and that different temporal patterns of receptor dephosphorylation emerge following brief exposure to either hNmU-25 or hNmS-33. Specifically, phosphorylation following brief exposure to hNmS-33 was more sustained compared to hNmU-25. Identification of the sites of NMU2 phosphorylation in response to either hNmU-25 or hNmS-33 was therefore of particular interest. Mass spectrometric analysis was used to determine the phosphorylation sites of NMU2 following challenge of HEK-NMU2-HA with hNmU-25, hNmS-33 (1 μM) or control (buffer) for 5 min. After solubilising and immunoprecipitating the NMU2-HA receptors, they were then resolved by gel electrophoresis and stained with coomassie blue **(see Methods)**. The results showed a band located at a molecular size of ~ 80 kDa **(Figure 6.1; a)**. Immunoblotting of the immunoprecipitated NMU2-HA also resulted in an intense band at ~ 80 kDa **(Figure 6.1; b)** consistent therefore with the coomassie-stained band being NMU2-HA. The immunoprecipitated NMU2-HA was excised from coomassie-stained gels in small cubes (~1 x 2 mm) and submitted for mass spectrometric analysis (PNACL, University of Leicester). Five serine and threonine phosphorylation sites were detected in the *C*-terminal fragment of NMU2-HA **(Figure 6.2; a, b, c, d, e)**. Unfortunately, a region of the *C*-terminus containing seven potential phosphorylation sites (serine/threonine residues) was not covered in any of the mass spectrometric analysis although tryptic digests with trypsin was used to cleave arginine and lysine and attempts using endoprotease, Glu-C to cut glutamic acid residue to maximize the coverage **(Figure 6.3; a)**. In those regions that were covered, there were differences in the number of times that each peptide fragment was detected and the times a particular serine or threonine residues. For example, in the peptide sequences representing NMU2 residues 330 - 345, that contains two serine residues, S341 was phosphorylated in 8 out of 58 observations following vehicle treatment, 4 out of 10 observations following hNmU-25 and 5 out of 12 observations following hNmS-33 **(Figure 6.3; b)**. However, in the sequences including residues 359 - 371 (containing one threonine residue) and residues 401 - 421 (containing one serine and two threonine residues), threonines 364 and 412 were observed as phosphorylated under basal conditions in 1 out of 1 and 1 out of 4 times respectively but never observed as phosphorylated under stimulated conditions **(Figure**

**6.3; b)**. Net Phos software was also used to assess the potential PKA or PKC sites, and identified two sites (S407 and T412) as potential PKC targets **(Figure 6.3; b)**.

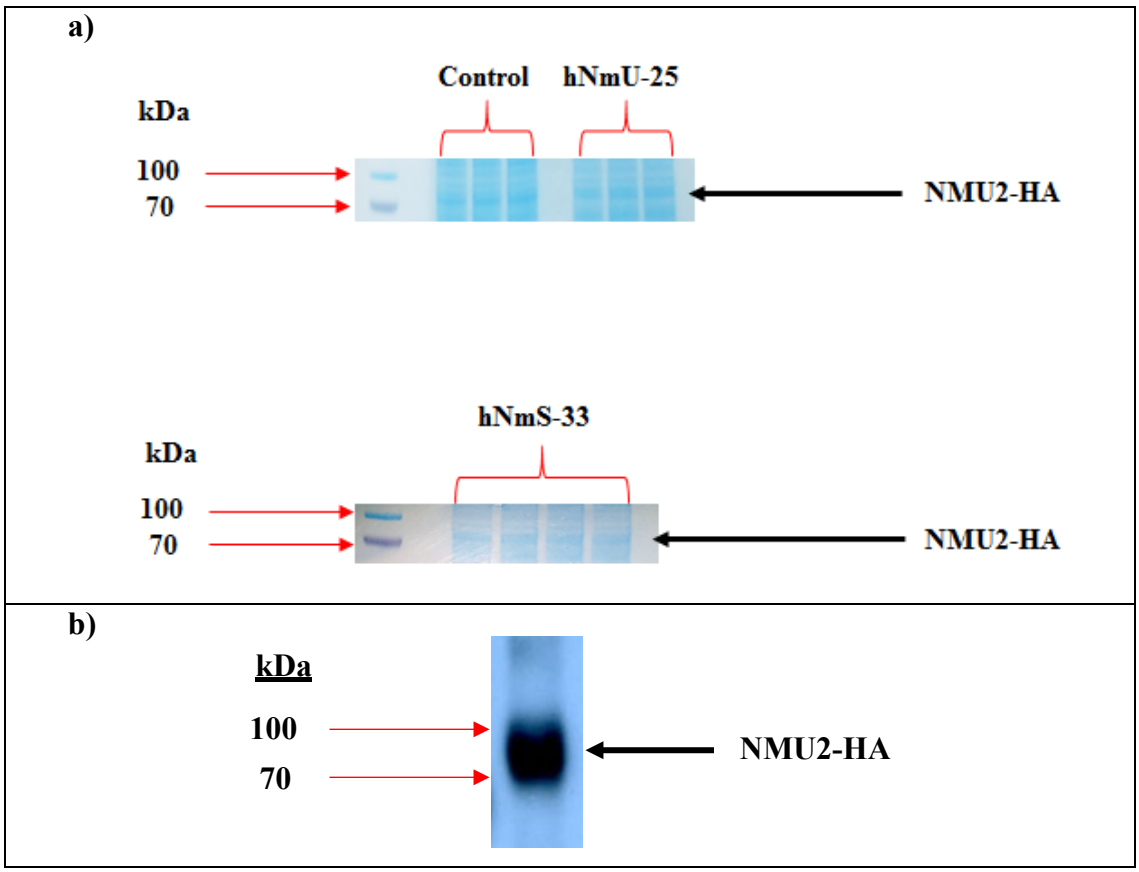


**Figure 6.1. NMU2-HA stimulation, purification and detection**

HEK-NMU2-HA cells were grown in 10 flasks (175 $cm^2$) to ~ 95 % confluency. On the day of the experiment, cells were washed, detached and re-suspended in KHB. After 1 h with shaking every 10 min, cells were then stimulated with hNmU-25 (1 µM), hNmS-33 (1 µM) or KHB (control) for 5 min before solubilisation. NMU2-HA was then captured using anti-HA antibody conjugated beads. Immunoprecipitated NMU2-HA receptors were resolved by polyacrylamide gel electrophoresis and stained with coomassie blue. The area of the gel was then cut into small cubes and submitted for analysis of the phosphorylation sites using an in-house service (Protein and Nucleic Acid Chemistry Laboratory (PNACL), University of Leicester) (a). NMU2-HA was immunoblotted from the same samples that ended with coomassie-stained gels using an anti-HA antibody for the validation of expected molecular weight (b).

a)

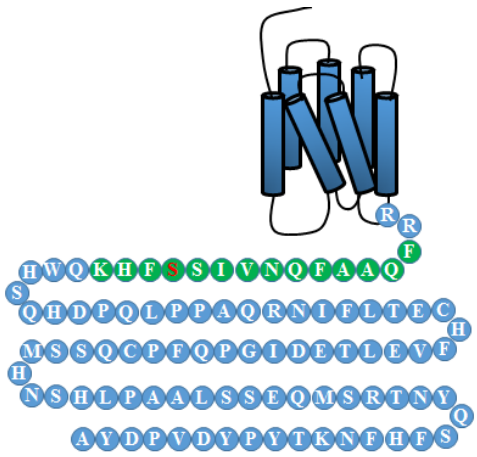

| AA sequence | Y ions |
|---|---|
| K | 147.1 |
| H | 284.2 |
| F | 431.2 |
| pS | 598.2 |
| S | 685.3 |
| I | 798.4 |
| V | 897.4 |
| N | 1011.5 |

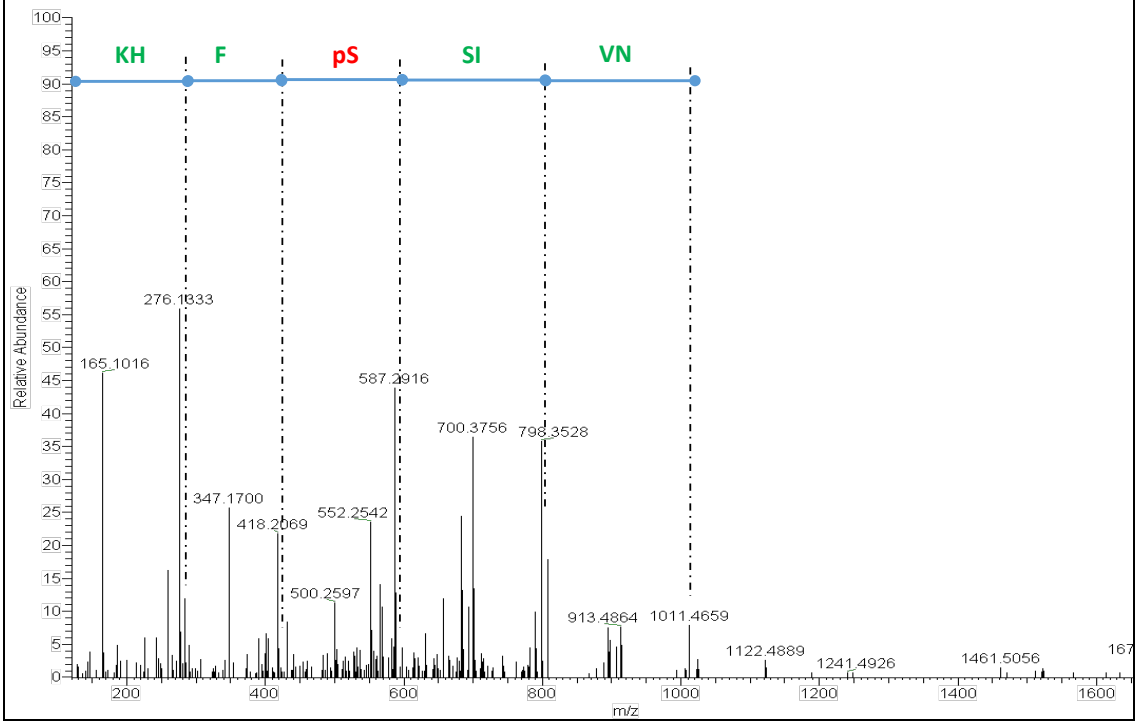

**b)**

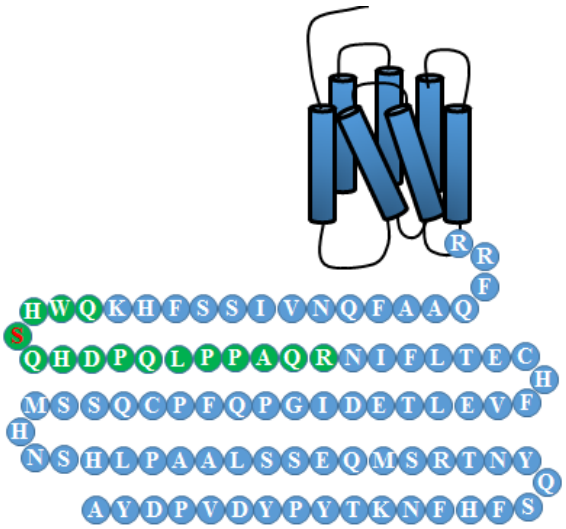

| AA sequence | Y ions |
|---|---|
| A | 374.2 |
| P | 471.3 |
| P | 568.3 |
| L | 681.4 |
| Q | 809.5 |
| P | 906.5 |
| D | 1021.5 |
| H | 1158.6 |
| Q | 1286.7 |
| pS | 1453.7 |
| H | 1590.7 |

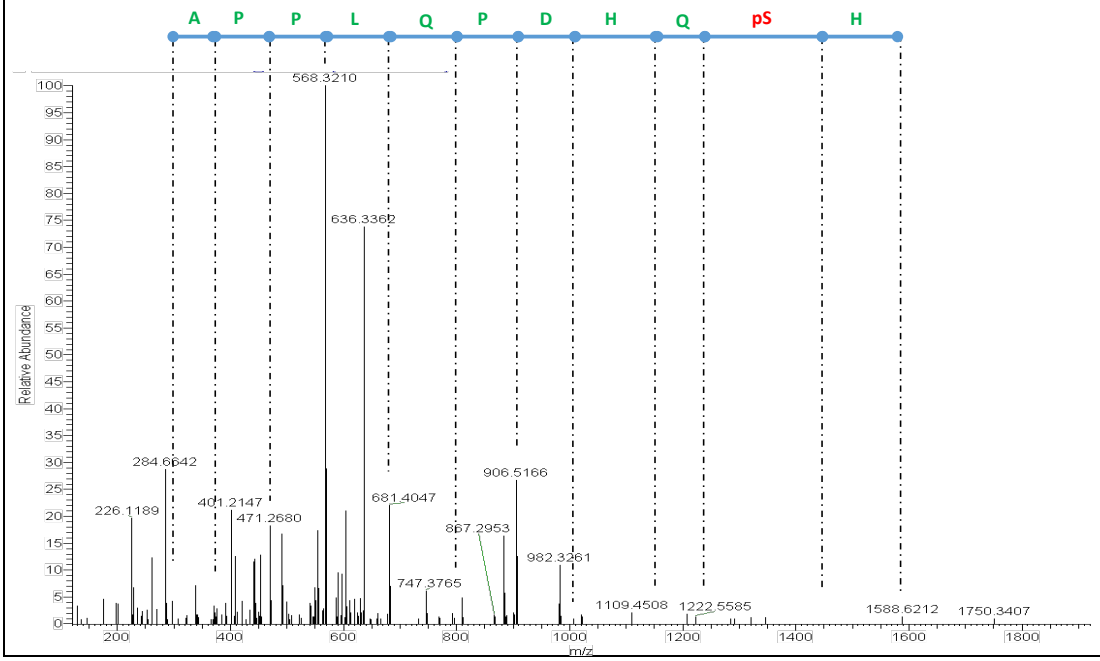

c)

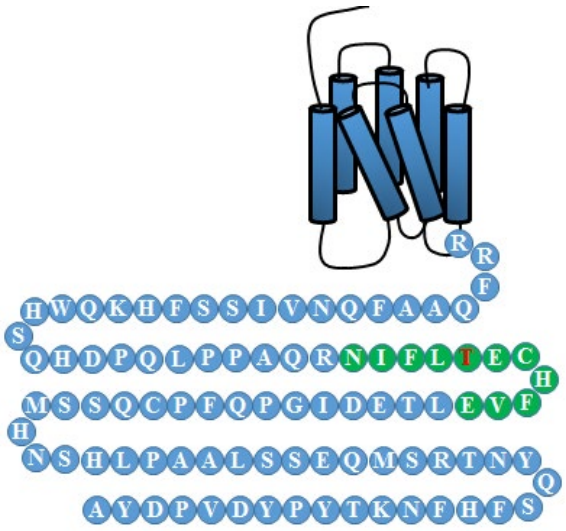

| AA sequence | Y ions |
|---|---|
| E | 148.1 |
| V | 247.1 |
| F | 394.2 |
| H | 531.3 |
| C | 691.3 |
| E | 820.3 |
| pT | 1001.3 |
| L | 1114.4 |

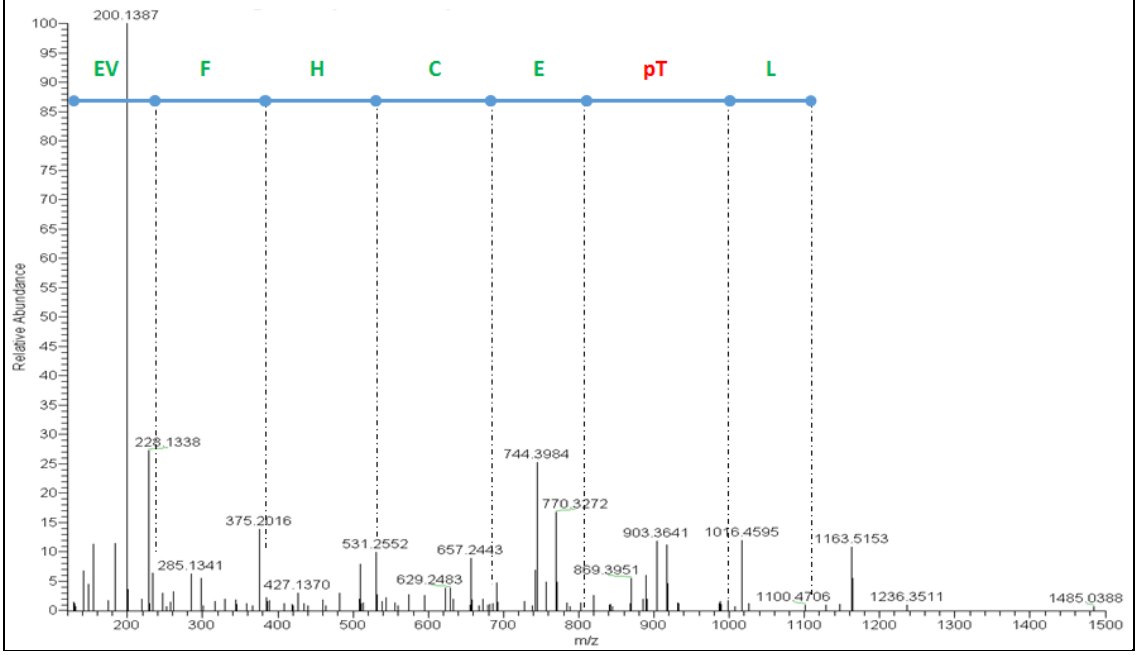

**d)**

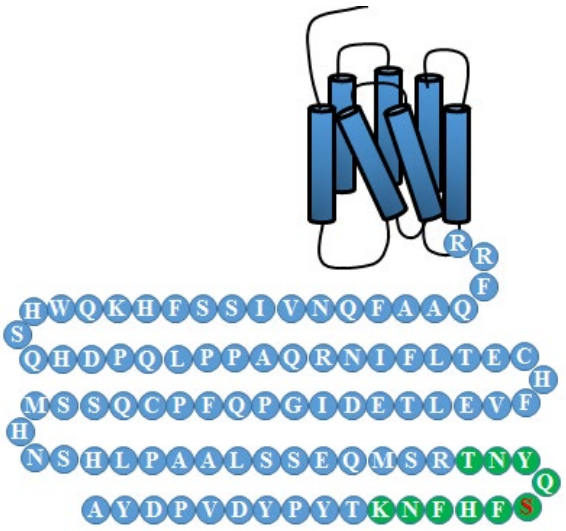


| AA sequence | Y ions |
|---|---|
| K | 147.1 |
| N | 261.2 |
| F | 408.2 |
| H | 545.3 |
| F | 692.4 |
| pS | 859.3 |
| Q | 987.4 |
| Y | 1150.5 |
| N | 1264.5 |
| T | 1365.6 |

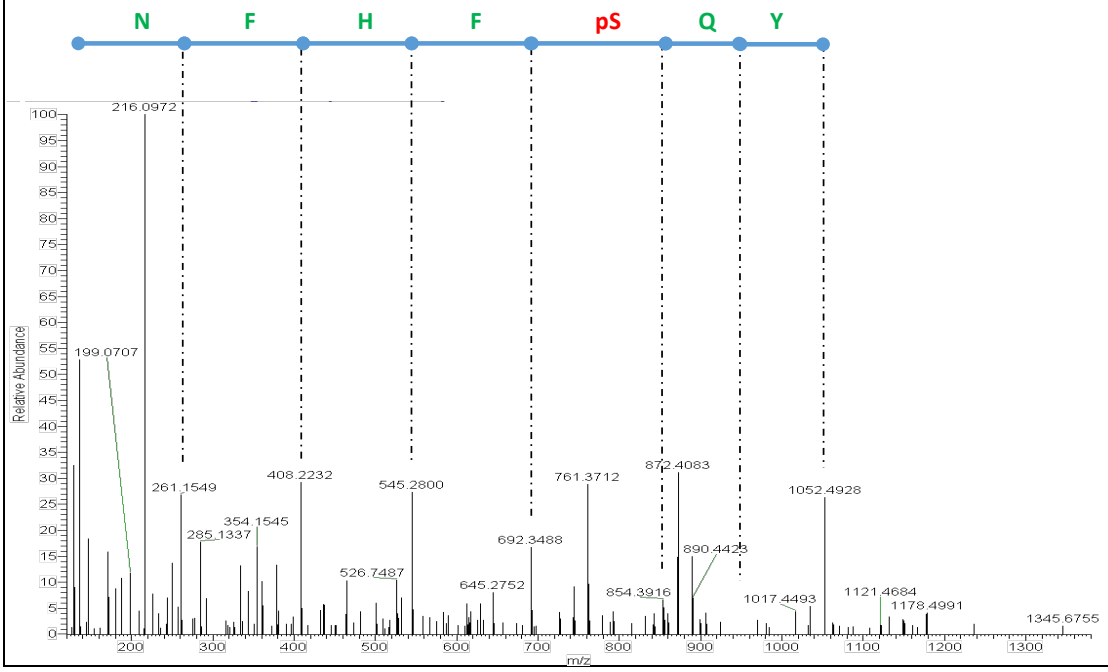

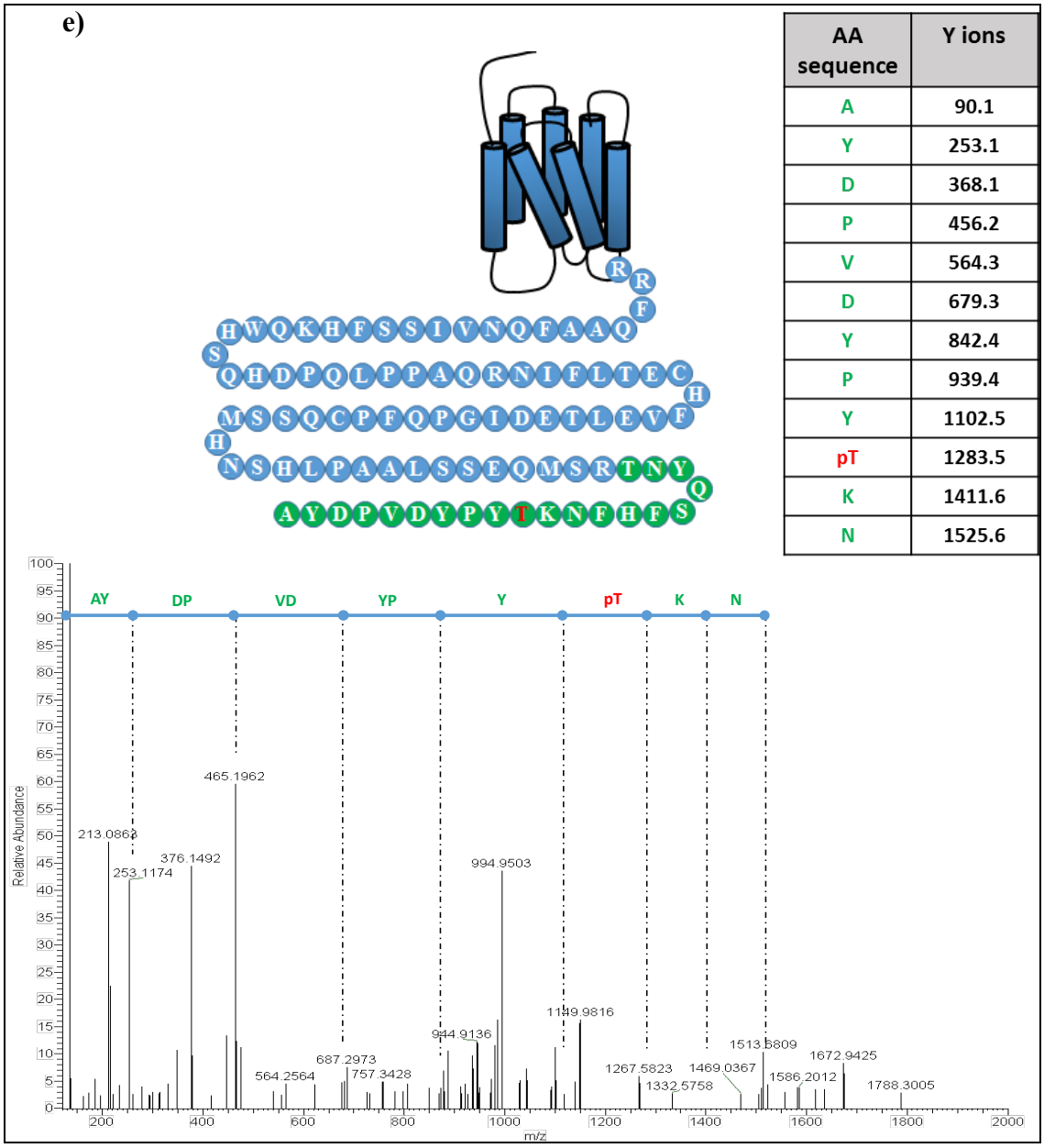


**Figure 6.2. Mass spectrometric analysis showing the detected sites of phosphorylation within NMU2-HA**

Immunoprecipitated NMU2-HA receptors were resolved by polyacrylamide gel electrophoresis and stained with coomassie blue. The area of the gel was then cut into small cubes and the samples submitted to the Protein and Nucleic Acid Chemistry Laboratory (PNACL) for LC-MS/MS analysis. Figures a - e show the sequence based on mass (m/z), allowing identification of phosphorylated residues. Also shown are the locations of the peptides detected by mass spectrometry (indicated by green circles) and phosphorylated sites within each peptide fragment (highlighted in red). The tables (right panels) represent the amino acid (AA) sequences of the peptide fragments detected via

mass spectrometry and indicate their expected molecular mass. Phosphorylated residues are identified in red as either pS or pT (phospho-serine or phospho-threonine).

**a) NMU2-HA sequence showing coverage by mass spectrometry and identified phosphorylation sites**

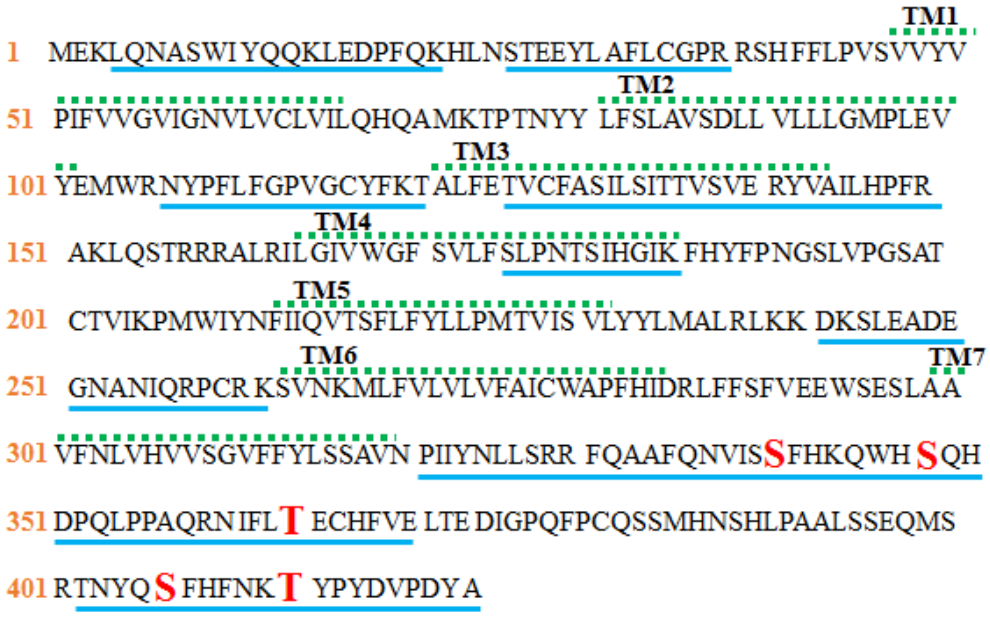


**b)**

| | | | Basal | | | hNmU-25 | | | hNmS-33 | | |
|---|---|---|---|---|---|---|---|---|---|---|---|
| **Peptide sequence** | **Residue numbers** | **Mascot ion score** | **N.P** | **N.P.P** | **PKC** | **N.P** | **N.P.P** | **PKC** | **N.P** | **N.P.P** | **PKC** |
| RFQAAFQNVISSFHKQ | (330-345) | 51.8 | 58 | 8 | | 10 | 4 | | 12 | 5 | |
| KQWHSQHDPQLPPAQRN | (344-360) | 25.3 | 148 | 12 | | 23 | 4 | | 22 | 4 | |
| RNIFLTECHFVEL | (359-371) | 22.7 | 1 | 1 | | - | - | | 1 | - | |
| RTNYQSFHFNKT | (401-412) | 44.6 | 53 | 10 | | 8 | 3 | | 8 | 2 | |
| RTNYQSFHFNKTYPYDVPDYA | (401-421) | 19.8 | 4 | 1 | | - | - | | | - | |

**Predicted by NetPhos**

**Figure 6.3. Summary of NMU2 mass spectrometry coverage, detected phosphorylation sites and potential second-messenger-dependent kinase phosphorylation sites**

The scheme (a) shows the five phosphorylation sites identified under basal (non-stimulated conditions) or following challenge with either hNmU-25 or hNmS-33. The peptide fragments covered by mass spectrometry are indicated by solid underlines (blue) and the detected phosphorylation sites highlighted in red. The dotted lines (green) represent the predicted positions of the seven transmembrane (TM) domains of NMU2. The table (b) shows each peptide in which a phosphorylated serine or threonine sites was observed. The table shows the total number of times the peptide fragment was detected and the number of times a phosphorylated residue was observed within the peptide. Two residues detected as phosphorylated (S406 and T412) were identified as potential PKC phosphorylation sites using NetPhos software (highlighted in grey) (b). PKA sites were identified by NetPhos software. The mass spectrometry experiments were performed twice for each of the hNmU-25- and hNmS-33-stimulated groups and three times for the vehicle-treated group. Abbreviation: total number of observations the peptide fragment was detected (N.P), total number of observations the phosphorylated residue within the peptide (N.P.P).

## 6.3 Generation of HEK293 cells with stable expression of NMU2-HA mutants (NMU2-HA-M1, -M2, -M3)

### 6.3.1 Strategy for designing NMU2-HA mutants

After identifying the five phosphorylation sites by mass spectrometry, strategies were adopted to generate NMU2-HA mutants with potential serine and threonine phosphorylation sites mutated to alanine to further characterise receptor phosphorylation and ultimately to assess the relationship of receptor phosphorylation to function. Strategies were designed to generate three NMU2-HA mutants; one (NMU2-HA-M1) was designed to mutate to alanine the five phosphorylation sites that had been identified by mass spectrometric analysis **(Figure 6.4; a)**. The second mutant (NMU2-HA-M2) was designed to replace with alanine all the potential *C*-terminal phosphorylation sites that were not covered by mass spectrometry **(Figure 6.4; b)**. Finally, NMU2-HA-M3 was designed to substitute all fourteen serine and threonine residues of the *C*-terminus with alanine including the five phosphorylation sites detected by mass spectrometry, seven potential phosphorylation sites that were not covered by mass spectrometry and two sites that, although covered by mass spectrometry had no evidence of phosphorylation **(Figure 6.4; c)**. **Figure 6.5** summarises the three NMU2-HA mutants. The strategy was to generate each NMU2-HA mutant from two fragments; one from the existing pcDNA 3.1+ plasmid containing the NMU2-HA sequence from the start codon to an AfeI restriction site in the middle of NMU2-HA **(Figure 6.6; a)**. The second fragment for each construct contained the mutated sites as indicated **(Figure 6.5)** and was synthesized by Eurofins (Wolverhampton, UK). This fragment started from an AfeI restriction site and ended in an XbaI restriction site in the end of the receptor **(Figure 6.6; a)**. Initially a ligation method was used in an attempt to sub-clone the second fragment into the pcDNA 3.1+ plasmid containing the first, to generate the full sequences of the NMU2-HA mutants. Unfortunately, this was not successful and a ligation-independent cloning method was performed by PROTEX Services (University of Leicester). Briefly, the first fragments of the constructs **(Figure 6.6; a)** (1-421 bp in length) were generated by PCR from an existing pcDNA 3.1+ plasmid containing the NMU2-HA sequence. The forward primer for this reaction contained a homologous sequence to the pLEICS-12 vector (PROTEX Services; University of Leicester) at the 5' prime ends and the reverse primers contained the AfeI restriction site present within the NMU2 sequence at the 3' prime ends as indicated in **Figure 6.7; a (Figure 6.6; b)**. The second fragments containing the mutated

sites were generated by PCR amplification. The forward primers contained the 15 bases from the end of the first fragments, before the AfeI restriction sites, followed by AfeI restriction sites and 15 bases of the NMU2 sequence at the 5' prime ends. The reverse primers contained a homologous sequence to the pLEICS-12 vector followed by a restriction site for NotI, a stop codon and the HA tag sequence at the 3' prime ends as indicated in **Figure 6.7; b**. Three pEX-A128 vectors (Eurofins, Wolverhampton, UK) each containing a mutant sequence were used as the template to generate the three constructs of the second fragments **(Figure 6.6; b)**. After generating the two fragments for each mutant, they were then used as templates for the forward primer of the first fragment and reverse primer of the second fragment to join the two fragments together using PCR amplification **(Figure 6.6; b)**.

After joining the two fragments, the resulting fragment was sub-cloned into the pLEICS-12 vector using ligation-independent cloning **(Figure 6.6; c)**. The three resulting constructs each contained an NMU2-HA mutant with restriction sites for NheI and NotI at the *C*- and *N*-termini of NMU2-HA respectively **(Figure 6.6; c)**. The NMU2-HA mutants were validated by DNA sequencing (PNACL; University of Leicester) (data not shown).

**a) Mutant NMU2-HA-M1**

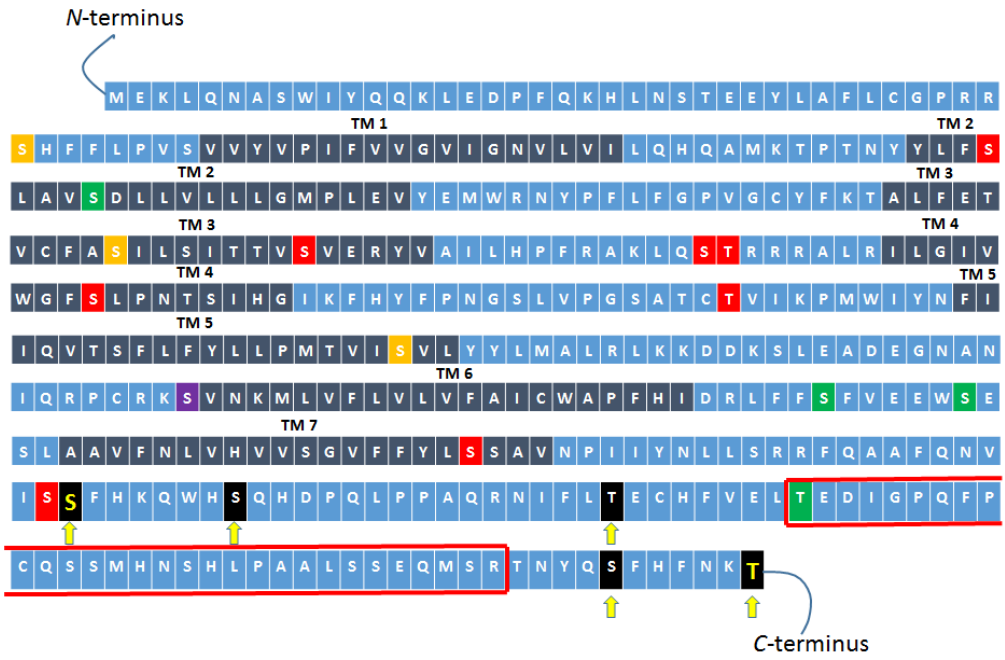


**b) Mutant NMU2-HA-M2**

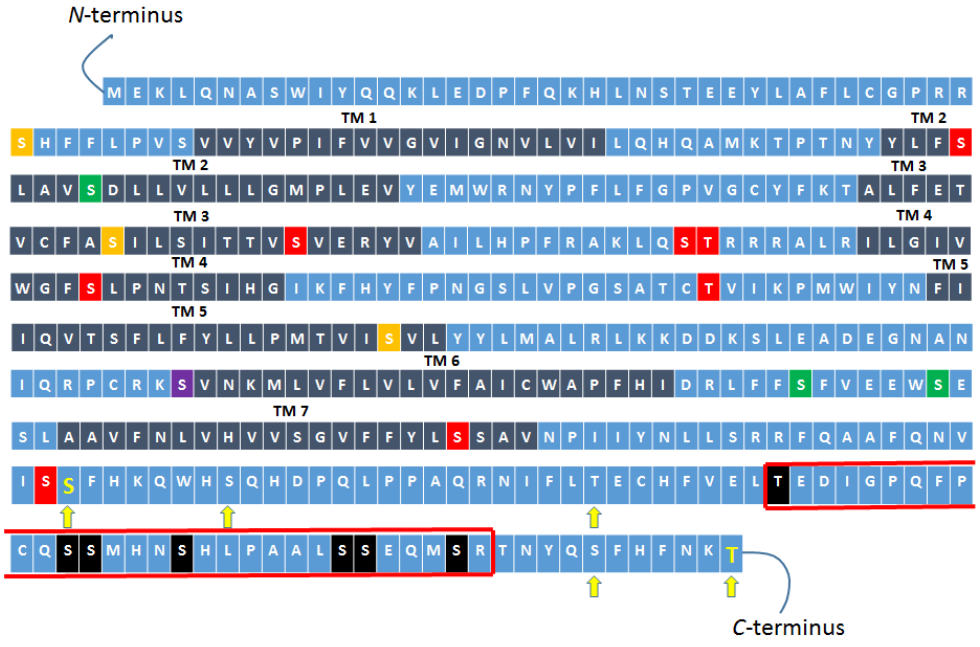

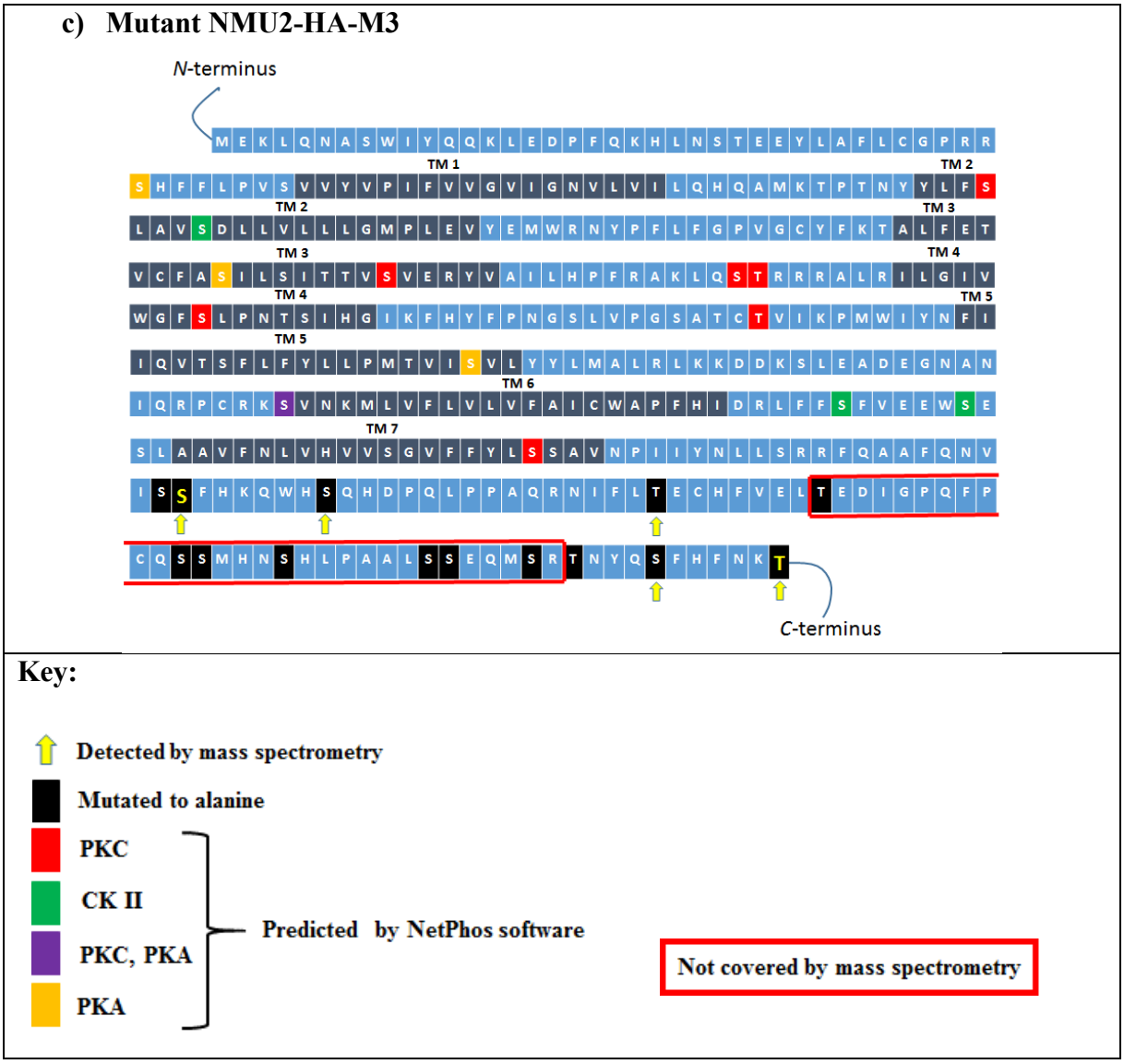


**Figure 6.4. Detected and potential phosphorylation sites within NMU2**

(a) NMU2-HA-M1 showing the five phosphorylation sites identified by mass spectrometry (yellow arrows) that were mutated to alanine (black boxes). (b) NMU2-HA-M2 scheme showing the seven potential S and T phosphorylation sites not covered by mass spectrometry that were mutated to alanine (black boxes). (c) NMU2-HA-M3 in which fourteen phosphorylation or potential phosphorylation sites including those detected and not detected by mass spectrometry were mutated to alanine (black boxes). Potential phosphorylation sites of PKC, PKA and CK II were identified using NetPhos software (highlighted by appropriate coloured boxes). Two of five phosphorylation sites identified by mass spectrometry were matched to the NetPhos results and predicted as substrates for PKC phosphorylation (yellow letters). The HA tag sequence is not shown in any of the constructs.

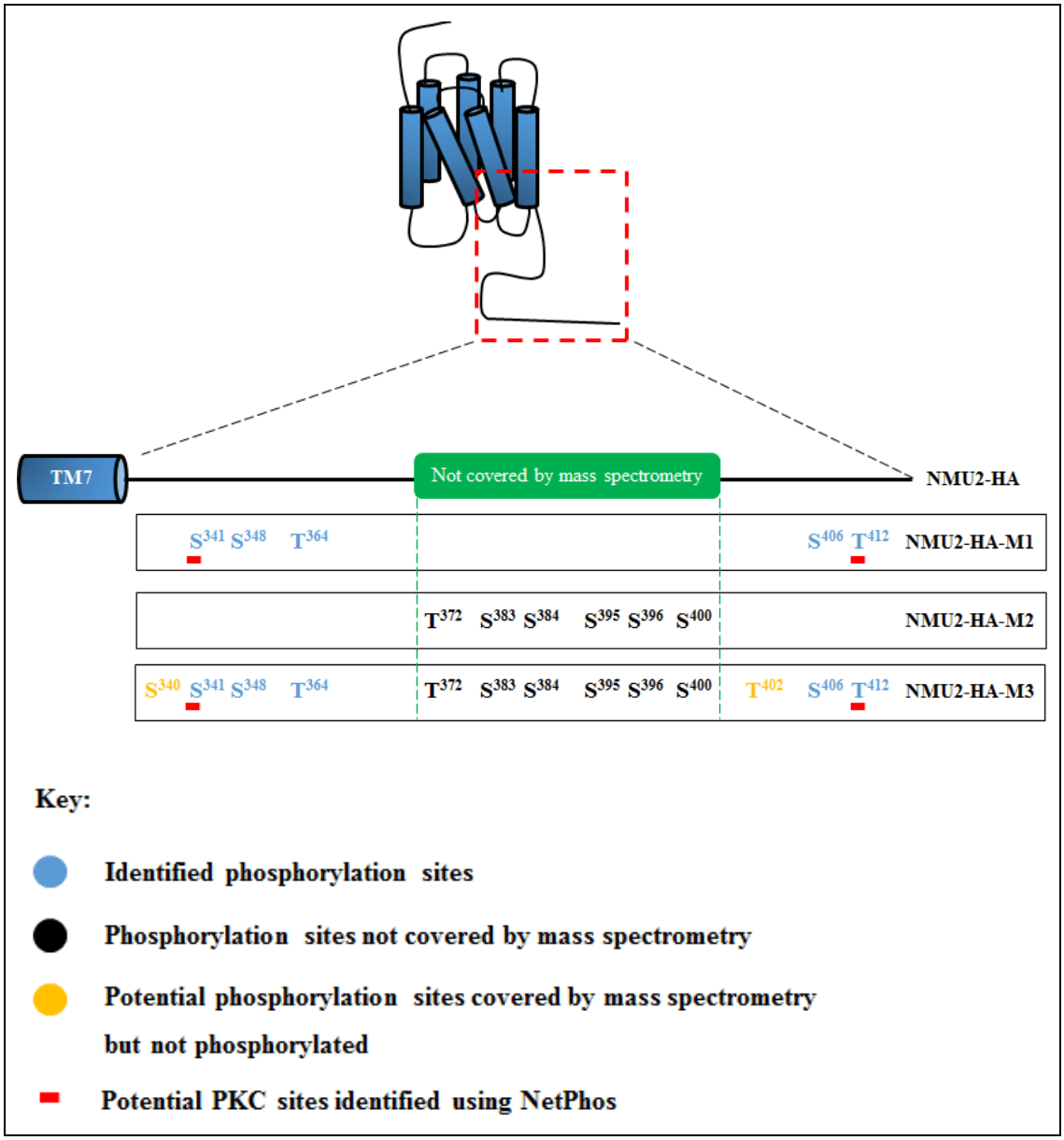


**Figure 6.5. Summary of the NMU2-HA mutants**

Scheme showing the designs of the three NMU2-HA mutants. NMU2-HA-M1 was designed to mutate to alanine the five phosphorylation sites that were identified by mass spectrometry (blue arrows). The NMU2-HA-M2 mutant was designed to mutate to alanine the potential phosphorylation sites that were not covered by mass spectrometry (black arrows). All the identified phosphorylation sites (blue), potential sites not covered by mass spectrometry (black) and sites that were covered by mass spectrometry but not phosphorylated (yellow) were mutated to alanine in the NMU2-HA-M3 mutant **(for more details see Figure 6.4)**. This included two phosphorylation sites predicted as PKC targets using NetPhos software (underlined in red).

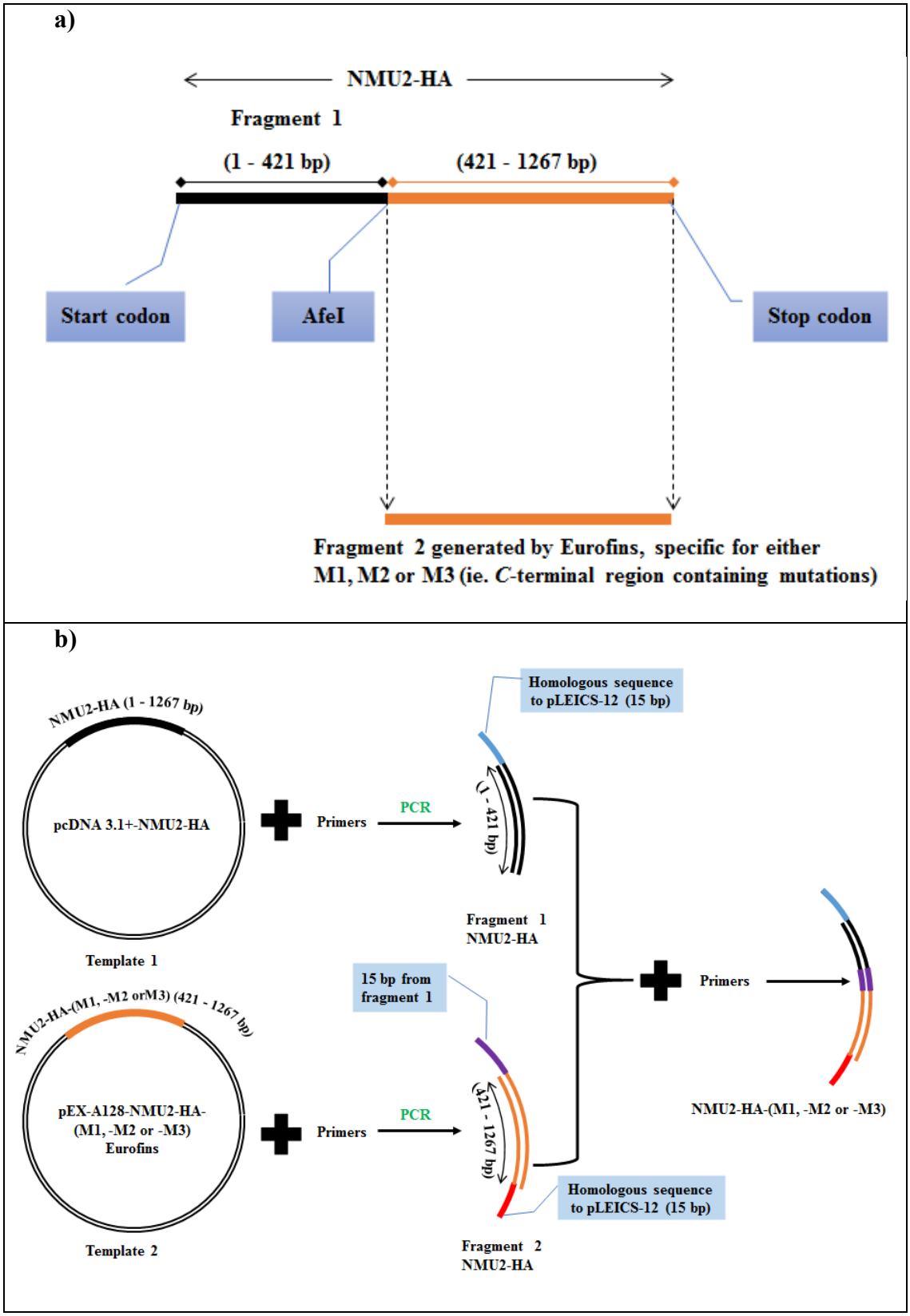
a)
NMU2-HA
Fragment 1
(1 - 421 bp)
(421 - 1267 bp)
Start codon
AfeI
Stop codon
Fragment 2 generated by Eurofins, specific for either M1, M2 or M3 (ie. C-terminal region containing mutations)
b)
NMU2-HA (1 - 1267 bp)
pcDNA 3.1+-NMU2-HA
Template 1
Primers
PCR
Homologous sequence to pLEICS-12 (15 bp)
(1 - 421 bp)
Fragment 1 NMU2-HA
NMU2-HA-(M1, -M2 orM3) (421 - 1267 bp)
pEX-A128-NMU2-HA-(M1, -M2 or -M3) Eurofins
Template 2
Primers
PCR
15 bp from fragment 1
(421 - 1267 bp)
Homologous sequence to pLEICS-12 (15 bp)
Fragment 2 NMU2-HA
Primers
NMU2-HA-(M1, -M2 or -M3)

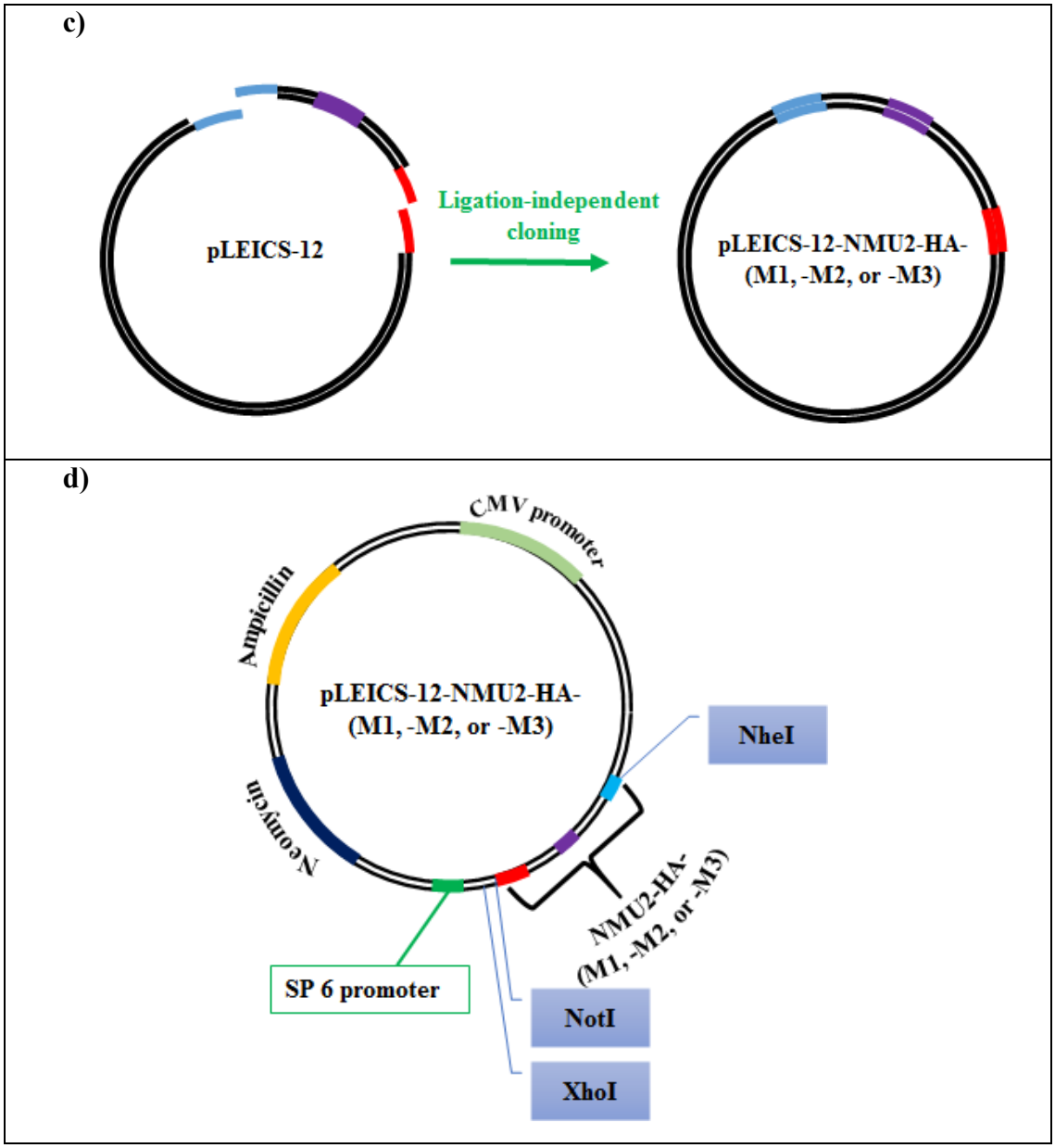


**Figure 6.6. Schematic representation of the strategy for generation of NMU2-HA-M1, NMU2-HA-M2 and NMU2-HA-M3 constructs**

The diagram represents the strategy for generation of NMU2-HA mutants highlighted in **Figure 6.5**. (a) The first fragment was from the start codon of NMU2-HA to the restriction site for AfeI (1 - 421 bp). The second fragment was synthesized by Eurofins and represents the section from the AfeI restriction site to the stop codon (421 - 1267 bp) and included the mutants that contained serine/threonine sites mutated to alanine. (b) The overall strategy for the generation of NMU2-HA-M1, -M2, and -M3 indicating PCR amplification of the fragments to generate NMU2-HA mutants using two homologous sequences from pLEICS-12 (blue, red). Two vectors were used as templates to generate the fragments; one was NMU2-HA in pcDNA 3.1+ (in-house) and three vectors, each

containing one of the three mutants (NMU2-HA-M1, -M2, or -M3) in pEX-A128 that were made by Eurofins. Fifteen bases were inserted from the end of the first fragment to connect the two fragments (purple). The two fragments were then joined together by PCR amplification using the forward primer of fragment 1, the reverse primer of fragment 2 with fragment 1 and 2 as templates. (c) Using ligation-independent cloning, the resulting fragment from (b) was cloned into pLEICS-12. (d) The resulting plasmids indicating important regions including the locations of genes providing resistance to ampicillin and neomycin.

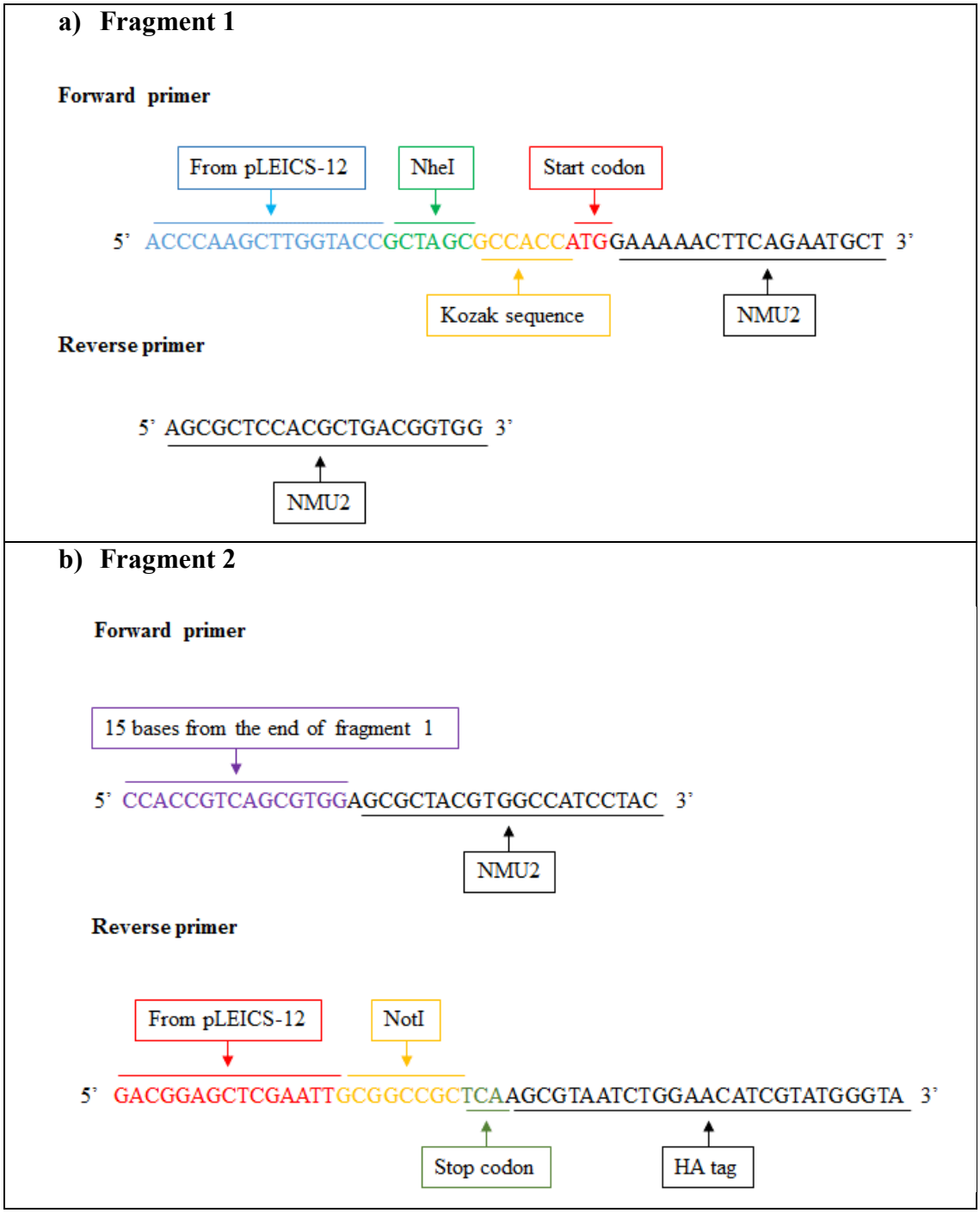


**Figure 6.7. Primer design for generation of NMU2-HA mutants**

Two fragments were used to generate each NMU2-HA mutant using ligation-independent cloning method (PROTEX Services, University of Leicester). (a) The forward and reverse primers were used to generate fragment 1 for each mutant, which begins from a start codon to an AfeI restriction site in the middle of the NMU2 sequence (1 - 421bp) using NMU2-HA in pcDNA 3.1+ as a template. The forward primer contained a homologous sequence from the pLEICS-12 vector (PROTEX Services) (blue) at the *N*-terminal of NMU2-HA, a restriction site for NheI (green), a Kozak sequence (orange), a

start codon (red) and 18 bases of the NMU2 sequence representing the *N*-terminal of the protein. The reverse primer contained 21 bases of NMU2-HA starting from the AfeI restriction site **(see Figure 6.6, a)**. (b) The second fragment was generated for each mutant using two primers and three vectors each containing NMU2-HA-M1, -M2, or -M3 in pEX-A128 vector that were synthesized by Eurofins. The forward primer was designed to include 15 bases from the end of fragment 1 (purple) and 21 bases of the NMU2 sequence (black) starting from the AfeI restriction site. The reverse primer contained a homologous sequence from pLEICS-12 (PROTEX Services) (red) at the *C*-terminal of NMU2-HA, a restriction site for NotI (orange), a stop codon (green) and the HA tag sequence.

### 6.3.2 Transient expression in HEK-293 cells of NMU2-HA-M1, NMU2-HA-M2 or NMU2-HA-M3

To assess the phosphorylation status of NMU2-HA mutants in response to either hNmU-25 or hNmS-33 following generation of the three mutants, transient transfection was performed to: 1) examine the efficiency of receptor expression and; 2) later study receptor phosphorylation. HEK-293 were transfected with NMU2-HA-M1, -M2 or -M3 and left for 48 h. Cells were then immediately solubilised and immunoblotting performed with an anti-HA antibody. Immunoblotting of cell lysates with an anti-HA antibody from cells with transient expression of NMU2-HA mutants resulted in multiple bands **(Figure 6.8)**. In contrast, the stable NMU2-HA cell line (control) demonstrated only one band at ~ 80 kDa whilst untransfected cells had no visible bands **(Figure 6.8)**. These results were similar to earlier results with the transient expression of NMU2-HA which also resulted in multiple bands and did not show phosphorylation following stimulation with either hnmU-25 or hNmS-33 **(see Figure 3.3 and Figure 4.1)**. Taken together, these data indicated that it was important to generate HEK-293 with stable expression of NMU2-HA-1, NMU2-HA-M2 or NMU2-HA-M3.

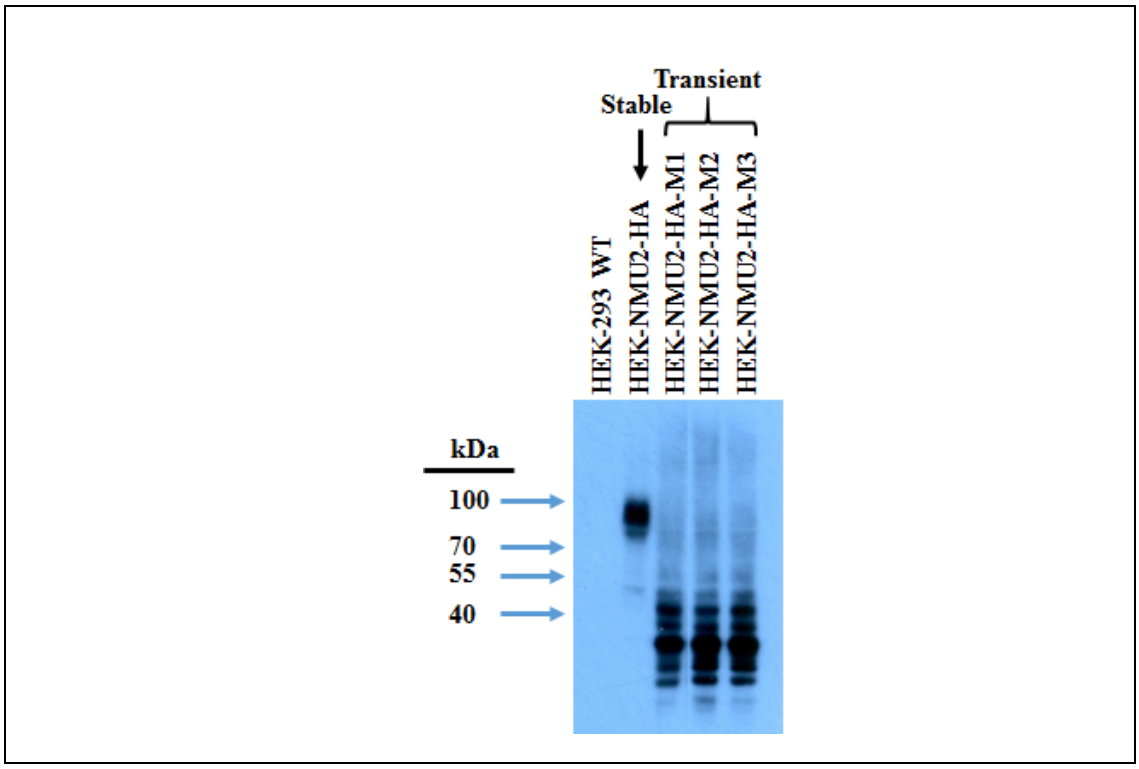


**Figure 6.8. Transient expression of NMU2-HA mutants**

HEK-293 cells transiently transfected with NMU2-HA mutants were washed twice with PBS buffer and then solubilised. The samples were resolved by gel electrophoresis and

immunoblotted with anti-HA tag antibody **(see Methods)**. HEK-293 and HEK-NMU2-HA were used as negative and positive controls respectively. Data are representative immunoblots of three independent experiments.

### 6.3.3 Stable expression of NM-HA-M1, NMU2-HA-M2 or NMU2-M3

Generation of HEK-293 cells with stable expression of NMU2-HA-M1, NMU2-HA-M2 or NMU2-HA-M3 was performed by transfecting HEK-293 with NMU2-HA-M1, -M2 or -M3 and left for 48 h. Cells were then treated with Geneticin (G418). The cells surviving in the presence of Geneticin were sub-cultured following high dilutions to obtain single cells. These were then grown into single colonies that were selected from 10 ml dishes and expanded into 24-well plates. The cells were then screened by immunoblotting with an anti-HA antibody. In some of the clones that grew under Geneticin treatment, there was no immunoreactivity detected using an anti-HA antibody. This included NMU2-HA-M1 colonies 52, 56, 57, 58 and 59 **(Figure 6.9; a)**, NMU2-HA-M2 colonies 25, 26, 27and 28 **(Figure 6.9; b)** and NMU2-HA-M3 colonies 18, 20and 32 **(Figure 6.9; c)**. Other colonies showed weak immunoreactivity but few colonies, such as NMU2-HA-M1 colonies 53, 55 and 60, NMU2-HA-M2 colonies 19, 21, 22 and 24 and NMU2-HA-M3 colonies 6, 7 and 16, resulted in strong immunoreactivity with an anti-HA antibody **(Figure 6.9; b)**. From each mutant cell line, one colony that showed immunoreactivity similar to the NMU2-HA cell line was selected for further examination. These were NMU2-HA-M1 colony 53, NMU2-HA-M2 colony 21 and NMU2-HA-M3 colony 7 **(Figure 6.9)**. After expanding the selected colonies, immunoblotting was again performed. The results of these were consistent with the initial blotting of the selected and expanded colonies (**Figure 6.10)**.

Immunoprecipitation of the NMU2-HA mutants followed by immunoblotting was also performed in order to ensure that immunoprecipitation was sufficient to allow the phosphorylation experiments to be performed. Immunoblotting of NMU2-HA mutants that had been immunoprecipitated with anti-HA conjugated beads resulted in two intense bands located at ~ 47 kDa and ~ 80 kDa which were similar to the immunoblotting of the NMU2-HA and mutants without immunoprecipitation **(Figure 6.11)**. These results also showed that the NMU2-HA mutants did not influence the efficiency of the immunoprecipitation compared to the NMU2-HA (control) **(Figure 6.11)**.

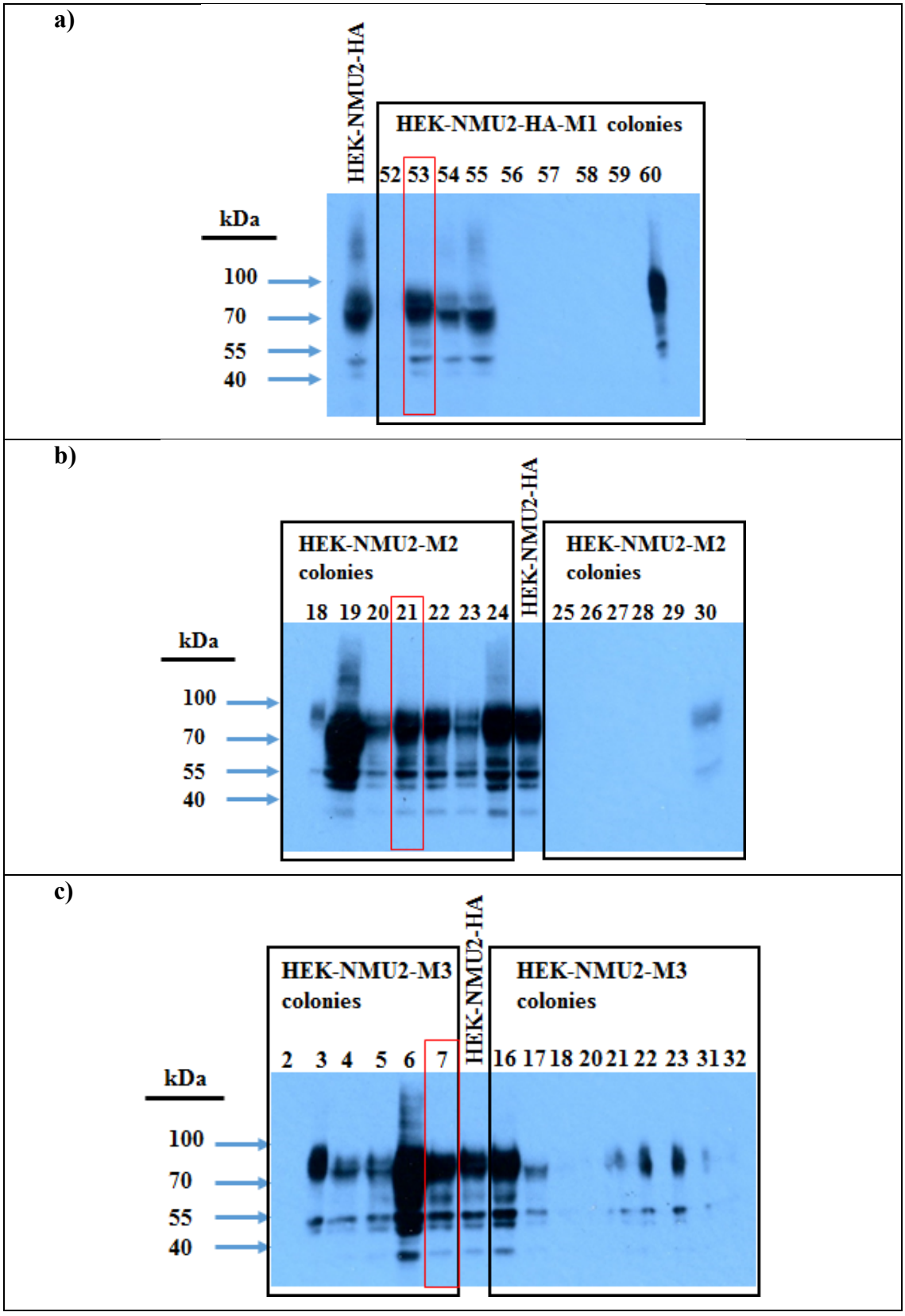


**Figure 6.9. Immunoblotting of colonies of HEK-NMU2-HA mutants**

HEK-293 cells were transfected with NMU2-HA-M1, -M2, or -M3. Stable cell lines were then generated by treating with Geneticin. After three weeks of treatment, the surviving

cells were sub-cultured in high dilutions to obtain single cells. Cells were then allowed to expand to single colonies. Each colony was selected and sub-cultured in 24-well plates for 24 h. Cells were then washed twice with PBS and solubilised. The samples were resolved by gel electrophoresis and immunoblotted with an anti-HA antibody **(see Methods)**. The representative immunoblots (a, b, c) are examples of blots from a large number of selected colonies. For each mutant, the colony identified by a red box (NMU2-HA-M1; colony 53, NMU2-HA-M2; colony 21 or NMU2-HA-M3; colony 7) was selected for further examination and characterisation.

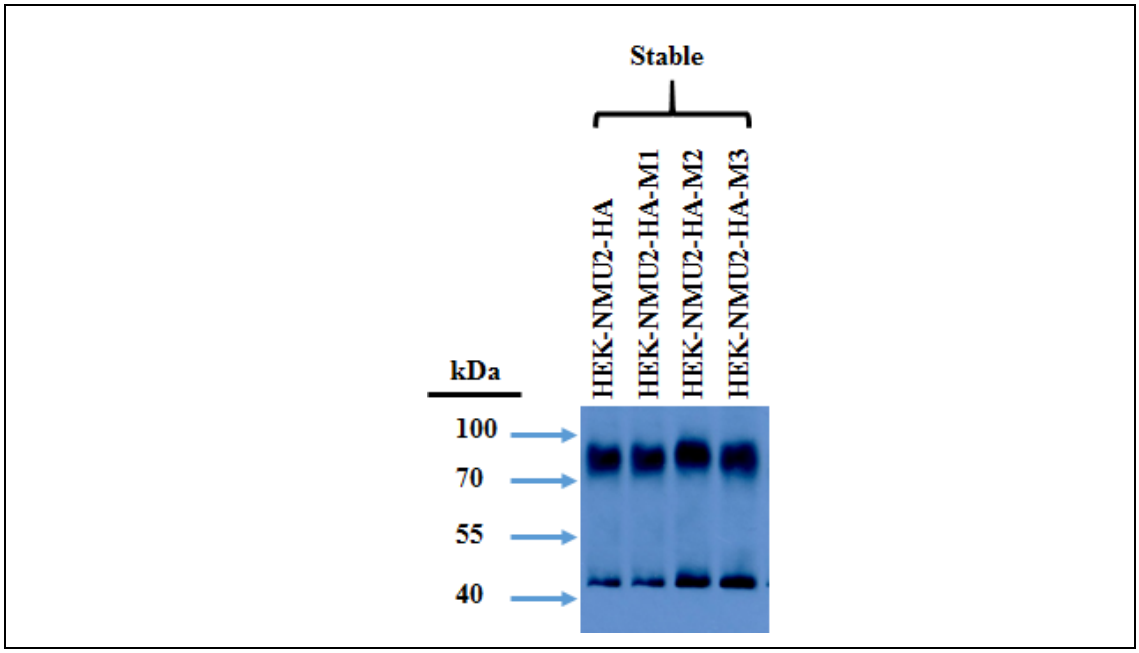


**Figure 6.10. Stable expression of NMU2-HA versus that of the selected NMU2-HA mutants**

After selection of the NMU2-HA mutant colonies, each cell line was grown to ~ 95 % confluence in 24-well plates. Cells were then washed with PBS and solubilised. The samples from each NMU2-HA mutant and NMU2-HA (positive control) cell lines were resolved by gel electrophoresis and immunoblotted with anti-HA antibody **(see Methods)**. Data are representative immunoblots of two independent experiments.

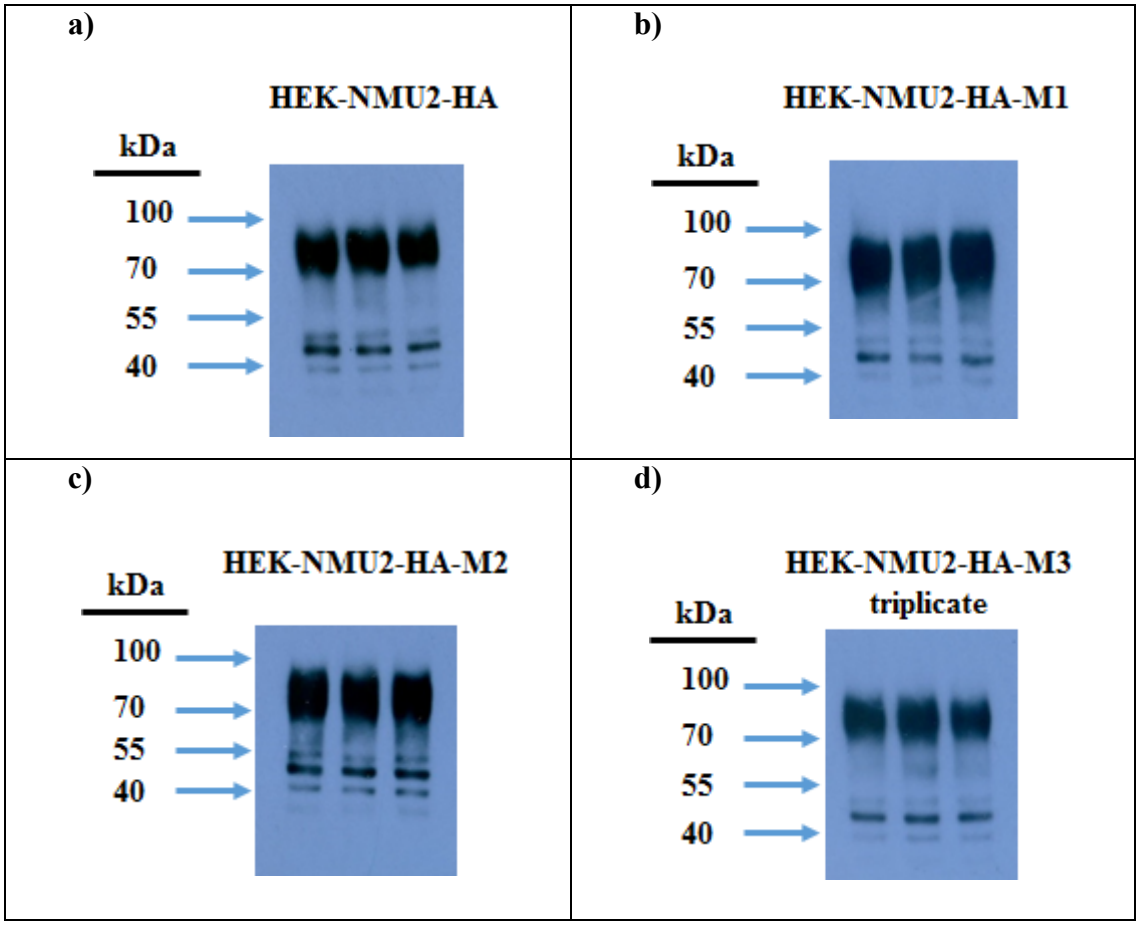


**Figure 6.11. Immunoblotting of immunoprecipitated NMU2-HA-M1, NMU2-HA-M2 or NMU2-HA-M3 with anti-HA antibody**

Cells with stable expression of NMU2-HA (a), NMU2-HA-M1 (b), NMU2-HA-M2 (c) or NMU2-HA-M3 (d) were grown in 6-well plates for 24 h. Cells were then washed twice with PBS and solubilised. NMU2-HA or NMU2-HA mutants were immunoprecipitated using anti-HA conjugated beads, resolved by gel electrophoresis and then immunoblotted with anti-HA antibody **(see Methods)**. Data are representative immunoblots of two independent similar experiments with similar results.

## 6.4 Phosphorylation of NMU2-HA mutants

### 6.4.1 hNmU-25- and hNmS-33-mediated phosphorylation of NMU2-HA mutants

After generating cell lines with stable expression of NMU2-HA-M1, NMU2-HA-M2 or NMU2-HA-M3, NMU2-HA phosphorylation in response to hNmU-25 or hNmS-33 was explored. Exposing NMU2-HA or NMU2-HA-M1 (containing five phosphorylation sites of serine and threonine residues mutated to alanine that were detected by mass spectrometric analysis) to either hNmU-25 or hNmS-33 (1 μM) for 5 min caused equivalent levels of NMU2-HA phosphorylation between hNmU-25 and hNmS-33 in each cell line (3.6 ± 0.1, 3.5 ± 0.1 and 3.3 ± 0.1, 3.3 ± 0.05 fold over basal levels in HEK-NMU2-HA and HEK-NMU2-HA-M1 respectively) **(Figure 6.12; a, b)**. Furthermore, the levels of receptor phosphorylation in HEK-NMU2-HA in response to either hNmU-25 or hNmS-33 were slightly higher compared to those in HEK-NMU2-HA-M1. For example, the calculated means by densitometry for hNmU-25 versus hNmS-33 were 1093061 versus 1063998 and 931693 versus 922364 in HEK-NMU2-HA and HEK-NMU2-HA-M1 respectively. These experiments were performed alongside each other with equivalent loading of NMU2-HA on the gels. There were clear differences between NMU2-HA and both NMU2-HA-M2 (containing seven potential phosphorylation sites of serine and threonine residues mutated to alanine that were not covered by mass spectrometry) and NMU2-HA-M3 (containing fourteen phosphorylation sites of serine and threonine residues mutated to alanine including five phosphorylation sites determined by mass spectrometry, seven potential phosphorylation that were not covered by mass spectrometry and two sites that were covered by mass spectrometry but not phosphorylated). Challenge with either hNmU-25 or hNmS-33 provoked an increase in NMU2-HA-M2 phosphorylation, although ligand-mediated phosphorylation of NMU2-HA by either ligand was higher (3.6 ± 0.1 versus 3.5 ± 0.1 and 2.5 ± 0.2 versus 3.3 ± 0.1 for hNmU-25 versus hNmS-33 in HEK-NMU2-HA and HEK-NMU2-HA-M2 respectively). Only in the NMU2-HA-M2, the increased level of phosphorylation was significantly higher following 5 min challenge with hNmS-33 compared to hNmU-25 **(Figure 6.12; c)**. Challenge of HEK-NMU2-HA-M3 with either hNmU-25 or hNmS-33 did not increase the levels of phosphorylation compared to the basal levels **(Figure 6.12; d)**. Immunoblotting demonstrated equal loading of NMU2-HA and the mutants **(Figure 6.13)**. Furthermore, receptor phosphorylation did not affect the ability to immunoprecipitate NMU2-HA or the mutants **(Figure 6.12: IB; $a_{ii}$, $b_{ii}$, $c_{ii}$, $d_{ii}$,)**.

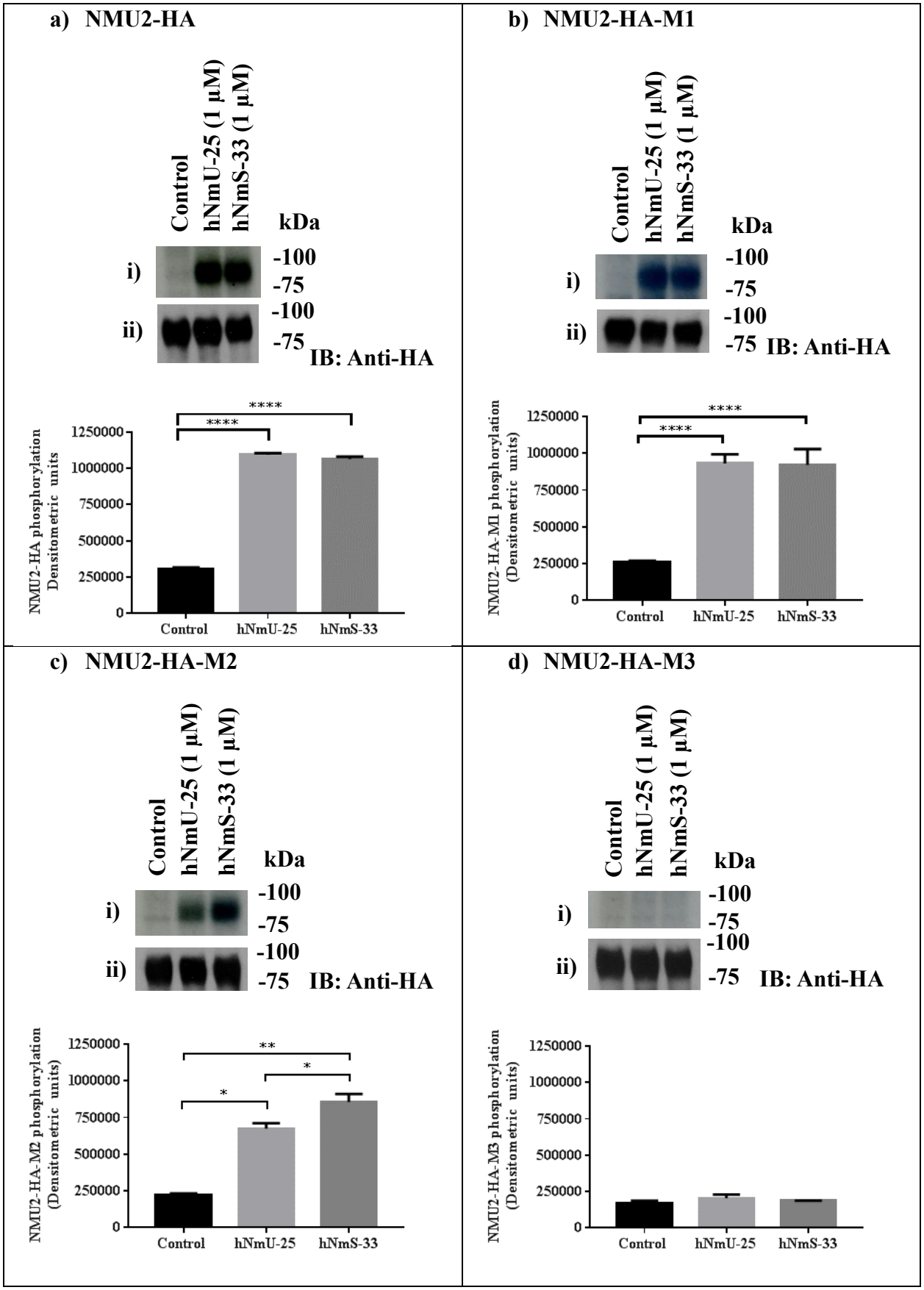


**Figure 6.12. Agonist-dependent phosphorylation of NMU2-HA mutants**

Cell were grown on poly-D-lysine coated 6-well plates for 24 h. Cells were washed twice with phosphate-free KHB and labelled with $^{32}P$ orthophosphate for 1 h. Cells were stimulated with hNmU-25 (1 μM), hNmS-33 (1 μM) or KHB (control) for 5 min. Following solubilisation of the cell monolayers, NMU2-HA or NMU2-HA mutants were immunoprecipitated and resolved by gel electrophoresis. The gel was then dried and visualised by autoradiography ($a_i$, $b_i$, $c_i$, $d_i$). Immunoblotting of the immunoprecipitate with an anti-HA antibody was used as a loading control for NMU2-HA and NMU2-HA mutants (IB; $a_{ii}$, $b_{ii}$, $c_{ii}$, $d_{ii,}$).The phosphorylation bands were quantified by densitometric analysis using Image J software (a, b, c, d). Data are either representative autoradiographs or blots of n = 3 or mean ± sem, n = 3. Statistical analysis was performed using a one way ANOVA followed by Bonferroni's test: $^{*}P < 0.05$, $^{**}P < 0.01$, $^{****}P < 0.0001$.

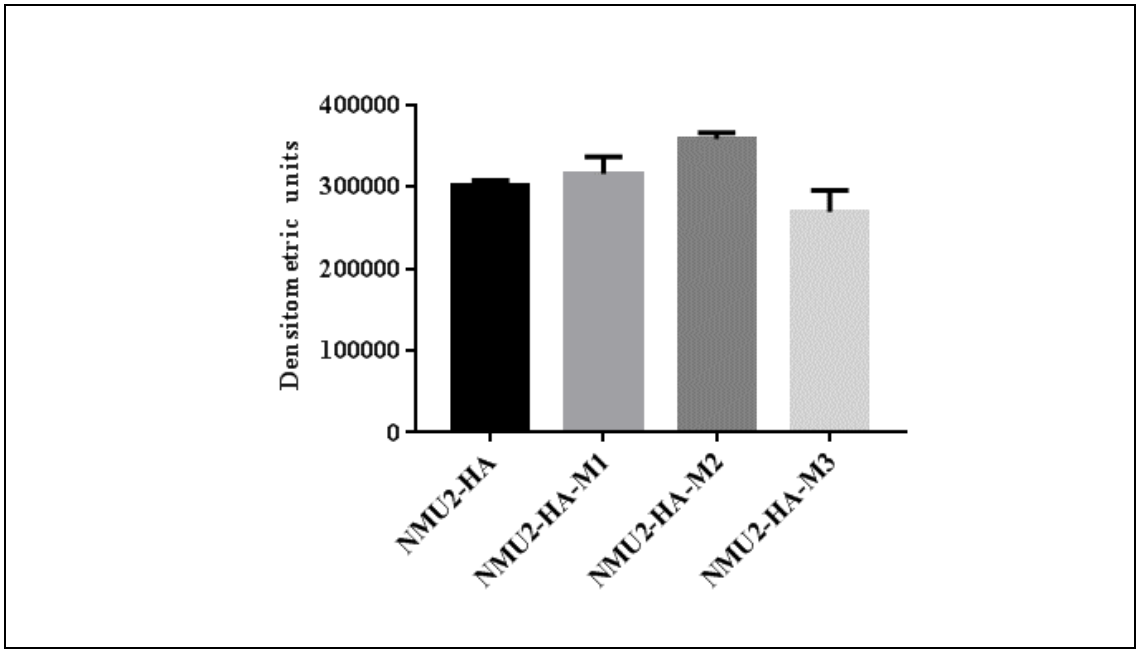


**Figure 6.13 Quantification of immunoblots of immunoprecipitated NMU2-HA and mutants as loading controls for the phosphorylation experiments**

NMU2-HA and the mutants were immunoprecipitated from equivalent volume aliquots of the samples from the receptor phosphorylation experiments. Samples were then resolved by the gel electrophoresis, transferred to the membranes and blotted with an anti-HA antibody **(see Methods)**. The immunoblots were quantified by densitometric analysis using Image J software. The data represent the mean of loading controls (mean ± sem, n = 3) **(see Figure 6.12: IB; $a_{ii}$, $b_{ii}$, $c_{ii}$, $d_{ii}$,)**.

### 6.4.2 Effect of PKC inhibition on the phosphorylation of wild-type and mutants of NMU2-HA in response to challenge with either hNmU-25 or hNmS-33

Challenge of HEK-NMU2-HA with either hNmU-25 or hNmS-33 for 5 min caused robust increases in the levels of phosphorylation which were similar in response to either ligand. However, these increases were significantly decreased when the cells were pre-incubated with the PKC inhibitor Ro 31-8220 (5 μM, 30 min) **(Figure 6.14; $a_i$)**. Stimulation of HEK-NMU2-HA-M1 with either hNmU-25 or hNmS-33 (1 μM) for 5 min caused marked increases in the levels of phosphorylation compared to the control group **(Figure 6.14; $b_i$)**. Pre-incubation of cells with Ro 31-8220 prior to challenging with either ligand did not influence the level of NMU2-HA-M1 phosphorylation **(Figure 6.14; $b_i$)**. Challenge of HEK-NMU2-HA-M2 with either hNmU-25 or hNmS-33 (1μM) for 5 min provoked marked increases in the levels of phosphorylation **(Figure 6.14; $c_i$)**. In contrast, following 5 min stimulation with either ligand in the presence of the PKC inhibitor, Ro 31-8220, phosphorylation of NMU2-HA-M2 was abolished **(Figure 6.14; $c_i$)**. Neither hNmU-25 nor hNmS-33 caused phosphorylation of NMU2-HA-M3 in either the presence or absence of Ro 31-8220 **(Figure 6.14; $d_i$)**.

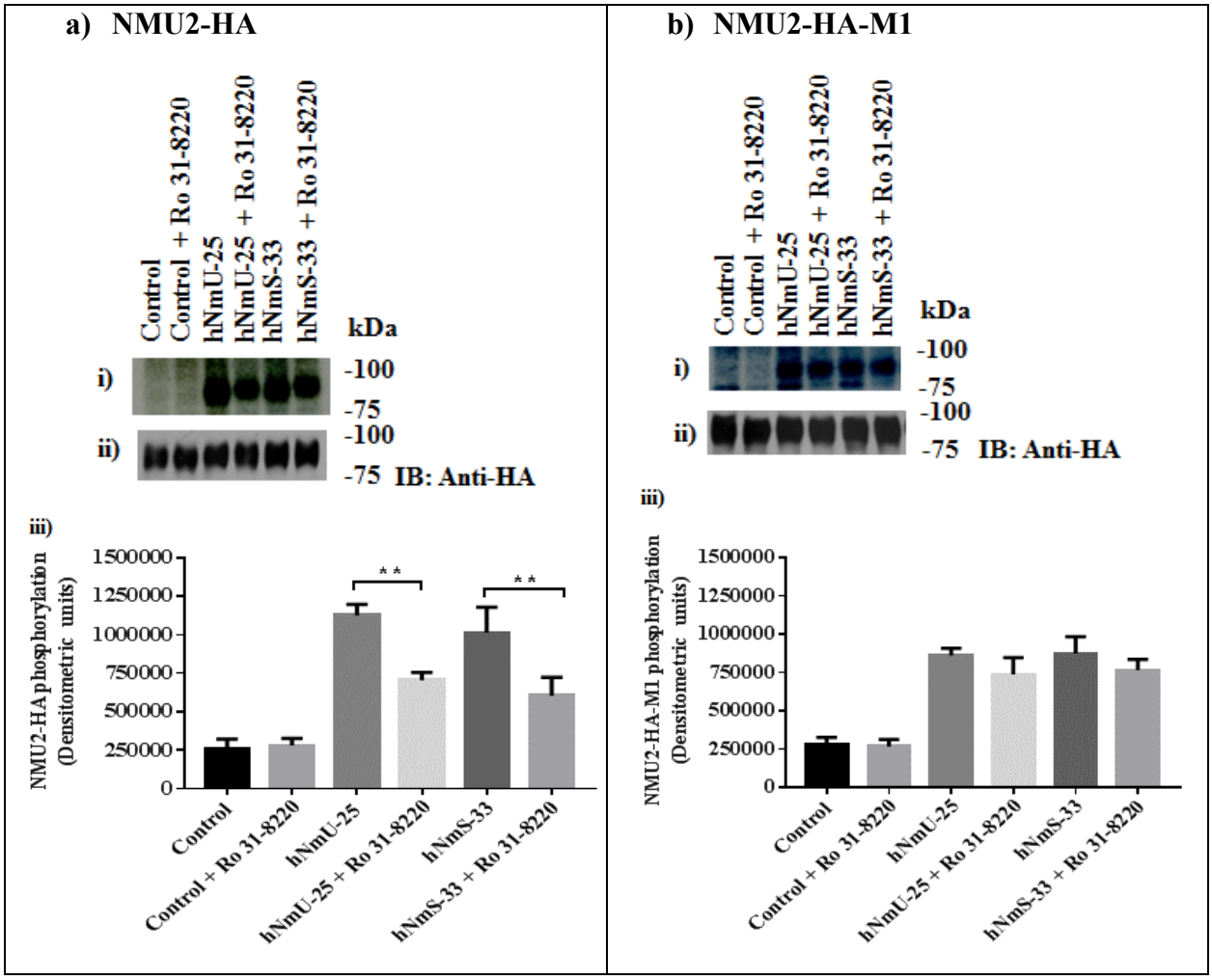
a) NMU2-HA
b) NMU2-HA-M1
Control
Control + Ro 31-8220
hNmU-25
hNmU-25 + Ro 31-8220
hNmS-33
hNmS-33 + Ro 31-8220
kDa
i)
ii)
-100
-75
IB: Anti-HA
iii)
NMU2-HA phosphorylation (Densitometric units)
NMU2-HA-M1 phosphorylation (Densitometric units)
1500000
1250000
1000000
750000
500000
250000
0
* *
* *

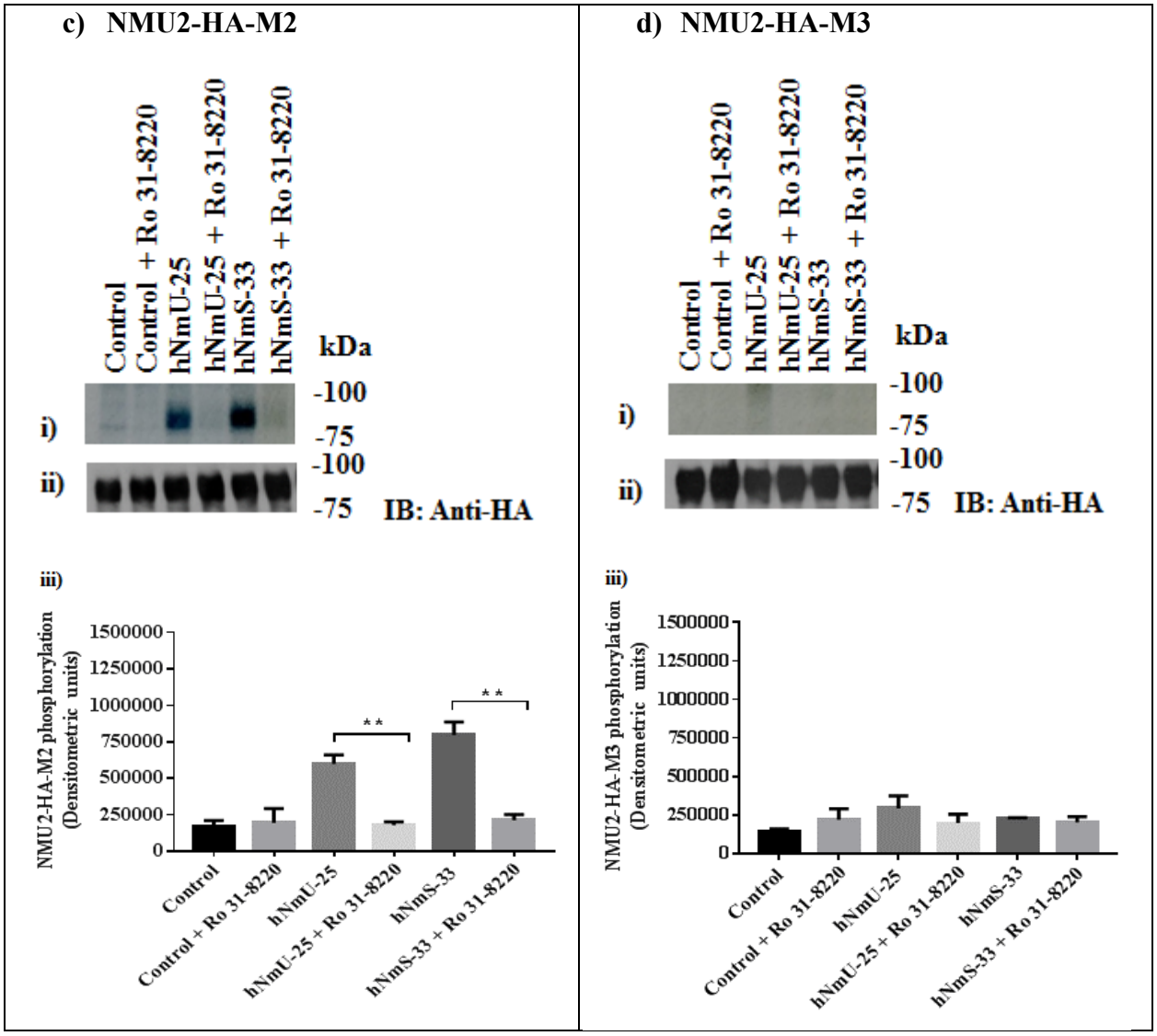


**Figure 6.14. Effect of PKC inhibition on agonist-dependent phosphorylation of NMU2-HA wild-type and mutants**

Cells were cultured on poly-D-lysine coated 6-well plates for 24 h before washing twice with phosphate-free KHB and labelling with $^{32}P$ orthophosphate for 1 h. Cells were pre-incubated with or without Ro 31-8220 (5µM) for 30 min and then stimulated with hNmU-25 (1 µM), hNmS-33 (1 µM) or KHB (control) for 5 min. Following solubilisation of the cell monolayers, NMU2-HA or NMU2-HA mutants were immunoprecipitated and resolved by gel electrophoresis. The gel was then dried and visualised by autoradiography ($a_i$, $b_i$, $c_i$, $d_i$). Immunoblotting of the immunoprecipitates with an anti-HA antibody were used as loading controls (IB; $a_{ii}$, $b_{ii}$, $c_{ii}$, $d_{ii,}$). The phosphorylation bands were quantified by densitometric analysis using Image J software (iii). Data are representative autoradiographs (i) or immunoblots (ii) of n = 3 or mean ± sem, n = 3 (iii). Statistical analysis was performed using a one way ANOVA followed by Bonferroni's test:$^{*}P<$

0.05, $^{**}P < 0.01$. Only comparisons between the presence or absence of Ro 31-8220 are shown for each condition

## 6.5 Discussion

The emergence of mass spectrometry has played an essential role in understanding the importance of receptor phosphorylation in the regulation of GPCR function. This technique allows determination of the precise phosphorylation sites which can then be manipulated by mutations to facilitating the study of their effects on GPCRs signalling. For example, mass spectrometry has previously been used to identify sixteen phosphorylation sites within the *C*-terminus and ICL3 of the muscarinic M3 receptor(Butcher *et al.*, 2011). These sites were predominantly serine residues although two phosphorylated threonine residues were identified (Butcher *et al.*, 2011). Of nineteen potential phosphorylation sites, only eight sites in the *C*-terminal tail of neuropeptide $FF_2$ receptor also determined by mass spectrometry were assigned as phosphorylated under both basal state and agonist activation including five serine and three threonine residues (Bray *et al.*, 2014).

Purification of NMU2-HA with anti-HA-conjugated beads and resolution by polyacrylamide gel electrophoresis generated a band at ~ 80 kDa. Although the predicted molecular mass of NMU2-HA is ~ 47 kDa suggesting that this greater molecular mass could from receptor post-translation modification processes such as glycosylation **(Discussion 3.3)**.

Protein phosphorylation is a crucial regulatory mechanism in protein post-translation modification and this is mediated by protein kinases which, in turn, adds a phosphate group ($PO_4$) to amino acids within the protein sequence. This, in turn, leads to changes in the conformation of protein through converting from hydrophobic to hydrophilic state thereby promoting its interaction with a variety of proteins (Hunter, 2012; Sacco *et al.*, 2012; Li *et al.*, 2013; Ardito *et al.*, 2017).

The present results of mass spectrometry show that of fourteen potential phosphorylation sites in the *C*-terminal tail of NMU2-HA, five residues were assigned as phosphorylated either following stimulation with agonists or under basal, non-stimulated, conditions. These sites included three serines and two threonines ($S^{341}$, $S^{348}$, $T^{364}$, $S^{406}$, and $T^{412}$). Unfortunately, mass spectrometric analysis of the tryptic digests of NMU2-HA did not cover a peptide sequence in the *C*-terminus containing seven potential phosphorylation including one threonine and six serine residues ($^{372}$TEDIGPQFPCQSSMHNSHLPAALSSEQMS$^{400}$). A possible explanation of this

might be this region contained few arginine and lysine residues that are targets for the trypsin digests. Attempts using Gluc-C to cleave glutamic acids to maximize the peptide coverage did not unfortunately digest peptide sequences within regions that were not covered following tryptic digest, despite the presence of glutamic acid within these regions. Alternative approach or modification that could be used to help to resolve this issue using phosphopeptide enrichment technique prior to the mass spectrometric analysis. This technique uses positively charged metal ions such as $Fe^{3+}$ or $Ti^{4+}$ to bind the negatively charged phosphopeptide molecules, thus facilitates purification of the phosphorylated peptides from complex mixtures (Thingholm *et al.*, 2016). In this study, it is difficult to identify the effect of agonist-dependent phosphorylation by mass spectrometry as the five phosphorylation sites detected by mass spectrometry as there was overlap between the treated groups and basal condition (untreated group). Given that some peptide sequences were not covered by mass spectrometry, these added a complexity in the interpretation of agonist-induced phosphorylation versus the basal condition and further work, probably involving point mutations, would be needed to precisely define the agonist-dependent phosphorylation sites.

Phosphorylation sites have been mapped for a number of GPCRs. For example, stimulation of the $G_{\alpha q}$-coupled FFA4 with TUG-891, a synthetic and a selective agonist, induces robust phosphorylation with five phosphorylation sites identified in the *C*-terminal tail. These sites included three serines and two threonines and mutations of these residues reduce both the potency and efficacy of TUG-891-mediated FFA4 interaction with arrestin 3 (Butcher *et al.*, 2014). In another study there was robust phosphorylation of GHSR1a following 5 min stimulation with ghrelin as shown by $^{32}P$ incorporation into immunoprecipitated receptor, which mass spectrometry assigned to three serines and two threonines. Amongst these, mutagenesis showed that $S^{362}$, $S^{363}$and $T^{366}$ were crucial for the recruitment of both arrestin 2 and arrestin 3 to in addition to receptor internalisation and arrestin-mediated ERK signalling. In contrast, $S^{349}$ and $T^{350}$ were responsible for increasing the stability of receptor-arrestin complexes as shown by a reduced affinity between the arrestins and receptor when $S^{349}$ and $T^{350}$ were mutated to alanine (Bouzo-Lorenzo *et al.*, 2016). Taken together, these studies highlight the importance of specific phosphorylation sites for the determination of specific functional consequences. Although under basal, non-stimulated, conditions MOP receptor was phosphorylated at $S^{363}$ and $T^{370}$ sites in the *C*-terminal region, stimulation of receptor with morphine or

synthetic opioid peptide, DAMGO phosphorylates additional sites including $S^{356}$, $T^{357}$ and $S^{375}$. Furthermore, *in vitro* assay using glutathione S transferase fusion proteins of *C*-terminus of the receptor, the purified GRK2 and PKC caused phosphorylation of $S^{375}$ and $S^{363}$ respectively, highlighting specific sites can be phosphorylated by different kinases and that might be crucial in regulation of GPCR functions (Chen *et al.*, 2013). Five phosphorylation sites were identified in NMU2-HA by mass spectrometry although unknown if these sites represent agonist-dependent phosphorylation or there are other sites, particularly in the section not covered by mass spectrometry. The time course of NMU2 dephosphorylation was different in response to brief exposure to hNmS-33 compared to hNmU-25. It is also possible that sites of NMU2 phosphorylation might differ between the two ligands. However, mass spectrometric analysis did not show a difference between the ligands although this was difficult due to the poor spectrum.

To further explore sites of phosphorylation including potential kinases in addition to explore differences between ligands to consider functional consequences of this phosphorylation, three NMU2-HA mutant constructs were generated. The first mutant (NMU2-HA-M1: $S^{341}$, $S^{348}$, $T^{364}$, $S^{406}$, and $T^{412}$) included five serine and threonine sites were assigned as phosphorylated and that were replaced with alanine. The second mutant (NMU2-HA-M2: $T^{372}$, $S^{383}$, $S^{384}$, $S^{388}$, $S^{395}$, $S^{396}$, and $S^{400}$) contained seven potential phosphorylation sites not covered by mass spectrometry that were mutated to alanine. The last mutant (NMU2-HA-M3: $S^{341}$, $S^{348}$, $T^{364}$, $S^{406}$, $T^{412}$, $T^{372}$, $S^{383}$, $S^{384}$, $S^{388}$, $S^{395}$, $S^{396}$, $S^{400}$, $S^{340}$ and $T^{402}$) included fourteen mutations which covered all of the serine and threonine residues of the *C*-terminal tail, whether they were detected as phosphorylated by mass spectrometry, not covered by mass spectrometry or covered by mass spectrometry but not phosphorylated **(**Error! Reference source not found.**)**. Immunoblotting of the transiently expressed constructs showed multiple bands similar to the transient expression of the NMU2-HA wild-type **(Figure 3.3; a, Figure 6.8)**. Furthermore, the cells in which the NMU2-HA wild-type was transiently expressed, stimulation with agonist did not induce receptor phosphorylation compared to non-stimulated group **(Figure 4.1)**. Therefore, three stable cell lines were generated, each expressing one of the mutants for study receptor phosphorylation. Mutation of all fourteen potential serine/threonine phosphorylation sites in the *C*-terminal tail of NMU2-HA-M3 completely inhibited receptor phosphorylation following stimulation with either ligand providing an evidence that one or more of these sites are responsible for NMU2

phosphorylation following either hNmU-25 or hNmS-33 challenge thereby excluding other intracellular regions such as ICL2 and ICL3 where potential phosphorylation sites have been suggested (Brighton *et al.*, 2004a). Although removal of all potential serine/threonine phosphorylation sites in the *C*-terminus of NMU2-HA (HEK-NMU2-HA-M3) could affect receptor functionality, a preliminary study in our laboratory (data not shown) demostrated robust $Ca^{2+}$ responses to either hNmU-25 or hNmS-33 in a cell line with stable expression of NMU2-HA-M3. These responses showed slightly higher potency and Emax values compared to responses in cells expressing NMU2-HA, indicating that this mutated receptor is functional.

Either hNmU-25 or hNmS-33 induced phosphorylation of NMU2-HA-M1 (five serine/threonine sites assigned as phosphorylated that were mutated to alanine) with equivalent magnitude albeit with a slightly lower Emax compared to NMU2-HA. NMU2-HA-M2 (seven potential phosphorylation sites not covered by mass spectrometry) showed a significantly lower phosphorylation in response to hNmU-25 than hNmS-33 suggesting that hNmS-33 either causes phosphorylation of different or more sites. There could also be partial or full overlap of phosphorylation sites but hNmS-33 clearly does more. Mass spectrometric analysis showed a difference between the total number of peptide fragment that were observed and the peptide residue that was assigned as phosphorylated within the peptide fragment, for example, the peptide sequence KQWHSQHDPQLPPAQRN was observed 23 times but only 4 times was assigned as phosphorylated in response to either ligand. This suggests that mass spectrometric analysis might not accurately detect all phosphorylation sites although sites were covered by mass spectrometry **(Figure 6.3)**. This might explain the possibility that $S^{340}$ and $T^{402}$ might responsible for greater phosphorylation of NMU2-HA-M2 in response to hNmS-33 although these two sites were covered by mass spectrometry but not phosphorylated **(Figure 6.5)**.

Data in Chapters, three and four have shown differences in the time courses of NMU2 signalling and dephosphorylation following brief exposure to hNmU-25 or hNmS-3. This highlights that different agonists can stabilise different conformations of the receptor leading to distinct signalling consequences (Peterhans *et al.*, 2016; Xiao *et al.*, 2016; Yang *et al.*, 2017). It has been demonstrated that carvedilol (non-selective β adrenoceptor antagonist but functions as inverse agonist for $G\alpha_s$-dependent AC activation) mediates different pattern of $\beta_2$ adrenoceptor phosphorylation compared to the unbiased ligand,

isoproterenol (full agonist). While isoproterenol induces phosphorylation of thirteen sites in $\beta_2$ adrenoceptor resulting in G-protein-dependent and independent signalling, only two of thirteen potential phosphorylation sites $S^{355}$ and $S^{356}$, were phosphorylated in response to receptor occupation by carvedilol and those sites were specifically targeted by GRK6, suggesting that carvedilol induces a specific change in receptor conformation and that leads to recruitment of specific GRK subtypes, thereby promoting arrestin interaction with the receptor (Nobles *et al.*, 2011a). It has also reported that GRK6 phosphorylation of receptor by carvedilol was responsible for arrestin 3 mediated ERK1/2 activation suggesting that biased ligands can activate specific subtype of GRK and stabilise specific conformation of arrestin, thereby engaging to different functional outcome (Wisler *et al.*, 2007; Nobles *et al.*, 2011a). Different phosphorylation profiles in the SST2 receptor were also generated in response to different ligands. While somatostatin and octreotide induced SST2 receptor phosphorylation at four threonine residues within the cluster $^{353}$TTETQRT$^{359}$, which are necessary for receptor internalisation, pasirotide only mediated phosphorylation of $^{356}$T and $T^{359}$, which failed to induce receptor internalisation (Poll *et al.*, 2010). Such examples demonstrate a clear connection between sites of receptor phosphorylation and signalling consequences and that are directed by the nature of the ligand-bound. In respect of NMU2, hNmS-33 might cause receptor phosphorylation at different sites to hNmU-25 and induce different conformation of the receptor. The phosphorylation status of NMU2-HA-M2 **(See Figure 6.12)** suggests that there may be some differences in phosphorylation sites between hNmU-25 and hNmS-33 that may lead to a specific conformation of the receptor that is induced by hNmS-33 thereby engaging the ligand-bound receptor to different intracellular components conferring a greater stability for example, resistance to phosphatases or proteolytic enzymes. This is at least in part consistent with a recent study that showed that ECE-1 plays a critical role in processing of hNmU-25 but not hNmS-33. In that study, silencing of ECE-1 by siRNA or inhibition with an ECE-1 inhibitor reduced the rate of the resensitisation of NMU2 and increased spatio-temporal profiles of NMU2-mediated ERK and P38 signalling in HEK-293 expressing NMU2 (Alhosaini *et al.*, 2018). This might suggest that hNmS-33 induces different conformation or different phosphorylation of the receptor (different sites or additional sites compared to hNmU-25) that lead to couple to proteins causing a limitation of access of ECE-1 enzyme and lacking of its dissociation from receptor. This might provide an explanation about the extended receptor

phosphorylation and sustained MAPK signalling following brief exposure to hNmS-33 compared to hNmU-25.

To explore the potential sites that are involved in receptor phosphorylation by kinases, PKC inhibitor was used as we showed in Chapter 4 that ~ 50 % of agonist-mediated NMU2 phosphorylation was PKC-dependent leaving the other part of phosphorylation for other kinases (potentially by GRKs) yet to be identified. NMU2-HA phosphorylation following stimulation with either ligand was reduced by ~ 50 % in the presence of PKC inhibitor. In contrast, NMU2-HA-M1 phosphorylation was not reduced by PKC inhibition suggesting that mutating the five phosphorylation sites that were assigned as being phosphorylated by mass spectrometry contain the PKC-dependent sites **(Figure 6.5)**. The lack of effect of PKC inhibition on phosphorylation highlights the likely presence of GRK-dependent phosphorylation sites within the remaining serine and threonine residues. Two of the five PKC-dependent sites are in agreement with the predicted PKC sites using NetPhos software (Brighton *et al.*, 2004a) **(See also Figure 6.4)**. Further support for the contribution of GRKs is that both hNmU-25 and hNmS-33 mediate arrestins recruitment to NMU2 as revealed in BRET assay **(Chapter five)**. This is consistent with the classic scheme of GPCR regulation in which the GRKs are involved (Pierce *et al.*, 2002; Lefkowitz *et al.*, 2005) **(Section 1.4.2.4)**. NMU2-HA-M2 phosphorylation by either ligand, which carries mutations of seven potential phosphorylation sites not covered by mass spectrometry, was abolished by inhibiting the PKC suggesting that at least some of five potential phosphorylation sites existed in NMU2-HA-HA are necessary for agonist-dependent PKC phosphorylation. PKC-dependent, agonist-mediated receptor phosphorylation has been shown for a number of GPCRs (Oppermann *et al.*, 1996; Chen *et al.*, 2013; Singh *et al.*, 2014). For example, phosphorylation of FFA4 in response to docosahexaenoic acid (DHA) at three serine/threonine sites ($T^{347}$, $S^{350}$ and $S^{357}$) in the *C*-terminus is mediated by both PKC and GRK. In that study, inhibition of PKC by bisindoylmaleimide II, PKC inhibitor reduced this phosphorylation which was completely abolished when both $S^{350}$ and $S^{357}$ sites were mutated suggesting that the $T^{347}$ site is PKC-dependent while the two serine residues were crucial for GRK phosphorylation (Burns *et al.*, 2014). This highlights the multiple levels of specificity, for example, specificity of kinases in phosphorylation of specific sites. This specificity may play a critical role in engaging the receptor with different intracellular compartments or proteins resulting in different functional outcomes. In respect of the

ligands of NMU2, hNmS-33 might differ from hNmU-25 mediating different conformation of the receptor and multiple levels of specificity regarding the sites of phosphorylation and the kinases involved in receptor phosphorylation causing differences in coupling of receptor to different functional consequences.

In conclusion, this chapter shows first a potential map of NMU2 phosphorylation sites in which five sites including $S^{341}$, $S^{348}$, $T^{364}$, $S^{406}$, and $T^{412}$ are phosphorylated using mass spectrometric analysis although other potential phosphorylation sites are not covered. Amongst fourteen phosphorylatable sites are responsible for agonist-mediated NMU2 phosphorylation. At least one or more of the five potential phosphorylation sites identified by mass spectrometry are essential for PKC phosphorylation. Different phosphorylation magnitudes emerges between hNmU-25 and hNmS-33-mediated NMU2 phosphorylation after mutating seven potential phosphorylation sites (NMU2-HA-M2: $T^{372}$, $S^{383}$, $S^{384}$, $S^{388}$, $S^{395}$, $S^{396}$, and $S^{400}$) to alanine. Here, 5 min stimulation with hNmS-33 induced NMU2-HA-M2 phosphorylation to a greater extent than that of hNmU-25, highlighting the importance of one or more of these sites on hNmU-25-mediated NMU2 phosphorylation but also possibly highlights that hNmU-25 and hNmS-33 could target at least some different sites. However several questions remain unanswered. For example, the GRK subtypes responsible for agonist-mediated NMU2 phosphorylation remain to be determined. Further, it is unknown if the different ligands recruit different GRKs or if this is related to different signalling outcomes. Further study would be merited looking at the functional aspects of the NMU2 mutants in response to either ligand to explore the roles of the mutated residues in ligand-dependent signalling profiles and resensitisation. Given the data presented that shows discrepancies between phosphorylation and arrestins recruitment, examination of the interaction of the mutants with the arrestins would be of particular value.

# 7 Chapter seven

## 7.1 Concluding discussion

NMU2, a member of family A GPCRs, mediates the actions of structurally-related but different neuropeptides, NmU and NmS. Upon ligand binding, NMU2 preferentially couples to $G\alpha_q$ to mediate a range of intracellular signalling events. Central expression of NMU2 plays a critical role in regulation of many effects including the suppression of feeding behaviour and increasing of energy expenditure **(Section 1.2.3.1.2 and 1.2.3.2.2 for more details)** highlighting a potential therapeutic target in the treatment of obesity (Mitchell *et al.*, 2009).

Different resensitisation rates and signalling profiles of NMU2 in response to either hNmU-25 (NmU) or hNmS-33 (NmS) were shown previously in recombinant system (Alhosaini *et al.*, 2018). Specifically, although hNmU-25 and hNmS-33 have equal potency in $Ca^{2+}$ signalling, the resensitisation of the $Ca^{2+}$ response was significantly different between the two ligands. Thus the rate of NMU2 resensitisation following hNmS-33 was considerably slower than that following hNmU-25. Given also that NMU2 is rapidly internalised and the ligand binds essentially irreversible (Brighton *et al.*, 2008; Alhosaini *et al.*, 2018), it is possible that the ligand may play a critical role in determining the fate of the internalised receptor and potential intracellular signalling. Studies with that have been observed with a variety of GPCRs. For example, activation of the $\beta_2$ adrenoceptor with isoproterenol mediates ERK activation via c-Src that is recruited to the receptor following arrestin binding. This was abolished by demonstration that ERK activation was abolished following overexpression of a dominant negative mutant of arrestin 2 (Luttrell *et al.*, 1997; Eichel *et al.*, 2018). Although the present study showed similar temporal patterns of NMU2-mediated ERK1/2 signalling in the continued presence of either hNmU-25 or hNmS-33, different temporal profiles of activation emerged following a brief challenge. Thus brief exposure to hNmS-33 resulted in a more sustained ERK activation than hNmU-25. This is consistent with earlier work from this laboratory (Alhosaini *et al.*, 2018). Such brief challenge might reflect the transient nature of *in vivo* exposure of peptidergic receptors to ligand given the episodic release of peptides and their removal by processes such as dilution and degradation.

The present study also shows that NMU2 mediates P38 and JNK activation by either hNmU-25 or hNmS-33 with similar patterns in the continued presence of ligand.

However, brief challenge with hNmS-33 caused a more sustained P38 and JNK activation than brief exposure to hNmU-25. Given the intracellular signalling including arrestin-dependent signalling described for a variety of GPCRs (Eichel *et al.*, 2018), the slow rate of resensitisation and sustained MAPK signalling of NMU2 in response to hNmS-33 compared to hNmU-25 could arise from ligand-dependent differences in the types or temporal profiles of arrestins recruitment to NMU2. These differences could also be as a consequence of different receptor conformations or ligand processing thereby resulting in different signalling consequences. It is well known that arrestins recruitment to the activated receptor is a consequence of receptor phosphorylation (Yang *et al.*, 2017). However, this may be not true for some GPCRs in which the phosphorylation appears to play no role in the recruitment of arrestins, for example, PAR1, substance P receptor and leukotriene B4 receptor (Chen *et al.*, 2004a; Jala *et al.*, 2005; Stalheim *et al.*, 2005). It is unknown if and where NMU2 is phosphorylated following agonist stimulation nor if this is related to arrestins recruitment. Study of these were major aims of the work described in this thesis. To study receptor phosphorylation, a stable cell line was generated in which NMU2 containing a *C*-terminal HA tag was expressed (NMU2-HA). This allowed efficient immunoprecipitation of the receptor that is critical step in the study of receptor phosphorylation. This approach has been previously applied for the study of phosphorylation of a number of GPCRs (Prihandoko *et al.*, 2015b). Data in Chapter 3 show that the functional responses of HEK-NMU2-HA to either hNmU-25 or hNmS-33 are similar to the cell line expressing wild-type receptor (HEK-NMU2), thereby demonstrating that, at least further responses examined, HEK-NMU2-HA behaves identically to HEK-NMU2 **(Discussion 3.3)**. This cell line was used to study NMU2 phosphorylation.

The results in Chapter 4 show that NMU2 is phosphorylated in response to either hNmU-25 or hNmS-33 with equivalent levels. Furthermore, inhibition of PKC but not PKA partially reduced agonist-dependent NMU2 phosphorylation by either ligand suggesting that other kinases most likely GRKs, play a role in this phosphorylation. This is consistent with the classic scheme for GPCRs in which binding of ligand to receptor causes its phosphorylation that is either by second messenger kinases (PKC and PKA) to mediate a heterologous desensitisation or by GRKs which recruit arrestins to the receptor to cause a homologous desensitisation by preventing G-protein coupling (Pierce *et al.*, 2002; Torrecilla *et al.*, 2007; Yang *et al.*, 2017).

Although NMU2 is phosphorylated to a similar extent by either hNmU-25 or hNmS-33, removal of the ligands after brief (5 min) exposure resulted in different rates of dephosphorylation. Thus the rate of dephosphorylation following hNmS-33 was slow compared to hNmU-25 suggesting the nature of the ligand may regulate receptor processing (dephosphorylation), trafficking and potentially therefore, signalling **(Figure 4.12)**. This is consistent with data presented in Chapter 3 that showed a more sustained activation of MAPKs (ERK, P38 and JNK) and a slower rate of NMU2 resensitisation following brief exposure to hNmS-33 compared to hNmU-25. One possibility that these events are connected is by differences in the stability of ligand-receptor-arrestin complex in which hNmS-33 could be protected from endosomal proteolysis thereby sustaining agonist occupation of the receptor and associated receptor phosphorylation and signalling and/or hNmS-33 could hold the receptor in a conformation that is more resistant to dephosphorylation **(Discussion 4.7)**. A recent study has highlighted a potential role of ECE-1 in the processing of hNmU-25 but not hNmS-33, demonstrating that inhibition of ECE-1 in HEK-293 expressing NMU2 increases the duration of NMU2-mediated ERK and P38 activation in response to brief exposure to hNmU-25 but not hNmS-33 (Alhosaini *et al.*, 2018). It would be worth to use ECE-1 inhibitor to examine the effect of ECE-1 on the dephosphorylation pattern of NMU2 following brief challenge with hNmU-25 to highlight role the specificity of ligand in determination of receptor trafficking (recycling/ resensitisation).

The present study also shows that the more sustained phosphorylation of NMU2 following brief exposure to hNmS-33 was not changed by PKC inhibition highlighting a potential ligand-specific role of GRK **(Figure 4.13)**. Further work is required to investigate the GRK subtypes that are critical for ligand-dependent NMU2 phosphorylation. This could be explored using genetic tools (siRNA) or commercially available chemical inhibitors of GRKs such as compound 101 (GRK2 and GRK3) and paroxetine (GRK2).

Given that NMU2 is phosphorylated in response to either hNmU-25 or hNmS-33 but that different profiles of dephosphorylation emerged following brief ligand exposure, arrestins recruitment to NMU2 was also examined. The results in Chapter 5 show that either hNmU-25 or hNmS-33 induce both arrestin 2 and arrestin 3 recruitment to NMU2 in a concentration-dependent fashion with evidence that NMU2 preferentially binds to arrestin 3. This would suggest a Class A GPCR in which they have higher affinity for

arrestin 3 than arrestin (Pierce *et al.*, 2002; Lefkowitz *et al.*, 2005). However, the data presented in Chapter 3 demonstrated slow rates of resensitisation in response to the two ligands (~ 6 h or more to fully recover depending on ligand bound) which is a marker of receptor recycling suggesting that NMU2 could belong to Class B GPCR.

Surprisingly, in addition to similar profiles of arrestins recruitment to NMU2 in the continued presence of ligand, no differences were found in the temporal profile of arrestins dissociation from NMU2 between hNmU-25 and hNmS-33 following brief exposure and removal of ligand suggesting that NMU2 interaction with arrestins are not responsible for the sustained temporal profile of NMU2-mediated MAPK signalling. Furthermore, this indicates a disparity between receptor phosphorylation and arrestins recruitment. It is likely that following brief exposure to ligand, NMU2 is phosphorylated by GRKs which lead to recruitment of arrestins to the receptor. Because of the interaction between NMU2 and arrestins is weak, arrestins dissociate from the receptor leaving the ligand-bound receptor being engaged with other intracellular compartments such as dynamin-dependent pathway or other mechanisms yet to be identified **(Discussion 5.11)**.

Data in Chapter 5 show that PKC is not responsible for agonist-mediated NMU2 interaction with the arrestins, suggesting a potential participation of GRKs. This is consistent with the general paradigm of GPCR activation by the cognate ligand which leads to receptor phosphorylation by GRKs, thereby resulting in arrestins recruitment and promoting homologous desensitisation (Pitcher *et al.*, 1992; Tobin *et al.*, 2008; Gurevich *et al.*, 2012). The recruitment of arrestins is able to induce G-protein-independent signalling (Yang *et al.*, 2017). Given that agonist stimulation may cause different conformational states of the receptor, this may lead to recruitment of a specific GRK subtype resulting in distinct biological consequences (Watari *et al.*, 2014), including the engagement of the ligand-bound receptor with different subcellular signalling molecules.

Using mass spectrometric analysis, data in Chapter 6 show that five residues ($S^{341}$, $S^{348}$, $T^{364}$, $S^{406}$, and $T^{412}$) within the *C*-terminal of NMU2 are phosphorylated. A region in the *C*-terminal of NMU2 containing seven potential phosphorylation sites (six serine and one threonine residues) was not covered by mass spectrometry. It would therefore be worth attempting a phosphopeptide enrichment method prior to mass spectrometric analysis using metal ions affinity to capture the negatively-charged phosphate groups **(Discussion 6.5)**.

Three NMU2 mutants were generated to further explore sites of phosphorylation including potential kinases and any possible differences between ligands to consider the effect of this phosphorylation on the functional consequences. In each of these, serine and threonine residues representing identified or potential phosphorylation sites were mutated to alanine. These mutants were NMU2-HA-M1 (five phosphorylation sites that had been determined by mass spectrometry to be phosphorylated), NMU2-HA-M2 (seven potential phosphorylation sites not covered by mass spectrometry) and NMU2-HA-M3 (fourteen phosphorylation sites including the five phosphorylation sites detected by mass spectrometry, seven potential phosphorylation sites not covered by mass spectrometry and two potential sites that were covered by mass spectrometry but not phosphorylated). The data presented show that NMU2 mutants had different levels of phosphorylation in response to agonist compared to the wild-type NMU2-HA. There is evidence that the phosphorylation sites amongst these fourteen residues in the *C*-terminal of NMU2 are responsible for either hNmU-25- or hNmS-33-induced NMU2 phosphorylation as revealed by a complete inhibition of NMU2 phosphorylation in NMU2-HA-M3 (fourteen phosphorylatable sites had been mutated to alanine) thereby indicating that phosphorylation of sites elsewhere in the receptor (ICL2 and ICL3) are probably not involved **(Figure 1.3)**. Furthermore, the results show that removal of seven potential phosphorylation sites in NMU2-HA-M2 generated a difference between hNmU-25- and hNmS-33-mediated NMU2 phosphorylation. In this mutant, the hNmU-25 phosphorylation response was significantly lower than of hNmS-33 suggesting that one or more of the seven potential phosphorylation sites removed might be critical specifically in hNmU-25-induced NMU2 phosphorylation. These data highlight potentially ligand-specific patterns of receptor phosphorylation and these could, of course generate different signalling outcomes (Tobin, 2008; Yang *et al.*, 2017). The results show that the five phosphorylation sites that were identified as phosphorylated by mass spectrometry contain PKC-dependent sites involved in agonist-dependent phosphorylation as phosphorylation in this NMU2-HA-M2 mutant was abolished by inhibition of PKC in response to either hNmU-25 or hNmS-33. Further studies are needed to investigate the effect of these mutations on the rate of NMU2 resensitisation, MAPKs signalling and temporal profile of ligand-dependent receptor dephosphorylation in response to either hNmU-25 or hNmS-33. To develop a fuller picture of NMU2 phosphorylation sites, it would be worth generating further mutations, including individual or double potential phosphorylation sites. This would help to identify the exact

sites or clusters that are critical for ligand-dependent NMU2 phosphorylation in addition to exploring the kinases that are involved in the phosphorylation of these sites, this might lead to establish a phosphorylation barcode **(Section 1.4.2.4.1)**. Having identified specific phosphorylation sites, it would be helpful to generate phospho-specific antibodies that target these sites. This would allow determination of the role of specific phosphorylation sites in response to individual ligands and to work out the signalling and functional consequences of phosphorylation of these sites. This might be useful tools to investigate role of these sites in agonist-dependent NMU2 phosphorylation and their effect on signalling outcomes in the hypothalamic tissues in which NMU2 is endogenously expressed

The results presented in this thesis demonstrate ligand-specific differences in NMU2 signalling and phosphorylation profiles suggesting that these differences might generate distinct biological responses. There is some evidence of physiological relevance of ligand-specific signalling profiles and regulation at NMU2. For example, while ICV injection of rats with NmU increases neuronal electrical activity in the PVN between 30 min and 60 min, ICV injection with NmS increases activity for at least 120 min (Ida *et al.*, 2005), highlighting that although the presence of potential extracellular effects on the ligands, there could well be effects at the level of the receptor. This also accords with the ICV administration of NmS to rats that resulted in a prolong suppression of eating compared to NmU-treated rats (Ida *et al.*, 2005; Miyazato *et al.*, 2008). The present study shows ligand-dependent differences in MAPK signalling and phosphorylation patterns between the two endogenous ligands, hNmU-25 and hNmS-33 at NMU2 using a brief ligand exposure protocol that may be more similar to transient *in vivo* exposure. The consequences of these to physiology and their implications for drug discovery require further study.

# 8 Summary

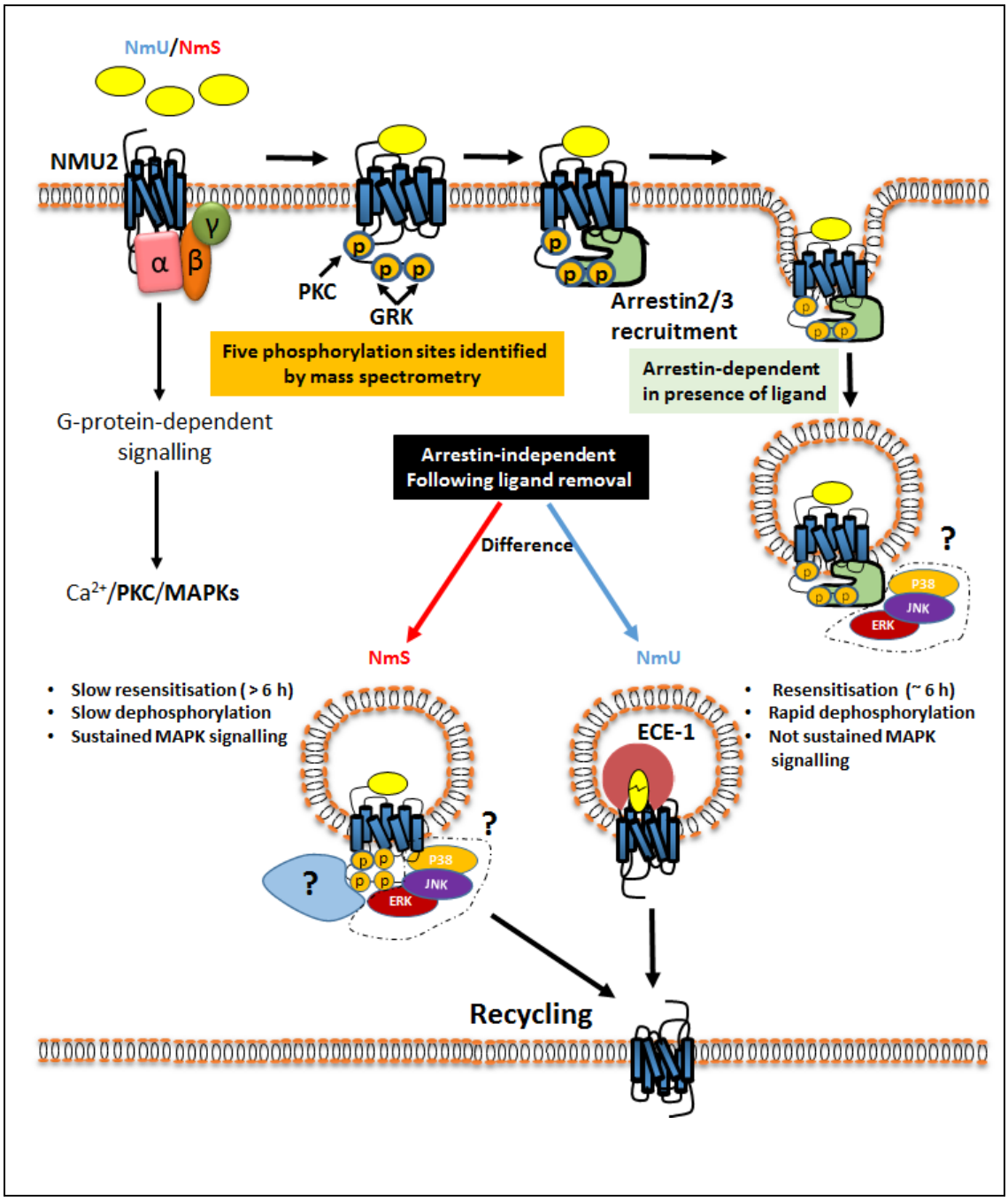


**Figure 8.1 NMU2 signalling and regulation**

The scheme summarises the main findings of the project. Both hNmU-25 and hNmS-33 activate NMU2 and mediate $Ca^{2+}$, ERK1/2 and P38 activation with equivalent potency. Both ligands induce NMU2 phosphorylation of equal magnitude and this phosphorylation is partially PKC-dependent (~ 50 %), suggesting the involvement of other kinases, most likely GRKs. In the continued presence of either hNmU-25 or hNmS-33, both ligands cause arrestin 2 and arrestin 3 recruitment to NMU2 and similar patterns of MAPK activation (ERK, P38, and JNK). The mechanisms of MAPK activation remain to be

established. Following brief (5 min) exposure to the ligands, differences in signalling and regulation emerged. This protocol may more accurately reflect the *in vivo* exposure of peptidergic receptors to ligands and demonstrated that the rate of NMU2 resensitisation was slower following hNmS-33 compared to hNmU-25. Furthermore, signalling of the MAPKs (ERK, P38 and JNK) was more sustained following brief exposure of NMU2 to hNmS-33 compared to hNmU-25. The rate of dephosphorylation of NMU2 was also slower following brief exposure to hNmS-33 compared to hNmU-25, although loss of arrestin-NMU2 interaction was not different between the ligands. This might suggest that NMU2 engages with intracellular proteins other than arrestins to sustain MAPK signalling. ECE-1 has been previously shown to play a role in processing of hNmU-25 but not hNmS-33. This might suggest that the difference in the conformation of receptor following agonist activation may limit access of phosphates or proteolytic enzymes to ligand-bound receptor in response to hNmS-33 compared to hNmU-25 resulting in distinct functional consequences. Five phosphorylation sites in the *C*-terminal tail of NMU2 were assigned as phosphorylated by mass spectrometry. Mutants of potential NMU2 serine and threonine phosphorylation sites established that *C*-terminus is critical for agonist-dependent phosphorylation excluding other potential regions such as intracellular loops. Ligand-dependent, PKC-dependent phosphorylation sites and ligand-dependent, PKC-independent phosphorylation sites been have shown by mutating the five sites that were indicated as phosphorylated by mass spectrometry. Probable differences in phosphorylation sites between hNmU-25 and hNmS-33 following removal of seven potential phosphorylation sites. This might suggest that phosphorylation sites in response to the two ligands are likely different and this may explain the difference in the temporal profile of dephosphorylation between hNmU-25 and hNmS-33.

# 9 Future experiments

1. Functional characterisation of mutant cell lines to address the importance of phosphorylation sites in the signalling and regulation of NMU2 in response to either hNmU-25 or hNmS-33.
2. Effects of phosphorylation sites on the interaction between NMU2 and the arrestins
3. Examination of the potential GRKs subtypes that might be critical for ligand-dependent NMU2 phosphorylation, particularly in terms of the time course of NMU2 dephosphorylation.

# 10 References


Abdalla MM (2017). Central and peripheral control of food intake. *Endocr Regul* 51**:** 52-70.

Adage T, Scheurink AJ, de Boer SF, de Vries K, Konsman JP, Kuipers F*, et al.* (2001). Hypothalamic, metabolic, and behavioral responses to pharmacological inhibition of CNS melanocortin signaling in rats. *J Neurosci* 21**:** 3639-3645.

Ahn S, Shenoy SK, Wei H, Lefkowitz RJ (2004). Differential kinetic and spatial patterns of beta-arrestin and G protein-mediated ERK activation by the angiotensin II receptor. *J Biol Chem* 279**:** 35518-35525.

Aiyar N, Disa J, Foley JJ, Buckley PT, Wixted WE, Pullen M*, et al.* (2004). Radioligand binding and functional characterization of recombinant human NmU1 and NmU2 receptors stably expressed in clonal human embryonic kidney-293 cells. *Pharmacology* 72**:** 33-41.

Alegria-Schaffer A, Lodge A, Vattem K (2009). Performing and optimizing Western blots with an emphasis on chemiluminescent detection. *Methods Enzymol* 463**:** 573-599.

Alevizos I, Mahadevappa M, Zhang X, Ohyama H, Kohno Y, Posner M*, et al.* (2001). Oral cancer in vivo gene expression profiling assisted by laser capture microdissection and microarray analysis. *Oncogene* 20**:** 6196-6204.

Alfa RW, Park S, Skelly KR, Poffenberger G, Jain N, Gu X*, et al.* (2015). Suppression of insulin production and secretion by a decretin hormone. *Cell Metab* 21**:** 323-334.

Alhosaini K, Bahattab O, Qassam H, Challiss J, Willars GB (2018). Ligand-Specific Signaling Profiles and Resensitization Mechanisms of the Neuromedin U2 Receptor. *Mol Pharmacol*.

Angrisani L, Santonicola A, Iovino P, Formisano G, Buchwald H, Scopinaro N (2015). Bariatric Surgery Worldwide 2013. *Obes Surg* 25**:** 1822-1832.

Antonny B, Burd C, De Camilli P, Chen E, Daumke O, Faelber K*, et al.* (2016). Membrane fission by dynamin: what we know and what we need to know. *EMBO J* 35**:** 2270-2284.

Ardito F, Giuliani M, Perrone D, Troiano G, Lo Muzio L (2017). The crucial role of protein phosphorylation in cell signaling and its use as targeted therapy (Review). *Int J Mol Med* 40**:** 271-280.

Audet M, Bouvier M (2012). Restructuring G-protein- coupled receptor activation. *Cell* 151**:** 14-23.

Augood SJ, Keast JR, Emson PC (1988). Distribution and characterisation of neuromedin U-like immunoreactivity in rat brain and intestine and in guinea pig intestine. *Regul Pept* 20**:** 281-292.

Austin C, Lo G, Nandha KA, Meleagros L, Bloom SR (1995). Cloning and characterization of the cDNA encoding the human neuromedin U (NmU) precursor: NmU expression in the human gastrointestinal tract. *J Mol Endocrinol* 14**:** 157-169.

Austin C, Oka M, Nandha KA, Legon S, Khandan-Nia N, Lo G*, et al.* (1994). Distribution and developmental pattern of neuromedin U expression in the rat gastrointestinal tract. *J Mol Endocrinol* 12**:** 257-263.

Bahouth SW, Nooh MM (2017). Barcoding of GPCR trafficking and signaling through the various trafficking roadmaps by compartmentalized signaling networks. *Cell Signal* 36**:** 42-55.

Ballesta J, Carlei F, Bishop AE, Steel JH, Gibson SJ, Fahey M*, et al.* (1988). Occurrence and developmental pattern of neuromedin U-immunoreactive nerves in the gastrointestinal tract and brain of the rat. *Neuroscience* 25**:** 797-816.

Batterham RL, Heffron H, Kapoor S, Chivers JE, Chandarana K, Herzog H*, et al.* (2006). Critical role for peptide YY in protein-mediated satiation and body-weight regulation. *Cell Metab* 4**:** 223-233.

Bechtold DA, Ivanov TR, Luckman SM (2009). Appetite-modifying actions of pro-neuromedin U-derived peptides. *Am J Physiol Endocrinol Metab* 297**:** E545-551.

Behary P, Cegla J, Tan TM, Bloom SR (2015). Obesity: Lifestyle management, bariatric surgery, drugs, and the therapeutic exploitation of gut hormones. *Postgrad Med* 127**:** 494-502.

Benaiges D, Pedro-Botet J, Flores-Le Roux JA, Climent E, Goday A (2017). Past, present and future of pharmacotherapy for obesity. *Clin Investig Arterioscler* 29**:** 256-264.

Benzon CR, Johnson SB, McCue DL, Li D, Green TA, Hommel JD (2014). Neuromedin U receptor 2 knockdown in the paraventricular nucleus modifies behavioral responses to obesogenic high-fat food and leads to increased body weight. *Neuroscience* 258**:** 270-279.

Berchiche YA, Gravel S, Pelletier M-E, St-Onge G, Heveker N (2011). Different Effects of the Different Natural CC Chemokine Receptor 2b Ligands on β-Arrestin Recruitment, Gα<sub>i</sub> Signaling, and Receptor Internalization. *Mol Pharmacol* 79**:** 488.

Bird RJ, Baillie GS, Yarwood SJ (2010). Interaction with receptor for activated C-kinase 1 (RACK1) sensitizes the phosphodiesterase PDE4D5 towards hydrolysis of cAMP and activation by protein kinase C. *Biochem J* 432**:** 207-216.

Bjorbaek C (2009). Central leptin receptor action and resistance in obesity. *J Investig Med* 57**:** 789-794.

Bonneterre J, Montpas N, Boularan C, Gales C, Heveker N (2016). Analysis of Arrestin Recruitment to Chemokine Receptors by Bioluminescence Resonance Energy Transfer. *Methods Enzymol* 570**:** 131-153.

Boughton CK, Murphy KG (2013). Can neuropeptides treat obesity? A review of neuropeptides and their potential role in the treatment of obesity. *Br J Pharmacol* 170**:** 1333-1348.

Bouvier M, Hausdorff WP, De Blasi A, O'Dowd BF, Kobilka BK, Caron MG*, et al.* (1988). Removal of phosphorylation sites from the beta 2-adrenergic receptor delays onset of agonist-promoted desensitization. *Nature* 333**:** 370-373.

Bouzo-Lorenzo M, Santo-Zas I, Lodeiro M, Nogueiras R, Casanueva FF, Castro M*, et al.* (2016). Distinct phosphorylation sites on the ghrelin receptor, GHSR1a, establish a code that determines the functions of ß-arrestins. *Scientific Reports* 6**:** 22495.

Bray L, Froment C, Pardo P, Candotto C, Burlet-Schiltz O, Zajac JM*, et al.* (2014). Identification and functional characterization of the phosphorylation sites of the neuropeptide FF2 receptor. *J Biol Chem* 289**:** 33754-33766.

Bray MS, Young ME (2007). Circadian rhythms in the development of obesity: potential role for the circadian clock within the adipocyte. *Obes Rev* 8**:** 169-181.

Brighton PJ, Szekeres PG, Willars GB (2004a). Neuromedin U and its receptors: structure, function, and physiological roles. *Pharmacol Rev* 56**:** 231-248.

Brighton PJ, Szekeres PG, Wise A, Willars GB (2004b). Signaling and ligand binding by recombinant neuromedin U receptors: evidence for dual coupling to Galphaq/11 and Galphai and an irreversible ligand-receptor interaction. *Mol Pharmacol* 66**:** 1544-1556.

Brighton PJ, Wise A, Dass NB, Willars GB (2008). Paradoxical behavior of neuromedin U in isolated smooth muscle cells and intact tissue. *J Pharmacol Exp Ther* 325**:** 154-164.

Budd DC, Rae A, Tobin AB (1999). Activation of the mitogen-activated protein kinase pathway by a Gq/11-coupled muscarinic receptor is independent of receptor internalization. *J Biol Chem* 274**:** 12355-12360.

Burke LK, Doslikova B, D'Agostino G, Garfield AS, Farooq G, Burdakov D*, et al.* (2014). 5-HT obesity medication efficacy via POMC activation is maintained during aging. *Endocrinology* 155**:** 3732-3738.

Burns RN, Moniri NH (2010). Agonism with the omega-3 fatty acids α-linolenic acid and docosahexaenoic acid mediates phosphorylation of both the short and long isoforms of the human GPR120 receptor. *Biochem Biophys Res Commun* 396**:** 1030-1035.

Burns RN, Singh M, Senatorov IS, Moniri NH (2014). Mechanisms of homologous and heterologous phosphorylation of FFA receptor 4 (GPR120): GRK6 and PKC mediate phosphorylation of Thr347, Ser350, and Ser357 in the C-terminal tail. *Biochemical Pharmacology* 87**:** 650-659.

Busillo JM, Armando S, Sengupta R, Meucci O, Bouvier M, Benovic JL (2010). Site-specific phosphorylation of CXCR4 is dynamically regulated by multiple kinases and results in differential modulation of CXCR4 signaling. *J Biol Chem* 285**:** 7805-7817.

Butcher AJ, Prihandoko R, Kong KC, McWilliams P, Edwards JM, Bottrill A*, et al.* (2011). Differential G-protein-coupled receptor phosphorylation provides evidence for a signaling bar code. *J Biol Chem* 286**:** 11506-11518.

Butcher AJ, Hudson BD, Shimpukade B, Alvarez-Curto E, Prihandoko R, Ulven T*, et al.* (2014). Concomitant action of structural elements and receptor phosphorylation determines arrestin-3 interaction with the free fatty acid receptor FFA4. *J Biol Chem* 289**:** 18451-18465.

Cabrera-Vera TM, Vanhauwe J, Thomas TO, Medkova M, Preininger A, Mazzoni MR*, et al.* (2003). Insights into G protein structure, function, and regulation. *Endocr Rev* 24**:** 765-781.

Calle EE, Rodriguez C, Walker-Thurmond K, Thun MJ (2003). Overweight, obesity, and mortality from cancer in a prospectively studied cohort of U.S. adults. *N Engl J Med* 348**:** 1625-1638.

Cao CQ, Yu XH, Dray A, Filosa A, Perkins MN (2003). A pro-nociceptive role of neuromedin U in adult mice. *Pain* 104**:** 609-616.

Castillo-Badillo JA, Sánchez-Reyes OB, Alfonzo-Méndez MA, Romero-Ávila MT, Reyes-Cruz G, García-Sáinz JA (2015). α1B-adrenergic receptors differentially associate

with Rab proteins during homologous and heterologous desensitization. *PLoS One* 10**:** e0121165-e0121165.

Chan AS, Clairfeuille T, Landao-Bassonga E, Kinna G, Ng PY, Loo LS*, et al.* (2016). Sorting nexin 27 couples PTHR trafficking to retromer for signal regulation in osteoblasts during bone growth. *Mol Biol Cell* 27**:** 1367-1382.

Chao TH, Hayashi M, Tapping RI, Kato Y, Lee JD (1999). MEKK3 directly regulates MEK5 activity as part of the big mitogen-activated protein kinase 1 (BMK1) signaling pathway. *J Biol Chem* 274**:** 36035-36038.

Chen CH, Paing MM, Trejo J (2004a). Termination of protease-activated receptor-1 signaling by beta-arrestins is independent of receptor phosphorylation. *J Biol Chem* 279**:** 10020-10031.

Chen J, Gopalakrishnan S, Lake MR, Bianchi BR, Locklear J, Reilly RM (2010). Application of large-scale transient transfection to cell-based functional assays for ion channels and GPCRs. *Methods Enzymol* 485**:** 293-309.

Chen TB, Zhou M, Walker B, Harriot P, Mori K, Miyazato M*, et al.* (2006). Structural and functional analogs of the novel mammalian neuropeptide, neuromedin S (NmS), in the dermal venoms of Eurasian bombinid toads. *Biochem Biophys Res Commun* 345**:** 377-384.

Chen Y-J, Oldfield S, Butcher AJ, Tobin AB, Saxena K, Gurevich VV*, et al.* (2013). Identification of phosphorylation sites in the COOH-terminal tail of the μ-opioid receptor. *J Neurochem* 124**:** 189-199.

Chen Z, Gaudreau R, Le Gouill C, Rola-Pleszczynski M, Staňková J (2004b). Agonist-Induced Internalization of Leukotriene B<sub>4</sub> Receptor 1 Requires G-Protein-Coupled Receptor Kinase 2 but Not Arrestins. *Mol Pharmacol* 66**:** 377.

Chen Z, Gaudreau R, Le Gouill C, Rola-Pleszczynski M, Stankova J (2004c). Agonist-induced internalization of leukotriene B(4) receptor 1 requires G-protein-coupled receptor kinase 2 but not arrestins. *Mol Pharmacol* 66**:** 377-386.

Chini B (2019). Expanding neuropeptide signalling by multiplying receptor functional states and sub-cellular locations. *Cell and Tissue Research* 375**:** 49-56.

Chu C, Jin Q, Kunitake T, Kato K, Nabekura T, Nakazato M*, et al.* (2002). Cardiovascular actions of central neuromedin U in conscious rats. *Regul Pept* 105**:** 29-34.

Cirmanova V, Bayer M, Starka L, Zajickova K (2008). The effect of leptin on bone: an evolving concept of action. *Physiol Res* 57 Suppl 1**:** S143-151.

Cisse M, Duplan E, Guillot-Sestier MV, Rumigny J, Bauer C, Pages G*, et al.* (2011). The extracellular regulated kinase-1 (ERK1) controls regulated alpha-secretase-mediated processing, promoter transactivation, and mRNA levels of the cellular prion protein. *J Biol Chem* 286**:** 29192-29206.

Claing A, Laporte SA, Caron MG, Lefkowitz RJ (2002). Endocytosis of G protein-coupled receptors: roles of G protein-coupled receptor kinases and beta-arrestin proteins. *Prog Neurobiol* 66**:** 61-79.

Claing A, Perry SJ, Achiriloaie M, Walker JKL, Albanesi JP, Lefkowitz RJ*, et al.* (2000a). Multiple endocytic pathways of G protein-coupled receptors delineated by GIT1 sensitivity. *Proceedings of the National Academy of Sciences* 97**:** 1119.

Claing A, Perry SJ, Achiriloaie M, Walker JK, Albanesi JP, Lefkowitz RJ*, et al.* (2000b). Multiple endocytic pathways of G protein-coupled receptors delineated by GIT1 sensitivity. *Proc Natl Acad Sci U S A* 97**:** 1119-1124.

Conn PM, Ulloa-Aguirre A (2010). Trafficking of G-protein-coupled receptors to the plasma membrane: insights for pharmacoperone drugs. *Trends Endocrinol Metab* 21**:** 190-197.

Cottrell GS, Padilla BE, Amadesi S, Poole DP, Murphy JE, Hardt M*, et al.* (2009). Endosomal endothelin-converting enzyme-1: a regulator of beta-arrestin-dependent ERK signaling. *J Biol Chem* 284**:** 22411-22425.

Coulthard LR, White DE, Jones DL, McDermott MF, Burchill SA (2009). p38(MAPK): stress responses from molecular mechanisms to therapeutics. *Trends Mol Med* 15**:** 369-379.

Cummings DE, Overduin J (2007). Gastrointestinal regulation of food intake. *J Clin Invest* 117**:** 13-23.

Daaka Y, Luttrell LM, Lefkowitz RJ (1997a). Switching of the coupling of the beta2-adrenergic receptor to different G proteins by protein kinase A. *Nature* 390**:** 88-91.

Daaka Y, Luttrell LM, Lefkowitz RJ (1997b). Switching of the coupling of the β2-adrenergic receptor to different G proteins by protein kinase A. *Nature* 390**:** 88.

Daaka Y, Luttrell LM, Ahn S, Della Rocca GJ, Ferguson SS, Caron MG*, et al.* (1998). Essential role for G protein-coupled receptor endocytosis in the activation of mitogen-activated protein kinase. *J Biol Chem* 273**:** 685-688.

Dass NB, Bassil AK, North-Laidler VJ, Morrow R, Aziz E, Tuladhar BR*, et al.* (2007). Neuromedin U can exert colon-specific, enteric nerve-mediated prokinetic activity, via a pathway involving NMU1 receptor activation. *Br J Pharmacol* 150**:** 502-508.

Davis D, Liu X, Segaloff DL (1995). Identification of the sites of N-linked glycosylation on the follicle-stimulating hormone (FSH) receptor and assessment of their role in FSH receptor function. *Mol Endocrinol* 9**:** 159-170.

Davis RJ (1994). MAPKs: new JNK expands the group. *Trends Biochem Sci* 19**:** 470-473.

De Angioletti M, Lacerra G, Sabato V, Carestia C (2004). Beta+45 G --> C: a novel silent beta-thalassaemia mutation, the first in the Kozak sequence. *Br J Haematol* 124**:** 224-231.

De Vries L, Zheng B, Fischer T, Elenko E, Farquhar MG (2000). The regulator of G protein signaling family. *Annu Rev Pharmacol Toxicol* 40**:** 235-271.

DeFea KA, Vaughn ZD, O'Bryan EM, Nishijima D, Dery O, Bunnett NW (2000a). The proliferative and antiapoptotic effects of substance P are facilitated by formation of a beta -arrestin-dependent scaffolding complex. *Proc Natl Acad Sci U S A* 97**:** 11086-11091.

DeFea KA, Zalevsky J, Thoma MS, Dery O, Mullins RD, Bunnett NW (2000b). beta-arrestin-dependent endocytosis of proteinase-activated receptor 2 is required for intracellular targeting of activated ERK1/2. *J Cell Biol* 148**:** 1267-1281.

Deslauriers B, Ponce C, Lombard C, Larguier R, Bonnafous JC, Marie J (1999). N-glycosylation requirements for the AT1a angiotensin II receptor delivery to the plasma membrane. *Biochem J* 339 ( Pt 2)**:** 397-405.

DeWire SM, Ahn S, Lefkowitz RJ, Shenoy SK (2007). Beta-arrestins and cell signaling. *Annu Rev Physiol* 69**:** 483-510.

Dhanasekaran DN, Reddy EP (2008). JNK signaling in apoptosis. *Oncogene* 27**:** 6245-6251.

Di Pizio A, Levit A, Slutzki M, Behrens M, Karaman R, Niv MY (2016). Chapter 18 - Comparing Class A GPCRs to bitter taste receptors: Structural motifs, ligand interactions and agonist-to-antagonist ratios. In: K. Shukla A (ed). *Methods in Cell Biology*, edn, Vol. 132: Academic Press. p^pp 401-427.

Diaz C, Angelloz-Nicoud P, Pihan E (2018). Modeling and Deorphanization of Orphan GPCRs. In: Heifetz A (ed). *Computational Methods for GPCR Drug Discovery*, edn. New York, NY: Springer New York. p^pp 413-429.

Doll C, Poll F, Peuker K, Loktev A, Gluck L, Schulz S (2012). Deciphering micro-opioid receptor phosphorylation and dephosphorylation in HEK293 cells. *Br J Pharmacol* 167**:** 1259-1270.

Domin J, Ghatei MA, Chohan P, Bloom SR (1987). Neuromedin U--a study of its distribution in the rat. *Peptides* 8**:** 779-784.

Domin J, Benito-Orfila MA, Nandha KA, Aitken A, Bloom SR (1992). The purification and sequence analysis of an avian neuromedin U. *Regul Pept* 41**:** 1-8.

Domin J, Yiangou Y, Spokes R, Aitken A, Parmar K, Chrysanthou BJ*, et al.* (1989). The Purification and Characterization of Amphibian Neuromedin-U. *Regul Pept* 26**:** 67-67.

Dong C, Filipeanu CM, Duvernay MT, Wu G (2007). Regulation of G protein-coupled receptor export trafficking. *Biochim Biophys Acta* 1768**:** 853-870.

Dutt P, Nguyen N, Toksoz D (2004). Role of Lbc RhoGEF in Galpha12/13-induced signals to Rho GTPase. *Cell Signal* 16**:** 201-209.

Duvernay MT, Filipeanu CM, Wu G (2005). The regulatory mechanisms of export trafficking of G protein-coupled receptors. *Cell Signal* 17**:** 1457-1465.

Egecioglu E, Ploj K, Xu X, Bjursell M, Salome N, Andersson N*, et al.* (2009). Central NMU signaling in body weight and energy balance regulation: evidence from NMUR2 deletion and chronic central NMU treatment in mice. *Am J Physiol Endocrinol Metab* 297**:** E708-716.

Eichel K, von Zastrow M (2018). Subcellular Organization of GPCR Signaling. *Trends Pharmacol Sci* 39**:** 200-208.

Elazar Z, Fuchs S (1991). Phosphorylation by Cyclic AMP-Dependent Protein Kinase Modulates Agonist Binding to the D2 Dopamine Receptor. *J Neurochem* 56**:** 75-80.

Erickson JC, Hollopeter G, Palmiter RD (1996). Attenuation of the obesity syndrome of ob/ob mice by the loss of neuropeptide Y. *Science* 274**:** 1704-1707.

Erlandson SC, McMahon C, Kruse AC (2018). Structural Basis for G Protein-Coupled Receptor Signaling. *Annu Rev Biophys*.

Euer NI, Kaul S, Deissler H, Mobus VJ, Zeillinger R, Weidle UH (2005). Identification of L1CAM, Jagged2 and Neuromedin U as ovarian cancer-associated antigens. *Oncol Rep* 13**:** 375-387.

Feinstein TN, Yui N, Webber MJ, Wehbi VL, Stevenson HP, King JD, Jr.*, et al.* (2013). Noncanonical control of vasopressin receptor type 2 signaling by retromer and arrestin. *J Biol Chem* 288**:** 27849-27860.

Ferguson SS (2001). Evolving concepts in G protein-coupled receptor endocytosis: the role in receptor desensitization and signaling. *Pharmacol Rev* 53**:** 1-24.

Fisher JM, Scheller RH (1988). Prohormone processing and the secretory pathway. *J Biol Chem* 263**:** 16515-16518.

Freedman NJ, Ament AS, Oppermann M, Stoffel RH, Exum ST, Lefkowitz RJ (1997). Phosphorylation and desensitization of human endothelin A and B receptors. Evidence for G protein-coupled receptor kinase specificity. *J Biol Chem* 272**:** 17734-17743.

Fujii R, Hosoya M, Fukusumi S, Kawamata Y, Habata Y, Hinuma S*, et al.* (2000). Identification of neuromedin U as the cognate ligand of the orphan G protein-coupled receptor FM-3. *J Biol Chem* 275**:** 21068-21074.

Fujioka K (2010). Benefits of moderate weight loss in patients with type 2 diabetes. *Diabetes Obes Metab* 12**:** 186-194.

Fukue Y, Sato T, Teranishi H, Hanada R, Takahashi T, Nakashima Y*, et al.* (2006). Regulation of gonadotropin secretion and puberty onset by neuromedin U. *FEBS Lett* 580**:** 3485-3488.

Fukuhara S, Chikumi H, Gutkind JS (2001). RGS-containing RhoGEFs: the missing link between transforming G proteins and Rho? *Oncogene* 20**:** 1661-1668.

Fukushima Y, Oka Y, Saitoh T, Katagiri H, Asano T, Matsuhashi N*, et al.* (1995). Structural and functional analysis of the canine histamine H2 receptor by site-directed mutagenesis: N-glycosylation is not vital for its action. *Biochem J* 310 ( Pt 2)**:** 553-558.

Funes S, Hedrick JA, Yang S, Shan L, Bayne M, Monsma FJ, Jr.*, et al.* (2002). Cloning and characterization of murine neuromedin U receptors. *Peptides* 23**:** 1607-1615.

Gadde KM, Martin CK, Berthoud HR, Heymsfield SB (2018). Obesity: Pathophysiology and Management. *J Am Coll Cardiol* 71**:** 69-84.

Gajjar S, Patel BM (2017). Neuromedin: An insight into its types, receptors and therapeutic opportunities. *Pharmacol Rep* 69**:** 438-447.

Garczyk S, Klotz N, Szczepanski S, Denecke B, Antonopoulos W, von Stillfried S*, et al.* (2017). Oncogenic features of neuromedin U in breast cancer are associated with NMUR2 expression involving crosstalk with members of the WNT signaling pathway. *Oncotarget* 8**:** 36246-36265.

Gardiner SM, Compton AM, Bennett T, Domin J, Bloom SR (1990). Regional hemodynamic effects of neuromedin U in conscious rats. *Am J Physiol* 258**:** R32-38.

Gartlon J, Szekeres P, Pullen M, Sarau HM, Aiyar N, Shabon U*, et al.* (2004). Localisation of NMU1R and NMU2R in human and rat central nervous system and effects of neuromedin-U following central administration in rats. *Psychopharmacology (Berl)* 177**:** 1-14.

Gesty-Palmer D, Chen M, Reiter E, Ahn S, Nelson CD, Wang S*, et al.* (2006). Distinct beta-arrestin- and G protein-dependent pathways for parathyroid hormone receptor-stimulated ERK1/2 activation. *J Biol Chem* 281**:** 10856-10864.

Ghosh M, Kao YJ, Schonbrunn A (2011). Ligand-Dependent Mechanisms of sst2A Receptor Trafficking: Role of Site-Specific Phosphorylation and Receptor Activation in the Actions of Biased Somatostatin Agonists. *Mol Endocrinol* 25**:** 1040-1054.

Gianfagna F, Cugino D, Ahrens W, Bailey ME, Bammann K, Herrmann D*, et al.* (2013). Understanding the links among neuromedin U gene, beta2-adrenoceptor gene and bone health: an observational study in European children. *PLoS One* 8**:** e70632.

Giebing G, Tölle M, Jürgensen J, Eichhorst J, Furkert J, Beyermann M*, et al.* (2005). Arrestin-Independent Internalization and Recycling of the Urotensin Receptor Contribute to Long-Lasting Urotensin II–Mediated Vasoconstriction. *Circulation Research* 97**:** 707-715.

Gilman AG (1987). G PROTEINS: TRANSDUCERS OF RECEPTOR-GENERATED SIGNALS. *Annu Rev Biochem* 56**:** 615-649.

Goldsmith ZG, Dhanasekaran DN (2007). G protein regulation of MAPK networks. *Oncogene* 26**:** 3122-3142.

Gong K, Li Z, Xu M, Du J, Lv Z, Zhang Y (2008). A novel protein kinase A-independent, beta-arrestin-1-dependent signaling pathway for p38 mitogen-activated protein kinase activation by beta2-adrenergic receptors. *J Biol Chem* 283**:** 29028-29036.

Graham ES, Turnbull Y, Fotheringham P, Nilaweera K, Mercer JG, Morgan PJ*, et al.* (2003). Neuromedin U and Neuromedin U receptor-2 expression in the mouse and rat hypothalamus: effects of nutritional status. *J Neurochem* 87**:** 1165-1173.

Greenway FL (2015). Physiological adaptations to weight loss and factors favouring weight regain. *Int J Obes (Lond)* 39**:** 1188-1196.

Grundmann M, Kostenis E (2017). Temporal Bias: Time-Encoded Dynamic GPCR Signaling. *Trends Pharmacol Sci* 38**:** 1110-1124.

Guan XM, Yu H, Jiang Q, Van Der Ploeg LH, Liu Q (2001). Distribution of neuromedin U receptor subtype 2 mRNA in the rat brain. *Brain Res Gene Expr Patterns* 1**:** 1-4.

Gupta MK, Mohan ML, Naga Prasad SV (2018). G Protein-Coupled Receptor Resensitization Paradigms. *Int Rev Cell Mol Biol* 339**:** 63-91.

Gurevich EV, Tesmer JJG, Mushegian A, Gurevich VV (2012). G protein-coupled receptor kinases: More than just kinases and not only for GPCRs. *Pharmacology & Therapeutics* 133**:** 40-69.

Gurevich VV, Gurevich EV (2018a). GPCRs and Signal Transducers: Interaction Stoichiometry. *Trends Pharmacol Sci* 39**:** 672-684.

Gurevich VV, Gurevich EV (2018b). Arrestin-mediated signaling: Is there a controversy? *World J Biol Chem* 9**:** 25-35.

Gutkind JS (2000). Regulation of mitogen-activated protein kinase signaling networks by G protein-coupled receptors. *Sci STKE* 2000**:** re1.

Gyombolai P, Toth AD, Timar D, Turu G, Hunyady L (2015). Mutations in the 'DRY' motif of the CB1 cannabinoid receptor result in biased receptor variants. *J Mol Endocrinol* 54**:** 75-89.

Halaas JL, Boozer C, Blair-West J, Fidahusein N, Denton DA, Friedman JM (1997). Physiological response to long-term peripheral and central leptin infusion in lean and obese mice. *Proc Natl Acad Sci U S A* 94**:** 8878-8883.

Hamm HE (1998). The many faces of G protein signaling. *J Biol Chem* 273**:** 669-672.

Hamrick MW, Pennington C, Newton D, Xie D, Isales C (2004). Leptin deficiency produces contrasting phenotypes in bones of the limb and spine. *Bone* 34**:** 376-383.

Hamrick MW, Della-Fera MA, Choi YH, Pennington C, Hartzell D, Baile CA (2005). Leptin treatment induces loss of bone marrow adipocytes and increases bone formation in leptin-deficient ob/ob mice. *J Bone Miner Res* 20**:** 994-1001.

Han SO, Kommaddi RP, Shenoy SK (2013). Distinct roles for beta-arrestin2 and arrestin-domain-containing proteins in beta2 adrenergic receptor trafficking. *EMBO Rep* 14**:** 164-171.

Hanada R, Nakazato M, Murakami N, Sakihara S, Yoshimatsu H, Toshinai K*, et al.* (2001). A role for neuromedin U in stress response. *Biochem Biophys Res Commun* 289**:** 225-228.

Hanada R, Teranishi H, Pearson JT, Kurokawa M, Hosoda H, Fukushima N*, et al.* (2004). Neuromedin U has a novel anorexigenic effect independent of the leptin signaling pathway. *Nat Med* 10**:** 1067-1073.

Hanada T, Date Y, Shimbara T, Sakihara S, Murakami N, Hayashi Y*, et al.* (2003). Central actions of neuromedin U via corticotropin-releasing hormone. *Biochem Biophys Res Commun* 311**:** 954-958.

Hasdemir B, Liao M, Bunnett NW, Mahajan S, Bhargava A (2012). Endothelin-Converting Enzyme-1 Actions Determine Differential Trafficking and Signaling of Corticotropin-Releasing Factor Receptor 1 at High Agonist Concentrations. *Mol Endocrinol* 26**:** 681-695.

Hashimoto T, Kurosawa K, Sakura N (1995). Structure-activity relationships of neuromedin U. II. Highly potent analogs substituted or modified at the N-terminus of neuromedin U-8. *Chem Pharm Bull (Tokyo)* 43**:** 1154-1157.

Hashimoto T, Masui H, Uchida Y, Sakura N, Okimura K (1991). Agonistic and antagonistic activities of neuromedin U-8 analogs substituted with glycine or D-amino acid on contractile activity of chicken crop smooth muscle preparations. *Chem Pharm Bull (Tokyo)* 39**:** 2319-2322.

Hausdorff WP, Bouvier M, O'Dowd BF, Irons GP, Caron MG, Lefkowitz RJ (1989). Phosphorylation sites on two domains of the beta 2-adrenergic receptor are involved in distinct pathways of receptor desensitization. *J Biol Chem* 264**:** 12657-12665.

Heasman SJ, Ridley AJ (2008). Mammalian Rho GTPases: new insights into their functions from in vivo studies. *Nat Rev Mol Cell Biol* 9**:** 690-701.

Hedrick JA, Morse K, Shan L, Qiao X, Pang L, Wang S*, et al.* (2000). Identification of a human gastrointestinal tract and immune system receptor for the peptide neuromedin U. *Mol Pharmacol* 58**:** 870-875.

Henry RR, Chilton R, Garvey WT (2013). New options for the treatment of obesity and type 2 diabetes mellitus (narrative review). *J Diabetes Complications* 27**:** 508-518.

Hirshman CA, Lande B, Croxton TL (1999). Role of M2 muscarinic receptors in airway smooth muscle contraction. *Life Sciences* 64**:** 443-448.

Holst JJ (2007). The physiology of glucagon-like peptide 1. *Physiol Rev* 87**:** 1409-1439.

Honzawa M, Sudoh T, Minamino N, Kangawa K, Matsuo H (1990). Neuromedin U-like immunoreactivity in rat intestine: regional distribution and immunohistochemical study. *Neuropeptides* 15**:** 1-9.

Hosoya M, Moriya T, Kawamata Y, Ohkubo S, Fujii R, Matsui H*, et al.* (2000). Identification and functional characterization of a novel subtype of neuromedin U receptor. *J Biol Chem* 275**:** 29528-29532.

Howard AD, Wang R, Pong SS, Mellin TN, Strack A, Guan XM*, et al.* (2000). Identification of receptors for neuromedin U and its role in feeding. *Nature* 406**:** 70-74.

Hsu SH, Luo CW (2007). Molecular dissection of G protein preference using Gsalpha chimeras reveals novel ligand signaling of GPCRs. *Am J Physiol Endocrinol Metab* 293**:** E1021-1029.

Huang G, Shi LZ, Chi H (2009). Regulation of JNK and p38 MAPK in the immune system: signal integration, propagation and termination. *Cytokine* 48**:** 161-169.

Huang Y, Willars GB (2011). Generation of epitope-tagged GPCRs. *Methods Mol Biol* 746**:** 53-84.

Huang Y, Wilkinson GF, Willars GB (2010). Role of the signal peptide in the synthesis and processing of the glucagon-like peptide-1 receptor. *Br J Pharmacol* 159**:** 237-251.

Hudson BD, Shimpukade B, Mackenzie AE, Butcher AJ, Pediani JD, Christiansen E*, et al.* (2013). The pharmacology of TUG-891, a potent and selective agonist of the free fatty acid receptor 4 (FFA4/GPR120), demonstrates both potential opportunity and possible challenges to therapeutic agonism. *Mol Pharmacol* 84**:** 710-725.

Hunter T (2012). Why nature chose phosphate to modify proteins. *Philosophical Transactions of the Royal Society B: Biological Sciences* 367**:** 2513-2516.

Ida T, Mori K, Miyazato M, Egi Y, Abe S, Nakahara K*, et al.* (2005). Neuromedin s is a novel anorexigenic hormone. *Endocrinology* 146**:** 4217-4223.

Illing S, Mann A, Schulz S (2014). Heterologous regulation of agonist-independent μ-opioid receptor phosphorylation by protein kinase C. *Br J Pharmacol* 171**:** 1330-1340.

Ingallinella P, Peier AM, Pocai A, Marco AD, Desai K, Zytko K*, et al.* (2012). PEGylation of Neuromedin U yields a promising candidate for the treatment of obesity and diabetes. *Bioorg Med Chem* 20**:** 4751-4759.

Ip YT, Davis RJ (1998). Signal transduction by the c-Jun N-terminal kinase (JNK) — from inflammation to development. *Current Opinion in Cell Biology* 10**:** 205-219.

Irannejad R, Tomshine JC, Tomshine JR, Chevalier M, Mahoney JP, Steyaert J*, et al.* (2013). Conformational biosensors reveal GPCR signalling from endosomes. *Nature* 495**:** 534.

Islam Z, Inui T, Ishibashi O (2019). Gpr137b is an orphan G-protein-coupled receptor associated with M2 macrophage polarization. *Biochem Biophys Res Commun* 509**:** 657-663.

Ivanov TR, Lawrence CB, Stanley PJ, Luckman SM (2002). Evaluation of neuromedin U actions in energy homeostasis and pituitary function. *Endocrinology* 143**:** 3813-3821.

Iyer V, Tran TM, Foster E, Dai W, Clark RB, Knoll BJ (2006). Differential phosphorylation and dephosphorylation of beta2-adrenoceptor sites Ser262 and Ser355,356. *Br J Pharmacol* 147**:** 249-259.

Jafri F, El-Shewy HM, Lee MH, Kelly M, Luttrell DK, Luttrell LM (2006). Constitutive ERK1/2 activation by a chimeric neurokinin 1 receptor-beta-arrestin1 fusion protein. Probing the composition and function of the G protein-coupled receptor "signalsome". *J Biol Chem* 281**:** 19346-19357.

Jala VR, Shao WH, Haribabu B (2005). Phosphorylation-independent beta-arrestin translocation and internalization of leukotriene B4 receptors. *J Biol Chem* 280**:** 4880-4887.

Jayadev S, Smith RD, Jagadeesh G, Baukal AJ, Hunyady L, Catt KJ (1999). N-linked glycosylation is required for optimal AT1a angiotensin receptor expression in COS-7 cells. *Endocrinology* 140**:** 2010-2017.

Jean-Charles P-Y, Rajiv V, Shenoy SK (2016a). Ubiquitin-Related Roles of β-Arrestins in Endocytic Trafficking and Signal Transduction. *Journal of Cellular Physiology* 231**:** 2071-2080.

Jean-Charles P-Y, Kaur S, Shenoy SK (2017). G Protein-Coupled Receptor Signaling Through β-Arrestin-Dependent Mechanisms. *Journal of cardiovascular pharmacology* 70**:** 142-158.

Jean-Charles PY, Rajiv V, Shenoy SK (2016b). Ubiquitin-Related Roles of beta-Arrestins in Endocytic Trafficking and Signal Transduction. *J Cell Physiol* 231**:** 2071-2080.

Jensen DD, Lieu T, Halls ML, Veldhuis NA, Imlach WL, Mai QN*, et al.* (2017). Neurokinin 1 receptor signaling in endosomes mediates sustained nociception and is a viable therapeutic target for prolonged pain relief. *Science Translational Medicine* 9**:** eaal3447.

Jensen MD, Ryan DH, Apovian CM, Ard JD, Comuzzie AG, Donato KA*, et al.* (2014). 2013 AHA/ACC/TOS guideline for the management of overweight and obesity in adults: a report of the American College of Cardiology/American Heart Association Task Force on Practice Guidelines and The Obesity Society. *J Am Coll Cardiol* 63**:** 2985-3023.

Jethwa PH, Small CJ, Smith KL, Seth A, Darch SJ, Abbott CR*, et al.* (2005). Neuromedin U has a physiological role in the regulation of food intake and partially mediates the effects of leptin. *Am J Physiol Endocrinol Metab* 289**:** E301-305.

Jiang L, Teng GMK, Chan EYM, Au SWN, Wise H, Lee SST*, et al.* (2012). Impact of Cell Type and Epitope Tagging on Heterologous Expression of G Protein-Coupled Receptor: A Systematic Study on Angiotensin Type II Receptor. *PLoS One* 7**:** e47016.

Jones NA, Morton MF, Prendergast CE, Powell GL, Shankley NP, Hollingsworth SJ (2006). Neuromedin U stimulates contraction of human long saphenous vein and gastrointestinal smooth muscle in vitro. *Regul Pept* 136**:** 109-116.

Kaczmarek P, Malendowicz LK, Pruszynska-Oszmalek E, Wojciechowicz T, Szczepankiewicz D, Szkudelski T*, et al.* (2006). Neuromedin U receptor 1 expression in the rat endocrine pancreas and evidence suggesting neuromedin U suppressive effect on insulin secretion from isolated rat pancreatic islets. *Int J Mol Med* 18**:** 951-955.

Kage R, O'Harte F, Thim L, Conlon JM (1991). Rabbit neuromedin U-25: lack of conservation of a posttranslational processing site. *Regul Pept* 33**:** 191-198.

Kahsai AW, Xiao K, Rajagopal S, Ahn S, Shukla AK, Sun J*, et al.* (2011). Multiple ligand-specific conformations of the beta2-adrenergic receptor. *Nat Chem Biol* 7**:** 692-700.

Kaisho T, Nagai H, Asakawa T, Suzuki N, Fujita H, Matsumiya K*, et al.* (2017). Effects of peripheral administration of a Neuromedin U receptor 2-selective agonist on food intake and body weight in obese mice. *Int J Obes (Lond)* 41**:** 1790-1797.

Kalsbeek A, Kreier F, Fliers E, Sauerwein HP, Romijn JA, Buijs RM (2007). Minireview: Circadian control of metabolism by the suprachiasmatic nuclei. *Endocrinology* 148**:** 5635-5639.

Kanematsu-Yamaki Y, Nishizawa N, Kaisho T, Nagai H, Mochida T, Asakawa T*, et al.* (2017). Potent Body Weight-Lowering Effect of a Neuromedin U Receptor 2-selective PEGylated Peptide. *J Med Chem* 60**:** 6089-6097.

Kangawa K, Minamino N, Fukuda A, Matsuo H (1983). Neuromedin K: a novel mammalian tachykinin identified in porcine spinal cord. *Biochem Biophys Res Commun* 114**:** 533-540.

Kasper JM, Smith AE, Hommel JD (2018). Cocaine-Evoked Locomotor Activity Negatively Correlates With the Expression of Neuromedin U Receptor 2 in the Nucleus Accumbens. *Front Behav Neurosci* 12**:** 271.

Kaufman RJ (1990). Vectors used for expression in mammalian cells. *Methods Enzymol* 185**:** 487-511.

Kelly E (2006). G-protein-coupled receptor dephosphorylation at the cell surface. *Br J Pharmacol* 147**:** 235-236.

Kelly E, Bailey CP, Henderson G (2008). Agonist-selective mechanisms of GPCR desensitization. *Br J Pharmacol* 153 Suppl 1**:** S379-S388.

Ketterer K, Kong B, Frank D, Giese NA, Bauer A, Hoheisel J*, et al.* (2009). Neuromedin U is overexpressed in pancreatic cancer and increases invasiveness via the hepatocyte growth factor c-Met pathway. *Cancer Lett* 277**:** 72-81.

Khan SM, Sleno R, Gora S, Zylbergold P, Laverdure JP, Labbe JC*, et al.* (2013). The expanding roles of Gbetagamma subunits in G protein-coupled receptor signaling and drug action. *Pharmacol Rev* 65**:** 545-577.

Khorgami Z, Shoar S, Andalib A, Aminian A, Brethauer SA, Schauer PR (2017). Trends in utilization of bariatric surgery, 2010-2014: sleeve gastrectomy dominates. *Surg Obes Relat Dis* 13**:** 774-778.

Kim J, Ahn S, Ren XR, Whalen EJ, Reiter E, Wei H*, et al.* (2005). Functional antagonism of different G protein-coupled receptor kinases for beta-arrestin-mediated angiotensin II receptor signaling. *Proc Natl Acad Sci U S A* 102**:** 1442-1447.

Kim JY, Yang MS, Oh CD, Kim KT, Ha MJ, Kang SS*, et al.* (1999). Signalling pathway leading to an activation of mitogen-activated protein kinase by stimulating M3 muscarinic receptor. *Biochem J* 337 ( Pt 2)**:** 275-280.

Kim KS, Seeley RJ, Sandoval DA (2018). Signalling from the periphery to the brain that regulates energy homeostasis. *Nat Rev Neurosci* 19**:** 185-196.

Kiselyov K, Shin DM, Muallem S (2003). Signalling specificity in GPCR-dependent Ca2+ signalling. *Cell Signal* 15**:** 243-253.

Kliewer A, Reinscheid RK, Schulz S (2017). Emerging Paradigms of G Protein-Coupled Receptor Dephosphorylation. *Trends Pharmacol Sci* 38**:** 621-636.

Klopfleisch R, Meyer A, Lenze D, Hummel M, Gruber AD (2013). Canine cutaneous peripheral nerve sheath tumours versus fibrosarcomas can be differentiated by neuroectodermal marker genes in their transcriptome. *J Comp Pathol* 148**:** 197-205.

Kocan M, Pfleger KDG (2011). Study of GPCR–Protein Interactions by BRET. In: Willars GB, Challiss RAJ (eds). *Receptor Signal Transduction Protocols: Third Edition*, edn. Totowa, NJ: Humana Press. p^pp 357-371.

Kocan M, See HB, Sampaio NG, Eidne KA, Feldman BJ, Pfleger KDG (2009). Agonist-independent interactions between beta-arrestins and mutant vasopressin type II receptors associated with nephrogenic syndrome of inappropriate antidiuresis. *Molecular endocrinology (Baltimore, Md.)* 23**:** 559-571.

Kohsaka A, Bass J (2007). A sense of time: how molecular clocks organize metabolism. *Trends Endocrinol Metab* 18**:** 4-11.

Kojima M, Haruno R, Nakazato M, Date Y, Murakami N, Hanada R*, et al.* (2000). Purification and identification of neuromedin U as an endogenous ligand for an orphan receptor GPR66 (FM3). *Biochem Biophys Res Commun* 276**:** 435-438.

Kong KC, Butcher AJ, McWilliams P, Jones D, Wess J, Hamdan FF*, et al.* (2010). M<sub>3</sub>-muscarinic receptor promotes insulin release via receptor phosphorylation/arrestin-dependent activation of protein kinase D1. *Proceedings of the National Academy of Sciences* 107**:** 21181.

Kowalski TJ, Spar BD, Markowitz L, Maguire M, Golovko A, Yang S*, et al.* (2005). Transgenic overexpression of neuromedin U promotes leanness and hypophagia in mice. *J Endocrinol* 185**:** 151-164.

Kramer HK, Simon EJ (2000). mu and delta-opioid receptor agonists induce mitogen-activated protein kinase (MAPK) activation in the absence of receptor internalization. *Neuropharmacology* 39**:** 1707-1719.

Kranenburg O, Moolenaar WH (2001). Ras-MAP kinase signaling by lysophosphatidic acid and other G protein-coupled receptor agonists. *Oncogene* 20**:** 1540-1546.

Krueger KM, Daaka Y, Pitcher JA, Lefkowitz RJ (1997). The role of sequestration in G protein-coupled receptor resensitization. Regulation of beta2-adrenergic receptor dephosphorylation by vesicular acidification. *J Biol Chem* 272**:** 5-8.

Kruse AC, Hu J, Pan AC, Arlow DH, Rosenbaum DM, Rosemond E*, et al.* (2012). Structure and dynamics of the M3 muscarinic acetylcholine receptor. *Nature* 482**:** 552-556.

Kuhar JR, Bedini A, Melief EJ, Chiu YC, Striegel HN, Chavkin C (2015). Mu opioid receptor stimulation activates c-Jun N-terminal kinase 2 by distinct arrestin-dependent and independent mechanisms. *Cell Signal* 27**:** 1799-1806.

Kurosawa K, Sakura N, Hashimoto T (1996). Structure-activity relationships of neuromedin U. III. Contribution of two phenylalanine residues in dog neuromedin U-8 to the contractile activity. *Chem Pharm Bull (Tokyo)* 44**:** 1880-1884.

Kushner RF, Ryan DH (2014). Assessment and lifestyle management of patients with obesity: clinical recommendations from systematic reviews. *JAMA* 312**:** 943-952.

Lander ES, Linton LM, Birren B, Nusbaum C, Zody MC, Baldwin J*, et al.* (2001). Initial sequencing and analysis of the human genome. *Nature* 409**:** 860-921.

Latorraca NR, Venkatakrishnan AJ, Dror RO (2017a). GPCR Dynamics: Structures in Motion. *Chemical Reviews* 117**:** 139-155.

Latorraca NR, Venkatakrishnan AJ, Dror RO (2017b). GPCR Dynamics: Structures in Motion. *Chem Rev* 117**:** 139-155.

Lee IT, Chang AS, Manandhar M, Shan Y, Fan J, Izumo M*, et al.* (2015). Neuromedin s-producing neurons act as essential pacemakers in the suprachiasmatic nucleus to couple clock neurons and dictate circadian rhythms. *Neuron* 85**:** 1086-1102.

Lee KB, Pals-Rylaarsdam R, Benovic JL, Hosey MM (1998). Arrestin-independent internalization of the m1, m3, and m4 subtypes of muscarinic cholinergic receptors. *J Biol Chem* 273**:** 12967-12972.

Lee WH, Liu SB, Shen JH, Jin Y, Lai R, Zhang Y (2005). Identification and molecular cloning of a novel neuromedin U analog from the skin secretions of toad Bombina maxima. *Regul Pept* 129**:** 43-47.

Lefkowitz RJ (1998). G protein-coupled receptors. III. New roles for receptor kinases and beta-arrestins in receptor signaling and desensitization. *J Biol Chem* 273**:** 18677-18680.

Lefkowitz RJ (2013). A brief history of G-protein coupled receptors (Nobel Lecture). *Angew Chem Int Ed Engl* 52**:** 6366-6378.

Lefkowitz RJ, Shenoy SK (2005). Transduction of receptor signals by beta-arrestins. *Science* 308**:** 512-517.

Lefkowitz RJ, Pierce KL, Luttrell LM (2002). Dancing with Different Partners: Protein Kinase A Phosphorylation of Seven Membrane-Spanning Receptors Regulates Their G Protein-Coupling Specificity. *Mol Pharmacol* 62**:** 971.

Li X, Wilmanns M, Thornton J, Köhn M (2013). Elucidating Human Phosphatase-Substrate Networks. *Sci Signal* 6**:** rs10.

Li X, Zhou M, Huang W, Yang H (2017a). N-glycosylation of the beta2 adrenergic receptor regulates receptor function by modulating dimerization. *FEBS J* 284**:** 2004-2018.

Li X, Niu M, Su J, Ma Z, Jin M, Qiao W*, et al.* (2017b). Cloning and expression patterns of neuromedin U and its receptors in pigs. *Neuropeptides* 64**:** 47-60.

Li Y, Song J, Tong Y, Chung SK, Wong YH (2017c). RGS19 upregulates Nm23-H1/2 metastasis suppressors by transcriptional activation via the cAMP/PKA/CREB pathway. *Oncotarget* 8**:** 69945-69960.

Lin TY, Wu FJ, Lee WY, Hsiao CL, Luo CW (2013). Ovarian regulation of neuromedin U and its local actions in the ovary, mediated through neuromedin U receptor 2. *Am J Physiol Endocrinol Metab* 304**:** E800-809.

Lin TY, Wu FJ, Chang CL, Li Z, Luo CW (2016). NMU signaling promotes endometrial cancer cell progression by modulating adhesion signaling. *Oncotarget* 7**:** 10228-10242.

Lohse MJ, Nuber S, Hoffmann C (2012). Fluorescence/bioluminescence resonance energy transfer techniques to study G-protein-coupled receptor activation and signaling. *Pharmacol Rev* 64**:** 299-336.

Lowe JD, Sanderson HS, Cooke AE, Ostovar M, Tsisanova E, Withey SL*, et al.* (2015). Role of G Protein–Coupled Receptor Kinases 2 and 3 in <em>μ</em>-Opioid Receptor Desensitization and Internalization. *Mol Pharmacol* 88**:** 347.

Lu J, Willars GB (2019). Endothelin-converting enzyme-1 regulates glucagon-like peptide-1 receptor signalling and resensitisation. *Biochemical Journal* 476**:** 513-533.

Luo J, Busillo JM, Benovic JL (2008a). M<sub>3</sub> Muscarinic Acetylcholine Receptor-Mediated Signaling Is Regulated by Distinct Mechanisms. *Mol Pharmacol* 74**:** 338.

Luo J, Busillo JM, Benovic JL (2008b). M3 muscarinic acetylcholine receptor-mediated signaling is regulated by distinct mechanisms. *Mol Pharmacol* 74**:** 338-347.

Luttrell LM (2008). Reviews in molecular biology and biotechnology: transmembrane signaling by G protein-coupled receptors. *Mol Biotechnol* 39**:** 239-264.

Luttrell LM, Lefkowitz RJ (2002). The role of beta-arrestins in the termination and transduction of G-protein-coupled receptor signals. *J Cell Sci* 115**:** 455-465.

Luttrell LM, Gesty-Palmer D (2010). Beyond desensitization: physiological relevance of arrestin-dependent signaling. *Pharmacol Rev* 62**:** 305-330.

Luttrell LM, Daaka Y, Della Rocca GJ, Lefkowitz RJ (1997). G protein-coupled receptors mediate two functionally distinct pathways of tyrosine phosphorylation in rat 1a fibroblasts. Shc phosphorylation and receptor endocytosis correlate with activation of Erk kinases. *J Biol Chem* 272**:** 31648-31656.

Luttrell LM, Roudabush FL, Choy EW, Miller WE, Field ME, Pierce KL*, et al.* (2001). Activation and targeting of extracellular signal-regulated kinases by beta-arrestin scaffolds. *Proc Natl Acad Sci U S A* 98**:** 2449-2454.

Luttrell LM, Ferguson SS, Daaka Y, Miller WE, Maudsley S, Della Rocca GJ*, et al.* (1999a). Beta-arrestin-dependent formation of beta2 adrenergic receptor-Src protein kinase complexes. *Science* 283**:** 655-661.

Luttrell LM, Ferguson SSG, Daaka Y, Miller WE, Maudsley S, Della Rocca GJ*, et al.* (1999b). β-Arrestin-Dependent Formation of β<sub>2</sub> Adrenergic Receptor-Src Protein Kinase Complexes. *Science* 283**:** 655.

Magni P, Dozio E, Ruscica M, Celotti F, Masini MA, Prato P*, et al.* (2009). Feeding behavior in mammals including humans. *Ann N Y Acad Sci* 1163**:** 221-232.

Makaronidis JM, Batterham RL (2018). Obesity, body weight regulation and the brain: insights from fMRI. *Br J Radiol* 91**:** 20170910.

Malendowicz LK, Nussdorfer GG, Nowak KW, Mazzocchi G (1993). Effects of neuromedin U-8 on the rat pituitary-adrenocortical axis. *In Vivo* 7**:** 419-422.

Malendowicz LK, Nussdorfer GG, Markowska A, Tortorella C, Nowak M, Warchol JB (1994a). Effects of neuromedin U (NMU)-8 on the rat hypothalamo-pituitary-adrenal axis. Evidence of a direct effect of NMU-8 on the adrenal gland. *Neuropeptides* 26**:** 47-53.

Malendowicz LK, Andreis PG, Markowska A, Nowak M, Warchol JB, Neri G*, et al.* (1994b). Effects of neuromedin U-8 on the secretory activity of the rat adrenal cortex: evidence for an indirect action requiring the presence of the zona medullaris. *Res Exp Med (Berl)* 194**:** 69-79.

Marchese A, Benovic JL (2001). Agonist-promoted ubiquitination of the G protein-coupled receptor CXCR4 mediates lysosomal sorting. *J Biol Chem* 276**:** 45509-45512.

Marchese A, Trejo J (2013). Ubiquitin-dependent regulation of G protein-coupled receptor trafficking and signaling. *Cell Signal* 25**:** 707-716.

Martínez-Morales Juan C, Romero-Ávila MT, Reyes-Cruz G, García-Sáinz JA (2018). S1P<sub>1</sub> receptor phosphorylation, internalization, and interaction with Rab proteins: effects of sphingosine 1-phosphate, FTY720-P, phorbol esters, and paroxetine. *Bioscience Reports* 38**:** BSR20181612.

Martinez VG, O'Driscoll L (2015). Neuromedin U: a multifunctional neuropeptide with pleiotropic roles. *Clin Chem* 61**:** 471-482.

Maruyama K, Konno N, Ishiguro K, Wakasugi T, Uchiyama M, Shioda S*, et al.* (2008). Isolation and characterisation of four cDNAs encoding neuromedin U (NMU) from the brain and gut of goldfish, and the inhibitory effect of a deduced NMU on food intake and locomotor activity. *J Neuroendocrinol* 20**:** 71-78.

Maxfield FR (2014). Role of endosomes and lysosomes in human disease. *Cold Spring Harb Perspect Biol* 6**:** a016931.

McCue DL, Kasper JM, Hommel JD (2017). Regulation of motivation for food by neuromedin U in the paraventricular nucleus and the dorsal raphe nucleus. *Int J Obes (Lond)* 41**:** 120-128.

McDonald PH, Chow CW, Miller WE, Laporte SA, Field ME, Lin FT*, et al.* (2000). Beta-arrestin 2: a receptor-regulated MAPK scaffold for the activation of JNK3. *Science* 290**:** 1574-1577.

McGarvey JC, Xiao K, Bowman SL, Mamonova T, Zhang Q, Bisello A*, et al.* (2016). Actin-Sorting Nexin 27 (SNX27)-Retromer Complex Mediates Rapid Parathyroid Hormone Receptor Recycling. *J Biol Chem* 291**:** 10986-11002.

Meng T, Su HR, Binkert C, Fischli W, Zhou L, Shen JK*, et al.* (2008). Identification of non-peptidic neuromedin U receptor modulators by a robust homogeneous screening assay. *Acta Pharmacol Sin* 29**:** 517-527.

Micewicz ED, Bahattab OS, Willars GB, Waring AJ, Navab M, Whitelegge JP*, et al.* (2015). Small lipidated anti-obesity compounds derived from neuromedin U. *Eur J Med Chem* 101**:** 616-626.

Millar RP, Newton CL (2010). The year in G protein-coupled receptor research. *Mol Endocrinol* 24**:** 261-274.

Miller-Gallacher JL, Nehme R, Warne T, Edwards PC, Schertler GF, Leslie AG*, et al.* (2014). The 2.1 A resolution structure of cyanopindolol-bound beta1-adrenoceptor identifies an intramembrane Na+ ion that stabilises the ligand-free receptor. *PLoS One* 9**:** e92727.

Milligan G, Kostenis E (2006). Heterotrimeric G-proteins: a short history. *Br J Pharmacol* 147 Suppl 1**:** S46-55.

Min C, Zheng M, Zhang X, Guo S, Kwon K-J, Shin CY*, et al.* (2015). N-linked Glycosylation on the N-terminus of the dopamine D2 and D3 receptors determines receptor association with specific microdomains in the plasma membrane. *Biochimica et Biophysica Acta (BBA) - Molecular Cell Research* 1853**:** 41-51.

Minamino N, Kangawa K, Matsuo H (1985). Neuromedin U-8 and U-25: novel uterus stimulating and hypertensive peptides identified in porcine spinal cord. *Biochem Biophys Res Commun* 130**:** 1078-1085.

Minamino N, Kangawa K, Honzawa M, Matsuo H (1988). Isolation and structural determination of rat neuromedin U. *Biochem Biophys Res Commun* 156**:** 355-360.

Mitchell JD, Maguire JJ, Davenport AP (2009). Emerging pharmacology and physiology of neuromedin U and the structurally related peptide neuromedin S. *Br J Pharmacol* 158**:** 87-103.

Miyazato M, Mori K, Ida T, Kojima M, Murakami N, Kangawa K (2008). Identification and functional analysis of a novel ligand for G protein-coupled receptor, Neuromedin S. *Regul Pept* 145**:** 37-41.

Mohan ML, Vasudevan NT, Gupta MK, Martelli EE, Naga Prasad SV (2012). G-protein coupled receptor resensitization-appreciating the balancing act of receptor function. *Current molecular pharmacology*.

Moore CA, Milano SK, Benovic JL (2007). Regulation of receptor trafficking by GRKs and arrestins. *Annu Rev Physiol* 69**:** 451-482.

Mores KL, Cassell RJ, van Rijn RM (2018). Arrestin recruitment and signaling by G protein-coupled receptor heteromers. *Neuropharmacology*.

Mori K, Miyazato M (2016). Chapter 13 - Neuromedin U/S. In: Takei Y, Ando H, Tsutsui K (eds). *Handbook of Hormones*, edn. San Diego: Academic Press. p^pp 94-e13-93.

Mori K, Miyazato M, Kangawa K (2008). Neuromedin S: discovery and functions. *Results Probl Cell Differ* 46**:** 201-212.

Mori K, Miyazato M, Ida T, Murakami N, Serino R, Ueta Y*, et al.* (2005). Identification of neuromedin S and its possible role in the mammalian circadian oscillator system. *EMBO J* 24**:** 325-335.

Moriyama M, Furue H, Katafuchi T, Teranishi H, Sato T, Kano T*, et al.* (2004). Presynaptic modulation by neuromedin U of sensory synaptic transmission in rat spinal dorsal horn neurones. *J Physiol* 559**:** 707-713.

Morley JE, Levine AS (1982). Corticotrophin releasing factor, grooming and ingestive behavior. *Life Sci* 31**:** 1459-1464.

Mullershausen F, Zecri F, Cetin C, Billich A, Guerini D, Seuwen K (2009). Persistent signaling induced by FTY720-phosphate is mediated by internalized S1P1 receptors. *Nature Chemical Biology* 5**:** 428.

Murphy JE, Roosterman D, Cottrell GS, Padilla BE, Feld M, Brand E*, et al.* (2011). Protein phosphatase 2A mediates resensitization of the neurokinin 1 receptor. *American Journal of Physiology-Cell Physiology* 301**:** C780-C791.

Murphy R, Turner CA, Furness JB, Parker L, Giraud A (1990). Isolation and microsequence analysis of a novel form of neuromedin U from guinea pig small intestine. *Peptides* 11**:** 613-617.

Muto T, Tsuchiya D, Morikawa K, Jingami H (2007). Structures of the extracellular regions of the group II/III metabotropic glutamate receptors. *Proc Natl Acad Sci U S A* 104**:** 3759-3764.

Nagai H, Kaisho T, Yokoyama K, Asakawa T, Fujita H, Matsumiya K*, et al.* (2018). Differential effects of selective agonists of neuromedin U1 and U2 receptors in obese and diabetic mice. *Br J Pharmacol* 175**:** 359-373.

Nakagawa T, Asahi M (2013). beta1-adrenergic receptor recycles via a membranous organelle, recycling endosome, by binding with sorting nexin27. *J Membr Biol* 246**:** 571-579.

Nakahara K, Kojima M, Hanada R, Egi Y, Ida T, Miyazato M*, et al.* (2004a). Neuromedin U is involved in nociceptive reflexes and adaptation to environmental stimuli in mice. *Biochem Biophys Res Commun* 323**:** 615-620.

Nakahara K, Katayama T, Maruyama K, Ida T, Mori K, Miyazato M*, et al.* (2010). Comparison of feeding suppression by the anorexigenic hormones neuromedin U and neuromedin S in rats. *J Endocrinol* 207**:** 185-193.

Nakahara K, Hanada R, Murakami N, Teranishi H, Ohgusu H, Fukushima N*, et al.* (2004b). The gut-brain peptide neuromedin U is involved in the mammalian circadian oscillator system. *Biochem Biophys Res Commun* 318**:** 156-161.

Nakazato M, Hanada R, Murakami N, Date Y, Mondal MS, Kojima M*, et al.* (2000). Central effects of neuromedin U in the regulation of energy homeostasis. *Biochem Biophys Res Commun* 277**:** 191-194.

Namkung Y, Sibley DR (2004). Protein kinase C mediates phosphorylation, desensitization, and trafficking of the D2 dopamine receptor. *J Biol Chem* 279**:** 49533-49541.

Narayanaswami V, Dwoskin LP (2017). Obesity: Current and potential pharmacotherapeutics and targets. *Pharmacol Ther* 170**:** 116-147.

Neuner P, Peier AM, Talamo F, Ingallinella P, Lahm A, Barbato G*, et al.* (2014). Development of a neuromedin U-human serum albumin conjugate as a long-acting candidate for the treatment of obesity and diabetes. Comparison with the PEGylated peptide. *J Pept Sci* 20**:** 7-19.

New DC, Wong YH (2007). Molecular mechanisms mediating the G protein-coupled receptor regulation of cell cycle progression. *J Mol Signal* 2**:** 2.

Niimi M, Murao K, Taminato T (2001). Central administration of neuromedin U activates neurons in ventrobasal hypothalamus and brainstem. *Endocrine* 16**:** 201-206.

Nijenhuis WA, Oosterom J, Adan RA (2001). AgRP(83-132) acts as an inverse agonist on the human-melanocortin-4 receptor. *Mol Endocrinol* 15**:** 164-171.

Nishimoto S, Nishida E (2006). MAPK signalling: ERK5 versus ERK1/2. *EMBO Rep* 7**:** 782-786.

Nobles KN, Xiao K, Ahn S, Shukla AK, Lam CM, Rajagopal S*, et al.* (2011a). Distinct phosphorylation sites on the β(2)-adrenergic receptor establish a barcode that encodes differential functions of β-arrestin. *Sci Signal* 4**:** ra51-ra51.

Nobles KN, Xiao K, Ahn S, Shukla AK, Lam CM, Rajagopal S*, et al.* (2011b). Distinct phosphorylation sites on the beta(2)-adrenergic receptor establish a barcode that encodes differential functions of beta-arrestin. *Sci Signal* 4**:** ra51.

Novak CM, Zhang M, Levine JA (2006). Neuromedin U in the Paraventricular and Arcuate Hypothalamic Nuclei Increases Non-Exercise Activity Thermogenesis. *J Neuroendocrinol* 18**:** 594-601.

Nuber S, Zabel U, Lorenz K, Nuber A, Milligan G, Tobin AB*, et al.* (2016). β-Arrestin biosensors reveal a rapid, receptor-dependent activation/deactivation cycle. *Nature* 531**:** 661.

O'Harte F, Bockman CS, Abel PW, Conlon JM (1991a). Isolation, structural characterization and pharmacological activity of dog neuromedin U. *Peptides* 12**:** 11-15.

O'Harte F, Bockman CS, Zeng W, Abel PW, Harvey S, Conlon JM (1991b). Primary structure and pharmacological activity of a nonapeptide related to neuromedin U isolated from chicken intestine. *Peptides* 12**:** 809-812.

Oakley RH, Laporte SA, Holt JA, Barak LS, Caron MG (1999). Association of beta-arrestin with G protein-coupled receptors during clathrin-mediated endocytosis dictates the profile of receptor resensitization. *J Biol Chem* 274**:** 32248-32257.

Oakley RH, Laporte SA, Holt JA, Caron MG, Barak LS (2000). Differential affinities of visual arrestin, beta arrestin1, and beta arrestin2 for G protein-coupled receptors delineate two major classes of receptors. *J Biol Chem* 275**:** 17201-17210.

Oakley RH, Laporte SA, Holt JA, Barak LS, Caron MG (2001). Molecular determinants underlying the formation of stable intracellular G protein-coupled receptor-beta-arrestin complexes after receptor endocytosis*. *J Biol Chem* 276**:** 19452-19460.

Oppermann M, Freedman NJ, Alexander RW, Lefkowitz RJ (1996). Phosphorylation of the type 1A angiotensin II receptor by G protein-coupled receptor kinases and protein kinase C. *J Biol Chem* 271**:** 13266-13272.

Ozaki Y, Onaka T, Nakazato M, Saito J, Kanemoto K, Matsumoto T*, et al.* (2002). Centrally administered neuromedin U activates neurosecretion and induction of c-fos messenger ribonucleic acid in the paraventricular and supraoptic nuclei of rat. *Endocrinology* 143**:** 4320-4329.

Padilla BE, Cottrell GS, Roosterman D, Pikios S, Muller L, Steinhoff M*, et al.* (2007). Endothelin-converting enzyme-1 regulates endosomal sorting of calcitonin receptor-like receptor and beta-arrestins. *J Cell Biol* 179**:** 981-997.

Paing MM, Stutts AB, Kohout TA, Lefkowitz RJ, Trejo J (2002). beta -Arrestins regulate protease-activated receptor-1 desensitization but not internalization or Down-regulation. *J Biol Chem* 277**:** 1292-1300.

Pal K, Mathur M, Kumar P, DeFea K (2013). Divergent beta-arrestin-dependent signaling events are dependent upon sequences within G-protein-coupled receptor C termini. *J Biol Chem* 288**:** 3265-3274.

Palczewski K, Kumasaka T, Hori T, Behnke CA, Motoshima H, Fox BA*, et al.* (2000). Crystal structure of rhodopsin: A G protein-coupled receptor. *Science* 289**:** 739-745.

Paschke R, Frenzel R, Lorenz S, Breitwieser GE, Miedlich SU (2007). Functional Desensitization of the Extracellular Calcium-Sensing Receptor Is Regulated via Distinct Mechanisms: Role of G Protein-Coupled Receptor Kinases, Protein Kinase C and β-Arrestins. *Endocrinology* 148**:** 2398-2404.

Patel D (2015). Pharmacotherapy for the management of obesity. *Metabolism* 64**:** 1376-1385.

Pavlos NJ, Friedman PA (2017). GPCR Signaling and Trafficking: The Long and Short of It. *Trends Endocrinol Metab* 28**:** 213-226.

Pearce A, Sanders L, Brighton PJ, Rana S, Konje JC, Willets JM (2017). Reciprocal regulation of beta2-adrenoceptor-activated cAMP response-element binding protein signalling by arrestin2 and arrestin3. *Cell Signal* 38**:** 182-191.

Peier A, Kosinski J, Cox-York K, Qian Y, Desai K, Feng Y*, et al.* (2009). The antiobesity effects of centrally administered neuromedin U and neuromedin S are mediated predominantly by the neuromedin U receptor 2 (NMUR2). *Endocrinology* 150**:** 3101-3109.

Pelayo J-C, Poole DP, Steinhoff M, Cottrell GS, Bunnett NW (2011). Endothelin-converting enzyme-1 regulates trafficking and signalling of the neurokinin 1 receptor in endosomes of myenteric neurones. *J Physiol* 589**:** 5213-5230.

Perron Bt, Roy S, Gallo-Payet N (2010). Role of Asparagine-Linked Glycosylation in Cell Surface Expression and Function of the Human Adrenocorticotropin Receptor (Melanocortin 2 Receptor) in 293/FRT Cells. *Endocrinology* 151**:** 660-670.

Peterhans C, Lally CCM, Ostermaier MK, Sommer ME, Standfuss J (2016). Functional map of arrestin binding to phosphorylated opsin, with and without agonist. *Scientific Reports* 6**:** 28686.

Peterson YK, Luttrell LM (2017). The Diverse Roles of Arrestin Scaffolds in G Protein-Coupled Receptor Signaling. *Pharmacol Rev* 69**:** 256-297.

Pfleger KD, Eidne KA (2006). Illuminating insights into protein-protein interactions using bioluminescence resonance energy transfer (BRET). *Nat Methods* 3**:** 165-174.

Pierce KL, Lefkowitz RJ (2001). Classical and new roles of beta-arrestins in the regulation of G-protein-coupled receptors. *Nat Rev Neurosci* 2**:** 727-733.

Pierce KL, Premont RT, Lefkowitz RJ (2002). Seven-transmembrane receptors. *Nat Rev Mol Cell Biol* 3**:** 639-650.

Pitcher J, Lohse MJ, Codina J, Caron MG, Lefkowitz RJ (1992). Desensitization of the isolated .beta.2-adrenergic receptor by .beta.-adrenergic receptor kinase, cAMP-dependent protein kinase, and protein kinase C occurs via distinct molecular mechanisms. *Biochemistry* 31**:** 3193-3197.

Pitcher JA, Freedman NJ, Lefkowitz RJ (1998). G protein-coupled receptor kinases. *Annu Rev Biochem* 67**:** 653-692.

Plotnikov A, Zehorai E, Procaccia S, Seger R (2011). The MAPK cascades: signaling components, nuclear roles and mechanisms of nuclear translocation. *Biochim Biophys Acta* 1813**:** 1619-1633.

Poll F, Doll C, Schulz S (2011). Rapid dephosphorylation of G protein-coupled receptors by protein phosphatase 1beta is required for termination of beta-arrestin-dependent signaling. *J Biol Chem* 286**:** 32931-32936.

Poll F, Lehmann D, Illing S, Ginj M, Jacobs S, Lupp A*, et al.* (2010). Pasireotide and octreotide stimulate distinct patterns of sst2A somatostatin receptor phosphorylation. *Mol Endocrinol* 24**:** 436-446.

Poulin B, Butcher A, McWilliams P, Bourgognon J-M, Pawlak R, Kong KC*, et al.* (2010). The M<sub>3</sub>-muscarinic receptor regulates learning and memory in a receptor phosphorylation/arrestin-dependent manner. *Proceedings of the National Academy of Sciences* 107**:** 9440.

Premont RT, Gainetdinov RR (2007). Physiological roles of G protein-coupled receptor kinases and arrestins. *Annu Rev Physiol* 69**:** 511-534.

Prendergast CE, Morton MF, Figueroa KW, Wu X, Shankley NP (2006). Species-dependent smooth muscle contraction to Neuromedin U and determination of the receptor subtypes mediating contraction using NMU1 receptor knockout mice. *Br J Pharmacol* 147**:** 886-896.

Prihandoko R, Bradley SJ, Tobin AB, Butcher AJ (2015a). Determination of GPCR Phosphorylation Status: Establishing a Phosphorylation Barcode. *Curr Protoc Pharmacol* 69**:** 2 13 11-26.

Prihandoko R, Bradley SJ, Tobin AB, Butcher AJ (2015b). Determination of GPCR Phosphorylation Status: Establishing a Phosphorylation Barcode. *Current Protocols in Pharmacology* 69**:** 2.13.11-12.13.26.

Prihandoko R, Alvarez-Curto E, Hudson BD, Butcher AJ, Ulven T, Miller AM*, et al.* (2016a). Distinct Phosphorylation Clusters Determine the Signaling Outcome of Free Fatty Acid Receptor 4/G Protein–Coupled Receptor 120. *Mol Pharmacol* 89**:** 505.

Prihandoko R, Alvarez-Curto E, Hudson BD, Butcher AJ, Ulven T, Miller AM*, et al.* (2016b). Distinct Phosphorylation Clusters Determine the Signaling Outcome of Free Fatty Acid Receptor 4/G Protein-Coupled Receptor 120. *Mol Pharmacol* 89**:** 505-520.

Qiu DL, Chu CP, Tsukino H, Shirasaka T, Nakao H, Kato K*, et al.* (2005). Neuromedin U receptor-2 mRNA and HCN channels mRNA expression in NMU-sensitive neurons in rat hypothalamic paraventricular nucleus. *Neurosci Lett* 374**:** 69-72.

Quan H, Funabashi T, Furuta M, Kimura F (2003). Effects of neuromedin U on the pulsatile LH secretion in ovariectomized rats in association with feeding conditions. *Biochem Biophys Res Commun* 311**:** 721-727.

Raddatz R, Wilson AE, Artymyshyn R, Bonini JA, Borowsky B, Boteju LW*, et al.* (2000). Identification and characterization of two neuromedin U receptors differentially expressed in peripheral tissues and the central nervous system. *J Biol Chem* 275**:** 32452-32459.

Rahman AA, Shahid IZ, Pilowsky PM (2011). Intrathecal neuromedin U induces biphasic effects on sympathetic vasomotor tone, increases respiratory drive and attenuates sympathetic reflexes in rat. *Br J Pharmacol* 164**:** 617-631.

Rahman AA, Shahid IZ, Pilowsky PM (2012). Differential cardiorespiratory and sympathetic reflex responses to microinjection of neuromedin U in rat rostral ventrolateral medulla. *J Pharmacol Exp Ther* 341**:** 213-224.

Rahman AA, Shahid IZ, Pilowsky PM (2013). Neuromedin U causes biphasic cardiovascular effects and impairs baroreflex function in rostral ventrolateral medulla of spontaneously hypertensive rat. *Peptides* 44**:** 15-24.

Rajagopal S, Shenoy SK (2018). GPCR desensitization: Acute and prolonged phases. *Cell Signal* 41**:** 9-16.

Rajagopal S, Rajagopal K, Lefkowitz RJ (2010a). Teaching old receptors new tricks: biasing seven-transmembrane receptors. *Nature Reviews Drug Discovery* 9**:** 373.

Rajagopal S, Rajagopal K, Lefkowitz RJ (2010b). Teaching old receptors new tricks: biasing seven-transmembrane receptors. *Nat Rev Drug Discov* 9**:** 373-386.

Rajagopal S, Ahn S, Rominger DH, Gowen-MacDonald W, Lam CM, Dewire SM*, et al.* (2011). Quantifying ligand bias at seven-transmembrane receptors. *Mol Pharmacol* 80**:** 367-377.

Raposinho PD, Pierroz DD, Broqua P, White RB, Pedrazzini T, Aubert ML (2001). Chronic administration of neuropeptide Y into the lateral ventricle of C57BL/6J male mice produces an obesity syndrome including hyperphagia, hyperleptinemia, insulin resistance, and hypogonadism. *Mol Cell Endocrinol* 185**:** 195-204.

Rasmussen SG, DeVree BT, Zou Y, Kruse AC, Chung KY, Kobilka TS*, et al.* (2011). Crystal structure of the beta2 adrenergic receptor-Gs protein complex. *Nature* 477**:** 549-555.

Ren X-R, Reiter E, Ahn S, Kim J, Chen W, Lefkowitz RJ (2005). Different G protein-coupled receptor kinases govern G protein and β-arrestin-mediated signaling of V2 vasopressin receptor. *Proc Natl Acad Sci U S A* 102**:** 1448.

Rincon M, Davis RJ (2009). Regulation of the immune response by stress-activated protein kinases. *Immunol Rev* 228**:** 212-224.

Rock CL, Flatt SW, Sherwood NE, Karanja N, Pakiz B, Thomson CA (2010). Effect of a free prepared meal and incentivized weight loss program on weight loss and weight loss

maintenance in obese and overweight women: a randomized controlled trial. *JAMA* 304**:** 1803-1810.

Roettger BF, Rentsch RU, Pinon D, Holicky E, Hadac E, Larkin JM*, et al.* (1995). Dual pathways of internalization of the cholecystokinin receptor. *J Cell Biol* 128**:** 1029.

Roosterman D, Cottrell GS, Padilla BE, Muller L, Eckman CB, Bunnett NW*, et al.* (2007). Endothelin-converting enzyme 1 degrades neuropeptides in endosomes to control receptor recycling. *Proc Natl Acad Sci U S A* 104**:** 11838-11843.

Ross EM, Wilkie TM (2000). GTPase-activating proteins for heterotrimeric G proteins: regulators of G protein signaling (RGS) and RGS-like proteins. *Annu Rev Biochem* 69**:** 795-827.

Rucinski M, Ziolkowska A, Tyczewska M, Szyszka M, Malendowicz LK (2008). Neuromedin U directly stimulates growth of cultured rat calvarial osteoblast-like cells acting via the NMU receptor 2 isoform. *Int J Mol Med* 22**:** 363-368.

Sacco F, Perfetto L, Castagnoli L, Cesareni G (2012). The human phosphatase interactome: An intricate family portrait. *FEBS Letters* 586**:** 2732-2739.

Sainz N, Barrenetxe J, Moreno-Aliaga MJ, Martinez JA (2015). Leptin resistance and diet-induced obesity: central and peripheral actions of leptin. *Metabolism* 64**:** 35-46.

Sakamoto T, Mori K, Nakahara K, Miyazato M, Kangawa K, Sameshima H*, et al.* (2007). Neuromedin S exerts an antidiuretic action in rats. *Biochem Biophys Res Commun* 361**:** 457-461.

Sakamoto T, Mori K, Miyazato M, Kangawa K, Sameshima H, Nakahara K*, et al.* (2008). Involvement of neuromedin S in the oxytocin release response to suckling stimulus. *Biochem Biophys Res Commun* 375**:** 49-53.

Sakura N, Kurosawa K, Hashimoto T (1995). Structure-activity relationships of neuromedin U. I. Contractile activity of dog neuromedin U-related peptides on isolated chicken crop smooth muscle. *Chem Pharm Bull (Tokyo)* 43**:** 1148-1153.

Sakura N, Ohta S, Uchida Y, Kurosawa K, Okimura K, Hashimoto T (1991). Structure-activity relationships of rat neuromedin U for smooth muscle contraction. *Chem Pharm Bull (Tokyo)* 39**:** 2016-2020.

Salahpour A, Espinoza S, Masri B, Lam V, Barak LS, Gainetdinov RR (2012). BRET biosensors to study GPCR biology, pharmacology, and signal transduction. *Frontiers in endocrinology* 3**:** 105-105.

Sampson CM, Kasper JM, Felsing DE, Raval SR, Ye N, Wang P*, et al.* (2018). Small-Molecule Neuromedin U Receptor 2 Agonists Suppress Food Intake and Decrease Visceral Fat in Animal Models. *Pharmacol Res Perspect* 6**:** e00425.

Sandoval DA, D'Alessio DA (2015). Physiology of proglucagon peptides: role of glucagon and GLP-1 in health and disease. *Physiol Rev* 95**:** 513-548.

Santos R, Ursu O, Gaulton A, Bento AP, Donadi RS, Bologa CG*, et al.* (2017). A comprehensive map of molecular drug targets. *Nat Rev Drug Discov* 16**:** 19-34.

Saper CB, Chou TC, Elmquist JK (2002). The need to feed: homeostatic and hedonic control of eating. *Neuron* 36**:** 199-211.

Sarma U, Ghosh I (2012). Different designs of kinase-phosphatase interactions and phosphatase sequestration shapes the robustness and signal flow in the MAPK cascade. *BMC systems biology* 6**:** 82-82.

Sasaki T, Shimizu T, Wakiguchi H, Yokotani K (2008). Centrally administered neuromedin U elevates plasma adrenaline by brain prostanoid TP receptor-mediated mechanisms in rats. *Eur J Pharmacol* 592**:** 81-86.

Sato E, Miyamoto Y (1988). [Cultivation of mouse oocytes in vitro: the ability to resume meiosis]. *Jikken Dobutsu* 37**:** 231-238.

Sato S, Hanada R, Kimura A, Abe T, Matsumoto T, Iwasaki M*, et al.* (2007). Central control of bone remodeling by neuromedin U. *Nat Med* 13**:** 1234-1240.

Sawutz DG, Lanier SM, Warren CD, Graham RM (1987). Glycosylation of the mammalian alpha 1-adrenergic receptor by complex type N-linked oligosaccharides. *Mol Pharmacol* 32**:** 565-571.

Schmidlin F, Dery O, DeFea KO, Slice L, Patierno S, Sternini C*, et al.* (2001). Dynamin and Rab5a-dependent trafficking and signaling of the neurokinin 1 receptor. *J Biol Chem* 276**:** 25427-25437.

Schwartz MW, Woods SC, Porte D, Jr., Seeley RJ, Baskin DG (2000). Central nervous system control of food intake. *Nature* 404**:** 661-671.

Seachrist JL, Anborgh PH, Ferguson SS (2000). beta 2-adrenergic receptor internalization, endosomal sorting, and plasma membrane recycling are regulated by rab GTPases. *J Biol Chem* 275**:** 27221-27228.

Seger R, Krebs EG (1995a). The MAPK signaling cascade. *FASEB J* 9**:** 726-735.

Seger R, Biener Y, Feinstein R, Hanoch T, Gazit A, Zick Y (1995b). Differential activation of mitogen-activated protein kinase and S6 kinase signaling pathways by 12-O-tetradecanoylphorbol-13-acetate (TPA) and insulin. Evidence for involvement of a TPA-stimulated protein-tyrosine kinase. *J Biol Chem* 270**:** 28325-28330.

Shan L, Qiao X, Crona JH, Behan J, Wang S, Laz T*, et al.* (2000). Identification of a novel neuromedin U receptor subtype expressed in the central nervous system. *J Biol Chem* 275**:** 39482-39486.

Shaul YD, Gibor G, Plotnikov A, Seger R (2009). Specific phosphorylation and activation of ERK1c by MEK1b: a unique route in the ERK cascade. *Genes Dev* 23**:** 1779-1790.

Shenoy SK, Lefkowitz RJ (2011). beta-Arrestin-mediated receptor trafficking and signal transduction. *Trends Pharmacol Sci* 32**:** 521-533.

Shenoy SK, McDonald PH, Kohout TA, Lefkowitz RJ (2001). Regulation of receptor fate by ubiquitination of activated beta 2-adrenergic receptor and beta-arrestin. *Science* 294**:** 1307-1313.

Shenoy SK, Xiao K, Venkataramanan V, Snyder PM, Freedman NJ, Weissman AM (2008). Nedd4 mediates agonist-dependent ubiquitination, lysosomal targeting, and degradation of the beta2-adrenergic receptor. *J Biol Chem* 283**:** 22166-22176.

Shenoy SK, Drake MT, Nelson CD, Houtz DA, Xiao K, Madabushi S*, et al.* (2006). beta-arrestin-dependent, G protein-independent ERK1/2 activation by the beta2 adrenergic receptor. *J Biol Chem* 281**:** 1261-1273.

Shetzline SE, Rallapalli R, Dowd KJ, Zou S, Nakata Y, Swider CR*, et al.* (2004). Neuromedin U: a Myb-regulated autocrine growth factor for human myeloid leukemias. *Blood* 104**:** 1833-1840.

Shimamura T, Shiroishi M, Weyand S, Tsujimoto H, Winter G, Katritch V*, et al.* (2011). Structure of the human histamine H1 receptor complex with doxepin. *Nature* 475**:** 65-70.

Shrager B, Jibara GA, Tabrizian P, Roayaie S, Ward SC (2012). Resection of nonalcoholic steatohepatitis-associated hepatocellular carcinoma: a Western experience. *Int J Surg Oncol* 2012**:** 915128.

Shukla AK, Xiao K, Lefkowitz RJ (2011a). Emerging paradigms of beta-arrestin-dependent seven transmembrane receptor signaling. *Trends Biochem Sci* 36**:** 457-469.

Shukla AK, Xiao K, Lefkowitz RJ (2011b). Emerging paradigms of β-arrestin-dependent seven transmembrane receptor signaling. *Trends in Biochemical Sciences* 36**:** 457-469.

Singh V, Raghuwanshi SK, Smith N, Rivers EJ, Richardson RM (2014). G Protein–Coupled Receptor Kinase-6 Interacts with Activator of G Protein Signaling-3 To Regulate CXCR2-Mediated Cellular Functions. *The Journal of Immunology* 192**:** 2186.

Smith AE, Kasper JM, Ara, Anastasio NC, Hommel JD (2019). Binge-Type Eating in Rats is Facilitated by Neuromedin U Receptor 2 in the Nucleus Accumbens and Ventral Tegmental Area. *Nutrients* 11.

Smith JS, Rajagopal S (2016). The beta-Arrestins: Multifunctional Regulators of G Protein-coupled Receptors. *J Biol Chem* 291**:** 8969-8977.

Smyth EM, Austin SC, Reilly MP, FitzGerald GA (2000). Internalization and sequestration of the human prostacyclin receptor. *J Biol Chem* 275**:** 32037-32045.

Sprang SR, Chen Z, Du X (2007). Structural basis of effector regulation and signal termination in heterotrimeric Galpha proteins. *Adv Protein Chem* 74**:** 1-65.

Sriram K, Insel PA (2018). GPCRs as targets for approved drugs: How many targets and how many drugs? *Mol Pharmacol***:** mol.117.111062.

Stalheim L, Ding Y, Gullapalli A, Paing MM, Wolfe BL, Morris DR*, et al.* (2005). Multiple Independent Functions of Arrestins in the Regulation of Protease-Activated Receptor-2 Signaling and Trafficking. *Mol Pharmacol* 67**:** 78-87.

Steinert RE, Feinle-Bisset C, Asarian L, Horowitz M, Beglinger C, Geary N (2017). Ghrelin, CCK, GLP-1, and PYY(3-36): Secretory Controls and Physiological Roles in Eating and Glycemia in Health, Obesity, and After RYGB. *Physiol Rev* 97**:** 411-463.

Sternson SM, Atasoy D (2014). Agouti-related protein neuron circuits that regulate appetite. *Neuroendocrinology* 100**:** 95-102.

Sumi S, Inoue K, Kogire M, Doi R, Takaori K, Suzuki T*, et al.* (1987). Effect of synthetic neuromedin U-8 and U-25, novel peptides identified in porcine spinal cord, on splanchnic circulation in dogs. *Life Sci* 41**:** 1585-1590.

Sweeting HN (2007). Measurement and definitions of obesity in childhood and adolescence: a field guide for the uninitiated. *Nutr J* 6**:** 32.

Syrovatkina V, Alegre KO, Dey R, Huang XY (2016). Regulation, Signaling, and Physiological Functions of G-Proteins. *J Mol Biol* 428**:** 3850-3868.

Szekeres PG, Muir AI, Spinage LD, Miller JE, Butler SI, Smith A*, et al.* (2000). Neuromedin U is a potent agonist at the orphan G protein-coupled receptor FM3. *J Biol Chem* 275**:** 20247-20250.

Tan CP, McKee KK, Liu Q, Palyha OC, Feighner SD, Hreniuk DL*, et al.* (1998). Cloning and characterization of a human and murine T-cell orphan G-protein-coupled receptor similar to the growth hormone secretagogue and neurotensin receptors. *Genomics* 52**:** 223-229.

Tanida M, Satomi J, Shen J, Nagai K (2009). Autonomic and cardiovascular effects of central neuromedin U in rats. *Physiol Behav* 96**:** 282-288.

Teixeira A, Chaverot N, Schroder C, Strosberg AD, Couraud PO, Cazaubon S (1999). Requirement of caveolae microdomains in extracellular signal-regulated kinase and focal adhesion kinase activation induced by endothelin-1 in primary astrocytes. *J Neurochem* 72**:** 120-128.

Thingholm TE, Larsen MR (2016). Phosphopeptide Enrichment by Immobilized Metal Affinity Chromatography. In: von Stechow L (ed). *Phospho-Proteomics: Methods and Protocols*, edn. New York, NY: Springer New York. p^pp 123-133.

Thompson EL, Murphy KG, Todd JF, Martin NM, Small CJ, Ghatei MA*, et al.* (2004). Chronic administration of NMU into the paraventricular nucleus stimulates the HPA axis but does not influence food intake or body weight. *Biochem Biophys Res Commun* 323**:** 65-71.

Thomsen ARB, Jensen DD, Hicks GA, Bunnett NW (2018). Therapeutic Targeting of Endosomal G-Protein-Coupled Receptors. *Trends Pharmacol Sci* 39**:** 879-891.

Thomsen ARB, Plouffe B, Cahill TJ, 3rd, Shukla AK, Tarrasch JT, Dosey AM*, et al.* (2016). GPCR-G Protein-β-Arrestin Super-Complex Mediates Sustained G Protein Signaling. *Cell* 166**:** 907-919.

Tian X, Irannejad R, Bowman SL, Du Y, Puthenveedu MA, von Zastrow M*, et al.* (2016). The alpha-Arrestin ARRDC3 Regulates the Endosomal Residence Time and Intracellular Signaling of the beta2-Adrenergic Receptor. *J Biol Chem* 291**:** 14510-14525.

Tobin AB (2008). G-protein-coupled receptor phosphorylation: where, when and by whom. *Br J Pharmacol* 153 Suppl 1**:** S167-176.

Tobin AB, Butcher AJ, Kong KC (2008). Location, location, location...site-specific GPCR phosphorylation offers a mechanism for cell-type-specific signalling. *Trends Pharmacol Sci* 29**:** 413-420.

Tohgo A, Pierce KL, Choy EW, Lefkowitz RJ, Luttrell LM (2002). beta-Arrestin scaffolding of the ERK cascade enhances cytosolic ERK activity but inhibits ERK-mediated transcription following angiotensin AT1a receptor stimulation. *J Biol Chem* 277**:** 9429-9436.

Topiol S, Sabio M (2015). The role of experimental and computational structural approaches in 7TM drug discovery. *Expert Opin Drug Discov* 10**:** 1071-1084.

Torrecilla I, Spragg EJ, Poulin B, McWilliams PJ, Mistry SC, Blaukat A*, et al.* (2007). Phosphorylation and regulation of a G protein-coupled receptor by protein kinase CK2. *J Cell Biol* 177**:** 127-137.

Torres R, Croll SD, Vercollone J, Reinhardt J, Griffiths J, Zabski S*, et al.* (2007). Mice genetically deficient in neuromedin U receptor 2, but not neuromedin U receptor 1, have impaired nociceptive responses. *Pain* 130**:** 267-278.

Toth AD, Prokop S, Gyombolai P, Varnai P, Balla A, Gurevich VV*, et al.* (2018). Heterologous phosphorylation-induced formation of a stability lock permits regulation of inactive receptors by beta-arrestins. *J Biol Chem* 293**:** 876-892.

Towbin H, Staehelin T, Gordon J (1979). Electrophoretic transfer of proteins from polyacrylamide gels to nitrocellulose sheets: procedure and some applications. *Proc Natl Acad Sci U S A* 76**:** 4350-4354.

Tran TM, Friedman J, Qunaibi E, Baameur F, Moore RH, Clark RB (2004). Characterization of Agonist Stimulation of cAMP-Dependent Protein Kinase and G Protein-Coupled Receptor Kinase Phosphorylation of the β<sub>2</sub>-Adrenergic Receptor Using Phosphoserine-Specific Antibodies. *Mol Pharmacol* 65**:** 196-206.

Tran TM, Friedman J, Baameur F, Knoll BJ, Moore RH, Clark RB (2007). Characterization of beta2-adrenergic receptor dephosphorylation: Comparison with the rate of resensitization. *Mol Pharmacol* 71**:** 47-60.

Trincavelli ML, Tuscano D, Cecchetti P, Falleni A, Benzi L, Klotz KN*, et al.* (2000). Agonist-induced internalization and recycling of the human A(3) adenosine receptors: role in receptor desensitization and resensitization. *J Neurochem* 75**:** 1493-1501.

Trzaskowski B, Latek D, Yuan S, Ghoshdastider U, Debinski A, Filipek S (2012). Action of molecular switches in GPCRs--theoretical and experimental studies. *Curr Med Chem* 19**:** 1090-1109.

Tschop M, Smiley DL, Heiman ML (2000). Ghrelin induces adiposity in rodents. *Nature* 407**:** 908-913.

Tusnady GE, Simon I (2001). The HMMTOP transmembrane topology prediction server. *Bioinformatics* 17**:** 849-850.

Upadhyay J, Farr O, Perakakis N, Ghaly W, Mantzoros C (2018). Obesity as a Disease. *Med Clin North Am* 102**:** 13-33.

Valsamakis G, Konstantakou P, Mastorakos G (2017). New Targets for Drug Treatment of Obesity. *Annu Rev Pharmacol Toxicol* 57**:** 585-605.

van der Klaauw AA (2018). Neuropeptides in Obesity and Metabolic Disease. *Clin Chem* 64**:** 173-182.

van Koppen CJ, Nathanson NM (1990). Site-directed mutagenesis of the m2 muscarinic acetylcholine receptor. Analysis of the role of N-glycosylation in receptor expression and function. *J Biol Chem* 265**:** 20887-20892.

Venter JC, Adams MD, Myers EW, Li PW, Mural RJ, Sutton GG*, et al.* (2001). The sequence of the human genome. *Science* 291**:** 1304-1351.

Vilardaga J-P, Jean-Alphonse FG, Gardella TJ (2014). Endosomal generation of cAMP in GPCR signaling. *Nature Chemical Biology* 10**:** 700-706.

Vilardaga J-P, Gardella TJ, Wehbi VL, Feinstein TN (2012). Non-canonical signaling of the PTH receptor. *Trends Pharmacol Sci* 33**:** 423-431.

Vilardaga JP, Krasel C, Chauvin S, Bambino T, Lohse MJ, Nissenson RA (2002). Internalization determinants of the parathyroid hormone receptor differentially regulate beta-arrestin/receptor association. *J Biol Chem* 277**:** 8121-8129.

Violin JD, Ren XR, Lefkowitz RJ (2006). G-protein-coupled receptor kinase specificity for beta-arrestin recruitment to the beta2-adrenergic receptor revealed by fluorescence resonance energy transfer. *J Biol Chem* 281**:** 20577-20588.

Wan Y, Zhang J, Fang C, Chen J, Li J, Li J*, et al.* (2018). Characterization of neuromedin U (NMU), neuromedin S (NMS) and their receptors (NMUR1, NMUR2) in chickens. *Peptides* 101**:** 69-81.

Wang W, Qiao Y, Li Z (2018). New Insights into Modes of GPCR Activation. *Trends Pharmacol Sci* 39**:** 367-386.

Wang X, Tournier C (2006). Regulation of cellular functions by the ERK5 signalling pathway. *Cell Signal* 18**:** 753-760.

Wang X, Destrument A, Tournier C (2007). Physiological roles of MKK4 and MKK7: insights from animal models. *Biochim Biophys Acta* 1773**:** 1349-1357.

Watari K, Nakaya M, Kurose H (2014). Multiple functions of G protein-coupled receptor kinases. *Journal of molecular signaling* 9**:** 1-1.

Wehbi VL, Stevenson HP, Feinstein TN, Calero G, Romero G, Vilardaga JP (2013). Noncanonical GPCR signaling arising from a PTH receptor-arrestin-Gbetagamma complex. *Proc Natl Acad Sci U S A* 110**:** 1530-1535.

Wei H, Ahn S, Barnes WG, Lefkowitz RJ (2004). Stable interaction between beta-arrestin 2 and angiotensin type 1A receptor is required for beta-arrestin 2-mediated activation of extracellular signal-regulated kinases 1 and 2. *J Biol Chem* 279**:** 48255-48261.

Wei H, Ahn S, Shenoy SK, Karnik SS, Hunyady L, Luttrell LM*, et al.* (2003). Independent beta-arrestin 2 and G protein-mediated pathways for angiotensin II activation of extracellular signal-regulated kinases 1 and 2. *Proc Natl Acad Sci U S A* 100**:** 10782-10787.

Weichert D, Kruse AC, Manglik A, Hiller C, Zhang C, Hubner H*, et al.* (2014). Covalent agonists for studying G protein-coupled receptor activation. *Proc Natl Acad Sci U S A* 111**:** 10744-10748.

Werry TD, Wilkinson GF, Willars GB (2003). Mechanisms of cross-talk between G-protein-coupled receptors resulting in enhanced release of intracellular Ca2+. *Biochem J* 374**:** 281-296.

Werry TD, Sexton PM, Christopoulos A (2005). "Ins and outs" of seven-transmembrane receptor signalling to ERK. *Trends Endocrinol Metab* 16**:** 26-33.

Westfall TD, McCafferty GP, Pullen M, Gruver S, Sulpizio AC, Aiyar VN*, et al.* (2002). Characterization of neuromedin U effects in canine smooth muscle. *J Pharmacol Exp Ther* 301**:** 987-992.

Wettschureck N, Offermanns S (2005). Mammalian G proteins and their cell type specific functions. *Physiol Rev* 85**:** 1159-1204.

Whalen EJ, Rajagopal S, Lefkowitz RJ (2011). Therapeutic potential of beta-arrestin- and G protein-biased agonists. *Trends Mol Med* 17**:** 126-139.

Wheatley M, Wootten D, Conner MT, Simms J, Kendrick R, Logan RT*, et al.* (2012). Lifting the lid on GPCRs: the role of extracellular loops. *Br J Pharmacol* 165**:** 1688-1703.

Willars GB, Müller-Esterl W, Nahorski SR (1999). Receptor phosphorylation does not mediate cross talk between muscarinic M3 and bradykinin B2 receptors. *American Journal of Physiology-Cell Physiology* 277**:** C859-C869.

Williams G, Bing C, Cai XJ, Harrold JA, King PJ, Liu XH (2001). The hypothalamus and the control of energy homeostasis: different circuits, different purposes. *Physiol Behav* 74**:** 683-701.

Wing RR, Tate DF, Gorin AA, Raynor HA, Fava JL (2006). A self-regulation program for maintenance of weight loss. *N Engl J Med* 355**:** 1563-1571.

Wisler JW, Rockman HA, Lefkowitz RJ (2018). Biased G Protein-Coupled Receptor Signaling: Changing the Paradigm of Drug Discovery. *Circulation* 137**:** 2315-2317.

Wisler JW, DeWire SM, Whalen EJ, Violin JD, Drake MT, Ahn S*, et al.* (2007). A unique mechanism of β-blocker action: Carvedilol stimulates β-arrestin signaling. *Proceedings of the National Academy of Sciences* 104**:** 16657-16662.

Wong SK (2003). G protein selectivity is regulated by multiple intracellular regions of GPCRs. *Neurosignals* 12**:** 1-12.

Wren AM, Small CJ, Abbott CR, Jethwa PH, Kennedy AR, Murphy KG*, et al.* (2002). Hypothalamic actions of neuromedin U. *Endocrinology* 143**:** 4227-4234.

Wu Y, McRoberts K, Berr SS, Frierson HF, Jr., Conaway M, Theodorescu D (2007). Neuromedin U is regulated by the metastasis suppressor RhoGDI2 and is a novel promoter of tumor formation, lung metastasis and cancer cachexia. *Oncogene* 26**:** 765-773.

Wuller S, Wiesner B, Loffler A, Furkert J, Krause G, Hermosilla R*, et al.* (2004). Pharmacochaperones post-translationally enhance cell surface expression by increasing conformational stability of wild-type and mutant vasopressin V2 receptors. *J Biol Chem* 279**:** 47254-47263.

Wynne K, Stanley S, McGowan B, Bloom S (2005). Appetite control. *J Endocrinol* 184**:** 291-318.

Xiao K, Liu H (2016). “Barcode” and Differential Effects of GPCR Phosphorylation by Different GRKs. In: Gurevich VV, Gurevich EV, Tesmer JJG (eds). *G Protein-Coupled Receptor Kinases*, edn. New York, NY: Springer New York. p^pp 75-120.

Xiao K, Sun J, Kim J, Rajagopal S, Zhai B, Villén J*, et al.* (2010). Global phosphorylation analysis of β-arrestin–mediated signaling downstream of a seven transmembrane receptor (7TMR). *Proceedings of the National Academy of Sciences* 107**:** 15299.

Yamashiro DJ, Maxfield FR (1987). Kinetics of endosome acidification in mutant and wild-type Chinese hamster ovary cells. *J Cell Biol* 105**:** 2713.

Yamashita K, Upadhyay S, Osada M, Hoque MO, Xiao Y, Mori M*, et al.* (2002). Pharmacologic unmasking of epigenetically silenced tumor suppressor genes in esophageal squamous cell carcinoma. *Cancer Cell* 2**:** 485-495.

Yamauchi J, Nagao M, Kaziro Y, Itoh H (1997). Activation of p38 mitogen-activated protein kinase by signaling through G protein-coupled receptors. Involvement of Gbetagamma and Galphaq/11 subunits. *J Biol Chem* 272**:** 27771-27777.

Yang F, Yu X, Liu C, Qu CX, Gong Z, Liu HD*, et al.* (2015). Phospho-selective mechanisms of arrestin conformations and functions revealed by unnatural amino acid incorporation and (19)F-NMR. *Nat Commun* 6**:** 8202.

Yang G, Su J, Yao Y, Lei Z, Zhang G, Liu Y*, et al.* (2012). Distribution of neuromedin S and its receptor NMU2R in pigs. *Res Vet Sci* 92**:** 180-186.

Yang Z, Yang F, Zhang D, Liu Z, Lin A, Liu C*, et al.* (2017). Phosphorylation of G Protein-Coupled Receptors: From the Barcode Hypothesis to the Flute Model. *Mol Pharmacol* 92**:** 201-210.

Yoon S, Seger R (2006). The extracellular signal-regulated kinase: multiple substrates regulate diverse cellular functions. *Growth Factors* 24**:** 21-44.

Yu SS, Lefkowitz RJ, Hausdorff WP (1993). Beta-adrenergic receptor sequestration. A potential mechanism of receptor resensitization. *J Biol Chem* 268**:** 337-341.

Yu XH, Cao CQ, Mennicken F, Puma C, Dray A, O'Donnell D*, et al.* (2003). Pro-nociceptive effects of neuromedin U in rat. *Neuroscience* 120**:** 467-474.

Zeng H, Gragerov A, Hohmann JG, Pavlova MN, Schimpf BA, Xu H*, et al.* (2006). Neuromedin U receptor 2-deficient mice display differential responses in sensory perception, stress, and feeding. *Mol Cell Biol* 26**:** 9352-9363.

Zhang W, Sakoda H, Miura A, Shimizu K, Mori K, Miyazato M*, et al.* (2017). Neuromedin U suppresses glucose-stimulated insulin secretion in pancreatic beta cells. *Biochem Biophys Res Commun* 493**:** 677-683.

Zhang ZY, Wang MW (2012). Obesity, a health burden of a global nature. *Acta Pharmacol Sin* 33**:** 145-147.

Zhou H, Tai HH (2000). Expression and functional characterization of mutant human CXCR4 in insect cells: role of cysteinyl and negatively charged residues in ligand binding. *Arch Biochem Biophys* 373**:** 211-217.

Zidar DA, Violin JD, Whalen EJ, Lefkowitz RJ (2009). Selective engagement of G protein coupled receptor kinases (GRKs) encodes distinct functions of biased ligands. *Proc Natl Acad Sci U S A* 106**:** 9649-9654.

Zindel D, Engel S, Bottrill AR, Pin JP, Prezeau L, Tobin AB*, et al.* (2016). Identification of key phosphorylation sites in PTH1R that determine arrestin3 binding and fine-tune receptor signaling. *Biochem J* 473**:** 4173-4192.